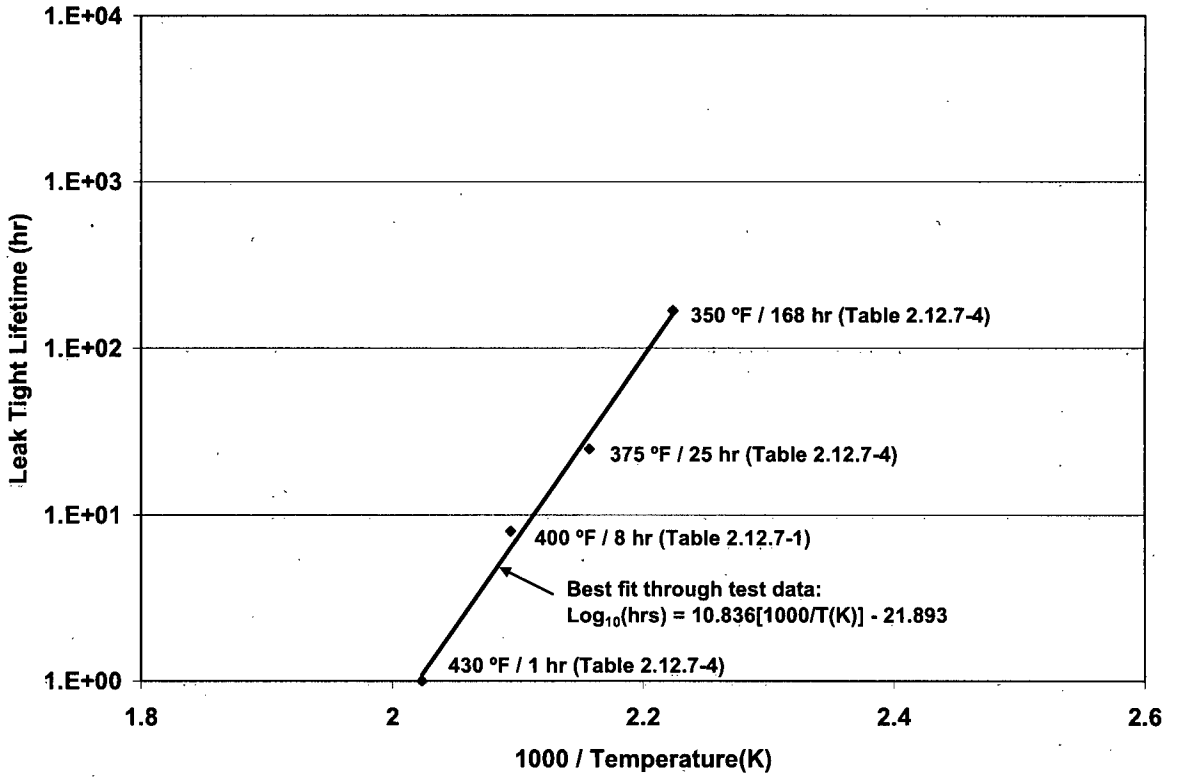

Figure 2.12.7-2 – R-0405-70 Test Data and Best Fit Curve

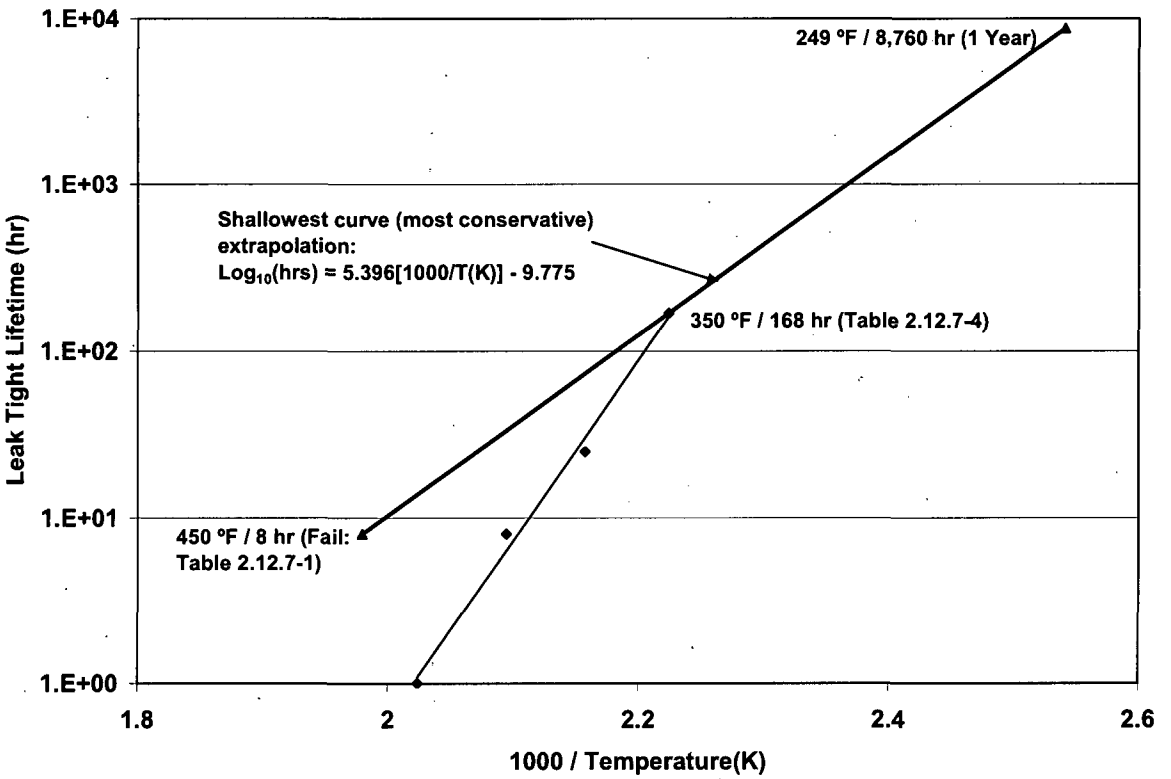

Figure 2.12.7-3 – Conservative Extrapolation to One Year

2.12.7.5 References

1. ANSI N14.5-1997, *American National Standard for Radioactive Materials – Leakage Tests on Packages for Shipment*, American National Standards Institute (ANSI), Inc.
2. *Safety Analysis Report for the TRUPACT-II Shipping Package*, USNRC Docket 71-9218, Revision 18, U.S. Department of Energy, Carlsbad Field Office, Carlsbad, New Mexico.
3. DOE Docket No. 94-6-9904, *Radioisotope Thermoelectric Generator Transportation System Safety Analysis Report for Packaging*, WHC-SD-RTG-SARP-001, prepared for the U.S. Department of Energy Office of Nuclear Energy under Contract No. DE-AC06-87RL10930 by Westinghouse Hanford Company, Richland, WA.
4. Westinghouse Hanford Company, *RTG Transportation System Packaging O-ring Material Thermal Validation Test Report for Face Seal Test Fixture*, WHC-SD-RTG-TRP-010, Rev 0.
5. Westinghouse Hanford Company, *Radioisotope Thermoelectric Generator (RTG) Transportation System Packaging O-ring Material Thermal Validation Test Report*, WHC-SD-RTG-TRP-001, Rev. 1.
6. Westinghouse Hanford Company, *Radioisotope Thermoelectric Generator (RTG) Transportation System Packaging O-ring Material Elevated Temperature Test Report*, WHC-SD-RTG-TRP-002, Rev. 0.
7. Nigrey, P. J., *Prediction of Packaging Seal Life Using Thermoanalytical Techniques*, Proceedings of the 12th International Conference on the Packaging and Transportation of Radioactive Materials, PATRAM 98, Vol. 4, p. 1730.

2.12.8 Fuel Basket Stress Analysis

This appendix provides details of the stress analysis evaluations of the four fuel baskets used in the BRR package under HAC free drop conditions. One basket corresponds to each type of fuel, which includes the University of Missouri Research Reactor (MURR), the Massachusetts Institute of Technology Nuclear Research Reactor (MITR-II), Advanced Test Reactor (ATR), and Training, Research, Isotopes, General Atomics (TRIGA) reactors.

The evaluations consist of manual calculations and buckling evaluations using ASME B&PV Code Case N-284-2 [13]. All buckling evaluations use a minimum factor of safety of 1.34, consistent with [13]. The bounding HAC impact acceleration of 120g is used for all analyses, which include free drops on the package end and on the package side. Basket and fuel weight is taken from Table 2.1-3. All of the material used in the fuel baskets is ASTM Type 304 stainless steel in various product forms including A240 (plate), A249 (tube), A269 (tube), A511 (tube), and A312 (pipe). Material properties are evaluated at the NCT maximum temperature of 400 °F, and taken from Table 2.2-1. Allowable stresses are taken from Table 2.1-1. The numeric values of allowable stress are given in Table 2.12.8-1. The analyses described in this appendix are based on the most critical load paths and demonstrate the structural integrity of the basket. Since each basket has a different design, the analyses which are most critical for each basket will be somewhat different.

Basket analyses do not include a dynamic load factor (DLF), since the impact acceleration used is nearly 50% higher than the maximum test result (see Section 2.12.5.3, *Reconciliation with Certification Test Results*), and because the basket structures are relatively stiff, which would result in a DLF not significantly different from unity.

2.12.8.1 MURR Basket

The MURR basket provides positioning and support for up to eight MURR fuel elements. The structure consists of an outer shell, an inner shell, eight radial separation plates, a support plate, and other stiffening components. From Table 2.1-3, the empty basket has a weight of 650 lb, and with eight fuel elements, the bounding weight is 770 lb. A cross sectional view of the basket is shown in Figure 2.12.8-1 and a view of the support plate is shown in Figure 2.12.8-2.

2.12.8.1.1 Fuel Support Plate Bending

The fuel support plate provides lower end support of the fuel elements. In the bottom-down vertical impact, the support plate is loaded by a maximum of eight fuel elements. Since each fuel element slot is supported by welds along three sides as shown in Figure 2.12.8-2, the loading of the plate can be analyzed for a single segment of the plate.

Stresses loading the plate can be modeled using [25], Table 24, Case 27. This is a conservative approach using the simply supported case. This method will ignore the in-plane moment reducing effects of the welds. The effective area of plate for the applied load is:

$$A_P = \frac{\pi}{4}(d_o^2 - d_i^2) - 8 \cdot \frac{\pi}{4} d_H^2 - 8 \cdot A_S = 106.3\,\text{in}^2$$

where d_o = 15.1 inches is the outer diameter of the plate, d_i = 7.0 inches is the center hole diameter of the plate, d_H = 0.8 inches is the diameter of the eight drain holes, and A_S = 3.781 in^2 is the area of the separator plates. For a density ρ = 0.29 lb/in^3 and a plate thickness t = 0.375 inches, the weight of the plate is:

$$W_P = A_P t\rho = 11.6 \text{ lb}$$

For a single sector of the plate, the plate load is:

$$P_P = (nW_{FE} + W_P) \cdot a = 15{,}792 \text{ lb}$$

where the number of fuel elements, n = 8, the weight of individual MURR element, W_{FE} = 15 lb, and the bounding acceleration is a = 120g. The distributed pressure load over each sector of the plate is equivalent to the total fuel load over the effective area of the plate.

$$q = \frac{P_P}{A_P} = 148.6 \text{ psi}$$

From Case 27 the maximum plate stress for each segment is:

$$\sigma_t = \beta_1 \frac{qa^2}{t^2} = 6{,}867 \text{ psi}$$

where $a = \frac{1}{2}d_o$ is the radius of the segment of plate, t = 0.375 inches is the thickness of the plate, and β_1 = 0.114 is a constant. The allowable combined membrane and bending stress is S = 64,000 psi from Table 2.12.8-1. The margin of safety is:

$$MS = \frac{S}{\sigma_t} - 1 = +8.32$$

Therefore the plate has sufficient capacity to support the applied load.

2.12.8.1.2 Outer Shell Slot Welds

The slot welds connect the outer shell to the inner components of the basket. In a bottom-down drop, the slot welds will take the full weight of the fuel, center shell, spacer plates, and fuel support plate. The ¼ inch fillet weld between the fuel support plate and the outer shell will be conservatively excluded from this calculation.

The combined slot weld area for the 32, 2.0 inch x 0.6 inch long slots with full radii is:

$$A_{SW} = 32[\frac{\pi}{4}(0.6)^2 + 2.0(0.6)] = 47.4 \text{ in}^2$$

For this load case, the applied load is conservatively taken as the full weight of the loaded basket at an acceleration, a = 120g:

$$P_{SW} = (nW_{FE} + W_b)a = 92{,}400 \text{ lb}$$

where the weight of the fuel basket is W_b = 650 lb. The shear stress due to the direct load is:

$$\tau_{SW} = \frac{P_{SW}}{A_{SW}} = 1{,}949 \text{ psi}$$

From Table NG-3352-1 of [32] the allowable stress of the weld is multiplied by a weld quality factor of 0.35, which applies to an intermittent or plug weld with surface PT examination. From Table 2.12.8-1, the allowable stress for pure shear is S = 22,320 psi. The margin of safety is:

$$MS = \frac{(0.35)S}{\tau_{SW}} - 1 = +3.00$$

Therefore the slot welds have sufficient capacity to support the applied load.

2.12.8.1.3 Lower Shell Buckling

The lower section of shell is an unsupported column for a length of about 17.50 inches. The buckling load is analyzed using the method of ASME Code Case N284-2 [13]. Using the full weight of the basket as before will yield a conservative result. The loading on the lower shell from Section 2.12.8.1.2, *Outer Shell Slot Welds*, is P_{SW} = 92,400 lb. The cross sectional area of the shell is based on the inner diameter, d_i, of 15.1 inches and the wall thickness, t, of 0.25 inches.

$$A_{LS} = \pi(d_i + t)t = 12.1\,in^2$$

The axial stress is then:

$$\sigma_\phi = \frac{P_{SW}}{A_{LS}} = 7{,}636\ psi$$

An inner diameter of 15.1 inches, an outer diameter of 15.6 inches, and a length of 18.0 inches are used in the buckling analysis. A factor of safety of 1.34 is used, consistent with the requirements of [13]. The results, shown in Table 2.12.8-2, show that all the interaction parameters are less than unity, as required. Therefore, buckling of the lower shell of the MURR basket under the HAC end drop will not occur.

2.12.8.2 MITR-II Basket

The MITR-II basket provides support and positioning for up to eight MITR-II fuel elements. The structure consists of a basket weldment fabricated from a stack of 28 plates that are machined to accept the fuel elements. The basket weldment sets upon a base support shell, and a fuel support plate. From Table 2.1-3, the empty basket has a weight of 560 lb, and with eight fuel elements, the bounding weight is 640 lb. A cross sectional view of the basket is shown in Figure 2.12.8-3.

2.12.8.2.1 Lower Shell Buckling

The lower section of shell is an unsupported column for a significant portion of its length. The buckling will be checked for an unbraced length of 26.3 inches which bounds the unbraced length. The buckling load is analyzed using the method of ASME Code Case N284-2 [13]. Using the full weight of the basket as before will yield a conservative result. The basket weight is W = 640 lb, the acceleration is a = 120g.

$$P = Wa = 76{,}800\ lb$$

The cross sectional area of the shell is based on the inner diameter, d_i, of 13.5 inches and the wall thickness, t, of 0.25 inches.

$$A_{LS} = \pi(d_i + t)t = 10.8\,in^2$$

The axial stress is then:

$$\sigma_\phi = \frac{P}{A_{LS}} = 7{,}111\ psi$$

An inner diameter of 13.5 inches, an outer diameter of 14.0 inches, and a length of 26.3 inches are used in the buckling analysis. A factor of safety of 1.34 is used, consistent with the requirements of [13]. The results, shown in Table 2.12.8-2, show that all the interaction parameters are less than unity, as required. Therefore, buckling of the lower shell of the MITR-II basket under the HAC end drop will not occur.

2.12.8.3 ATR Basket

The ATR basket provides support and positioning for up to eight ATR fuel elements. The structure consists of an outer shell, an inner shell, eight radial separation plates, a support plate, and other stiffening components. From Table 2.1-3, the empty basket has a weight of 450 lb, and with eight fuel elements, the bounding weight is 650 lb. A cross sectional view of the basket is shown in Figure 2.12.8-4 and a view of the support plate is shown in Figure 2.12.8-5.

2.12.8.3.1 Fuel Support Plate Bending

The fuel support plate provides lower end positioning of the fuel elements. In a bottom-down end drop, the support plate is loaded by a maximum of eight fuel elements. Each fuel element section of the plate is supported by welds along three sides as shown in Figure 2.12.8-4.

The plate is modeled using [25] Table 24, Case 27. This is the same conservative approach used in Section 2.12.8.1.1, *Fuel Support Plate Bending*. The load applied by eight fuel elements is averaged over the entire plate. The effective area of plate for the applied load is:

$$A_P = \frac{\pi}{4}(d_o^2 - d_i^2) - 8\frac{\pi}{4}d_H^2 - 8A_S = 86.3\,in^2$$

where d_o = 13.0 inches is the outer diameter of the plate, d_i = 6.5 inches is the center hole diameter of the plate, d_H = 0.8 inches is the diameter of the eight drain holes, and A_S = 1.15 in^2 is the area of the separator plates. For a density ρ = 0.29 lb/in^3, and a plate thickness t = 0.5 inches, the weight of the plate is:

$$W_P = A_P t\rho = 12.5\ lb$$

For a single sector of the plate, the plate load is:

$$P_P = (nW_{FE} + W_P)a = 25{,}512\ lb$$

where the number of fuel elements, n = 8, the weight of an individual element, W_{FE} = 25 lb, and the acceleration, a = 120g. The distributed pressure load of the plate is:

$$q = \frac{P_P}{A_P} = 296 \text{ psi}$$

From [25] Table 24, Case 27, the maximum plate stress for each plate is:

$$\sigma_P = \beta_1 \frac{qa^2}{t^2} = 5{,}703 \text{ psi}$$

Where $a = \frac{1}{2}d_o$ is the radius of the segment of plate, t = 0.5 inches is the thickness of the plate, and $\beta_1 = 0.114$ is a constant. The allowable combined membrane and bending stress is S = 64,000 psi from Table 2.12.8-1. The margin of safety is:

$$MS = \frac{S}{\sigma_P} - 1 = +10.2$$

Therefore the plate has sufficient capacity to support the applied load.

2.12.8.3.2 Outer Shell Slot Welds

The slot welds connect the outer shell to the inner components of the basket. In a bottom-down drop, the slot welds are assumed to take the full load of the fuel, center shell, spacer plates, and fuel support plate. Conservatively, the full basket weight W = 650 lb will be applied. The combined slot weld area for the 72, 0.8 inch x 0.3 inch long slots with full radii is:

$$A_{SW} = 72[\frac{\pi}{4}(0.3)^2 + 0.8(0.3)] = 20.2 \text{ in}^2$$

The applied load is the full weight at an acceleration of a = 120g.

$$P_{SW} = Wa = 78{,}000 \text{ lb}$$

The shear stress due to the direct load is:

$$\tau_{SW} = \frac{P}{A_{SW}} = 3{,}861 \text{ psi}$$

From Table NG-3352-1 of [32], the allowable stress of the weld is multiplied by a weld quality factor of 0.35, which applies to an intermittent or plug weld with surface PT examination. From Table 2.12.8-1, the allowable stress for pure shear is S = 22,320 psi. The margin of safety is:

$$MS = \frac{(0.35)S}{\tau_{SW}} - 1 = +1.02$$

Therefore the slot welds have sufficient capacity to support the applied load.

2.12.8.3.3 Side Drop Bending

For the side drop impact, the ATR basket can be modeled as a simply supported beam, supported on the end plates. Conservatively, the support plates at intermediate spacings will be neglected. The applied load, assumed to be distributed along the beam, is equal to the bounding weight of 650 lb and the acceleration of a = 120g. The full basket load from Section 2.12.8.3.2, *Outer Shell Slot Welds*, is P_{SW} = 78,000 lb. The bending moment is:

$$M = \frac{wL_S^2}{8} = \frac{P_{SW}L_S}{8} = 500{,}955 \text{ in} - \text{lb}$$

where L_S = 51.38 inches, which is the full length of the inner shell. The moment of inertia from the combination of the two shells, (neglecting the contribution of any other components) is:

$$I = \frac{\pi}{64}\left[d_{1o}^4 - d_{1i}^4\right] + \frac{\pi}{64}\left[d_{2o}^4 - d_{2i}^4\right] = 272.7 \text{ in}^4$$

Where d_{1o} = 13.5 inches and d_{1i} = 13.0 inches are the inner and outer diameters of the outer shell, and d_{2o} = 7.2 inches and d_{2i} = 6.5 inches are the inner and outer diameters of the inner shell after machining. The highest bending stress is located at the outer radius of the outer shell, c = 6.75 inches. The bending stress is:

$$\sigma_b = \frac{Mc}{I} = 12{,}400 \text{ psi}$$

The allowable combined membrane and bending stress is S = 64,000 psi from Table 2.12.8-1. The margin of safety is:

$$MS = \frac{S}{\sigma_b} - 1 = +4.16$$

Therefore bending of the ATR basket in the side drop will not occur.

2.12.8.4 TRIGA Basket

The TRIGA basket provides support and positioning for up to nineteen TRIGA fuel elements. The structure consists of nineteen support tubes arranged in two concentric circles, a base plate, a center stiffener, and a top plate. The base plate is supported by two concentric circular shells. Fuel spacers are used with shorter versions of TRIGA fuel. From Table 2.1-3, the empty basket has a weight of 290 lb, and with nineteen fuel elements, the bounding weight is 480 lb. A cross sectional view of the basket is shown in Figure 2.12.8-6 and a view of the support plate is shown in Figure 2.12.8-7.

2.12.8.4.1 Fuel Support Plate Bending

The fuel support plate provides lower end support of the fuel elements. In the bottom-down vertical impact, the support plate is loaded by a maximum of nineteen fuel elements, the top plate, center plate, and the fuel tubes and fuel spacers. Conservatively, the full weight of the basket will be taken as a distributed load across the plate. This load is distributed evenly over the plate and is reacted by the outer and inner shells which support the plate.

The loaded surface area of the plate consists of the basic plate surface between the outer support shell outer diameter, d_p = 13.0 inches, and the inner support shell inner diameter of d_i = 3.5 inches. This area is further reduced by the 19 drain holes with a diameter of d_h = 0.8 inches.

$$A_p = \frac{\pi}{4}(d_p^2 - d_i^2 - 19d_h^2) = 113.6 \text{ in}^2$$

The load per unit area on the plate is:

$$q = \frac{Wa}{A_p} = 507 \text{ psi}$$

where the weight on the plate is W = 480 lb, and the acceleration, a = 120g.

The maximum plate stress can be calculated from [25] Table 24, Case 2c. The distributed load is applied over the area between the outer edge (radius a = $d_p/2$) of the outer base shell to the inner edge (radius b = $d_i/2$) of the schedule 40 pipe inner base shell. The interpolated values from case 2c of K_{Mrmax} = 0.0575 and K_{Mtb} = -0.0754 are based on the ratio of the outer and inner plate radii b/a = 0.27. The maximum moment in the plate is based on the maximum absolute value of these to factors, K_{Max} = 0.0754. The maximum bending moments is:

$$M_{Max} = K_{Max} q a^2 = 1{,}615 \text{ lb}$$

The maximum bending stress using the material thickness of the plate, t = 0.5 in, is:

$$\sigma_b = -\frac{6M_{Max}}{t^2} = 38{,}760 \text{ psi}$$

The allowable combined membrane and bending stress is S = 64,000 psi from Table 2.12.8-1. The margin of safety is:

$$MS = \frac{S}{\sigma_b} - 1 = +0.65$$

Therefore the plate has sufficient capacity to support the applied load.

2.12.8.4.2 Shear Load on Pedestal Spacer Screw

Once adjusted, the length of the pedestal assembly is held in one of three positions by a single ¼-20 UNC screw (minimum diameter, d_n = 0.196 inches). The load on this screw will be in double shear and consist of the weight of one fuel element plus the weight of the spacer cap.

The weight of a single maximum length TRIGA fuel element is W_L = 10 lbs. Conservatively using the weight of the heaviest element, even though the pedestals are only used with short fuel elements, the maximum shear load on the screw is:

$$P_{SS} = W_L(120) = 1{,}200 \text{ lb}$$

The shear area of the screw (double shear) is:

$$A_S = 2\frac{\pi}{4}(d_n^2) = 0.0603 \text{ in}^2$$

The shear stress is:

$$\tau_S = \frac{P_{SS}}{A_S} = 19{,}900 \text{ psi}$$

From Table 2.12.8-1, the allowable for pure shear is S = 22,320 psi. The margin of safety for HAC is:

$$MS_{HAC} = \frac{S}{\tau_S} - 1 = +0.12$$

Therefore the screw has sufficient capacity to sustain the applied load.

2.12.8.4.3 Buckling of Fuel Tubes (Top Down Drop)

The TRIGA assembly may be supported by the 19 fuel tubes during a top down drop orientation. For consistency, this buckling case will be evaluated using the full weight of the assembly, W = 290 lb distributed over the 19 tubes. The buckling load is analyzed using the method of ASME Code Case N284-2 [13]. The complete length of the tube will be used as if it was not braced at the middle of its span. The applied load for each tube is:

$$P_{ft} = \frac{Wa}{19} = 1{,}832 \text{ lb}$$

The area of each tube is:

$$A_{ft} = \pi(d_i + t)t = 0.71 \text{ in}^2$$

where the inner diameter of each tube is d_i = 1.76 inches and the wall thickness is 0.12 inches. Based on this area the axial stress is:

$$\sigma_{ft} = \frac{P_{ft}}{A_{ft}} = 2{,}580 \text{ psi}$$

An inner diameter of 1.76 inches, an outer diameter of 2.0 inches, and a length of 48.00 inches are used. A factor of safety of 1.34 is used, consistent with the requirements of [13]. The results, shown in Table 2.12.8-2, show that all the interaction parameters are less than unity, as required. Therefore, buckling of the TRIGA basket fuel tubes under the HAC end drop will not occur.

2.12.8.4.4 Side Drop Bending

For the side drop impact, each fuel tube in the TRIGA basket is modeled as a simply supported beam. For an inner and outer diameter of the tube d_i = 1.76 inches, d_o = 2.0 inches, a length L_t = 48.00 inches, and a density ρ = 0.29 lb/in^3, the weight of the tube is:

$$V_b = \frac{\pi}{4}(d_o^2 - d_i^2)L_t = 34.0 \text{ in}^3$$

$$W_T = V_b\rho = 9.86 \text{ lb}$$

The applied load, assumed to be distributed along the beam, will be equal to the bounding weight of the largest fuel element W_F = 10 lbs. For the combined weight the load is:

$$P = 120(W_F + W_T) = 2{,}383 \text{ lb}$$

The bending moment is:

$$M = \frac{wL_t^2}{8} = \frac{PL_t}{8} = 7{,}149 \text{ in} - \text{lb}$$

where the reaction point separation is the unbraced length of the tube, L_t = 24.0 inches. The moment of inertia and area of a single tube is:

$$I = \frac{\pi}{64}\left[d_o^4 - d_i^4\right] = 0.314\ in^4$$

The bending stress is

$$\sigma_b = \frac{Mc}{I} = 22{,}767\ psi$$

where $c = \frac{1}{2}d_o$. From Table 2.12.8-1, the allowable stress is S = 64,000 psi for the combined membrane and bending stress. The margin of safety is:

$$MS = \frac{S}{\sigma_b} - 1 = +1.81$$

Therefore bending of the TRIGA fuel tubes will not occur.

2.12.8.5 Summary

Table 2.12.8-3 summarizes the margins of safety of the BRR package fuel baskets, as established in the sections above. Since all margins of safety are positive, and all Code Case N-284-2 interaction checks are less than unity, the BRR package fuel baskets are not of concern.

Table 2.12.8-1 – Material Properties and Allowable Stress

Parameter	(ASTM, Type 304)[1][4]
NCT Hot Bounding Temperature, °F	400
Elastic Modulus, psi	26.4×10^6
Design Stress, S_m, psi	18,600
Yield Stress, S_y, psi	20,700
Ultimate Stress, S_u, psi	64,000
HAC Allowable Stresses	
Primary Membrane Stress Intensity (P_m), psi	Lesser of: **$2.4S_m$ = 44,640** $0.7S_u$ = 44,800
Primary Membrane + Bending Stress Intensity ($P_m + P_b$), psi	Lesser of: **S_u = 64,000** $3.6S_m$ = 66,960
Pure Shear Stress Intensity, psi	Lesser of: $0.42S_u$ = 26,880[2] **$1.2S_m$ = 22,320**[3]

Notes:

1. ASTM A240, A249, A269, A276, A511, and A312.
2. ASME Code, Section III, Appendix F, Paragraph F-1334.2.
3. ASME Code, Section III, Subsection NG, Article NG-3225.
4. Governing values of allowable stress are in bold type.

Table 2.12.8-2 - Code Case N-284-2 Results Summary

Parameter	MURR	MITR-II	TRIGA	Remarks
Capacity Reduction Factors (-1511)				
$\alpha_{\varphi L}$ =	0.2070	0.2070	0.2070	
$\alpha_{\theta L}$ =	0.8000	0.8000	0.8000	
$\alpha_{\varphi\theta L}$ =	0.8000	0.8000	0.8000	
Plasticity Reduction Factors (-1610)				
η_{φ} =	0.1876	0.1706	0.0490	
η_{θ} =	0.3655	0.4924	0.2187	
$\eta_{\varphi\theta}$ =	0.0865	0.0970	0.0510	
Theoretical Buckling Values (-1712.1.1)				
C_{φ} =	0.6050	0.6050	0.6050	
$\sigma_{\varphi eL}$ =	520,261 psi	580,800 psi	2,038,979 psi	
$C_{\theta r}$ =	0.0778	0.0487	0.0351	
$\sigma_{\theta eL} = \sigma_{reL}$ =	66,906 psi	46,753 psi	118,324 psi	
C_h =	0.0744	0.0474	0.0351	
$\sigma_{\theta eL} = \sigma_{heL}$ =	64,015 psi	45,468 psi	118,324 psi	
$C_{\varphi\theta}$ =	0.2087	0.1668	0.0904	
$\sigma_{\varphi\theta eL}$ =	179,445 psi	160,127 psi	304,652psi	
Elastic Interaction Equations (-1713.1.1)				
σ_{xa} =	80,369 psi	89,721 psi	314,977 psi	
σ_{ha} =	38,218 psi	27,145 psi	70,641 psi	
σ_{ra} =	39,944 psi	27,912 psi	70,641 psi	
$\sigma_{\tau a}$ =	107,131 psi	95,598 psi	181,882 psi	
Axial + Hoop ⇨ Check (a):	N/A	N/A	N/A	<1 ∴ OK
Axial + Hoop ⇨ Check (b):	N/A	N/A	N/A	<1 ∴ OK
Axial + Shear ⇨ Check (c):	0.0950	0.0793	0.0082	<1 ∴ OK
Hoop + Shear ⇨ Check (d):	0.0000	0.0000	0.0000	<1 ∴ OK
Axial + Hoop + Shear ⇨ Check (e,a):	N/A	N/A	N/A	<1 ∴ OK
Axial + Hoop + Shear ⇨ Check (e,b):	N/A	N/A	N/A	<1 ∴ OK
Inelastic Interaction Equations (-1714.2.1)				
σ_{xc} =	15,077 psi	15,305 psi	15,448 psi	
σ_{rc} =	14,601 psi	13,745 psi	15,448 psi	
$\sigma_{\tau c}$ =	9,269 psi	9,269 psi	9,269 psi	
Max(Axial, Hoop) ⇨ Check (a):	0.5065	0.4646	0.1670	<1 ∴ OK
Axial + Shear ⇨ Check (b):	0.5065	0.4646	0.1670	<1 ∴ OK
Hoop + Shear ⇨ Check (c):	0.0000	0.0000	0.0000	<1 ∴ OK

Table 2.12.8-3 – Fuel Basket Stress Analysis Results

Analysis Description	Reference Section	Margin of Safety
MURR Basket		
Fuel Support Plate Bending	2.12.8.1.1	+8.32
Outer Shell Slot Welds	2.12.8.1.2	+3.00
Lower Shell Buckling	2.12.8.1.3	Pass*
MITR-II Basket		
Lower Shell Buckling	2.12.8.2.1	Pass*
ATR Basket		
Fuel Support Plate Bending	2.12.8.3.1	+10.2
Outer Shell Slot Welds	2.12.8.3.2	+1.02
Side Drop Bending	2.12.8.3.3	+4.16
TRIGA Basket		
Fuel Support Plate Bending	2.12.8.4.1	+0.65
Spacer Screw Shear Load	2.12.8.4.2	+0.12
Fuel Tube Buckling	2.12.8.4.3	Pass*
Side Drop Bending	2.12.8.4.4	+1.81

*Interaction equation checks are less than unity, as required by [13].

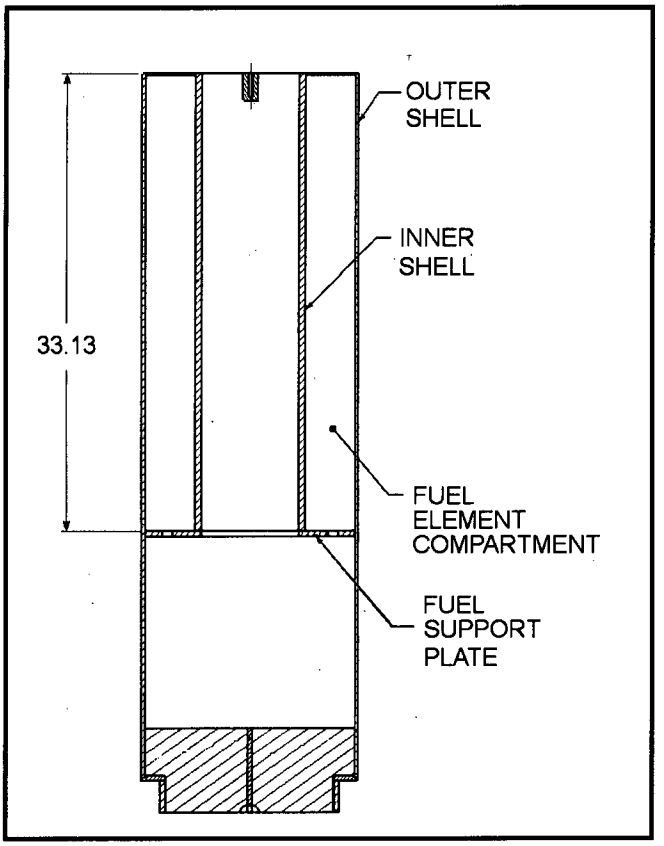

Figure 2.12.8-1 - MURR Fuel Basket Cross Section

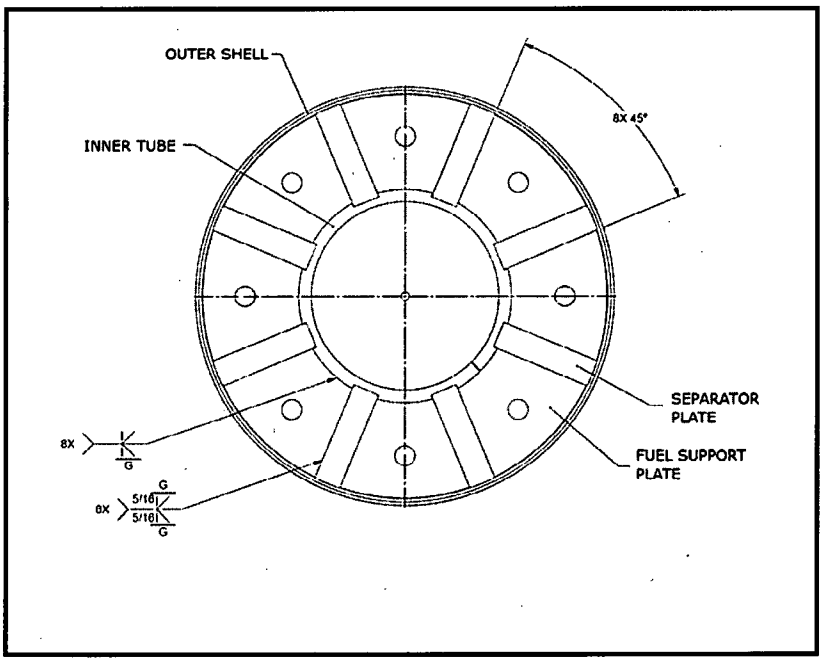

Figure 2.12.8-2 - MURR Fuel Basket View of Support Plate

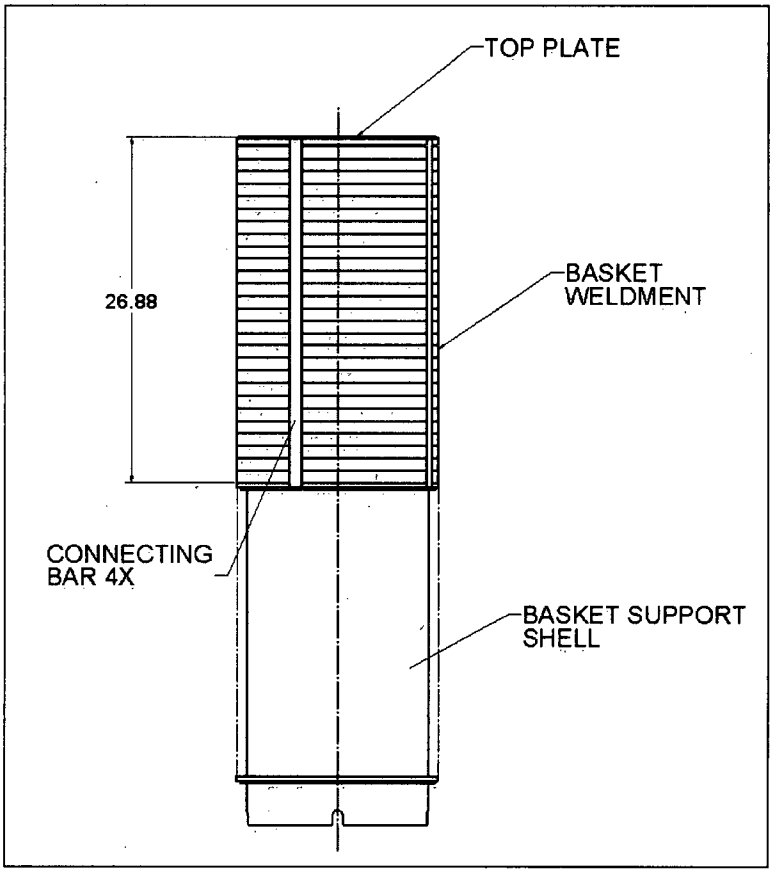

Figure 2.12.8-3 - MITR-II Fuel Basket Cross Section

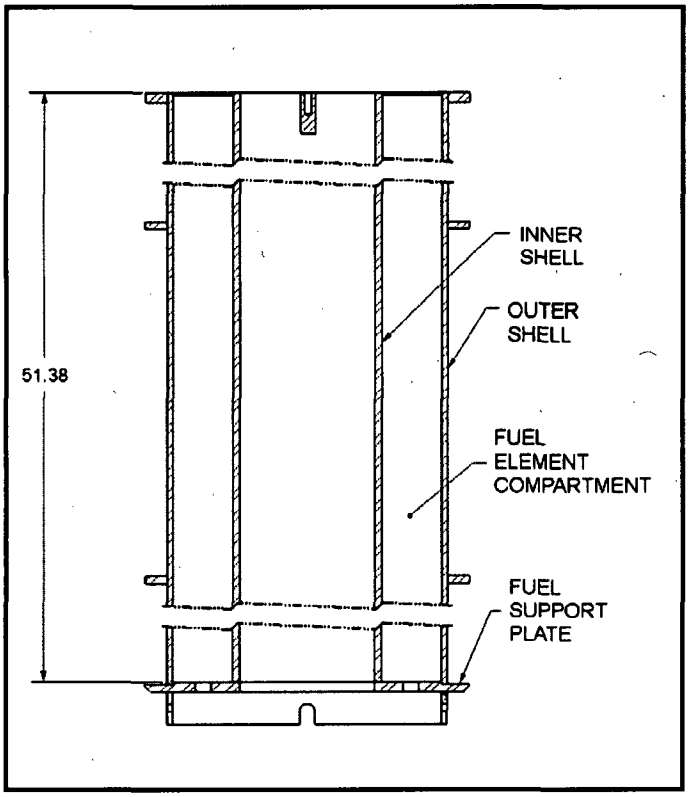

Figure 2.12.8-4 - ATR Fuel Basket Cross Section

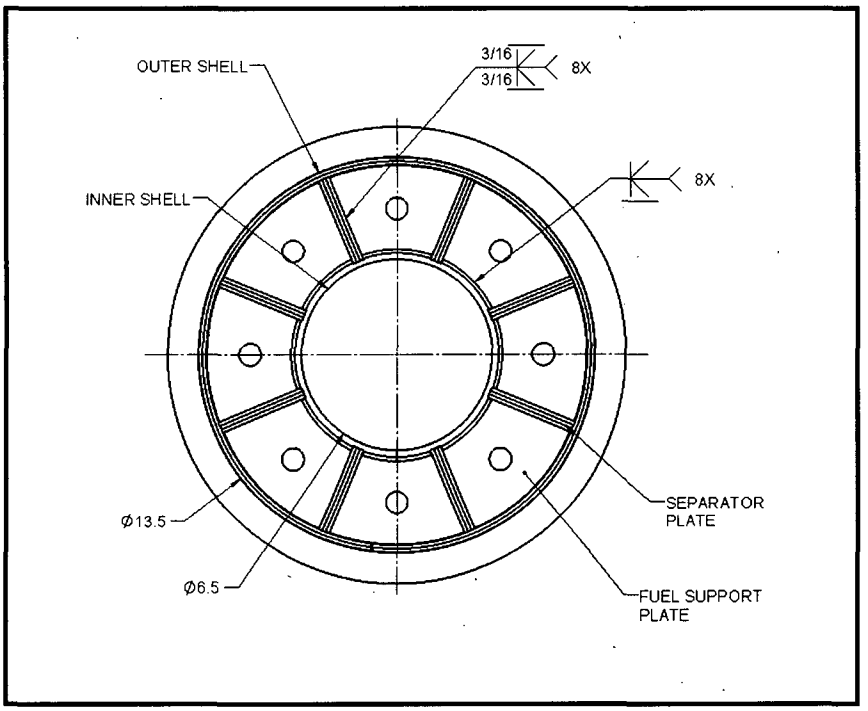

Figure 2.12.8-5 - ATR Fuel Basket View of Support Plate

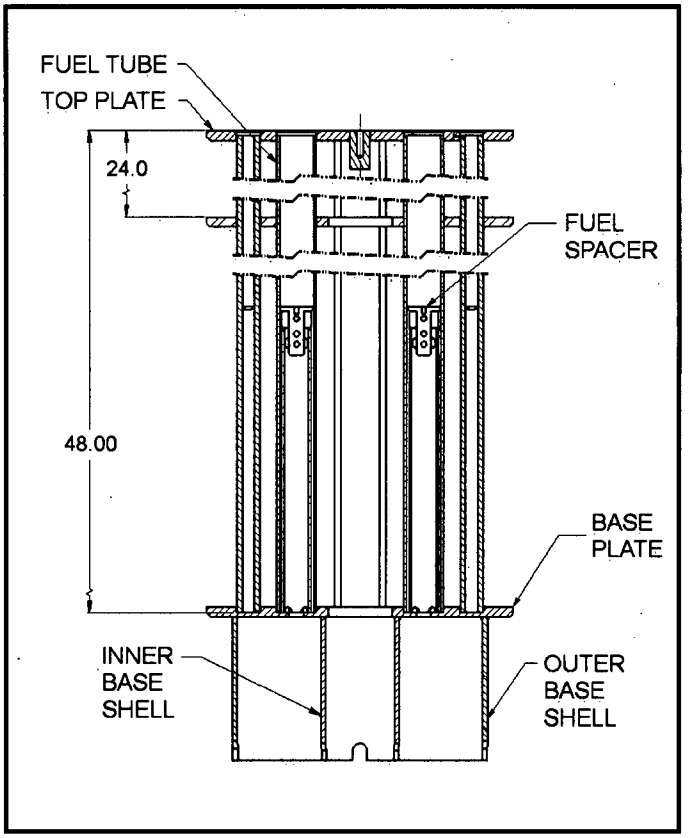

Figure 2.12.8-6 - TRIGA Fuel Basket Cross Section

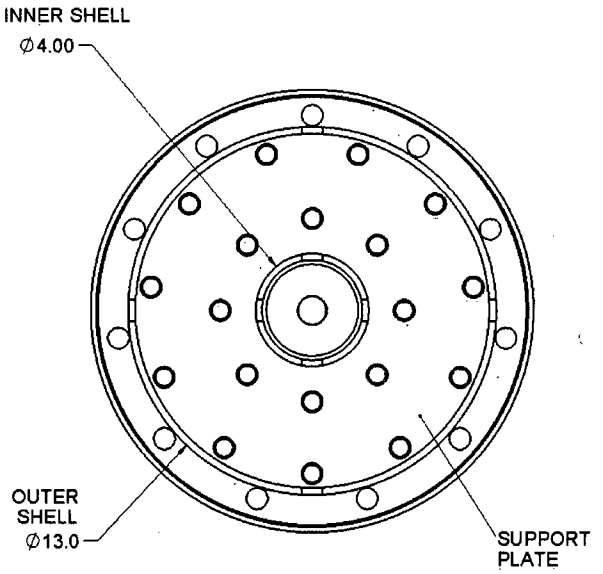

Figure 2.12.8-7 - TRIGA Fuel Basket View of Support Plate

3.0 THERMAL EVALUATION

This chapter identifies and describes the principal thermal design aspects of the BEA Research Reactor (BRR) package. The evaluations presented in this chapter demonstrate the compliance of the BRR package[1] as a Type B(U)F-96 shipping container with the thermal requirements of Title 10, Part 71 of the Code of Federal Regulations [1] when transporting a payload of irradiated fuel assemblies from various test and research reactors. These reactors include the Missouri University Research Reactor (MURR), the Massachusetts Institute of Technology Nuclear Research Reactor (MITR-II), Advanced Test Reactor (ATR), and Training, Research, Isotopes, General Atomics (TRIGA) reactors.

Specifically, all package components are shown to remain within their respective temperature limits under the normal conditions of transport (NCT). Further, per 10 CFR §71.43(g), the maximum temperature of the accessible package surfaces is demonstrated to be less than 185 °F for the maximum decay heat loading, an ambient temperature of 100 °F, and no insolation. Finally, the BRR package is shown to retain sufficient thermal protection following the HAC free and puncture drop scenarios to maintain all package component temperatures within their respective short term limits during the regulatory fire event and subsequent package cool-down.

3.1 Description of Thermal Design

The principal components of the BRR package are illustrated in Figure 1.2-1 through Figure 1.2-3 of Section 1.0, *General Information*. The principal components are: 1) a lead-shielded cask body, 2) a separate, removable upper shield plug, 3) a bolted closure lid, 4) upper and lower impact limiters containing polyurethane foam, and 5) a payload basket specific to the type of fuel being transported. Except for the closure bolts, the lead shielding, and the impact limiter attachment pins, the package is primarily of welded construction, using Type 304 austenitic stainless steel.

3.1.1 Design Features

The primary heat transfer mechanisms within the BRR packaging are conduction and radiation. The principal heat transfer from the exterior of the packaging is via convection and radiation to the ambient environment. The upper and lower impact limiter assemblies serve as the primary impact protection for the BRR package and its enclosed payload. The impact limiters also provide the principal thermal protection to the ends of the packaging, while a thermal shield is used to protect the portion of the packaging between the limiters from the high heat flux generated during the transient HAC fire event.

There is no pressure relief system included in the BRR packaging design. The thermal design features of the principal package components are described in the following paragraphs. See Section 1.0, *General Information*, for more detail.

[1] In the remainder of this chapter, the term 'packaging' refers to the assembly of components necessary to ensure compliance with the regulatory requirements, but does not include the payload. The term 'package' includes both the packaging components and the payload.

3.1.1.1 BRR Cask Body

The BRR cask body is a right circular cylinder approximately 77.1 inches long and 38 inches in diameter (not including the impact limiter attachments and the thermal shield). It is composed of upper and lower end structures that connect circular inner and outer shells. Lead located between the two circular shells, in the lower end closure structure, and in the shield plug provides radiological shielding for the package. This design results in a large thermal mass to surface area ratio capable of absorbing the high heat flux generated during the HAC fire event and limiting the temperature rise within the interior of the package. The payload cavity has a diameter of 16 inches and a length of 54 inches. Figure 1.2-3 provides an overview of the packaging dimensions.

The inner and outer shells and the end structures may be cast or forged from Type F304 stainless steel. Since the BRR package is designed to permit loading and unloading under water, the lower end structure contains a drain to allow removal of water from the payload cavity. The drain is sealed using a brass plug, butyl rubber seal, and a dust cap.

A thermal shield, composed of an outer sheet of 12 gauge (0.105-inch thick) Type 304 stainless steel and offset from the outer shell by small strips of the same 12 gauge material, covers the region of the outer shell not covered by the impact limiters. The shield serves to protect the outer shell from direct exposure to the high heat fluxes associated with the HAC fire accident event.

The lead shielding is made from ASTM B29, chemical lead, or optionally, from lead per Federal Specification QQ-L-171E, Grade A or C. The 8 inches thick lead shield in the side of the cask body is cast-in-place through openings in the upper end structure, thus eliminating/minimizing gaps between the lead and the steel shells. The shield at the bottom is made from lead sheet material which is packed firmly into place to yield a nominal thickness of 7.7 inches.

3.1.1.2 Removable Shield Plug

The removable shield plug rests on a shoulder located approximately half way along the length of the plug. The plug has a total thickness of 11.2 inches and a lead thickness of 9.7 inches. The outer shell is made from Type 304 plate material of various thicknesses and the cavity is filled with lead sheet material packed firmly into place. A ¾-inch diameter tube passes diagonally through the plug to ensure proper draining and drying of the cask while preventing a harmful shine path. Besides providing radiological shielding, the shield plug ensures a thermally significant separation distance between the basket's decay heat and the temperature sensitive closure seals.

3.1.1.3 BRR Cask Closure

The closure lid is made from 2-inch thick Type 304 stainless steel plate. It is attached to the cask using 12, 1-8 UNC electroless nickel plated bolts made of ASTM A320, Grade L43 material. The closure lid includes two O-ring seals made from butyl rubber of 3/8-inch cross sectional diameter. The inner O-ring is the containment seal, and the outer is the test seal. The seals are retained in dovetail grooves in the lid.

The BRR package features two ports which are also part of the containment boundary: a vent port in the closure lid, and a drain port in the lower end structure. Both ports are closed with threaded brass plugs and sealed with butyl rubber washers. A brass dust cover protects the port plugs. The seal test port is not part of the containment boundary.

3.1.1.4 Impact Limiters

The impact limiters attached to ends of the BRR packaging, each with essentially identical designs, provide a significant level of thermal protection to the package. Each limiter is 78 inches in diameter and 34.6 inches long overall, with a conical section 15 inches long towards the outer end. The impact limiters are filled with rigid, closed-cell polyurethane foam with a nominal 9 lb/ft^3 density that is poured in place. As described in Appendix 3.5.4, *'Last-A-Foam' Response under HAC Conditions*, the thermal decomposition of the closed-cell polyurethane foam during the HAC event absorbs a majority of the heat energy entering the impact limiters.

The foam is encased in a stainless steel shell for structural protection. The external shells (except for the outer end plates) are ¼ inches thick, while the internal shells which interface with the cask body are ½ inches thick. The outer end plates of the impact limiters are ½-inches thick. Plastic melt-out plugs are incorporated into the exterior shells of the limiters. The plugs are designed to soften and be expelled during the HAC fire event, thus relieving any pressure buildup in the limiters due to foam decomposition under elevated temperatures. The external surfaces of the impact limiter shell are covered with a white acrylic polyurethane coating to control solar absorptivity and raise thermal emissivity.

Each impact limiter is attached to the cask body via a set of eight (8) bayonet type connectors. The connectors consist of eight sets of two closely spaced plates, 1/2 inch thick, which go through the thermal shield and are welded to the outer shell of the cask. Mating with these plates are eight 3/4 inch thick plates attached to each limiter and which pass between the receptacle plates on the cask body. Each connection is completed by a stainless steel ball lock pin that passes through the three plates (two receptacle plates and one impact limiter plate).

3.1.1.5 Fuel Baskets

Four fuel baskets will be used with the BRR packaging, one for each type of fuel to be transported. Section 1.0, *General Information*, presents a description and illustration of each basket and fuel type to be loaded in the package. The baskets are made from welded construction using Type 304 stainless steel in plate, bar, pipe, and tubular forms. Each basket has a maximum diameter of 15.63 inches and a maximum length of 53.45 inches. The fuel cavities incorporated into each basket are sized and shaped to minimize free play between each fuel type and the basket, while ensuring the free insertion and removal of the elements. The baskets are open on the top with the basket designed to hold the fuel elements within approximately 3/8-inches of the basket's top end, nearest the shield plug. The baskets are designed to freely drain water when the cask is lifted out of the spent fuel pool.

3.1.2 Content's Decay Heat

The design basis decay heat loading for the irradiated fuel to be transported within the BRR packaging is a function of the irradiation history and the cooling time since discharge. Section

1.2.2, *Contents*, provides details of the fuel elements to be transported. For the purposes of this evaluation, the design basis decay heat loadings are as follows:

- MURR fuel: 158 W maximum per element, 1,264 W per basket
- MITR-II fuel: 150 W maximum per element, 1,200 W per basket
- ATR fuel: 30 W maximum per element, 240 W per basket
- TRIGA fuel: 20 W maximum per element, 380 W per basket

3.1.3 Summary Tables of Temperatures

Table 3.1-1 provides a summary of the package component temperatures under normal and accident conditions. The temperatures for normal conditions are based on an analytical model of the BRR package for steady-state operation with an ambient temperature of 100 °F and the 10 CFR §71.71(c)(1) prescribed insolation averaged over 24 hours. The temperatures for accident conditions are based on a transient simulation using an analytical model of a damaged BRR package. The damage conditions represent the worst-case hypothetical pre-fire damage predicted from a combination of physical drop testing using a half-scale certification test unit (CTU) and analytical structural evaluations.

The results for NCT conditions demonstrate that significant thermal margin exists for all package components. Further, the NCT evaluations demonstrate that the accessible surface temperatures will be below the maximum temperature of 185 °F permitted by 10 CFR §71.43(g) in an exclusive use shipment when transported in a 100 °F environment with no insolation. The results for HAC conditions also demonstrate that the design of the BRR package provides sufficient thermal protection to yield component temperatures that are significantly below the acceptable limits defined for each component. See Sections 3.2.2, *Technical Specifications of Components*, Section 3.3.1.1, *Maximum Temperatures*, and Section 3.4.3, *Maximum Temperatures and Pressure*, for more discussion.

Table 3.1-3 summarizes the permitted fuel basket loadings determined by this safety evaluation.

3.1.4 Summary Tables of Maximum Pressures

Table 3.1-2 presents a summary of the maximum pressures predicted under NCT and HAC conditions. The BRR package has a design maximum pressure of 25 psig (39.7 psia). Since the release of fission generated gases from uranium-aluminide and uranium-zirconium hydride based fuels is diffusion-limited as opposed to the direct release mechanism for commercial spent nuclear fuel, the pressurization of the cask cavity due to gaseous release from breached fuel elements will be insignificant [30, 31]. Based on an assumed fill gas temperature of 70 °F, the maximum pressure rise under NCT will be less than 6 psig, while the pressure rise under HAC conditions will be less than 9 psig. Based on the NCT pressure, the maximum normal operating pressure (MNOP) is set at a bounding level of 10 psig.

Table 3.1-1 – Maximum Temperatures for NCT and HAC Conditions

Location / Component ①	NCT Hot Conditions, °F	Accident Conditions, °F	Maximum Allowable	
			Normal	Accident
Fuel Element Plate	350	451	400	1,100
Fuel Element Side Plate	348	449	400	1,100
Fuel Basket	334	437	800	800
Inner Shell	237	393	800	800
Lead	234	482	620	620
Outer Shell	216	704	800	2,700
Thermal Shield	185	1,256	800	2,700
Lower End Structure	205	335	800	800
Upper End Structure	222	485	800	800
Shield Plug	230	317	620 ②	620 ②
Cask Lid	218	306	800	800
Closure/Vent Port Elastomeric Seals	217	306	250	400
Drain Port Elastomeric Seal	202	373	250	400
Upper Impact Limiter				
- Max. Foam	217	-	300	N/A
- Avg. Foam	147	-	300	N/A
- Shell	217	1,475	250 ③	2,700 ④
Lower Impact Limiter				
- Max. Foam	200	-	300	N/A
- Avg. Foam	142	-	300	N/A
- Shell	200	1,475	250 ③	2,700 ④
Max. Accessible Surface without Insolation	185 ⑤	-	185	N/A
Cask Cavity Bulk Gas	259	388	N/A	N/A

Notes: ① Results based on either a payload of eight (8) MURR fuel elements dissipating 158 W each or a payload of eight (8) MITR-II fuel elements dissipating 150 W each and helium as the backfill gas.

② Temperature criterion based on melting point of the enclosed lead shielding.

③ Temperature criterion based on long term temperature limit for shell coating.

④ Temperature criterion based on melting point for the shell. No criteria for the polyurethane foam since its thermal decomposition serves as it principal means of providing thermal protection during the HAC event.

⑤ Maximum temperature occurs at the root of the upper cask impact limiter attachment lugs.

Table 3.1-2 – Summary of Maximum Pressures

Condition	Cask Cavity Pressure
NCT Hot	5.2 psi gauge
HAC Hot	8.8 psi gauge

Table 3.1-3 – Summary of Permissible BRR Package Fuel Basket Loadings

Payload	Backfill Gas for Transport	Max. Decay Heat Per Element	Max. Package Decay Heat
MURR Fuel	Helium	158	1,264
MITR-II Fuel	Helium	150	1,200
ATR Fuel	Helium	30	240
TRIGA Fuel	Helium	20	380

3.2 Material Properties and Component Specifications

The BRR packaging is fabricated primarily of a variety of Type 304 stainless steel product forms, lead, and polyurethane foam. The payload materials include 6061-T6 and/or 6061-0 aluminum, uranium-aluminide (UAlx), and uranium-zirconium hydride (UZrH).

3.2.1 Material Properties

While a variety of Type 304 stainless steel specifications apply to the various components of the BRR packaging, each type exhibits the same thermal properties. Table 3.2-1 presents the thermal properties used to simulate the various Type 304 stainless steels used in the packaging. The thermal properties are taken from the ASME material properties database [2] and the density is taken from an on-line database [6]. Properties for temperatures between the tabulated values are calculated via linear interpolation within the heat transfer code.

Table 3.2-1 also presents the thermal properties for ASTM B29 chemical lead, as taken from reference [4]. The density value is taken from an on-line database [6].

The 9 lb_m/ft^3 (pcf) polyurethane foam used in the package impact limiters is based on a proprietary formulation that provides predictable impact-absorption performance under dynamic loading, while also providing an intumescent char layer that insulates and protects the underlying materials when exposed to HAC fire conditions. The thermal properties under NCT conditions are obtained from the manufacturer's on-line website [18]. Since the thermal conductivity of the material is tied to its density and the manufacturing process can yield densities that are $\pm$15% of the targeted value, this safety evaluation addresses the properties associated with both the low and high tolerance density foam (see Table 3.2-1). Since the low tolerance foam yields a lower thermal conductivity, it is assumed for NCT operations, while the higher thermal conductivity of the high tolerance density foam is used for HAC evaluation to conservatively bound the heat flow into the package.

Table 3.2-2 presents the thermal properties for the reactor fuel element material. The MURR, MITR-II, and ATR fuel elements are uranium-aluminide (UAlx) based fuels, while the TRIGA fuel element is a uranium-zirconium hydride (UZrH) based fuel. The thermophysical properties for the MURR, MITR-II, and ATR fuel elements are based on information provided in reference [5]. While the reference was developed specifically for the ATR fuel element, the thermal properties are also applicable to the MURR and MITR-II fuel elements (after adjustment for fuel plate geometry and composition) for the purposes of this safety evaluation given the similarity in the base materials for all three fuel elements. For analysis purposes, the material used for the side plates, covers, and fuel cladding are assumed to be 6061-0 aluminum. The thermal properties for the fuel plates are determined as a composite of the cladding and the fuel core materials based on the fuel design drawings [12, 13, and 14] and the thermal properties for the materials of fabrication [5].

The details of the computed values for the MURR, MITR-II, and ATR fuel elements are presented in Appendix 3.5.3.9, *Determination of Composite Thermal Properties for Fuel Plates*. For simplicity, the thermal properties are assumed to be constant with temperature based on the use of conservatively high thermal conductivity and conservatively low specific heat values.

This approach maximizes the heat transfer into the fuel components during the HAC event, while under estimating the ability of the components to store the heat.

The TRIGA fuel element uses uranium-zirconium hydride metal (UZrH) as its active fuel component, graphite as a spacer material, and aluminum or stainless steel for the end fixtures and for the fuel cladding. While a variety of TRIGA fuel designs exist, the active fuel length is either 14 or 15 inches. Table 3.2-2 presents representative thermal properties for the simulated TRIGA fuel element. The properties for graphite are based on representative values for KK-8 graphite [16], while the thermal properties for UZrH are based on [17]. The properties for the end fixtures and fuel cladding are assumed to be stainless steel (Type 304) for the purposes of this safety evaluation since this conservatively limits the axial heat spreading within the fuel element given its lower conductivity versus that of aluminum.

The thermal properties for air and helium, presented in Table 3.2-3 and Table 3.2-4, respectively, are derived from curve fits provided in [19]. Because the gas thermal conductivity varies significantly with temperature, the computer model calculates the thermal conductivity across the gas filled spaces and between the package and the ambient as a function of the mean film temperature. All void spaces within the BRR cask cavity are assumed to be filled with helium at a pressure of one atmosphere following draining and drying.

The emissivity of 'as-received' Type 304 stainless steel has been measured as 0.25 to 0.28 [7], while the emissivity of weathered Type 304 stainless steel has been measured as being between 0.46 to 0.50 [8]. For the purpose of this analysis, an emissivity of 0.25 is assumed for the emittance from all radiating stainless steel surfaces of the cask cavity to account for the surface finish required for decontamination considerations. The exterior surfaces of the upper and lower end structures of the cask body assume a slightly higher emissivity of 0.30 assuming a lower level of surface finish and greater wear and tear.

The exterior surface of the outer shell covered by the thermal shield is assumed to have an emissivity of 0.587 [9] to account for its elevated surface oxidation following the lead pour procedure. Since this surface will not be directly exposed to the pool, it will receive only limited surface finishing following fabrication. The emissivity for the exterior surfaces of the package thermal shield is assumed to be 0.45 to account for weathering, while an emissivity of 0.40 is used for the inner surface of the thermal shield to account for its lower level of weathering. The solar absorptivity of Type 304 stainless steel is approximately 0.52 [9].

The surfaces of the fuel baskets are assumed to have an emissivity of 0.30 to account for the degree of polishing, etc. required for these surfaces due to decontamination considerations. This is slightly higher than the 0.25 value assumed for the cask cavity interior surfaces due to the greater wear and tear on these surfaces and the higher operating temperatures.

Exposed surfaces of lead are expected to oxidize rapidly and exhibit an emissivity of 0.6 [9].

The 6061-0 aluminum used for the MURR, MITR-II, and ATR fuel cladding, end fittings, and side plates is assumed to have a surface coating of boehmite ($Al_2O_3H_2O$). Per [10], a 25 μm boehmite film will exhibit a surface emissivity of approximately 0.92.

The exterior surfaces of the impact limiters will be finished with a white color coating system [11]. This coating system is expected to yield an emissivity in excess of 0.9 and a solar

absorptivity of approximately 0.20. For conservatism, an emissivity of 0.9 and a solar absorptivity of 0.30 are assumed by this evaluation.

The char layer associated with the decomposed polyurethane foam has a conservative surface emissivity of approximately 0.95 based on a combination of the material type, color, and surface roughness. No free surfaces will exist for the 'poured in place' foam under NCT conditions.

Under HAC conditions, all exterior surfaces of the package are assumed to attain an emissivity of 0.9. This assumption exceeds the minimum requirements of 10 CFR §71.73(c)(4) [1].

3.2.2 Technical Specifications of Components

The materials used in the BRR packaging that are considered temperature sensitive are the lead used for the radiological shielding, the polyurethane foam used in the impact limiters, the epoxy coating used on the impact limiter exterior surfaces, the butyl rubber compound used for the containment boundary seals, and the aluminum cladding and UAl_x fuel matrix used for the enclosed fuel assemblies. The other materials either have temperature limits above the maximum expected temperatures or are not considered essential to the function of the package.

Type 304 stainless steel has a melting point above 2,700 °F [6], but in compliance with the ASME B&PV Code [3], its allowable temperature is limited to 800 °F if the component serves a structural purpose (e.g., the material's structural properties are relied on for loads postulated to occur in the respective operating mode or accidental free drop condition). As such, the appropriate upper temperature limit under normal conditions is 800 °F for stainless steel components that form the containment boundary or are used in the fuel baskets. The upper limit for all other stainless steel components is 2,700 °F for both normal and accident conditions.

The applicable temperature criterion for the ASTM B29 lead is its melting point of approximately 620 °F [6].

Below 250 °F the variation in the thermal properties of the proprietary polyurethane foam with temperature are slight and reversible. While small variations in the foam properties will occur between 250 and 500 °F as water vapor and non-condensable gases are driven out of the foam, the observed changes are very slight. For conservatism, a long-term limit of 300 °F is assumed for the foam. There is no short term temperature limit for the foam as its decomposition under exposure to high temperatures is part of its mechanism for providing thermal protection during the HAC fire event. A detailed description of the foam's behavior under elevated temperatures is presented in Appendix 3.5.4, *'Last-A-Foam' Response under HAC Conditions*.

The exterior surfaces of the impact limiter shells are to be coated in a two step process consisting of a primer coat of polyamide epoxy, followed by an acrylic polyurethane top coat [11]. The color is white. The coating system is resistant to long term temperature exposure up to 250 °F and for intermittent exposure up to 275 °F.

The butyl rubber compound used for the containment seals is fabricated from Rainier Rubber compound R-0405-70 [20]. Butyl rubber has a long term temperature range of -75 °F to 250 °F [21]. Per Appendix 2.12.7, *Seal Performance Tests*, an acceptable short duration limit for this compound is 400 °F for 8 hours, 380 °F for 24 hours, and 350 °F for 144 hours. For conservatism, a long-term limit of 250 °F, a short-term limit of 400 °F for 8 hours, and a low temperature limit of -40 °F are assumed for this analysis.

Aluminum has a melting point of approximately 1,100 °F [6]; however for strength purposes the normal operational temperature of the fuel cladding and the UAl_x fuel matrix are limited to 400°F based on structural strength considerations for aluminum [3]. The limit under HAC conditions is 1,100°F. The same allowable temperature limits are conservatively used for the TRIGA fuel elements as well.

The minimum allowable service temperature for all BRR package components is below -40 °F.

Table 3.2-1 – Thermal Properties of Packaging Materials

Material	Temperature (°F)	Thermal Conductivity (Btu/hr-ft-°F)	Specific Heat (Btu/lb_m-°F)	Density (lb_m/in^3)
Stainless Steel① Type 304	-40	8.2	0.112	0.289
	70	8.6	0.114	
	100	8.7	0.115	
	200	9.3	0.119	
	300	9.8	0.123	
	400	10.4	0.126	
	500	10.9	0.129	
	600	11.3	0.130	
	700	11.8	0.132	
	800	12.3	0.134	
	1000	13.1	0.135	
	1200	14.0	0.138	
	1400	14.9	0.141	
	1500	15.3	0.142	
Lead② ASTM B29, chemical lead	-58	21.67	0.030	0.4097
	32	20.4	0.030	
	80.6	19.99	0.030	
	158	19.88	0.031	
	260.6	19.36	0.032	
	428	18.43	0.033	
	608	16.49	0.033	
	620.6	16.35	0.036	
Polyurethane Foam	-	0.01872③	0.353	0.00599③
	-	0.01728④	0.353	0.00443④

Notes:

① Reference [2], Material Group J. Properties valid for ASTM A351, Grade CF8A, ASTM A182, Type F304, ASTM A451, Grade CPF8A, and ASTM A240, Type 304 stainless steels.

② Reference [4].

③ Based on FR3709 'Last-a-Foam' high tolerance foam density (i.e., 9 pcf + 15%) properties [18].

④ Based on FR3709 'Last-a-Foam' low tolerance foam density (i.e., 9 pcf - 15%) properties [18].

Table 3.2-2 – Thermal Properties of Fuel Element Materials

Material	Temperature (°F)	Thermal Conductivity (Btu/hr-ft-°F)	Specific Heat (Btu/lb$_m$-°F)	Density (lb$_m$/in^3)
Aluminum① Type 6061-0	32	102.3	-	0.0976
	62	-	0.214	
	80	104.0	-	
	170	107.5	-	
	260	109.2	0.225	
	350	109.8	-	
	440	110.4	0.236	
	530	110.4	-	
	620	109.8	0.247	
	710	108.6	-	
	800	106.9	0.258	
	890	105.2	-	
	980	103.4	0.269	
	1080	101.1	0.275	
MURR Fuel Plate②	-	49.2	0.195	0.119
MITR-II Fuel Plate②	-	66.6	0.208	0.113
ATR Fuel Plate 1②	-	46.6	0.193	0.120
ATR Fuel Plates 2 to 18②	-	69.6	0.210	0.112
ATR Fuel Plate 19②	-	38.9	0.188	0.122
TRIGA Graphite③	-	46.2	0.250	0.060
TRIGA Fuel④	-	10.40	0.191	0.134

Notes:

① Reference [5]

② Values determined based on composite value of aluminum cladding and fuel core material (see Appendix 3.5.3.9, *Determination of Composite Thermal Properties for Fuel Plates*). Thermal conductivity value valid for axial and circumferential heat transfer within fuel plates.

③ Representative value, based on Reference [16].

④ Representative value, based on Reference [17].

Table 3.2-3 – Thermal Properties of Air

Temperature (°F)	Density lb_m/in^3 ①	Specific Heat (Btu/lb_m-°F)	Dynamic Viscosity (lb_m /ft-hr)	Thermal Conductivity (Btu/hr-ft-°F)	Prandtl Number ②	Coef. Of Thermal Exp. ($°R^{-1}$) ③
-40	Use Ideal Gas Law w/ Molecular wt = 28.966	0.240	0.03673	0.0121	Compute as $Pr = c_p\mu / k$	Compute as $\beta = 1/(°F+459.67)$
0		0.240	0.03953	0.0131		
50		0.240	0.04288	0.0143		
100		0.241	0.04607	0.0155		
200		0.242	0.05207	0.0178		
300		0.243	0.05764	0.0199		
400		0.245	0.06286	0.0220		
500		0.248	0.06778	0.0240		
600		0.251	0.07242	0.0259		
700		0.253	0.07680	0.0278		
800		0.256	0.08098	0.0297		
900		0.259	0.08500	0.0315		
1000		0.262	0.08887	0.0333		
1200		0.269	0.09620	0.0366		
1400		0.274	0.10306	0.0398		
1500		0.277	0.10633	0.0412		

Table Notes:

① Density computed from ideal gas law as $\rho = PM/RT$, where R= 1545.35 ft-lbf/lb-mole-R, T= temperature in °R, P= pressure in lbf/ft^2, and M= molecular weight of air. For example, at 100 °F and atmospheric pressure of $14.69 lbf/in^2$, $\rho = (14.69*144\ in^2/ft^2*28.966\ lbm/lb\text{-}mole)/1545.35*(100+459.67) = 0.071\ lbm/ft^3 = 4.099x10^{-5}\ lbm/in^3$.

② Prandtl number computed as $Pr = c_p\mu / k$, where c_p = specific heat, μ = dynamic viscosity, and k = thermal conductivity. For example, at 100 °F, $Pr = 0.241*0.04607/0.0155 = 0.72$.

③ Coefficient of thermal expansion is computed as the inverse of the absolute temperature. For example, at 100 °F, $\beta = 1/(100+459.67) = 0.00179$.

Table 3.2-4 – Thermal Properties of Helium

Temperature (°F)	Density lb_m/in^3 ①	Specific Heat (Btu/lb_m-°F)	Dynamic Viscosity (lb_m /ft-hr)	Thermal Conductivity (Btu/hr-ft-°F)	Prandtl Number②	Coef. Of Thermal Exp. ($°R^{-1}$)③
-40	Use Ideal Gas Law w/ Molecular wt = 4.0026 g/mole	1.240	0.04032	0.0738	Compute as $Pr = c_p\mu / k$	Compute as $\beta = 1/(°F+459.67)$
0		1.240	0.04306	0.0784		
50		1.240	0.04634	0.0837		
100		1.240	0.04944	0.0886		
200		1.240	0.05520	0.0981		
300		1.240	0.06088	0.1075		
400		1.240	0.06643	0.1177		
500		1.240	0.07153	0.1291		
600		1.240	0.07640	0.1403		
700		1.240	0.08116	0.1508		
800		1.240	0.08580	0.1607		
900		1.240	0.09033	0.1702		
1000		1.240	0.09475	0.1793		
1200		1.240	0.10327	0.1971		
1400		1.240	0.11139	0.2144		
1500		1.240	0.11531	0.2231		

Table Notes:

① Density computed from ideal gas law as $\rho = PM/RT$, where R= 1545.35 ft-lbf/lb-mole-R, T= temperature in °R, P= pressure in lbf/ft^2, and M= molecular weight of helium.

② Prandtl number computed as $Pr = c_p\mu / k$, where c_p = specific heat, μ = dynamic viscosity, and k = thermal conductivity.

③ Coefficient of thermal expansion is computed as the inverse of the absolute temperature.

3.3 Thermal Evaluation for Normal Conditions of Transport

This section presents the thermal evaluation of the BRR for normal conditions of transport (NCT). Under NCT, the package will be transported in a vertical orientation. This establishes the orientation of the exterior surfaces of the package for determining the free convection heat transfer coefficients and insolation loading. The package support system is configured to mate with the lower impact limiter such that the conical and base surfaces of the limiter are fully enclosed. As such, the NCT evaluations conservatively assume an adiabatic condition for these surfaces (i.e. there is no heat transfer to or from the ambient).

3.3.1 Heat and Cold

The NCT thermal performance is determined using a three-dimensional thermal model of the BRR packaging and its enclosed payloads. The models provide a full height, half symmetry representation of the packaging and payload components. The modeling approach permits simulation of the varying insolation loads along the length of the package, captures the various degrees of symmetry within the fuel baskets, and allows the non-symmetry conditions of the HAC free drop damage to be simulated. A separate thermal model is used to evaluate the NCT thermal performance for each of the four potential fuel payloads. The details of the NCT thermal modeling are provided in Appendix 3.5.3, *Analytical Thermal Model.*

The safety evaluation for the BRR packaging components is based on a payload of eight (8) MURR fuel elements and a payload of eight (8) MITR-II fuel elements since their maximum decay heat loadings of 1,264 W and 1,200 W, respectively, exceeds by a factor of over 3 the maximum package decay heat loading of 380 W for the TRIGA fuel payload and the 240 W for the ATR fuel payload. As such, the peak temperatures achieved by the packaging components for the transport of the ATR and TRIGA payloads are bounded by those predicted for either the MURR or MITR-II fuel payloads. The peak packaging component temperatures for the MITR-II payload are similar to those achieved with the MURR payload given their similar decay heat loadings.

3.3.1.1 Maximum Temperatures

MURR Fuel Basket

Table 3.3-1 presents the predicted BRR package temperatures under NCT conditions for the transportation of a fully loaded MURR fuel basket dissipating 1,264 W of decay heat. The analysis assumes a helium gas backfill in order to limit the peak temperature of the MURR fuel plates to 400 °F or less, based on structural considerations.

The results demonstrate that large thermal margins exist for essentially all of the packaging and payload components. The minimum thermal margin of 34 °F (i.e., 250 - 216 °F), occurs for the cask closure seals. A similar thermal margin of 35 °F occurs for the coating used on the external surfaces of the impact limiters. These margins are adequate given the conservative assumptions used in the modeling, including neglecting the beneficial contribution of the stand-off strips when computing the temperature rise between the thermal shield and the outer shell and the assumption of a small, but uniform gap between the lead and the outer shell. Removing these

conservatisms will decrease the cask body surface temperatures and increase the thermal margins for the seals and the impact limiter coating by an estimated 9 °F.

Figure 3.3-1 to Figure 3.3-4 present the predicted temperature distribution within the BRR package for the NCT Hot condition. The elevation of the MURR fuel payload within the cask cavity is clearly evident from the temperature distribution seen in Figure 3.3-1 and Figure 3.3-3. The temperature distribution within the impact limiters illustrated in Figure 3.3-2 also reflects the elevation of the payload, plus the upright orientation of the package for NCT conditions in that the inside face of the lower impact limiter experiences the solar loading for a flat horizontal surface, while the same face for the upper impact limiter has a zero solar loading because of its downward orientation.

Figure 3.3-3 illustrates the temperature distribution in the structural shell of the cask. The presence of the impact limiter attachment lugs can be seen by the localized 'cool' spots in the temperature distribution of the outer shell. As noted in the description of the NCT thermal model provided in Appendix 3.5.3, *Analytical Thermal Model*, the NCT Hot results are based on an earlier cask design that used 6 instead of the current 8 attachment lugs per limiter, cask lug plates that are 0.38-inches thick by 2.75-inches wide vs. the current 0.5-inches thick by 3.63-inches wide, and a 0.25-inch vs. 0.125-inch radial gap between the limiter and the cask shell. Since the earlier design version provides slightly conservative results for NCT due to its lower surface area for heat dissipation to the ambient, it is appropriate for predicting the peak NCT temperatures.

Figure 3.3-4 presents the predicted temperature distribution within the MURR fuel basket under the NCT Hot condition.

Evaluation of the package for an ambient air temperature of 100 °F without insolation loads demonstrates that the temperatures of all exterior surfaces of the packaging are below the maximum temperature of 185 °F permitted by 10 CFR §71.43(g) for accessible surface temperature in an exclusive use shipment. The peak accessible surface temperature occurs at the root of the upper impact limiter attachment lugs. A sensitivity analysis, based on the revised lug design, as described in Appendix 3.5.3, *Analytical Thermal Model*, confirms that the peak accessible surface temperature in the vicinity of the upper impact limiter attachment lugs (see temperature distribution in Figure 3.3-5) is 185 °F or less.

MITR-II Fuel Basket

Table 3.3-2 presents the predicted maximum temperature achieved within the MITR-II fuel basket and the BRR package under the NCT Hot condition with a helium gas backfill. A design basis maximum decay heat loading of 150 W per element, or 1,200 W for a payload of eight (8) fuel elements, is assumed for the transportation of the MITR-II payload. As expected, given their similar total decay heat loads, the peak temperatures achieved within the BRR packaging components are similar to those presented in Table 3.3-1. The MITR-II fuel element is shorter than the MURR fuel element. As a result, the MITR-II payload decay heat source resides a little higher in the cask cavity which, in turn, leads to reduced heat flow into the lower components of the BRRC packaging (i..e, the lower end structure, the drain port, etc.), and lower temperatures versus those seen with the MURR payload.

The results in Table 3.3-2 demonstrate that the design criterion of a maximum fuel plate temperature of 400 °F is met if helium is used as the backfill gas. Figure 3.3-6 presents the predicted temperature distribution within the MITR-II fuel basket under the NCT Hot condition.

ATR Fuel Basket

Table 3.3-3 presents the predicted maximum temperature achieved within the ATR fuel basket under the NCT Hot condition with a helium gas backfill. The peak temperatures for the BRR packaging are again bounded by those presented in Table 3.3-1. The design basis maximum decay heat loading for the ATR fuel elements to be transported is 30 W per element, or 240 W for a payload of eight (8) fuel elements. Although this level of decay heat loading could be accommodated using air as the backfill gas, a helium gas backfill is to be used to maintain consistency with the loading procedures for the other payloads. Figure 3.3-7 presents the predicted bounding temperature distribution within the ATR fuel basket under the NCT Hot condition.

TRIGA Fuel Basket

Table 3.3-4 presents the predicted maximum temperature achieved within the TRIGA fuel basket under the NCT Hot condition with a helium backfill. The design basis maximum decay heat loading for the TRIGA fuel elements to be transported is 20 W per element, or 380 W for a payload of nineteen (19) fuel elements. As seen from Table 3.3-4, the results demonstrate that the design criterion of a maximum fuel element temperature of 400 °F is met. Figure 3.3-8 presents the predicted bounding temperature distribution within the TRIGA fuel basket under the NCT Hot condition.

3.3.1.2 Minimum Temperatures

The minimum temperature achieved within each of the fuel baskets would be achieved with a zero decay heat load and an ambient air temperature of -40 °F per 10 CFR §71.71(c)(2). The evaluation of this thermal condition requires no thermal calculation. Instead, all package components will eventually achieve the -40 °F temperature under steady-state conditions. As discussed in Section 3.2.2, *Technical Specifications of Components*, the -40 °F temperature is within the allowable operating temperature range for all package components.

3.3.2 Maximum Normal Operating Pressure

The cask cavity is to be filled with helium at atmospheric pressure following the draining and drying process. Since the release of fission generated gases from uranium-aluminide and uranium-zirconium hydride based fuel is diffusion-limited as opposed to the direct release mechanism for commercial spent nuclear fuel, the pressurization of the cask cavity due to gaseous release from breached fuel elements will be insignificant [30, 31] and is ignored for this safety evaluation.

The peak pressure developed within the cask cavity under NCT conditions can be conservatively estimated by assuming that the cavity gas reaches a bulk average temperature that is equal to the mean of the average inner shell temperature and the average fuel basket temperature. Under the NCT Hot condition with the MURR fuel payload the average temperature of the inner shell is

225 °F. Combining this temperature with the average fuel basket temperature of 293 °F yields a predicted bulk average backfill gas temperature of 259 °F.

Assuming the backfill gas has an initial temperature of 70 °F at the time of filling and that a fill pressure of one atmosphere is used, the predicted maximum operating pressure within the cask cavity for the transport of the MURR payload can be estimated via:

$$\text{Cavity Pressure} = 14.7\text{psia}\frac{(259^{o}\text{F} + 460^{o}\text{F})}{(70^{o}\text{F} + 460^{o}\text{F})} - 14.7\text{ psia}$$

$$\text{Cavity Pressure} = 5.2\text{ psig}$$

The equivalent peak bulk average fill gas temperatures for the MITR-II, ATR, and TRIGA baskets are 254, 164, and 174 °F, respectively. As such, the associated peak cask cavity pressures under NCT conditions are 5.1, 2.6, and 2.9 psig, respectively. Based on these NCT pressures, the maximum normal operating pressure (MNOP) within the cask cavity is set at a bounding level of 10 psig.

3.3.3 Vacuum Drying Operations

An evaluation of the proposed vacuum drying operation was conducted to ensure that the component temperatures will remain within their normal temperature limits. The vacuum drying operations consist of the following general steps:

1) the cask body, without the impact limiters, bottom drain plug, cask lid, and cask shield plug are placed in the reactor pool.
2) the fuel elements to be transported are placed in the fuel basket within the cask,
3) the shield plug is placed into the cask,
4) the loaded cask is lifted above the pool and the enclosed water allowed to drain back into the pool. At this point, the cask cavity is filled with air.
5) following decon operations, the loaded cask is moved to the facility work area where the drain port and cask lid is installed. The vent port tool is installed and vacuum drying is initiated.
6) the minimum pressure achieved under vacuum drying is 1 to 3 torr.

The transient evaluation of these operations used a modification of the NCT thermal model described in Appendix 3.5.3, *Analytical Thermal Model*. The modifications made for this evaluation consisted of assuming air as the backfill gas. While the impact limiters will not be installed during vacuum drying operations, and the cask lid will not be installed until just before vacuum drying begins, leaving these components in the thermal model greatly simplified the model modifications required and is seen as having no significant impact on the transient temperatures. The effect of being submerged in the reactor pool is addressed by assuming all cask components are at equilibrium with a maximum temperature of 80 °F.

At time = 0, the loaded cask is assumed to be lifted from the pool, the water drained and the cask cavity filled with air, the ambient conditions are conservatively assumed to be 100 °F without insolation. The transient analysis is conducted for a period of 8 hours and followed by a steady-state evaluation to establish the peak temperatures that would occur if the helium backfill is not

established. The MURR fuel element payload is selected as a basis for the vacuum drying evaluation since its decay heat loading is governing over the other three potential payloads.

The thermal analysis of vacuum drying assumes that the thermal conductivity of the gas filling the voids of the packaging and the payload remain unchanged from its base value at atmospheric pressure conditions for vacuum pressures of 1 torr or greater. There are two states that define the process by which heat is transferred by a gas [32]:

> **viscous state**, in which the totality of molecules is responsible for the heat transfer. The viscous state occurs as long as the pressure is higher than the range in which the molecular state occurs. Within the viscous state the thermal conductivity of a gas is independent of pressure.
>
> **molecular state**, heat conductivity in the molecular state is when the gas pressure is so low that the molecular mean free path is about equal or greater than the distance between the plates. The thermal conductivity of the gas is no longer characterized by the viscous state for conductivity and therefore the conductivity is dependent on pressure. The heat transfer process under these conditions is called free molecular conduction.

The pressure at which the molecular mean free path is equal to the minimum distance between the surfaces within the packaging is determined below for air as the fill gas. Per [33], the mean free path of the fill gas molecules is computed via:

$$L = \frac{k \times T}{\pi \times \sqrt{2} \times P \times d^2}$$

where:

k = 1.380658 x 10^{-23} J/K, the Boltzmann constant
P = pressure in Pa
T = temperature in K
d = molecule diameter, in m

At the lowest practical vacuum pressure of 1 torr (133 Pa) used for vacuum drying and a conservatively high gas temperature of 525 °F (547K) based on the hottest fuel element (as determined from the steady-state analysis), the mean free path for air with a molecule diameter of about 3×10^{-10} m (based on oxygen, [33]) is:

$$L = \frac{1.380658 \times 10^{-23} \times 547}{\pi \times \sqrt{2} \times 133 \times (3 \times 10^{-10})^2}$$

$$L = 1.42 \times 10^{-4} \text{ m} = 0.006 \text{ inches}$$

Since this mean free path is much smaller than the smallest significant gap in the model (i.e., the gap between fuel plates), the gas heat transfer everywhere within the model can be characterized as being in the viscous state and independent of the gas pressure.

Figure 3.3-9 illustrates the predicted package heat up following removal from the fuel pool. The illustrated thermal transient conservatively ignores the cooling effect provided by the water remaining in the cask cavity as it evaporates and the increased thermal conductivity provided by moist air over the dry air conductivity assumed by the thermal modeling. As seen by the transient curves presented in Figure 3.3-9, a minimum of 8 hours exists before the peak fuel plate temperature reaches the NCT limit of 400 °F. Since this temperature limit is set by structural considerations for the accident drop events and since no credible drop event exists between the time the cask is placed in the facility work area and the vacuum drying is completed and the cask is prepared for transportation, the actual temperature limit for the fuel elements under vacuum drying can be higher.

Oxidization of aluminum fuel has been studied for long term exposure to moist air and saturated water vapor at temperatures up to 400 °F (200 °C) [34, 35]. The results show no significant oxidization and no damage to the fuel cladding as a result of the exposure. As such, no fuel damage is expected for the limited time and exposure temperatures seen under vacuum drying.

In conclusion, the transient results in Figure 3.3-9 demonstrate that adequate time and thermal margin exists to allow the necessary vacuum drying operations to be completed without exceeding the maximum allowable component temperature limits. While even the steady-state temperatures with air as the backfill gas will not result in any damage to the fuel elements, the vacuum drying operations will include a provision to backfill the cask cavity with helium gas if the vacuum drying has not been completed within 8 hours. Once filled with the helium gas, the package temperatures are bounded by those presented in Section 3.3.1.1, *Maximum Temperatures*, for NCT conditions.

Table 3.3-1 – NCT Temperatures for BRR Packaging with MURR Fuel

Component	Temperature (°F) ①		
	NCT Hot ④	NCT Hot without Solar	Max. Allowable
MURR Fuel Plate	350	331	400
MURR Side Plate	348	329	400
MURR Fuel Basket	334	315	800
Inner Shell	237	216	800
Lead	233	213	620
Outer Shell	216	195	800
Thermal Shield	185	182	800
Lower End Structure	205	184	800
Upper End Structure	220	200	800
Shield Plug	225	205	620 ②
Cask Lid	216	197	800
Closure/Vent Port Elastomeric Seals	216	197	250
Drain Port Elastomeric Seal	202	181	250
Upper Impact Limiter			
- Max. Foam	215	196	300
- Avg. Foam	146	132	300
- Shell	215	196	250 ③
Lower Impact Limiter			
- Max. Foam	200	179	300
- Avg. Foam	142	127	300
- Shell	200	179	250 ③
Max. Accessible Surface	-	185 ⑤	185
Cask Cavity Bulk Gas	259	239	N/A

Notes: ① Results assume a payload of eight (8) MURR fuel elements dissipating 158 W each and helium as the backfill gas.

② Temperature criterion based on melting point of the enclosed lead shielding.

③ Temperature criterion based on long term temperature limit for shell coating.

④ Results conservatively based on an earlier design for the cask and impact limiter attachment lugs. See Appendix 3.5.3 for a description of the design change and the conservative impact of ignoring the design change for NCT Hot modeling.

⑤ Maximum temperature occurs at the root of the upper cask impact limiter attachment lugs.

Table 3.3-2 – NCT Hot Temperatures for BRR Packaging with MITR-II Fuel

Component ①	Temperature (°F)	
	8 Elements @ 150 W Each④	Max. Allowable
MITR-II Fuel Plate	348	400
MITR-II Side Plate	347	400
MITR-II Fuel Basket	331	800
Inner Shell	237	800
Lead	234	620
Outer Shell	216	800
Thermal Shield	185	800
Lower End Structure	197	800
Upper End Structure	222	800
Shield Plug	230	620②
Cask Lid	218	800
Closure/Vent Port Elastomeric Seals	217	250
Drain Port Elastomeric Seal	194	250
Upper Impact Limiter		
- Max. Foam	217	300
- Avg. Foam	147	300
- Shell	217	250③
Lower Impact Limiter		
- Max. Foam	192	300
- Avg. Foam	140	300
- Shell	192	250③
Cask Cavity Bulk Gas	254	N/A

Notes: ① Results assume a payload of eight (8) MITR-II fuel elements dissipating 150 W each and helium as the backfill gas.

② Temperature criterion based on melting point of the enclosed lead shielding.

③ Temperature criterion based on long term temperature limit for shell coating.

④ Results conservatively based on an earlier design for the cask and impact limiter attachment lugs. See Appendix 3.5.3 for a description of the design change and the conservative impact of ignoring the design change for NCT Hot modeling.

Table 3.3-3 – NCT Hot Temperatures for BRR Packaging with ATR Fuel

Component ①	Temperature (°F)	
	8 Elements @ 30 W Each	Max. Allowable
ATR Fuel Plate	197	400
ATR Side Plate	197	400
ATR Fuel Basket	195	800
Cask Cavity Bulk Gas	164	NA

Note: ① Temperatures for packaging components bounded by values in Table 3.3-1.

Table 3.3-4 – NCT Hot Temperatures for BRR Packaging with TRIGA Fuel

Component ①	Temperature (°F)	
	19 Elements @ 20 W Each	Max. Allowable
TRIGA Fuel Element	355	400
TRIGA End Fitting	308	400
TRIGA Fuel Basket	287	800
Cask Cavity Bulk Gas	174	NA

Note: ① Temperatures for packaging components bounded by values in Table 3.3-1.

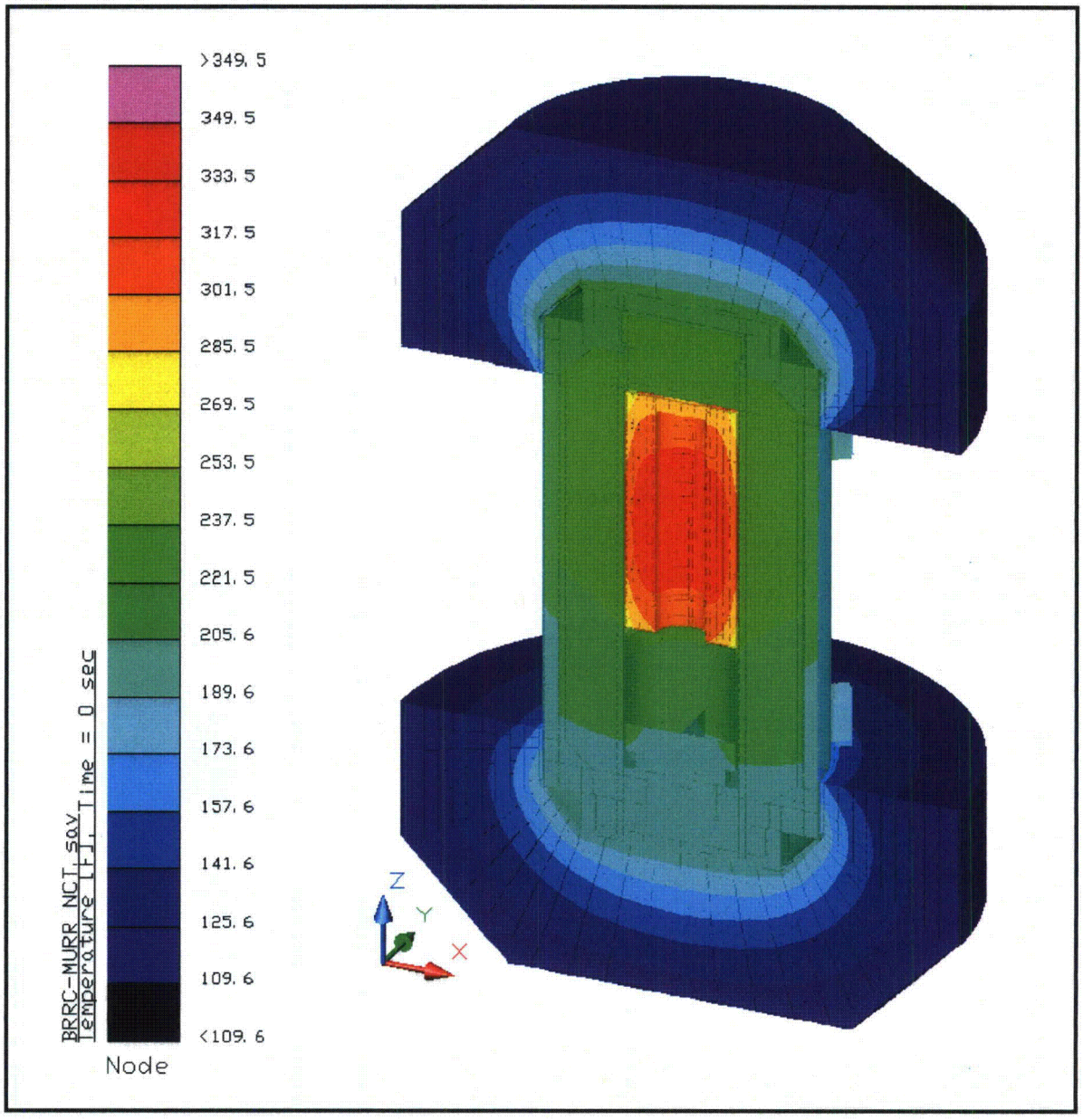

Figure 3.3-1 – BRR Package Temperature Distribution for NCT Hot Condition with MURR Fuel Basket

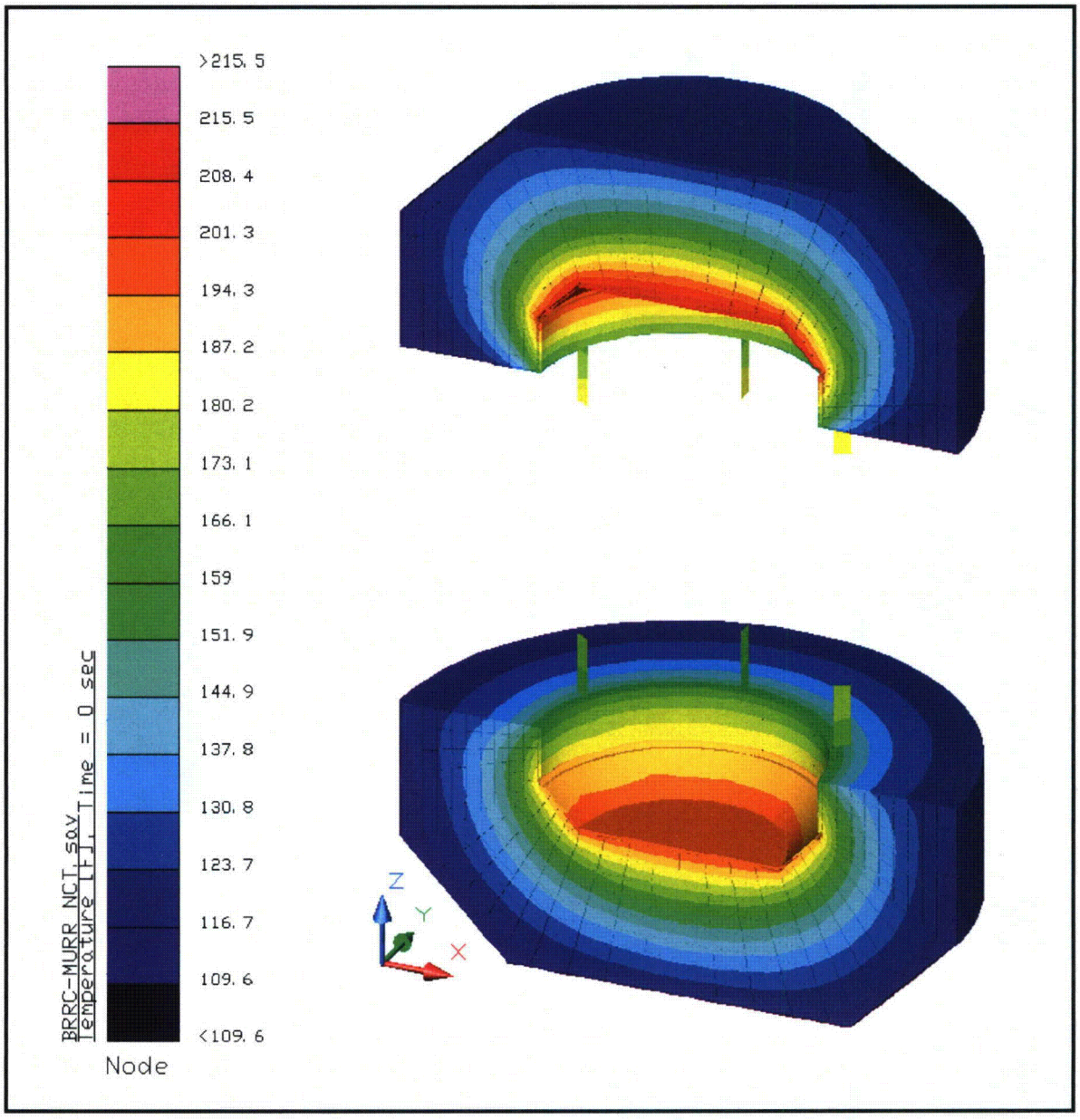

Note: Earlier design of 6 vs. 8 attachment lugs per limiter depicted. Results bound the revised design under NCT

Figure 3.3-2 – Impact Limiter Temperature Distribution for NCT Hot Condition with MURR Fuel Basket

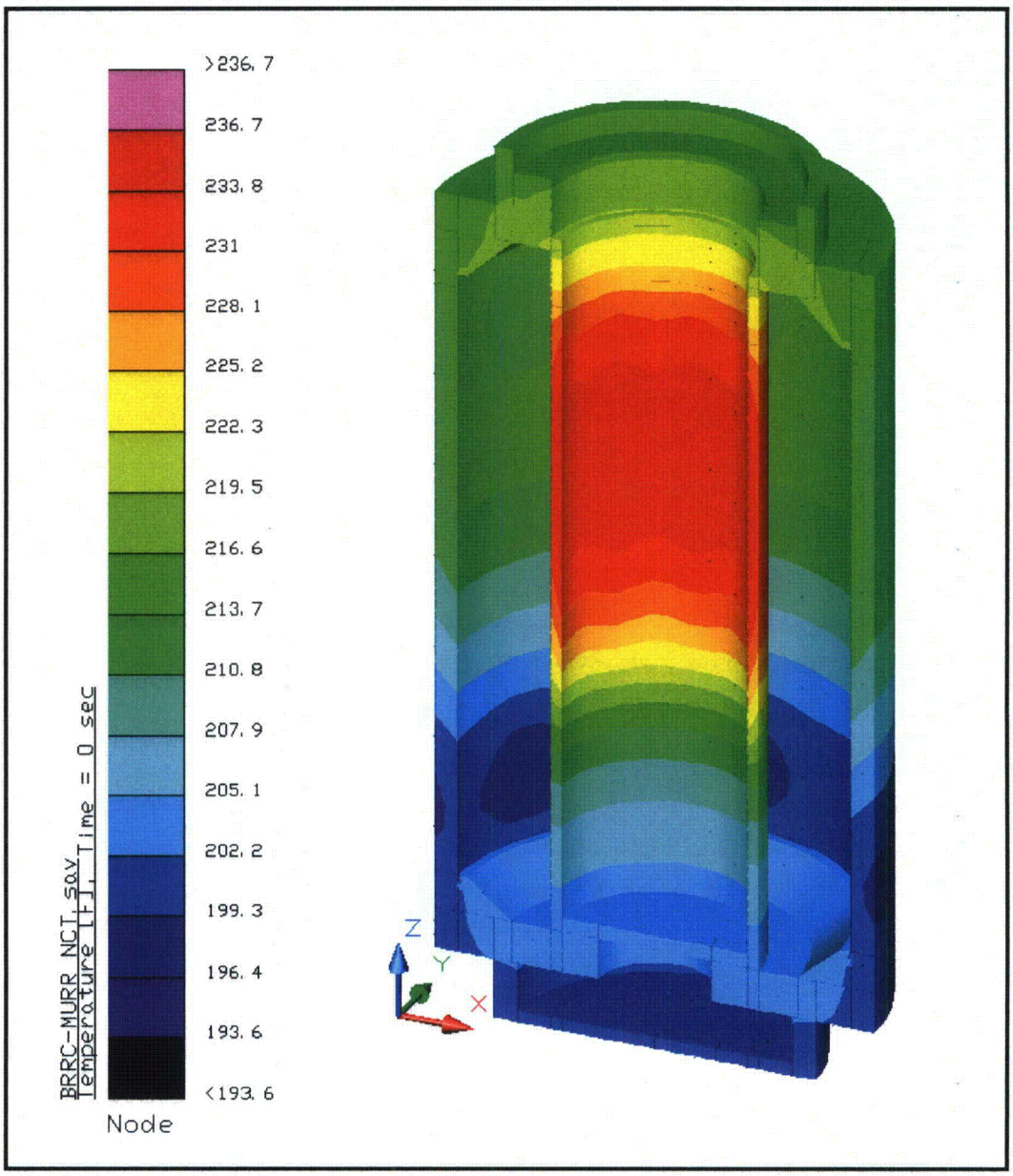

Figure 3.3-3 – Structural Shell Temperature Distribution for NCT Hot Condition with MURR Fuel Basket

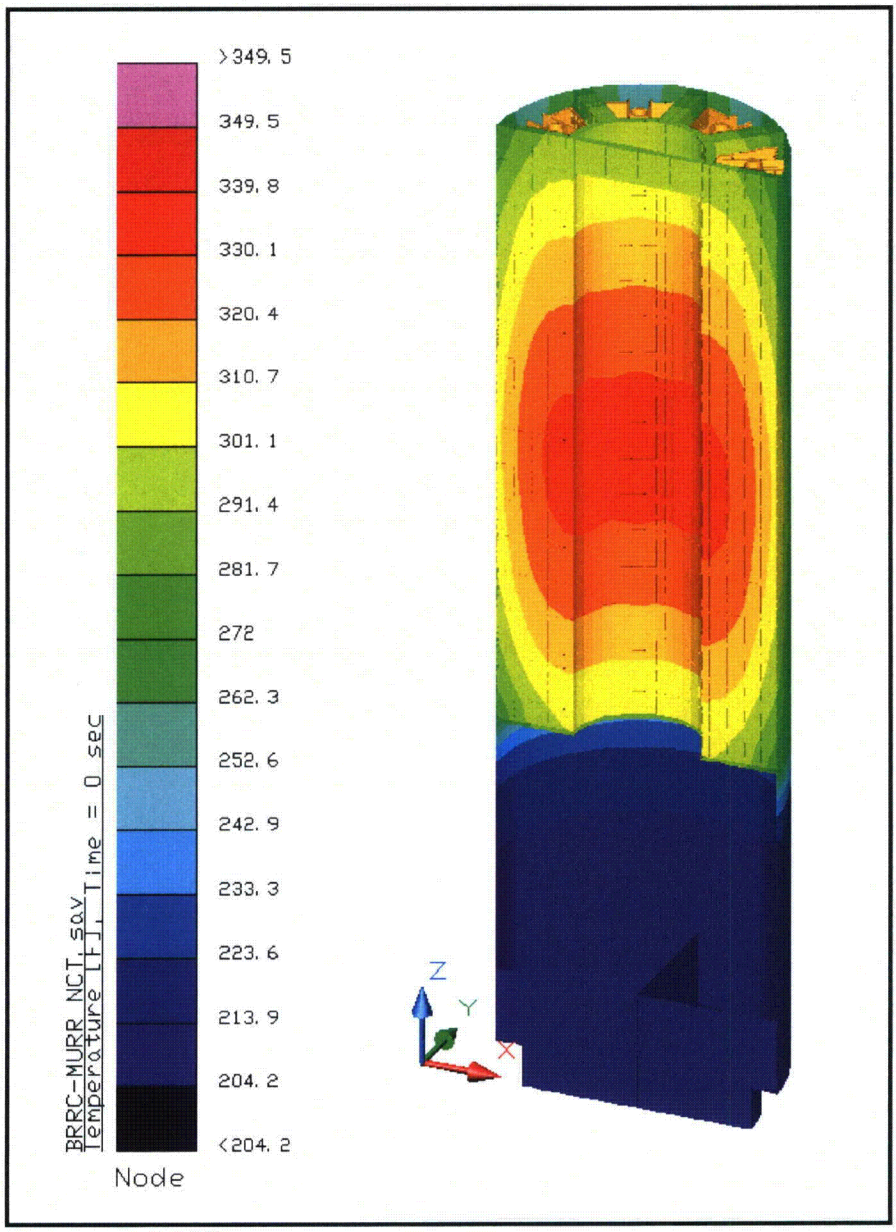

Figure 3.3-4 – MURR Fuel Basket Temperature Distribution for NCT Hot Condition

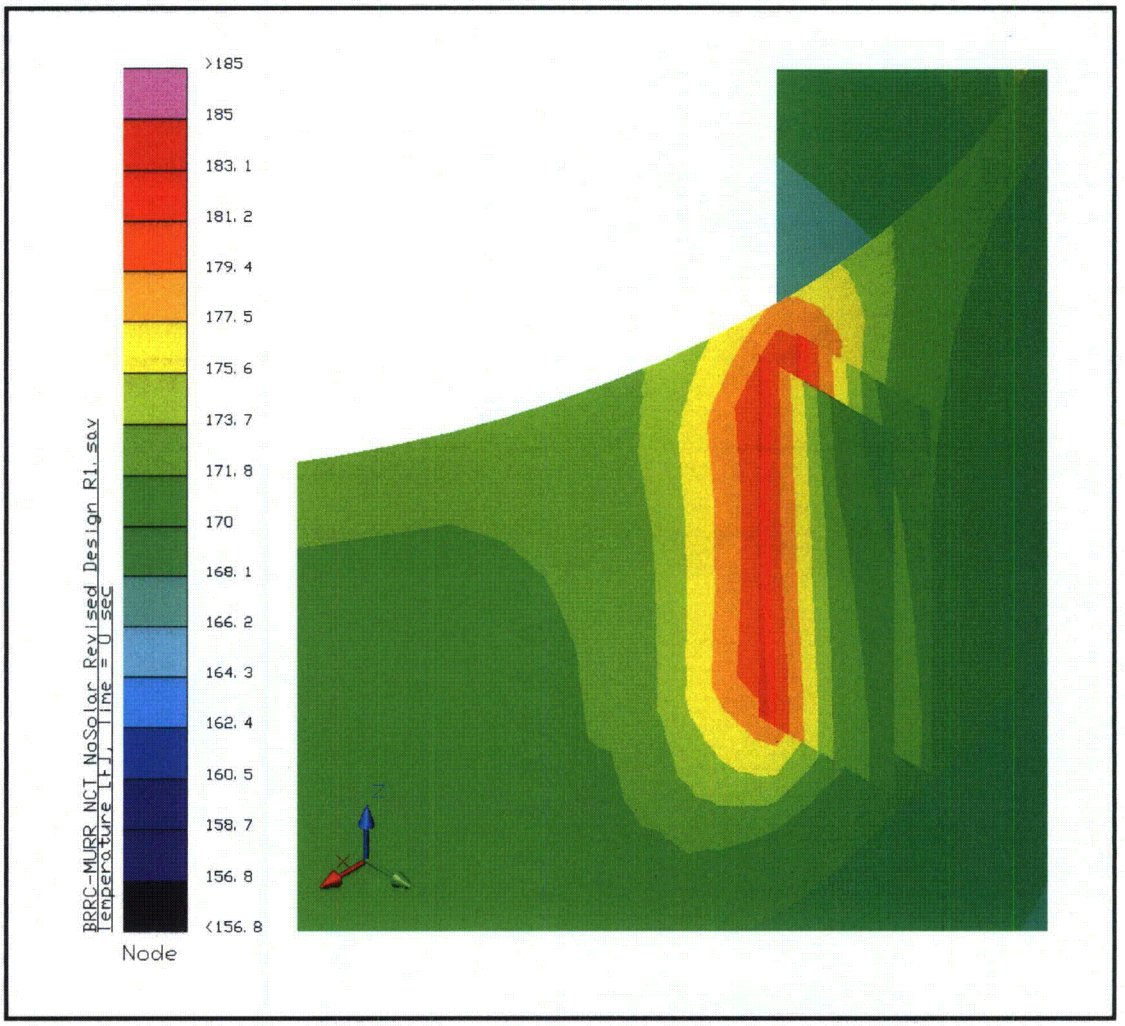

Surface Temperature Distribution in Vicinity of Impact Limiter Attachment Lugs

Figure 3.3-5 – Peak Accessible Surface Temperature for NCT No Solar

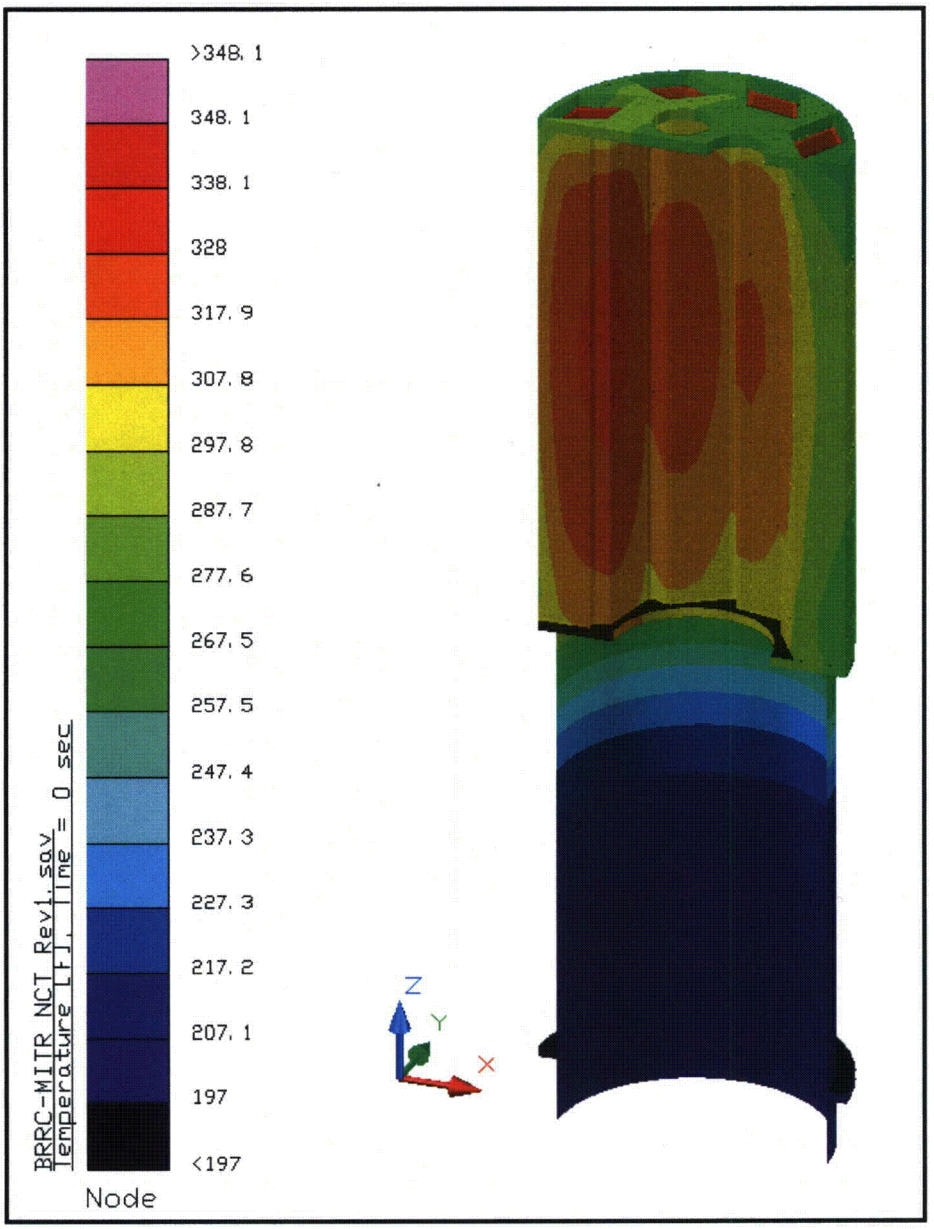

Note: Results are for basket decay heat loading of 1,200 W

Figure 3.3-6 – MITR-II Fuel Basket Temperature Distribution for NCT Hot Condition

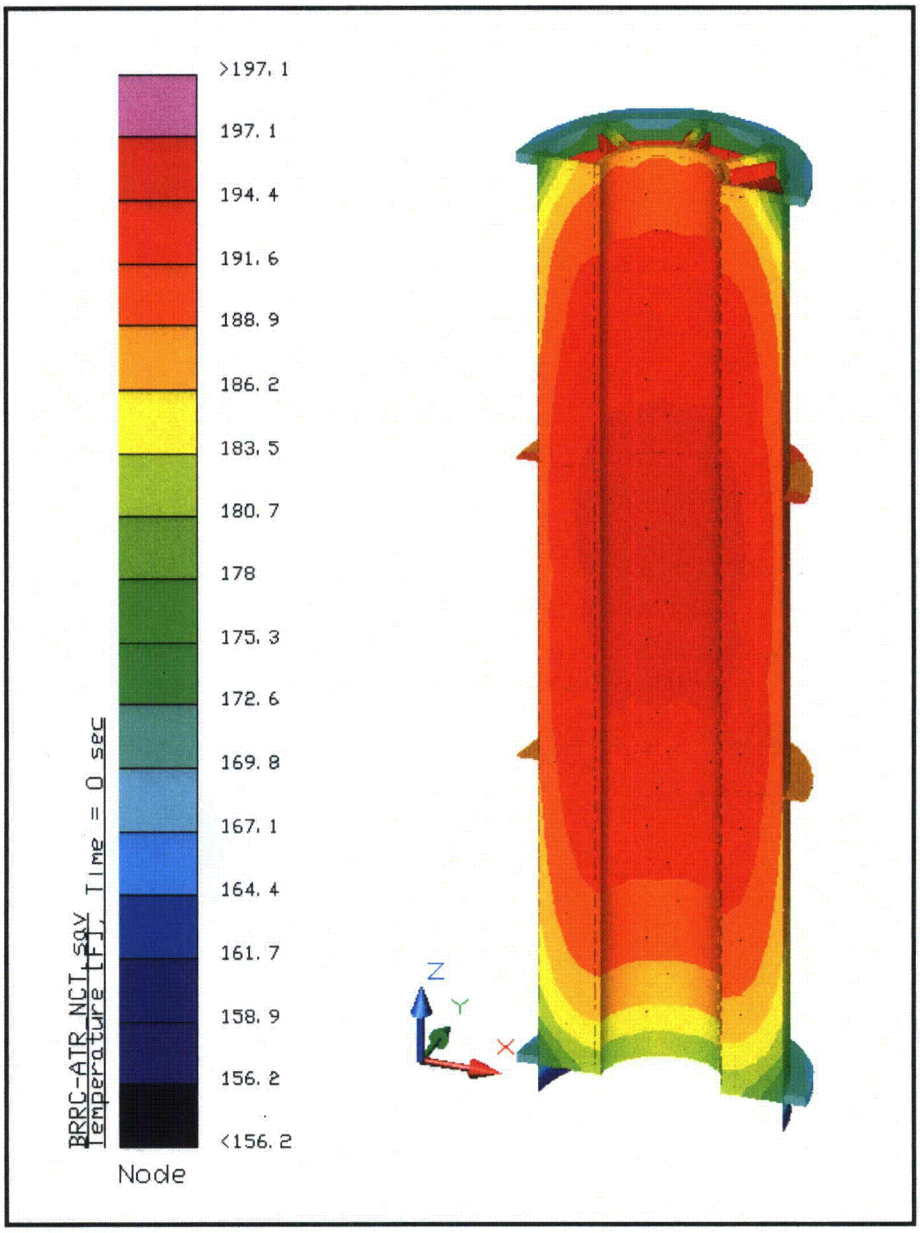

Note: Results are for basket decay heat loading of 240 W

Figure 3.3-7 – ATR Fuel Basket Temperature Distribution for NCT Hot Condition

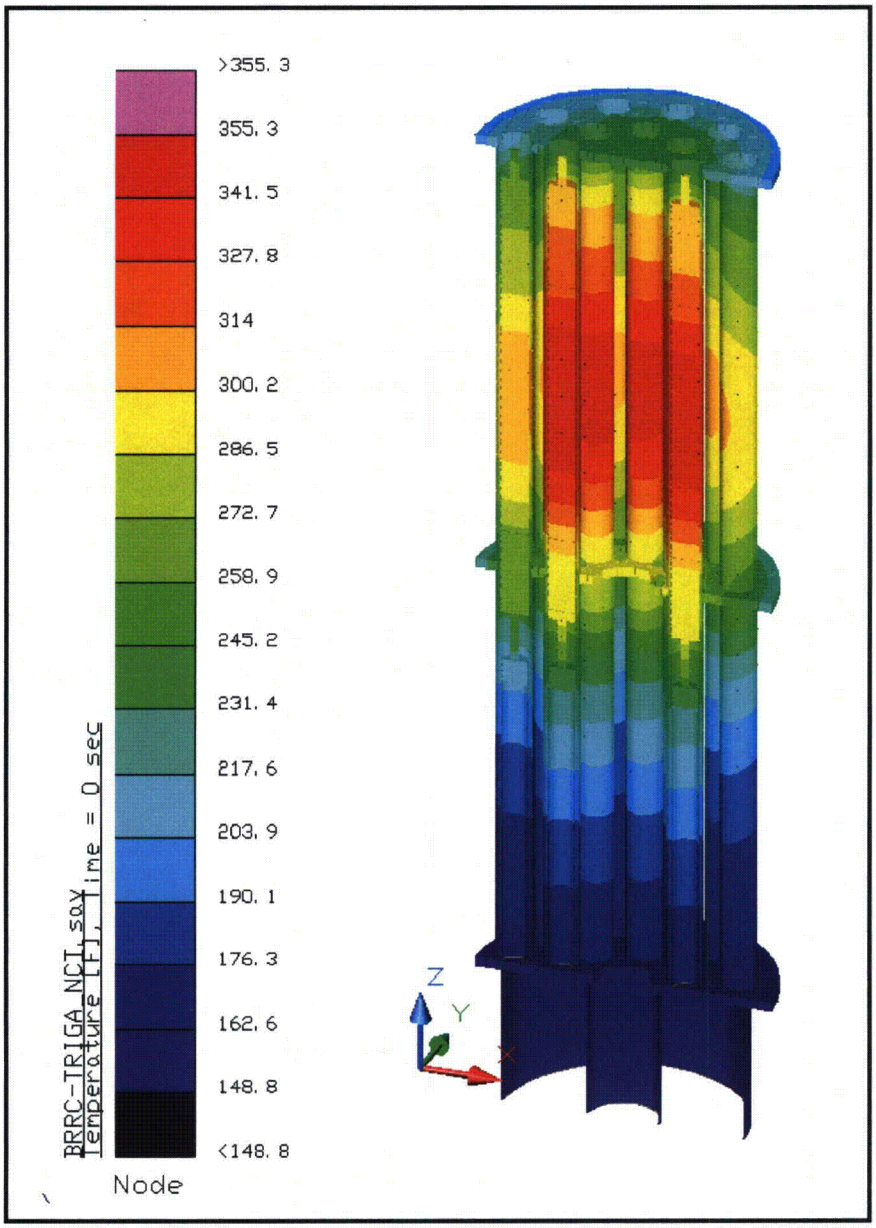

Note: Results are for basket decay heat loading of 380 W

Figure 3.3-8 – TRIGA Fuel Basket Temperature Distribution for NCT Hot Condition

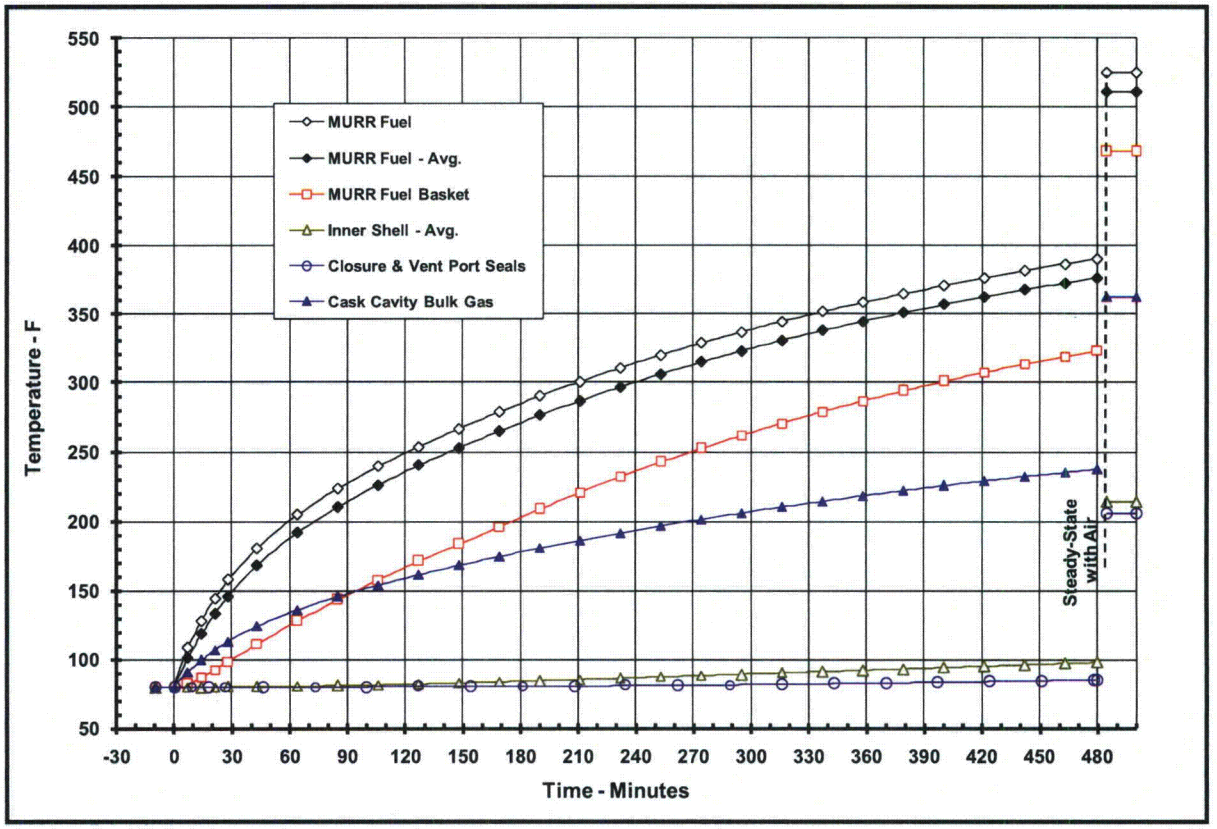

Figure 3.3-9 – Bounding Transient Heat Up During Vacuum Drying

3.4 Thermal Evaluation for Hypothetical Accident Conditions

This section presents the thermal evaluation of the BRR package under the hypothetical accident condition (HAC) specified in 10 CFR §71.73(c)(4) based on an analytical thermal model of the BRR. The analytical model for HAC is a modified version of the half symmetry NCT model described in Appendix 3.5.3.1, *Description of BRR Packaging Thermal Model for NCT Conditions*, with the MURR fuel element payload. The MURR payload is selected as a basis for the HAC evaluation since its decay heat loading is more than 3 times greater than either the TRIGA fuel payload or ATR fuel payloads and since its decay heat loading of 1,264 W exceeds the 1,200 W for the MITR-II fuel payload. As such, the peak HAC temperatures for the TRIGA and ATR payloads will be bounded by those achieved for the MURR payload, while those for the MITR-II payload will be essentially the same given the similar decay heat loading and the similar initial package temperatures.

The principal model modifications made to convert the NCT thermal model to the HAC model consists of modifying the impact limiter attachment thermal model to reflect the design modifications following the drop testing, simulating the expected package damage resulting from the HAC defined drop events, capturing the thermal decomposition of the polyurethane foam under HAC conditions, changing the package surface emissivities to reflect the assumed presence of soot and/or surface oxidization, assumed contact between the thermal shield and the outer shell and zero lead gap to maximize the heat flow into the package, and changing the package orientation from upright to horizontal to reflect its probable orientation following the HAC drop event.

Physical testing using a half scale certified test unit (CTU) is used to establish the expected level of damage sustained by the BRR package from the 10 CFR 71.73 prescribed free and puncture drops that are assumed to precede the HAC fire event. Appendix 2.12.3, *Certification Test Results*, provides the configuration and initial conditions of the test articles, the test facilities and instrumentation used, and the test results. Appendix 3.5.3.7, *Description of Thermal Model for HAC Conditions*, provides an overview of the test results, the rationale for selecting the worst-case damage scenario, and the details of the thermal modeling used to simulate the package conditions during the HAC fire event.

3.4.1 Initial Conditions

The initial conditions assumed for the package prior to the HAC event are described below in terms of the modifications made to the NCT thermal model to simulate the assumed package conditions prior to and during the HAC event. These modifications are:

- Simulated the worst-case damage arising from the postulated HAC free and puncture drops as described in Appendix 3.5.3.7, *Description of Thermal Model for HAC Conditions*,
- Changed the package orientation from upright to horizontal to reflect the assumed position of the package following an HAC accident event,
- Increased the emissivity of all external surfaces to 0.9 and the solar absorptivity to 0.9 to account for possible oxidation and/or soot accumulation on the surfaces,

- Increased the emissivity of the interior surface of the thermal shield from 0.4 to 0.6 to account for oxidization during the HAC event,
- Added heat transfer via radiation within the impact limiter enclosures with an emissivity of 0.95 to account for the potential loss of polyurethane foam from thermal decomposition,
- Assumed an initial temperature distribution equivalent to the package at steady-state conditions with a 100 °F ambient and no insolation. This assumption complies with the requirement of 10 CFR §71.73(b).

Following the free and puncture bar drop events, the BRR package is assumed come to rest in a horizontal position prior to the initiation of the fire event. The MURR basket and the fuel element are predicted to remain intact and experience no significant re-positioning as a result of the drop events. Since the package geometry is essentially axi-symmetrical, the thermal performance under HAC conditions is independent of the rotational orientation of the package.

3.4.2 Fire Test Conditions

The fire test conditions analyzed to address the 10 CFR §71.73(c) requirements are as follows:

- The initial ambient conditions are assumed to be 100 °F ambient with no insolation,
- At time = 0, a fully engulfing fire environment consisting of a 1,475 °F ambient with an effective emissivity of 1.0 is used to simulate the average flame temperature of the hydrocarbon fuel/air fire event. The assumption of an average flame emissivity coefficient of 1.0 conservatively bounds the minimum 0.9 flame emissivity specified by 10 CFR Part §71.73(c)(4).
- The convection heat transfer coefficients between the package and the ambient during the 30-minute fire event are based on an average gas velocity of 10 m/sec [29]. Following the 30-minute fire event the convection coefficients are based on still air.
- The ambient condition of 100 °F with insolation is assumed following the 30-minute fire event. A solar absorptivity of 0.9 is assumed for the exterior surfaces to account for potential soot accumulation on the package surfaces.

The transient analysis is continued for 4.5 hours after the end of the 30-minute fire to capture the peak package temperatures.

3.4.3 Maximum Temperatures and Pressure

3.4.3.1 Maximum HAC Temperatures

Table 3.4-1 presents the predicted peak temperature for the BRR package with the MURR fuel payload under HAC conditions. As seen from the table, significant thermal margins exist for all components. The closure and vent/drain port seals remain below their maximum allowable temperature due to a combination of their location, the amount of foam remaining, even after the conservative damage assumptions, and the surrounding thermal mass of the upper and lower end structures. For example, the peak temperature predicted for the vent/drain port seals arises for the improbable condition of the worst case damage described in Appendix 3.5.3.7, *Description of*

Thermal Model for HAC Conditions, for the impact limiter aligning directly opposite of the drain port location. Without that conservative assumption, the peak vent/drain port temperature would be approximately 300 °F.

Figure 3.4-1 illustrates the temperature profile within the BRR package at the end of the 30-minute hypothetical fire. The illustrated profile demonstrates the thermal protection afforded to the package by the thermal shield and the polyurethane filled impact limiters since the high temperatures are limited to narrow regions on the exterior of the packaging. This thermal protection occurs despite the conservative level of damage assumed for the impact limiters.

Figure 3.4-2 and Figure 3.4-3 illustrate the temperature response profiles for selected package components. The relatively low temperature rise seen for the fuel elements and the fuel basket over the HAC event further demonstrates the thermal protection afforded by the BRR package design.

3.4.3.2 Maximum HAC Pressures

The peak cask cavity pressure under HAC conditions is conservatively estimated in the same manner as for NCT conditions (i.e., the bulk average cavity gas temperature is assumed to be equal to the mean of the average inner shell temperature and the average fuel basket temperature). The potential pressurization of the cask cavity due to failed cladding on the uranium-aluminide and uranium-zirconium hydride based fuel elements is ignored for this safety evaluation since the release of fission generated gases from these fuel types is diffusion-limited as opposed to the direct release mechanism for commercial spent nuclear fuel. At the conditions seen within the BRR package, the pressurization of the cask cavity due to gaseous release from breached fuel elements will be insignificant [30, 31] and is ignored for this safety evaluation.

Under the HAC condition with the MURR fuel payload, the peak bulk average gas temperature achieved during the HAC transient is 388 °F. Based on an assumed backfill gas temperature of 70 °F, the predicted maximum pressure within the cask cavity is computed via:

$$\text{Cavity Pressure} = 14.7\text{psia}\frac{(388^{o}\text{F}+460^{o}\text{F})}{(70^{o}\text{F}+460^{o}\text{F})}-14.7\text{ psia}$$

$$\text{Cavity Pressure} = 8.8\text{ psig}$$

Given the significantly greater decay heat of the MURR fuel element payload, the computed peak HAC pressure will bound those achieved for the ATR and TRIGA baskets. The peak HAC pressure reached with the MITR-II payload will be slightly lower given the slightly lower decay heat loading and the similar pre-fire package starting temperatures.

3.4.4 Maximum Thermal Stresses

The maximum thermal stresses under the HAC condition are addressed in Section 2.7.4, *Thermal.*

Table 3.4-1 – HAC Temperatures

Component	Temperature (°F) ①			
	End of Fire	Peak	Post-fire Steady State	Max. Allowable
MURR Fuel Plate	344	451	326	1,100
MURR Side Plate	341	449	324	1,100
MURR Fuel Basket	326	437	310	800
Inner Shell	301	393	211	800
Lead	471	482	207	620
Outer Shell	704	704	200	2,700
Thermal Shield	1,256	1,256	180	2,700
Lower End Structure	318	335	182	800
Upper End Structure	485	485	198	800
Shield Plug	234	317	201	620 ②
Cask Lid	215	306	196	800
Closure/Vent Port Elastomeric Seals	212	306	196	400
Drain Port Elastomeric Seal	365	373	195	400
Upper Impact Limiter				
- Max. Foam	-	-	-	N/A ③
- Avg. Foam	-	-	-	N/A ③
- Shell	1,475	1,475	195	2,700 ③
Lower Impact Limiter				
- Max. Foam	-	-	-	N/A ③
- Avg. Foam	-	-	-	N/A ③
- Shell	1,475	1,475	190	2,700 ③
Cask Cavity Bulk Gas	305	388	257	N/A

Notes: ① Results assume a payload of eight (8) MURR fuel elements dissipating 158 W each and helium as the backfill gas.

② Temperature criterion based on melting point of the enclosed lead shielding.

③ Temperature criterion based on melting point for the shell. No criteria for the polyurethane foam since its thermal decomposition serves as it principal means of providing thermal protection during the HAC event.

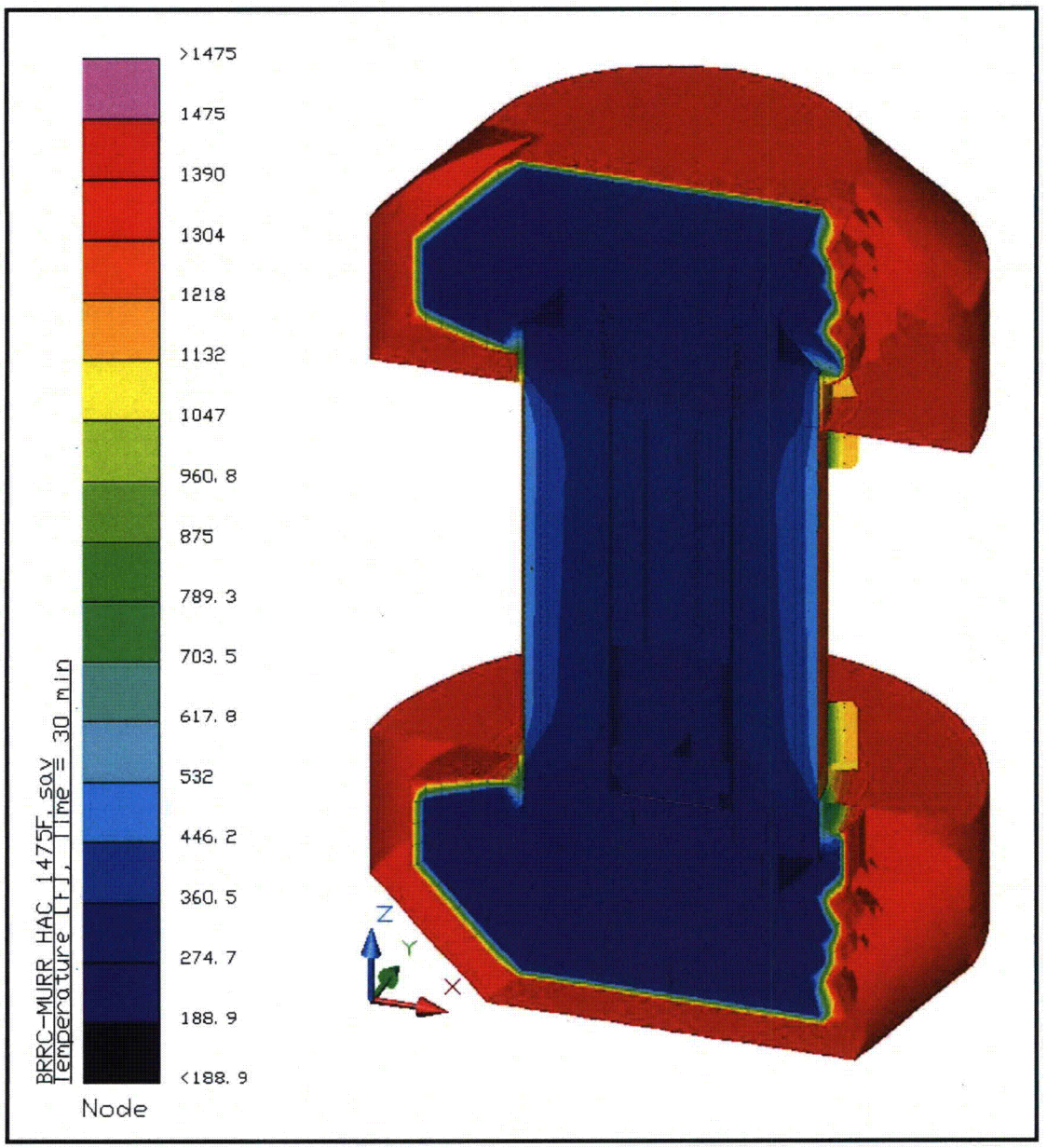

Figure 3.4-1 – BRR Package HAC Temperature Distribution at End of 30 Minute Fire

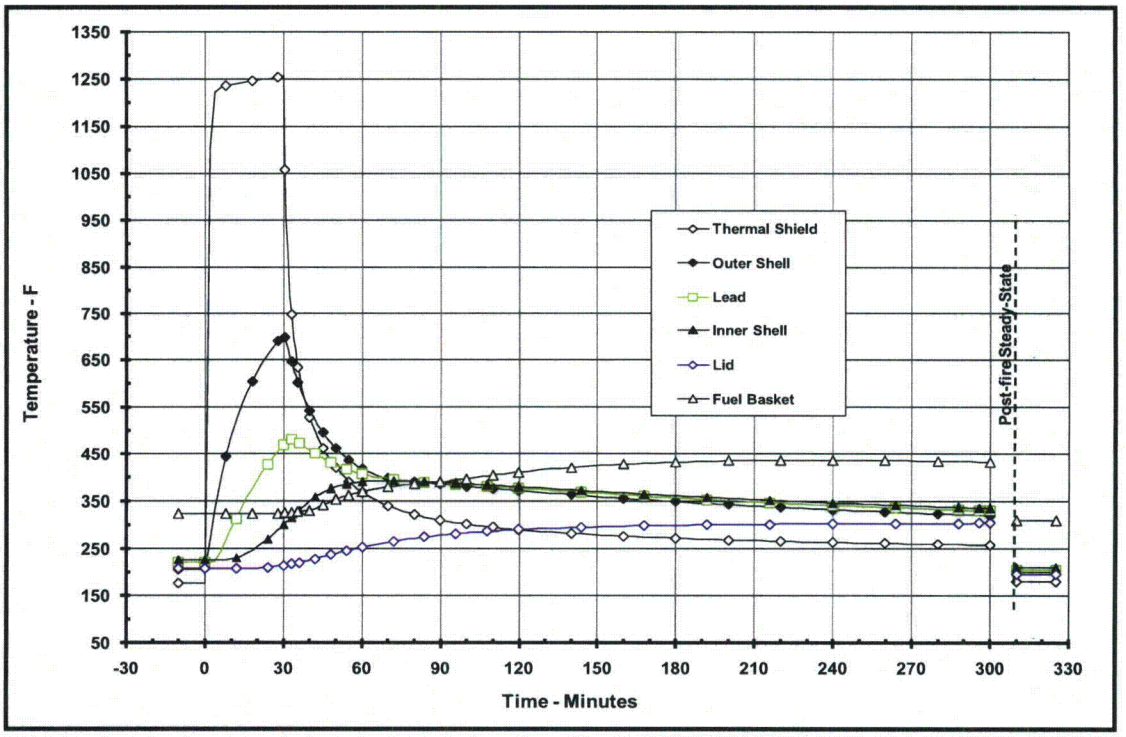

Figure 3.4-2 –Thermal Response to HAC Event, Package Components

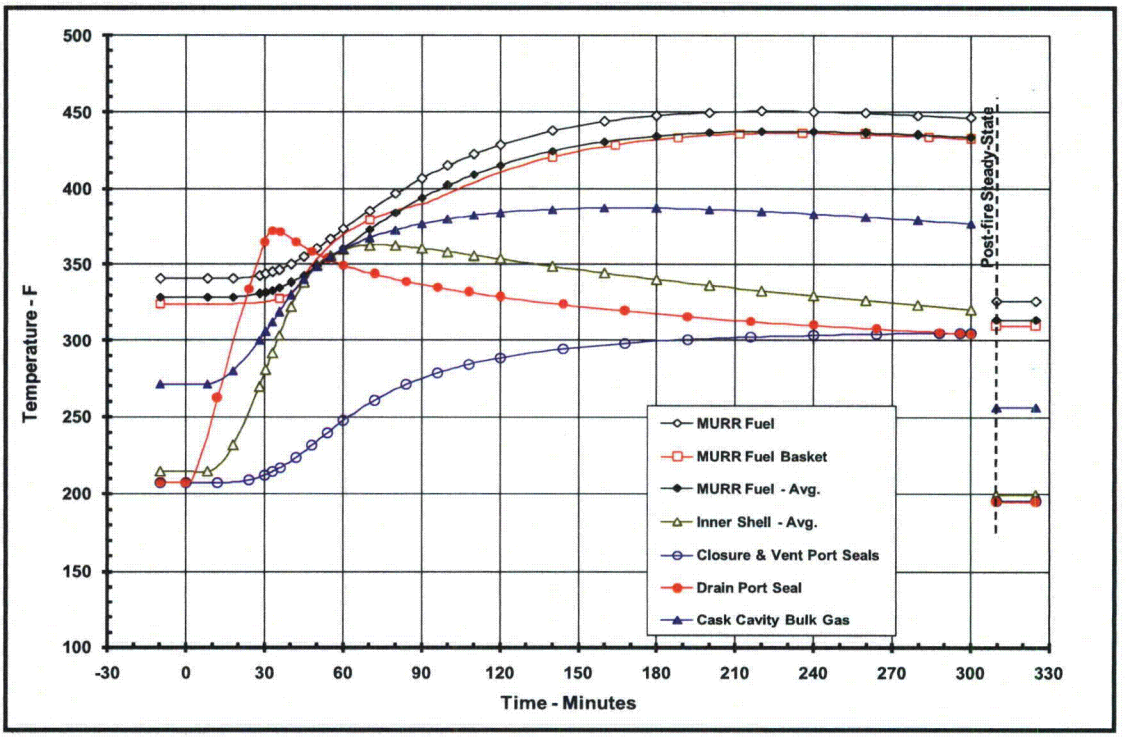

Figure 3.4-3 – Thermal Response to HAC Event, Payload, Seals, and Bulk Gas

3.5 Appendices

3.5.1 References

3.5.2 Computer Analysis Results

3.5.3 Analytical Thermal Model

3.5.4 'Last-A-Foam' Response under HAC Conditions

3.5.1 References

1. Title 10, Code of Federal Regulations, Part 71 (10 CFR 71), *Packaging and Transportation of Radioactive Materials*, United States Nuclear Regulatory Commission (USNRC), 01–01–08 Edition.
2. American Society of Mechanical Engineers (ASME) Boiler and Pressure Vessel (B&PV) Code, Section II, Part D, 2007.
3. American Society of Mechanical Engineers (ASME) Boiler & Pressure Vessel Code, Section III, Rules for Construction of Nuclear Facility Components, Division 1, Subsection NB, Class 1 Components, & Subsection NG, Core Support Structures, 2007 Edition.
4. Y.S. Touloukian, Thermophysical Properties of Matter, the TPRC Data Series, Plenum Publishing Corp., New York, NY, 1970.
5. Polkinghorne, S. and Lacy, J., *Thermophysical And Mechanical Properties Of ATR Core Materials*, Report No. PG-T-91-031, August 1991, EG&G Idaho, Inc.
6. Matweb, Online Material Data Sheets, *www.matweb.com*.
7. Frank, R., and Plagemann, W., *Emissivity Testing of Metal Specimens*, Boeing Analytical Engineering coordination sheet No. 2-3623-2-RF-C86-349, August 21, 1986. Testing accomplished in support of the TRUPACT-II design program.
8. Azzazy, M., *Emissivity Measurements of 304 Stainless Steel*, prepared for Southern California Edison, September 6, 2000, Transnuclear File No. SCE-01.0100.
9. Gubareff, G., Janssen, J., and Torborg, R., *Thermal Radiation Properties Survey*, 2nd Edition, Honeywell Research Center, 1960.
10. Gustavsen, Arild, *Heat Transfer in Window Frames with Internal Cavities*, PhD Thesis, Norwegian University of Science and Technology, Trondheim, Norway, September 2001.
11. Series 66 and 73 Product Data Sheets, Tnemec Company, Inc. 6800 Corporate Drive Kansas City, MO, *www.tnemec.com*.
12. MURR Fuel Drawings, EG&G Drawings No. 409406, Rev E and 409407, Rev N.
13. MITR-II Fuel Drawings, EG&G Drawings No. 410368, Rev A, 410369, Rev C, and 419486, Rev A.
14. ATR Mark VII Fuel Element Assembly, INEEL Drawing No. DWG-405400, Rev-19.
15. TRIGA Fuel Element Description, University of Utah Class Notes, Nuclear Engineering, CVEEN 5700/6700.
16. *KK-8 Graphite High Temperature Thermal Characteristics with Supporting Data*, letter from Harold E. Cook (Carbon/Graphite Group, Inc.) to Corwin Robinson (EG&G Mound Applied Technologies), dated March 13, 1992.
17. Greenspan, E., *Hydride Fuel for Improving the Design and Performance of LWRs*, Presentation to 233rd ACS National Meeting, Chicago, IL, 2007.
18. Last-A-Foam™ On-line Data Sheet, *www.generalplastics.com*.

19. Rohsenow, Hartnett, and Choi, Handbook of Heat Transfer, 3rd edition, McGraw-Hill, 1998.

20. Rainier Rubber Company, Seattle, WA, www.rainierrubber.com.

21. *Parker O-Ring Material Offering Guide*, ORD 5712, August 2002, *www.parkerorings.com*.

22. Thermal Desktop®, Version 5.1 and 5.3, Cullimore & Ring Technologies, Inc., Littleton, CO, 2007 and 2010.

23. SINDA/FLUINT, *Systems Improved Numerical Differencing Analyzer and Fluid Integrator*, Version 5.1 and 5.3, Cullimore & Ring Technologies, Inc., Littleton, CO, 2007 and 2010.

24. AFS Report TR-VV-06-001, Rev. 0, *Thermal Desktop® and SINDA/FLUINT Testing and Acceptance Report*, Version 5.1, AREVA Federal Services, LLC, 2008.

25. Kreith, Frank, Principles of Heat Transfer, 3rd edition, Harper & Row, 1973.

26. Guyer, Eric, Handbook of Applied Thermal Design, McGraw-Hill, Inc., 1989.

27. Williamson, C., and Iams, Z., *Thermal Assault and Polyurethane Foam - Evaluating Protective Mechanisms for Transport Containers*, General Plastics Manufacturing Company, Tacoma, WA, Waste Management '05 Symposium, Tucson, AZ, 2005.

28. Williamson, C., and Iams, Z., *Thermal Assault and Polyurethane Foam - Evaluating Protective Mechanisms*, General Plastics Manufacturing Company, Tacoma, WA, presented at PATRAM International Symposium, Berlin, Germany, 2004.

29. Schneider, M.E and Kent, L.A., *Measurements of Gas Velocities and Temperatures in a Large Open Pool Fire*, Heat and Mass Transfer in Fire - HTD Vol. 73, 1987, ASME, New York, NY.

30. Vinson, D., Sindelar, R., and Iyer, N., *Containment Evaluation of Breached AL-SNF For Cask Transport*, Savannah River National Laboratory - Materials Science & Technology, Aiken, SC 29808.

31. TRIGA® Fuel Description, General Atomics website, http://triga.ga.com.

32. Roth A, Vacuum Technology, 2nd Edition, Elsevier Science, 1982.

33. Lide, D., Handbook of Chemistry and Physics, 83rd Edition, The Chemical Rubber Co., 2002-2003.

34. Peacock Jr., H. B., et. al., *Evaluation of Corrosion of Aluminum Based Reactor Fuel Cladding Materials During Dry Storage*, WSRC-TR-95-0345, Westinghouse Savannah River Company.

35. Lam, P, Sindelar, R, and Barrett, K., *Corrosion of Aluminum-Uranium Alloys in Water Vapor at 200°C*, WSRC-MS-98-00858, Westinghouse Savannah River Company.

36. AFS Report AFS-TR-VV-013, Rev. 0, *Thermal Desktop® and SINDA/FLUINT Testing and Acceptance Report*, Version 5.3, AREVA Federal Services, LLC, 2010.

3.5.2 Computer Analysis Results

Due to the size and number of the output files associated with each analyzed condition, results from the computer analysis are provided on a CD-ROM.

3.5.3 Analytical Thermal Model

The analytical thermal model of the BRR package was developed for use with the Thermal Desktop® [22] and SINDA/FLUINT [23] computer programs. These programs are designed to function together to build, exercise, and post-process a thermal model. The Thermal Desktop® computer program is used to provide graphical input and output display function, as well as computing the radiation exchange conductors for the defined geometry and optical properties. Thermal Desktop® is designed to run as an AutoCAD® application. As such, all of the CAD tools available for generating geometry within AutoCAD® can be used for generating a thermal model. In addition, the use of the AutoCAD® layers tool presents a convenient means of segregating the thermal model into its various elements.

The SINDA/FLUINT computer program is a general purpose code that handles problems defined in finite difference (i.e., lumped parameter) and/or finite element terms and can be used to compute the steady-state and transient behavior of the modeled system. Although the code can be used to solve any physical problem governed by diffusion-type equations, specialized functions used to address the physics of heat transfer and fluid flow make the code primarily a thermal code.

The SINDA/FLUINT and Thermal Desktop® computer programs have been validated for safety basis evaluations for nuclear related projects [24, 36].

Together, the Thermal Desktop® and SINDA/FLUINT codes provide the capability to simulate steady-state and transient temperatures using temperature dependent material properties and heat transfer via conduction, convection, and radiation. Complex algorithms may be programmed into the solution process for the purposes of computing heat transfer coefficients as a function of the local geometry, gas thermal properties as a function of species content, temperature, and pressure, or, for example, to estimate the effects of buoyancy driven heat transfer as a function of density differences and flow geometry.

3.5.3.1 Description of BRR Packaging Thermal Model for NCT Conditions

The BRR packaging is represented by a 3-dimensional, half symmetry thermal model for the NCT evaluations. This modeling choice captures the full height of the packaging components and allows the incorporation of the varying insolation loads that will occur along the length of the package, the various degrees of symmetry within the fuel baskets, and the non-symmetry of the HAC free drop damage. The various packaging components are defined using a combination of planar and solid elements. Program features within the Thermal Desktop® computer program automatically compute the various areas, lengths, thermal conductors, and view factors involved in determining the individual elements that make up the thermal model of the complete assembly.

It should be noted that the NCT thermal model described below is based on an earlier design that used 6 instead of the current 8 attachment lugs per limiter, lug plates that are 0.38-inches thick by 2.75-inches wide vs. the current 0.5-inches thick by 3.63-inches wide, and a 0.25-inch vs. 0.125-inch radial gap between the limiter and the cask shell. Since these variations from the current design result in a lower surface area for heat dissipation to the ambient, the predicted NCT temperatures will be slightly higher than those expected for the current design. Because of this conservatism, the results are valid for the safety evaluations under NCT conditions. The design variations are incorporated for the HAC evaluations.

Figure 3.5-1 to Figure 3.5-5 illustrates 'solid' views of the BRR packaging thermal model. The model is composed of solid and plate type elements representing the various packaging components. Thermal communication between the various components is via conduction, radiation, and surface-to-surface contact. A total of approximately 20,500 nodes, 110 planar elements, and 4,900 solid elements are used to simulate the modeled components. Nearly 80 of the solid elements are finite difference solids (i.e., FD solids), a Thermal Desktop® computer program feature that permits a group of solid elements to be represented by a single entity. As such, the number of individual solid 'bricks' utilized in the modeling is actually significantly larger than the 4,900 value indicated above. In addition, one boundary node is used to represent the ambient environment for convection purposes and two boundary nodes is used to represent the ambient temperature for the purpose of radiation heat transfer. The use of separate boundary nodes for radiation heat transfer allows the model to capture the effective emissivity of the ambient environment.

As seen from Figure 3.5-1, the modeling accurately captures the geometry of the various components of the packaging, including the impact limiters, the inner and outer shells, the upper and lower end structures, the closure lid and shield plug, and lead sections. Also captured, but not easily seen in the figure due to the scale of the figures, is the thermal shield and the impact limiter attachment lugs. The minimal spatial resolution provided by the thermal modeling for the cask body components is approximately 1.75 inches in the radial direction, 2 inches in the axial direction, and every 10° in the circumferential direction. Greater spatial resolution (i.e., smaller radial and axial distances) is provided near the cask ends where larger thermal gradients are expected. A slightly lower spatial resolution is provided for the exterior portions of the impact limiters since the relatively low thermal conductivity of the polyurethane foam will yield correspondingly low heat flows.

Figure 3.5-2 illustrates the thermal modeling used for the various stainless steel components of the BRR cask body, while Figure 3.5-3 illustrates the thermal modeling of the lead structures within the cask body. The figures demonstrate that the geometry of the cask components is accurately captured by the thermal modeling.

Figure 3.5-4 illustrates the modeling used for the shell of the shield plug. While the height, radius, and shell thickness of the shield plug are accurately captured, the diagonal pipe and 4° taper are not included for modeling simplicity and because these details have no significant effect on the thermal performance of the packaging. Although the lead sheets used to fill the shield plug cavity are to be oversized and then hammered into place, the thermal modeling conservatively assumes a small (i.e., 0.0625-inch) uniform gap exists between the lead sheets and the shield plug shell.

The thermal modeling of the impact limiters, as illustrated in Figure 3.5-5, accurately captures the compound shape of the limiter's inner shell and the placement of the attachment lugs. Since the fabrication tolerance of the polyurethane foam used to fill the impact limiters can yield foam densities that are ±15% of the targeted 9 lb_m/ft^3 (pcf) foam density and since the foam's conductivity is a function of its density, the thermal modeling conservatively assumes a low tolerance foam density (i.e., 9 pcf less 15% ≈ 7.65 pcf) for NCT evaluations and a high tolerance foam density (i.e., 9 pcf plus 15% ≈ 10.35 pcf) for HAC evaluations.

3.5.3.2 Description of MURR Fuel and Basket Thermal Model

Figure 3.5-6 illustrates the thermal modeling of the MURR fuel basket and fuel element used for this evaluation. Approximately 2,600 nodes, 160 planar elements, and 1,000 solid elements are used to simulate the modeled components of the fuel basket, while approximately 3,300 nodes, 340 planar elements, and 550 solid elements are used to simulate the modeled components of each MURR fuel element.

The fuel basket modeling captures the inner and outer shells, the plates used to section off or divide the basket into compartments to house the individual fuel elements, and the base. While the inner shell and the divider plates are simulated using solid elements, the 0.25-inch thick outer shell and the base plates are represented by planar elements since the temperature difference though their thickness will be small. All of the basket components are assumed to be Type 304 stainless steel. The fuel elements are assumed to be essentially centered within in each compartment with the heat transfer between the fuel elements and the basket assumed to be via conduction and radiation across the separation gap and via contact with the plate supporting the fuel elements.

The fuel element simulation includes separate representation of the twenty-four (24) curved composite fuel plates, the side plates, and the upper and lower end box castings. Heat transfer between the individual fuel plates is simulated via conduction and radiation, while the heat transfer between the fuel plates and the side plates is via radiation and conduction through the crimped edges. The size, curvature, distance between the fuel plates, and the composite thermal properties of the plates are based on the information presented in Appendix 3.5.3.9, *Determination of Composite Thermal Properties for Fuel Plates*. The decay heat loading for the fuel elements is applied as a surface heat flux over the active fuel length of the plates.

Heat transfer between the fuel basket and the BRR packaging is assumed to be via conduction and radiation across the assumed uniform gap between the basket and the inner shell of the packaging. Direct contact is assumed between the base of the fuel basket and the base of the cask cavity. Because of the combination of decay heat and the criterion to limit the maximum fuel plate temperature to 400 °F or less (see Section 3.2.2), the BRR cask cavity is to be filled with helium gas at a pressure of one atmosphere following the draining and drying process.

3.5.3.3 Description of MITR-II Fuel and Basket Thermal Model

Figure 3.5-7 illustrates the thermal modeling of the MITR-II fuel basket and fuel element used for this evaluation, while Figure 3.5-8 illustrates the layout of the solids modeling for the basket internal geometry. Approximately 4,500 nodes, 2 planar elements, and 2,200 solid elements are used to simulate the modeled components of the fuel basket, while approximately 1,480 nodes,

75 planar elements, and 230 solid elements are used to simulate the modeled components of each MITR-II fuel element.

The fuel basket modeling captures the geometry of the machined stainless steel plates used to house the fuel elements, the top plate, the individual tie bars used to hold the basket together, and the pedestal base. All of the basket components are assumed to be Type 304 stainless steel. The fuel elements are assumed to be essentially centered within in each compartment with the heat transfer between the fuel elements and the basket assumed to be via conduction and radiation across the separation gap and via contact with the plate supporting the fuel elements.

The fuel element simulation includes separate representation of the fifteen (15) composite fuel plates, the side plates, and the upper and lower end box castings. Heat transfer between the individual fuel plates is simulated via conduction and radiation, while the heat transfer between the fuel plates and the side plates is via radiation and conduction through the crimped edges. The size, distance between the fuel plates, and the composite thermal properties of the plates are based on the information presented in Appendix 3.5.3.9, *Determination of Composite Thermal Properties for Fuel Plates*. The decay heat loading for the fuel elements is applied as a uniform surface heat flux over the active fuel length of the plates.

Heat transfer between the fuel basket and the BRR packaging is assumed to be via a combination of conduction and radiation across the gaps between the various basket surfaces and the inner shell of the packaging. The cask cavity is to be filled with helium gas to limit the maximum fuel plate temperature to 400 °F or less (see Section 3.2.2).

3.5.3.4 Description of ATR Fuel and Basket Thermal Model

Figure 3.5-9 illustrates the thermal modeling of the ATR fuel basket and fuel element used for this evaluation. Approximately 3,000 nodes, 50 planar elements, and 90 FD solid elements are used to simulate the modeled components of the fuel basket, while approximately 3,300 nodes, 95 planar elements, and 325 solid elements are used to simulate the modeled components of each ATR fuel element. As previously explained, an FD solid is a Thermal Desktop® computer program feature that permits a group of solid elements to be represented by a single entity. As such, the number of individual solid 'bricks' utilized in the modeling of the ATR fuel basket is actually significantly larger than 90.

The fuel basket modeling captures the inner and outer shells, the plates used to section off or divide the basket into compartments to house the individual fuel elements, the stiffening ribs, and the base. All of the basket components are assumed to be Type 304 stainless steel. The fuel elements are assumed to be essentially centered within in each compartment with the heat transfer between the fuel elements and the basket assumed to be via conduction and radiation across the separation gap.

The fuel element simulation includes separate representation of the nineteen (19) curved composite fuel plates and the side plates (including the cutouts). The upper and lower end boxes are to be removed prior to loading of the fuel assemblies within the basket. Heat transfer between the individual fuel plates is simulated via conduction and radiation, while the heat transfer between the fuel plates and the side plates is via radiation and conduction through the crimped edges. The size, curvature, distance between the fuel plates, and the composite thermal properties of the plates are based on the information presented in Appendix 3.5.3.9,

Determination of Composite Thermal Properties for Fuel Plates The decay heat loading for the fuel elements is applied as a uniform surface heat flux over the active fuel length of the plates.

Heat transfer between the fuel basket and the BRR packaging is assumed to be via a combination of conduction and radiation across the gaps between the various basket surfaces and the inner shell of the packaging. The thermal evaluations assume the cask cavity is filled with helium gas.

3.5.3.5 Description of TRIGA Fuel and Basket Thermal Model

Figure 3.5-10 illustrates the thermal modeling of the TRIGA fuel basket and fuel element used for this evaluation, while Figure 3.5-11 illustrates the solids modeling used to represent the void spaces between the fuel tubes. Approximately 7,500 nodes, 60 planar elements, and 1,000 solid elements are used to simulate the modeled components of the fuel basket, while approximately 1,030 nodes and 7 FD solid elements are used to simulate the modeled components of each TRIGA fuel element. As previously explained, an FD solid is a Thermal Desktop® computer program feature that permits a group of solid elements to be represented by a single entity. As such, the number of individual solid 'bricks' utilized in the modeling of each TRIGA fuel element is actually significantly larger than 7.

The fuel basket modeling captures the individual tubes used to house each fuel element, stiffening ribs, and the spacers used to position the shorter length fuel elements within the basket. All of the basket components are assumed to be fabricated of Type 304 stainless steel. The fuel elements are assumed to be essentially centered within in each compartment with the heat transfer between the fuel elements and the basket assumed to be via conduction and radiation across the separation gap and via contact with the plate supporting the fuel elements.

The fuel element simulation includes separate representation of the uranium zirconium hydride metal section, the graphite section, and the upper and lower end fittings. Since the temperature difference across the fuel cladding is small for the decay heats involved, the cladding is not modeled separately. The TRIGA fuel has two design active fuel lengths; 14 and 15 inches. The decay heat loading for the fuel elements is applied as a uniform volumetric heat flux over the active fuel length. The modeling assumes the shorter length to conservatively bound the maximum volumetric heat generation.

Heat transfer between the fuel basket and the BRR packaging is assumed to be via a combination of conduction and radiation across the gaps between the various basket surfaces and the inner shell of the packaging. The thermal evaluations assume the cask cavity is filled with helium.

3.5.3.6 Insolation Loads

The insolation loading on the BRR package is based on the 10CFR71.71(c)(1) specified insolation values over a 24-hour period. Since the BRR packaging is characterized by thermally massive shells and large foam filled impact limiters, the interior temperatures of the packaging will be effectively 'decoupled' from the diurnal changes in insolation loading. As such, a steady-state thermal model based on the application of the 10CFR71.71(c)(1) specified insolation values averaged over 24 hours is used to evaluate the design basis package temperatures under NCT conditions.

3.5.3.7 Description of Thermal Model for HAC Conditions

The thermal evaluations for the hypothetical accident condition (HAC) are conducted using an analytical thermal model of the BRR package. The HAC thermal model is a modified version of the half symmetry NCT model described above. The principal model modifications consist of simulating the expected package damage resulting from the drop events that are assumed to precede the HAC fire, changing the package surface emissivities to reflect the assumed presence of soot and/or surface oxidization, and simulating the thermal performance of the polyurethane foam used in the impact limiters.

Physical testing using a half scale certification test unit (CTU) is used to establish the expected level of damage sustained by the BRR packaging as a result of the 10 CFR 71.73 prescribed free and puncture drops that are assumed to precede the HAC fire event. The configuration and initial conditions of the test article, a description of the test facility, test article instrumentation, and the test results are documented Section 2.12.3, *Certification Test Results*. The drop tests covered a range of hypothetical free drop orientations and puncture bar drops. An overview of the results of the drop tests is provided below. For full details, including photographs and figures, see Section 2.12.3, *Certification Test Results*. It should be noted that all of the noted dimensions in this discussion are for the half scale model and need to be doubled to yield the equivalent full scale results.

1) The worst case physical damage to the exterior of the package occurs from an oblique slap down free drop. Overall, the resulting damage is thermally insignificant: an inward crush of approximately 4 inches and two small breaches in the joint along the outer diameter of the limiter. However, a subsequent drop on a puncture bar caught the fold in the limiter shell created by the oblique slap down drop and tore the damaged joint open. The total chord length of the damaged area measured approximately 26 inches. The width of the opening at the center was 5 inches and tapering to nearly zero at the ends. The chord length of the flap opening is approximately 22.6 inches. Negligible amounts of foam were lost from the limiter from the opening.

2) The CG over corner drop resulted in a crush distance of 5.5 inches. A subsequent puncture bar drop on the damage area resulted in the partial penetration of the shell. The puncture bar penetrated the underlying foam to a depth of 2-1/4 inches. The width of the breach/torn flap in the limiter shell was 4 inches and its length was 5 inches.

3) The vertical end drop resulted in impact limiter deformation that was a combination of outside-in and inside-out. The drop resulted in no tearing of the limiter shell and no exposure of the underlying foam. The crush distance was 3.4 inches. A subsequent puncture bar drop on the damaged area created a dent approximately 1-3/4 inches deep. One or two rebound impacts also occurred with negligible deformation. There were no signs of cracking in the dent or in the nearby weld seam.

4) The drop testing showed the original impact limiter attachment design was not adequate to fully retain the impact limiters on the package for the slapdown free drop event. The attachments were redesigned and retested to ensure complete attachment of the limiters. See Section 2.12.3, *Certification Test Results,* for further discussion.

5) No deformation of the impact limiter inner shell was noted.

Subsequent to the drop test, the impact limiter design was modified to improve its performance. These modifications increased the number of attachment lugs from 6 to 8 per limiter, increased the size and thickness of each lug from 0.38-inches thick by 2.75-inches wide to 0.5-inches thick by 3.63-inches wide, increased the size of the attachment pins, reduced the gap between the cask and the impact limiter inner shell from 0.25 to 0.125 inches, and a re-design of the limiter joint that cracked under the side/slap down drop (see Item 1 above).

Besides scaling the noted crush dimensions to the full scale design, the projected damage also needs to reflect the effect of temperature on the polyurethane foam's structural properties since the drop test was conducted under cold conditions and the worst case crush will arise under warm conditions. Figure 3.5-12 depicts the predicted crush depths under hot conditions for the vertical end, C.G. over corner, and side/slap down drop orientations based on an evaluation presented in Section 2.12.5, *Impact Limiter Performance Evaluation*. As seen from the figure, the side/slap down drop orientation is predicted to result in both the greatest crush depth and the closest approach to the inner shell of the limiter. Per Appendix 3.5.4, *'Last-A-Foam' Response under HAC Conditions*, approximately 3.5 to 3.8 inches of the nominally 9 pcf polyurethane foam will decompose during a 30 minute HAC fire event. This foam loss (or recession depth) will be even less for foam in the vicinity of crush damage since its effective density will have increased as a result of the crush damage. Any foam depths greater than 4 inches remaining after the HAC drop events will result in the underlying temperatures rising only marginally during the HAC fire event. Examination of Figure 3.5-12 demonstrates that the vertical end drop and C.G. over corner drops will leave more than 4 inches of foam everywhere, even without credit for increased foam density due to crush. As such, the side/slap down drop event is selected as the controlling scenario for impact limiter damage for the HAC evaluations.

The controlling puncture bar damage is determined from the half-scale drop results described in Section 2.12.3, *Certification Test Results*. Since the polyurethane foam forms an intumescent char that swells and tends to fill voids or gaps created by the puncture bar damage, the level of damage incurred by direct attack to the impact limiter's exterior shell would be thermally insignificant. An untested puncture bar scenario consisting of an impact to the thermal shield of the cask is also considered. This type of impact can be expected to cause a local depression in the thermal shield and potentially a small tear. However, overall, the thermal shield would retain its functionality with the region of elevated temperatures being localized to the size of the puncture bar and similar in temperature level to that seen at the impact limiter attachment lug locations. Therefore, the controlling puncture bar damage is assumed to be an attack on the impact limiter skin joint that tears a flap type opening in the limiter skin (see Item 1 above). While the re-design of the impact limiters following the drop tests is expected to eliminate this type of damage, it is assumed for the HAC evaluation to conservatively bound all other potential puncture bar damage scenarios.

Based on the above observations and the general assumptions for the package condition for the HAC evaluations, the NCT thermal model described above was modified for the HAC evaluations via the following steps:

1) Assume the package has been ejected from its support stand and is lying on its side. As such, the convective heat transfer from the package's exterior surfaces is based on a horizontal orientation. In addition, the adiabatic boundary condition assumed for selected surfaces of the lower impact limiter under NCT conditions are switched to active heat transfer surfaces.

2) The surface emissivity for all exterior surfaces is assumed to be 0.9 to account for potential oxidation and/or soot accumulation. The emissivity of all inside surfaces of the impact limiter exposed as the result of foam decomposition is assumed to be 0.95 to account for adherence of foam char.

3) The small, uniform gap conservatively assumed between the lead and the outer shell under NCT conditions is eliminated to maximize the heat flow into package.

4) Thermal conductance via the stand-off strips under the thermal shield is assumed for the HAC condition. Thermal credit for the stand-off strips was conservatively ignored for the NCT evaluations.

5) The number and size of the impact limiter attachments are increased for the HAC evaluation to reflect the re-design of the impact limiter following the drop testing. The NCT evaluations ignored this change since neglecting the added surface area yields conservative results.

6) A minimum of 3.8 inches of foam is removed from around the perimeter of the impact limiters at the start of the HAC evaluation. This change conservatively bounds the impact of the gradual decomposition of the foam over the 30 minute fire event. The conductivity of the remaining foam is set to that associated with foam fabricated at the high end of the density tolerance range (i.e., 9 pcf + 15%) in order to conservatively bound the heat transfer into the package.

7) Simulate the sideways crushing of the upper and lower impact limiters under hot drop conditions. This consisted of removing approximately 15.8 inches from one side of the impact limiters.

8) Simulate the conservative assumption that a puncture bar attack tears a flap in the upper impact limiter. This consisted of removing a total of 6.1 inches of foam over a 60° segment of the impact limiter to conservatively capture the additional recession depth over 3.8 inches that may occur due to the direct exposure of the foam surfaces to the flame (see Appendix 3.5.4, *'Last-A-Foam' Response under HAC Conditions*). Added radiation and convection conductors to the exposed region of the impact limiter's inner shell to reflect the conservative assumption that a flap opening has occurred in the upper impact limiter.

9) Simulated the possible shifting of the impact limiter by replacing the 0.125 inch nominal gap between the inner shell of the limiters and the cask shell with a direct contact conductance over an approximate 1 inch x 7.2 inch area (i.e., the modeled height of the cylindrical portion of the limiter's inner shell). The contact is placed in the center of the side drop foam crush damage and conservatively bounds the line-contact expected between two cylindrical bodies with no deformation.

Figure 3.5-13 illustrates the revised thermal model of the impact limiters used for the HAC evaluations. All other aspects of the BRR packaging remain the same as used for the NCT thermal evaluations.

3.5.3.8 Convection Coefficient Calculation

The BRR package thermal model uses semi-empirical relationships to determine the level of convection heat transfer from the exterior package surfaces under both the regulatory NCT and HAC conditions. The convective heat transfer coefficient, h_c, has a form of:

$$h_c = Nu\frac{k}{L}$$

where k is the thermal conductivity of the gas at the mean film temperature and L is the characteristic length of the vertical or horizontal surface. The convection coefficient is correlated via semi-empirical relationships against the local Rayleigh number and the characteristic length. The Rayleigh number is defined as:

where $$Ra_L = \frac{\rho^2 g_c \beta L^3 \Delta T}{\mu^2} \times Pr$$

g_c = gravitational acceleration, 32.174 ft/s^2 β = coefficient of thermal expansion, °R^{-1}

ΔT = temperature difference, °F ρ = density of air at the film temperature, lb$_m$/ft^3

μ = dynamic viscosity, lb$_m$/ft-s Pr = Prandtl number = (c_p μ) / k

L = characteristic length , ft k = thermal conductivity at film temp., Btu/ft-hr-°F

c_p = specific heat, Btu/ lb$_m$ -°F Ra_L = Rayleigh #, based on length 'L'

Note that k, c_p, and μ are each a function of air temperature as taken from Table 3.2-3. Values for ρ are computed using the ideal gas law, β for an ideal gas is simply the inverse of the absolute temperature of the gas, and Pr is computed using the values for k, c_p, and μ from Table 3.2-3. Unit conversion factors are used as required to reconcile the units for the various properties used.

The natural convection from a discrete vertical surface is computed using Equations 4-13, 4-24, 4-31, and 4-33 of reference [19], which is applicable over the range 1 < Rayleigh number (Ra) < 10^{12}:

$$Nu^T = \overline{C}_L Ra^{1/4}$$

$$\overline{C}_L = \frac{0.671}{\left(1+(0.492/Pr)^{9/16}\right)^{4/9}}$$

$$Nu_L = \frac{2.0}{\ln(1+2.0/Nu^T)}$$

$$Nu_t = C_t^V Ra^{1/3} / \left(1+1.4\times10^9 Pr/Ra\right)$$

$$C_t^V = \frac{0.13\,Pr^{0.22}}{\left(1+0.61\,Pr^{0.81}\right)^{0.42}}$$

$$Nu = \frac{h_c L}{k} = \left[(Nu_L)^6 + (Nu_t)^6\right]^{1/6}$$

The natural convection from a vertical cylindrical surface is computed by applying a correction factor to the laminar Nusselt number (Nu_L) determined using the same methodology and Nu_t for a vertical plate (see above). The characteristic dimension, L, is the height of the vertical cylinder and D is the cylinder's diameter. The correction factor as defined by Equations 4-44 of reference [19] is:

$$Nu_{L\text{-Cylinder}} = \frac{\delta}{\ln(1+\delta)} Nu_{L\text{-Plate}}$$

$$\delta = \frac{1.8 \times L/D}{Nu_{Plate}^T}$$

$$Nu_{Vert.\,Cylinder} = \frac{h_c L}{k} = \left[(Nu_{L\text{-Cylinder}})^6 + (Nu_{t\text{-Plate}})^6\right]^{1/6}$$

Natural convection from horizontal surfaces is computed from Equations 4-13, 4-25, 4-39, and 4-40 of reference [19], where the characteristic dimension (L) is equal to the plate surface area divided by the plate perimeter. For a heated surface facing upwards or a cooled surface facing downwards and Ra > 1:

$$Nu = \frac{h_c L}{k} = \left[(Nu_L)^{10} + (Nu_t)^{10}\right]^{1/10}$$

$$Nu_L = \frac{1.4}{\ln\left(1+1.4/\left(0.835 \times \overline{C}_L Ra^{1/4}\right)\right)}$$

$$\overline{C}_L = \frac{0.671}{\left(1+(0.492/Pr)^{9/16}\right)^{4/9}}$$

$$Nu_t = 0.14 \times \left(\frac{1+0.0107 \times Pr}{1+0.01 \times Pr}\right) \times Ra^{1/3}$$

For a heated surface facing downwards or a cooled surface facing upwards and $10^3 < Ra < 10^{10}$, the correlation is as follows:

$$Nu = Nu_L = \frac{2.5}{\ln\left(1+2.5/Nu^T\right)}$$

$$Nu^T = \frac{0.527}{\left(1+(1.9/Pr)^{9/10}\right)^{2/9}} Ra^{1/5}$$

Calculation of the convection coefficient from a horizontal cylindrical surface is computed using Equation 3-43, Chapter 1, from [26], where the characteristic length, D, is the outer diameter of the cylinder. This equation, applicable for $10^{-5} < Ra < 10^{12}$, is as follows:

$$Nu = \frac{h_c D}{k} = \left\{ 0.60 + \frac{0.387 Ra_D^{1/6}}{\left[1 + (0.559/Pr)^{9/16}\right]^{8/27}} \right\}^2$$

The forced convection coefficients applied during the HAC fire event are computed using the relationships in Table 6-5 of reference [25] for a flat surface, where the characteristic dimension (L) is equal to the length along the surface and the free stream flow velocity is V. The heat transfer coefficient is computed based on the local Reynolds number, where the Reynolds number is defined as:

$$Re_L = \frac{V \times \rho \times L}{\mu}$$

For $Re < 5x10^5$ and $Pr > 0.1$: $Nu = 0.664 \times Re_L^{0.5} \times Pr^{0.33}$

For $Re > 5x10^5$ and $Pr > 0.5$: $Nu = 0.036 \times Pr^{0.33} \times \left[Re_L^{0.8} - 23{,}200\right]$

Given the turbulent nature of the 30-minute fire event, a characteristic length of 0.25 feet is used for all surfaces to define the probable limited distance for boundary growth. Figure 3.5-14 presents an illustration of the level of convective heat transfer coefficient predicted by the above equation during the HAC transient.

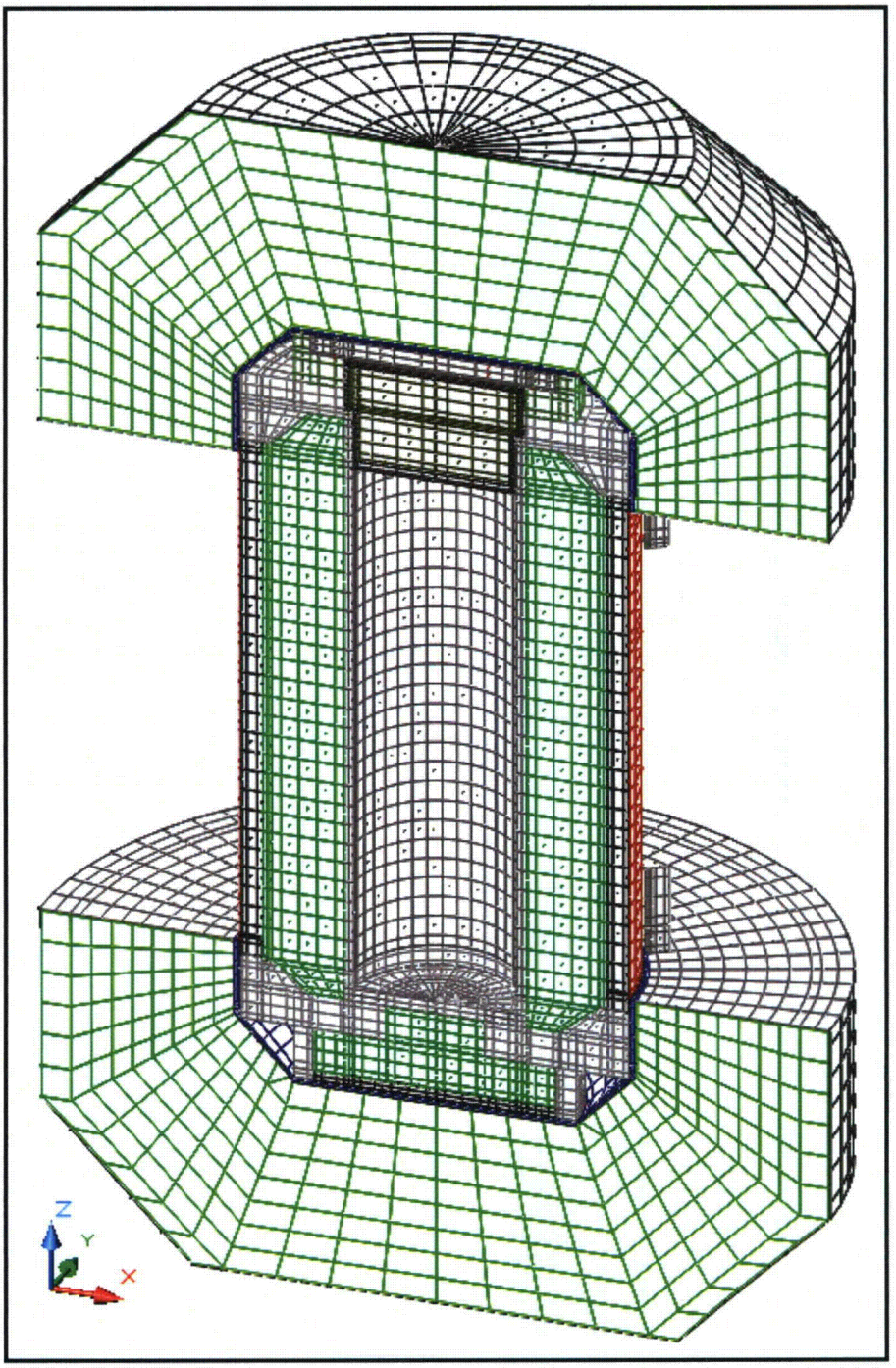

Figure 3.5-1 – Isometric View of 'Solids' Thermal Model for BRR Packaging

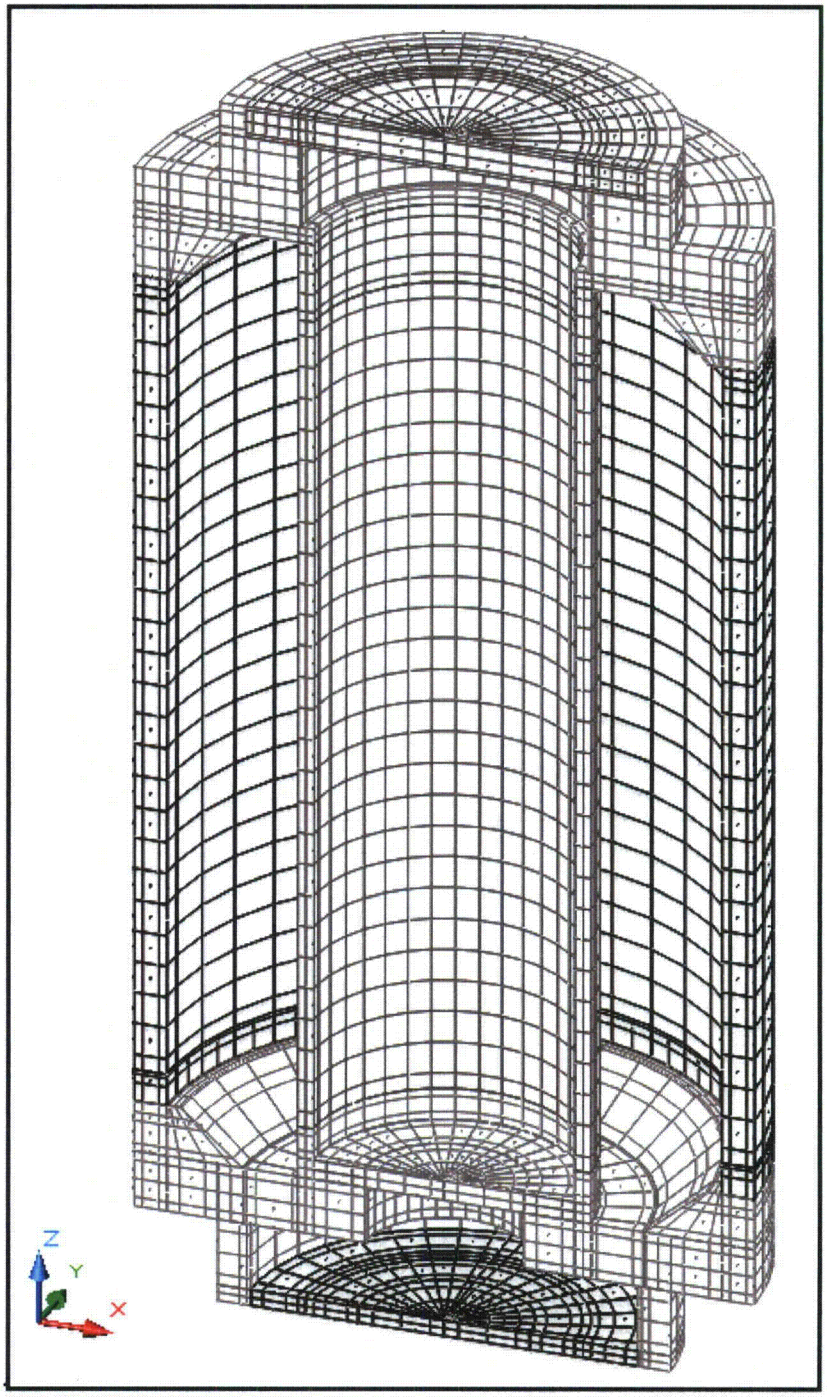

Figure 3.5-2 – Isometric View of 'Solids' Thermal Model for Inner/Outer Shells and Upper/Lower Structures

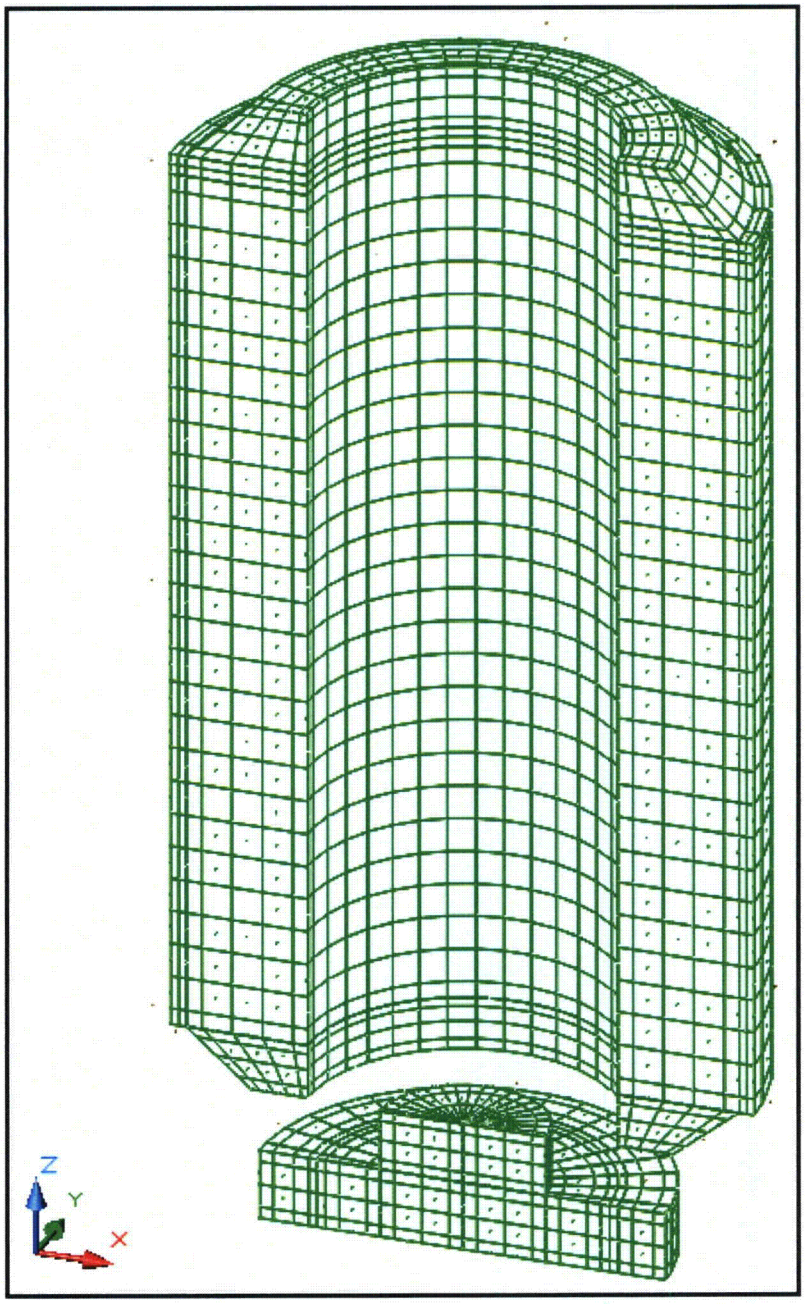

Figure 3.5-3 – Isometric View of 'Solids' Thermal Model for Cask Lead Sections

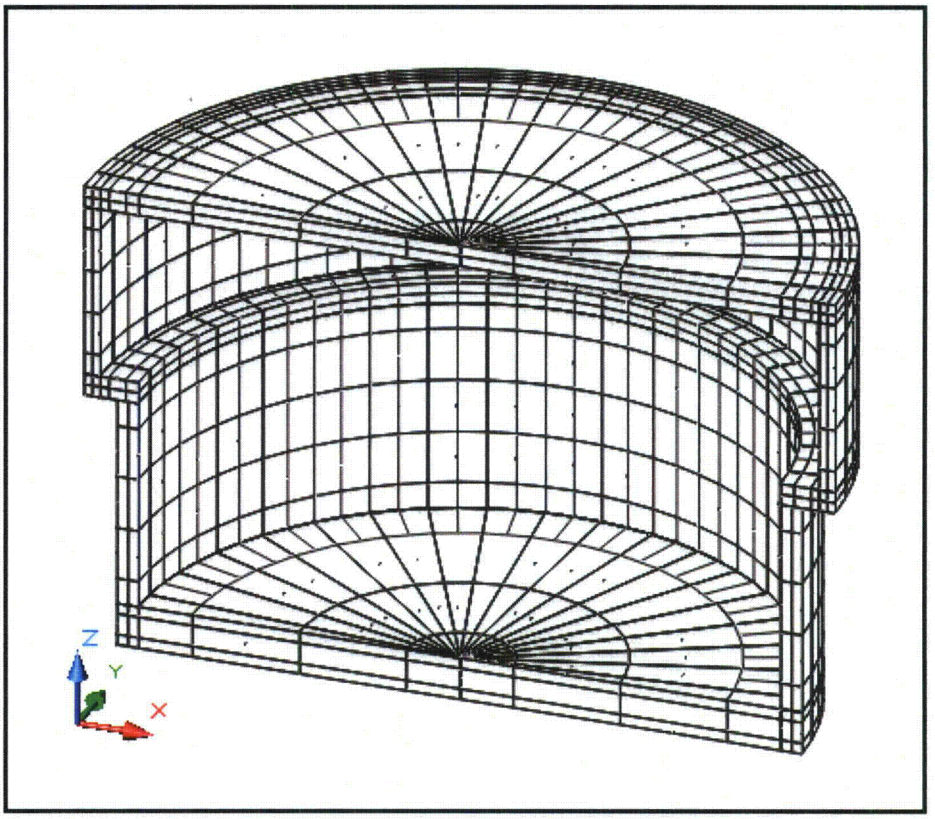

Figure 3.5-4 – Isometric View of 'Solids' Thermal Model for Shield Plug Shell

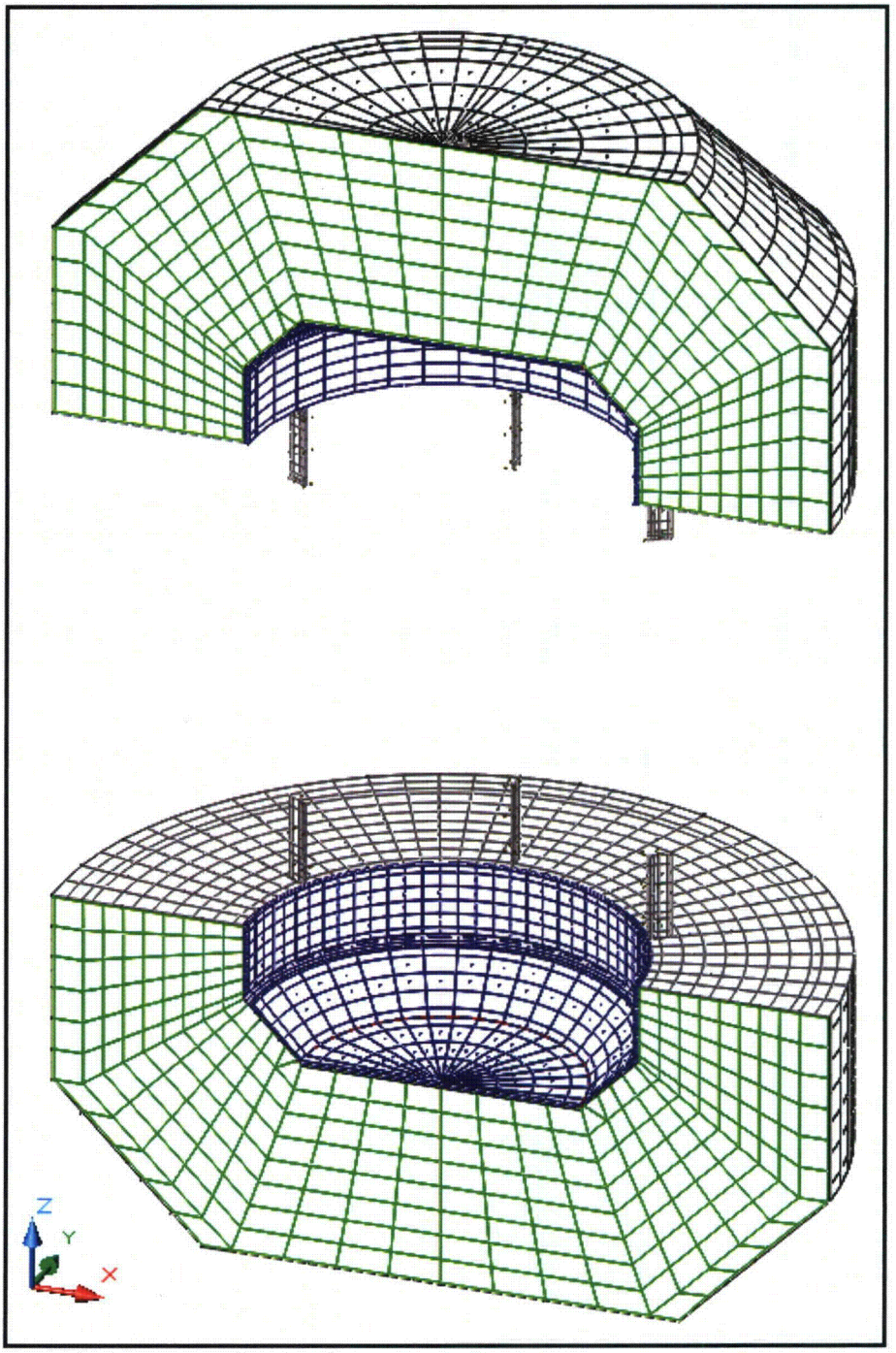

Figure 3.5-5 – Isometric View of 'Solids' Thermal Model for Impact Limiters

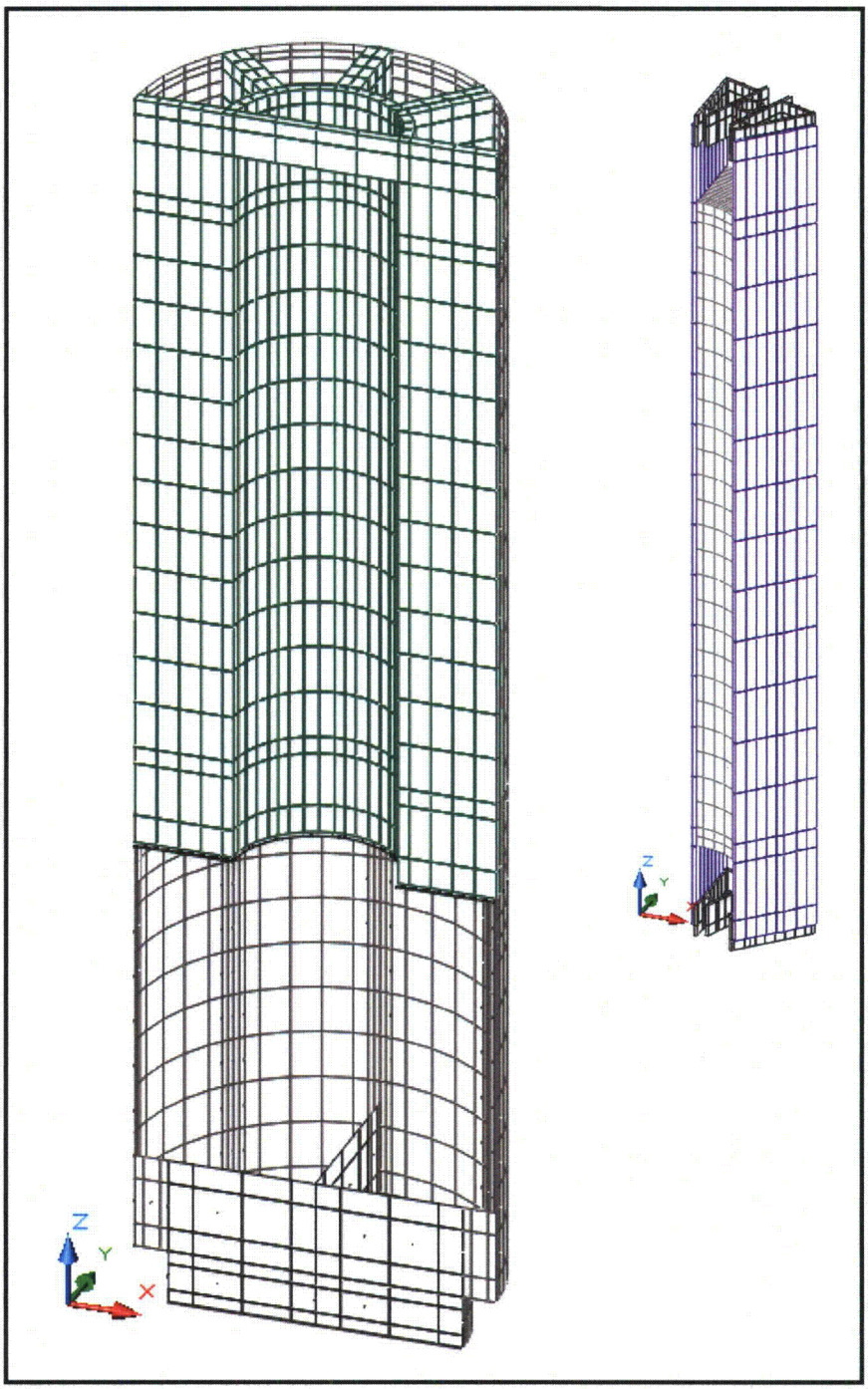

Figure 3.5-6 – Isometric View of 'Solids' Thermal Model for MURR Fuel Basket and Element

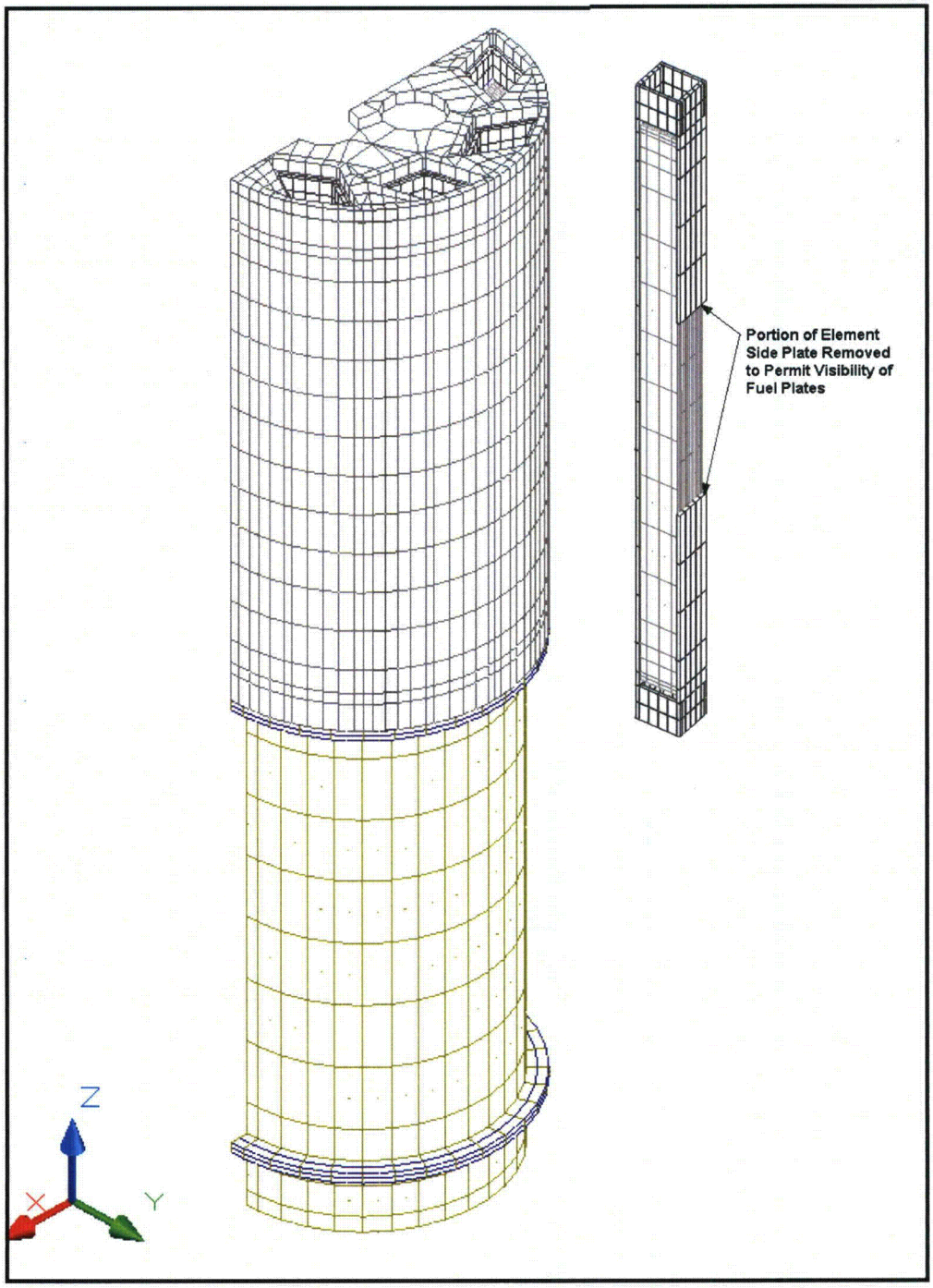

Figure 3.5-7 – Isometric View of 'Solids' Thermal Model for MITR-II Fuel Basket and Element

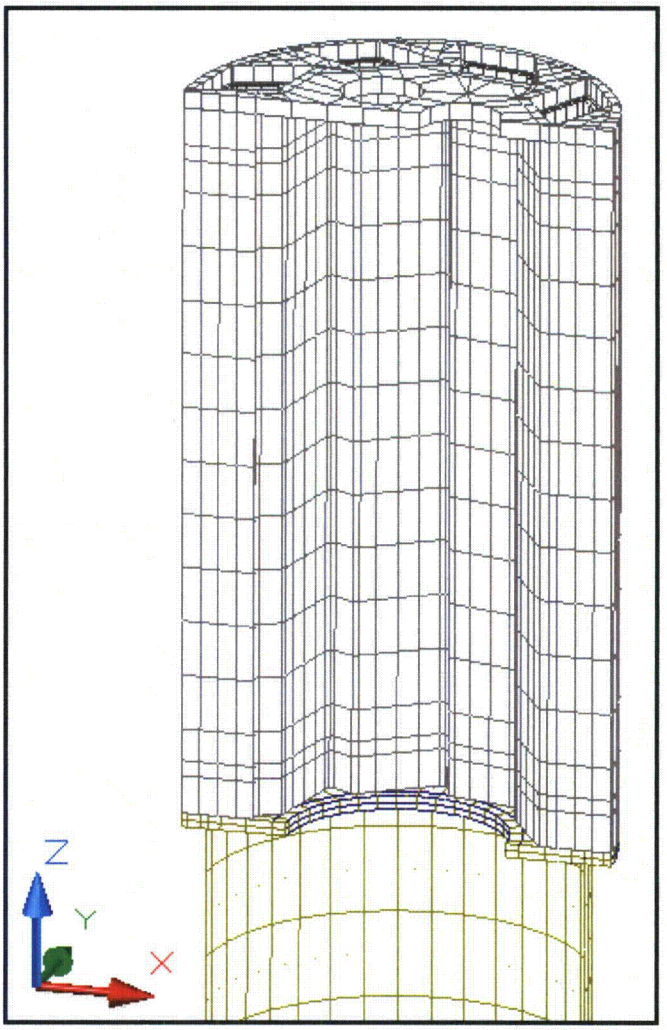

Figure 3.5-8 – Isometric View of Internal MITR-II Basket Model

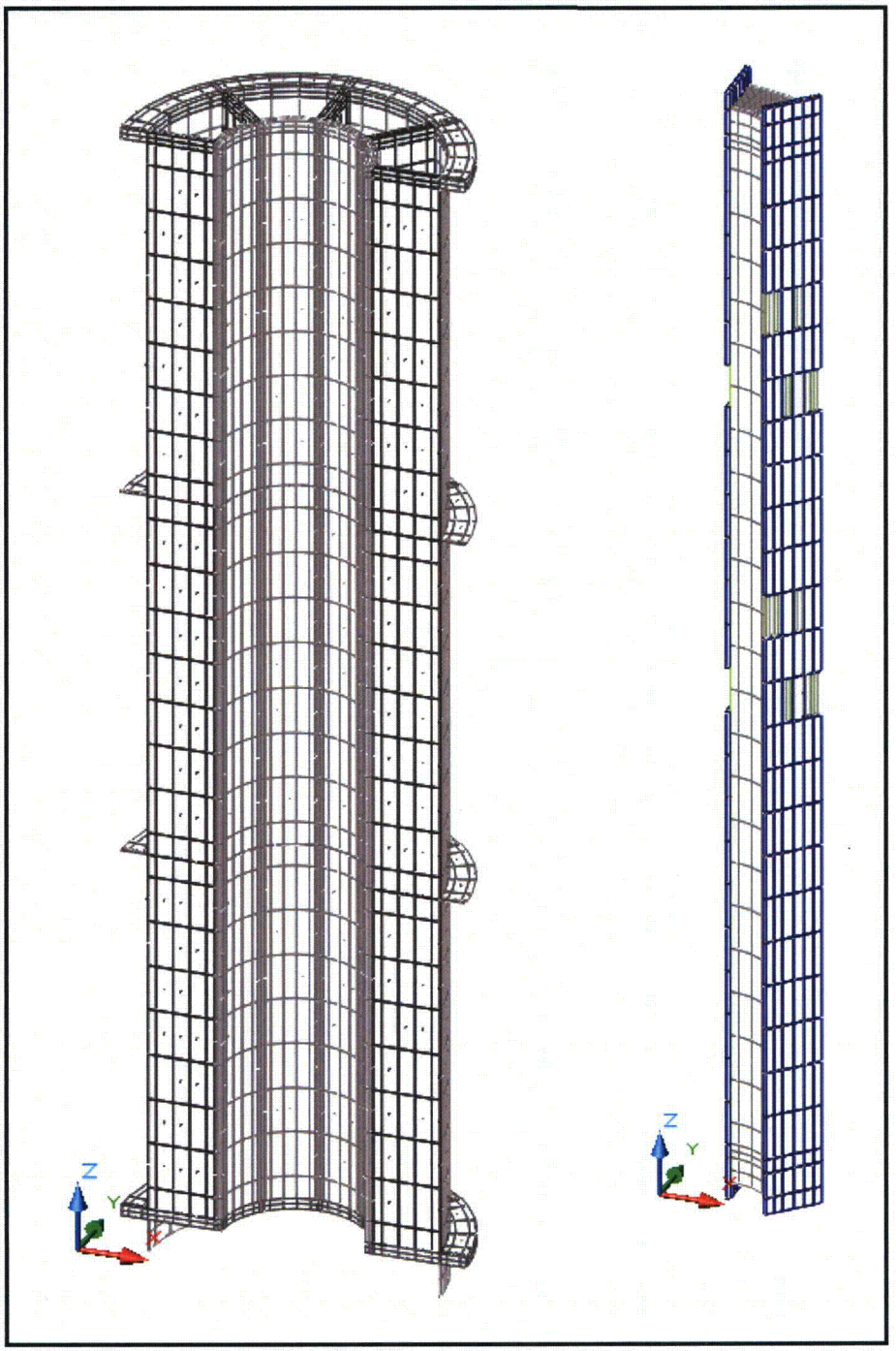

Figure 3.5-9 – Isometric View of 'Solids' Thermal Model for ATR Fuel Basket and Element

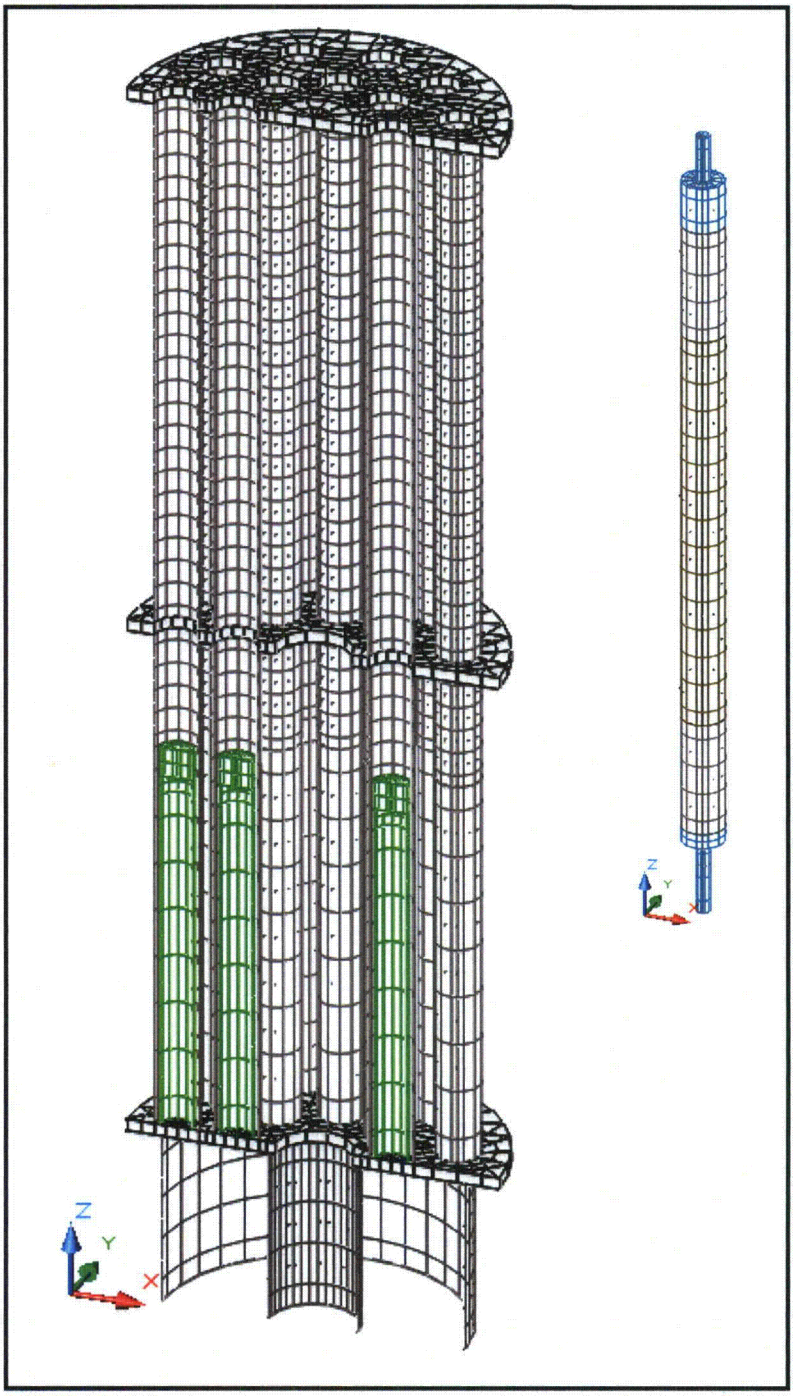

Figure 3.5-10 – Isometric View of 'Solids' Thermal Model for TRIGA Fuel Basket and Element

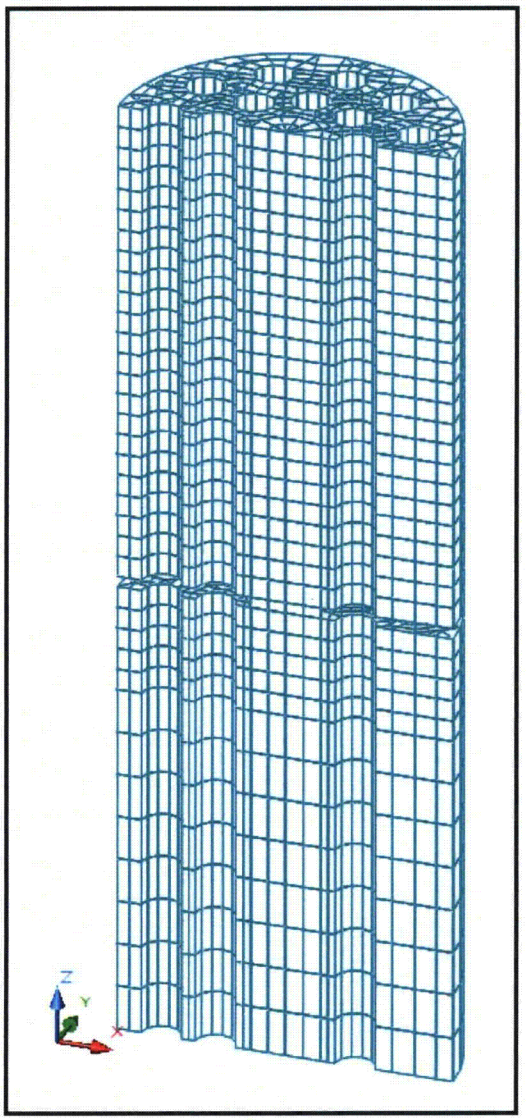

Figure 3.5-11 – Isometric View of 'Void Space' Modeling for TRIGA Basket

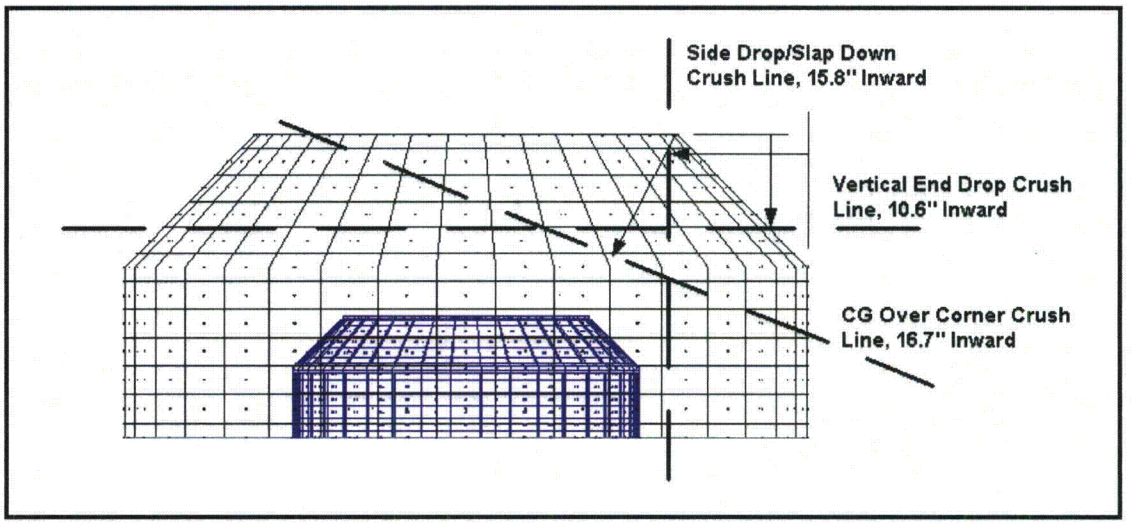

Figure 3.5-12 – Impact Limiter HAC Drop Crush Distances

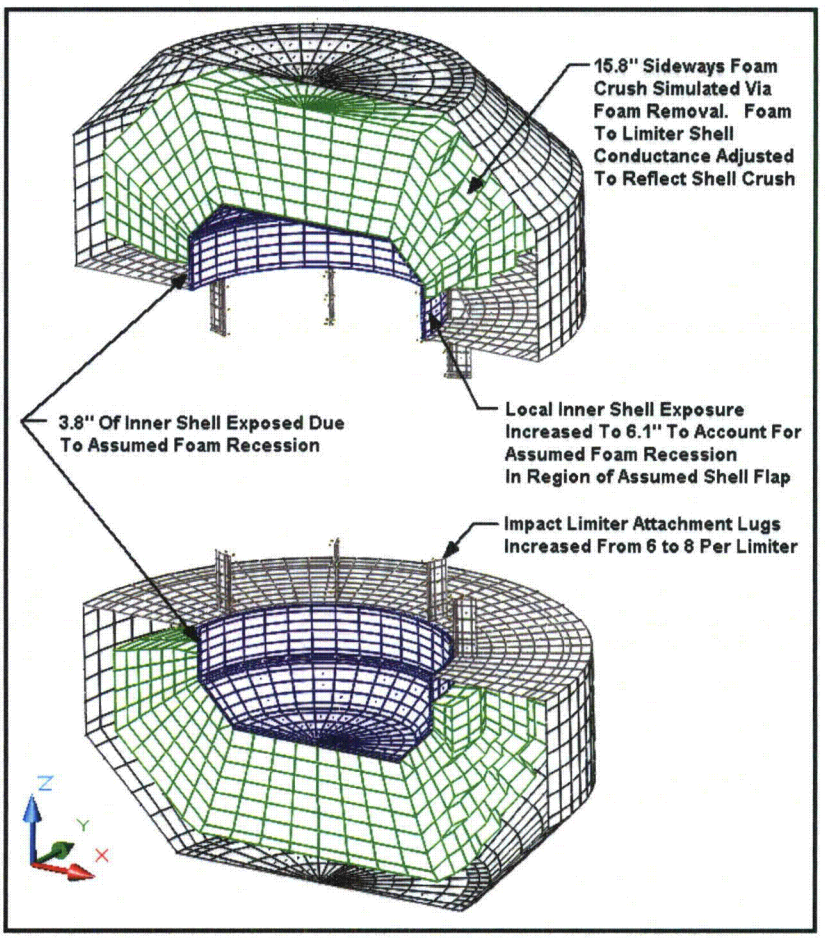

Figure 3.5-13 – Simulated HAC Damage to Impact Limiters

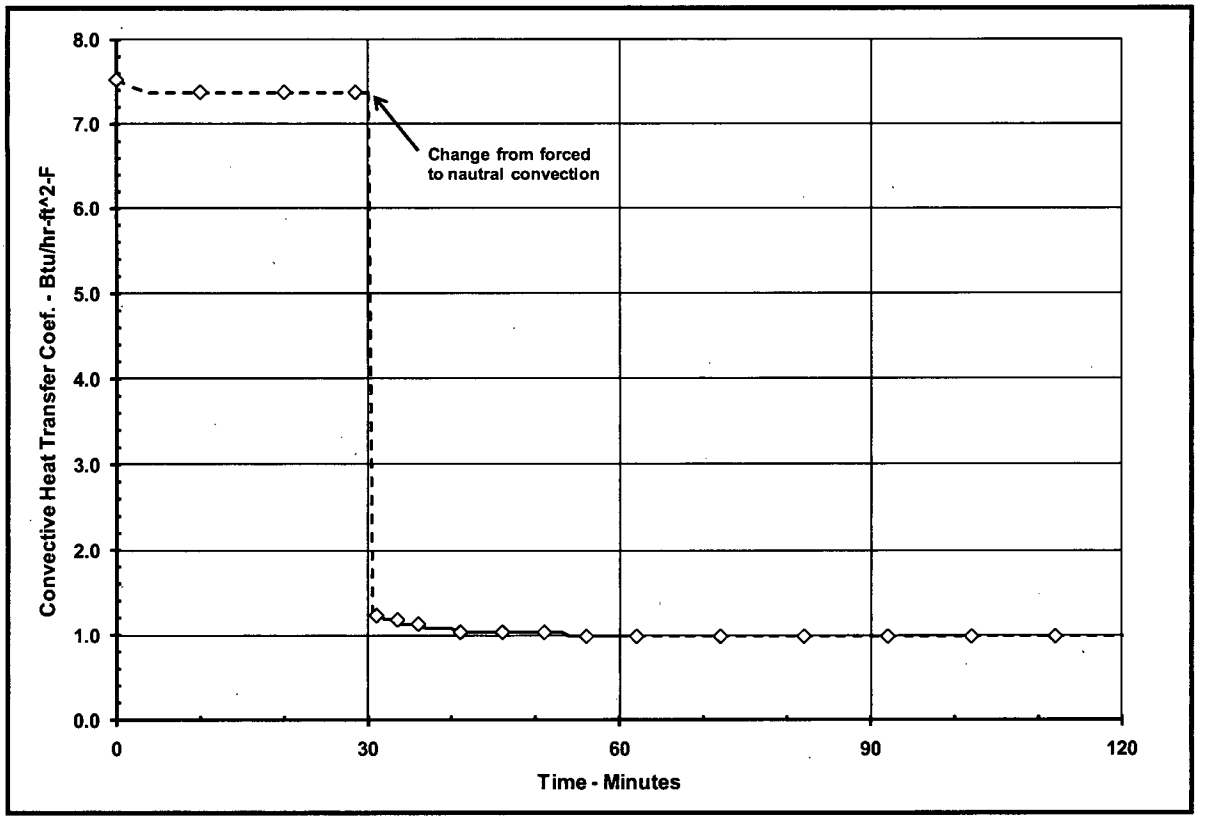

Figure 3.5-14 – Convection Coefficient Variation During HAC Transient

3.5.3.9 Determination of Composite Thermal Properties for Fuel Plates

Thermal Properties for ATR Fuel Plates

The ATR fuel plates are a composite material consisting of a fissile fuel matrix sandwiched within aluminum cladding. For the purposes of this calculation, the fuel composite is treated as a homogenous material with lumped thermal properties as defined below. This modeling approach is justified since the thermal gradient within the fuel element will be very low given that the un-irradiated fuel has essentially no decay heat.

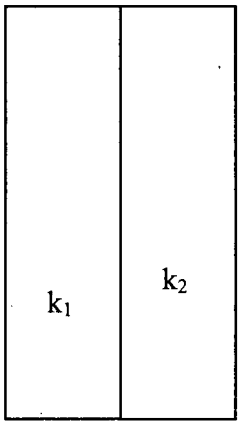

Because of the thinness of the plates, the average conductivity is required only for the axial and circumferential direction. Conductivity through the plates is not required as this analysis assumes a zero temperature gradient in that direction. Mean density and specific heat values are also defined below.

Circumferential and Axial Conductivity

Ignoring the affect of curvature, the heat flow can be written as,

$$q = -\Delta x \Delta z\, \bar{k} \frac{\Delta T}{\Delta y} = -\Delta x_1 \Delta z\, k_1 \frac{\Delta T}{\Delta y} - \Delta x_2 \Delta z\, k_2 \frac{\Delta T}{\Delta y}$$

where $\Delta x = \sum_i \Delta x_i$

From which, $\bar{k} = \dfrac{\Delta x_1 k_1 + \Delta x_2 k_2}{\Delta x}$

Mean Density

The mean density of the fuel plates is computed from:

$$Mass = \Delta x \Delta y \Delta z\, \bar{\rho} = \Delta x_1 \Delta y \Delta z\, \rho_1 + \Delta x_2 \Delta y \Delta z\, \rho_2, \text{ from which } \bar{\rho} = \frac{\Delta x_1 \rho_1 + \Delta x_2 \rho_2}{\Delta x}$$

Mean Specific Heat

In the same manner used to define the mean density, the mean specific heat for the fuel plates is computed as;

$$\bar{\rho}\, \bar{c}_p \Delta x \Delta y \Delta z = \rho_1 c_{p_1} \Delta x_1 \Delta y \Delta z + \rho_2 c_{p_2} \Delta x_2 \Delta y \Delta z, \text{ from which, } \bar{c}_p = \frac{\rho_1 c_{p_1} \Delta x_1 + \rho_2 c_{p_2} \Delta x_2}{\bar{\rho} \Delta x}$$

The thermal properties for the individual plates making up the ATR fuel element are computed using the above approach and thermophysical [5] and geometric data [14] for the ATR fuel element.

Based on these data sources, the radius of the inner plate is 3.015 inches, while the radius of the outer plate is 5.44 inches. The gap between the plates is 0.078 inches. The thickness of the aluminum cladding is 0.015 inches.

While the thermal properties for the aluminum cladding and the fissile fuel matrix material will vary with temperature, for the purposes of this evaluation, fixed material properties are assumed in order to simplify the calculation. To provide conservatism for this modeling approach, conservatively low value is assumed for the specific heat for each component, while a conservatively high thermal conductivity value is used. This methodology will result in over-predicting the temperature rise within the composite material during the HAC fire event.

The thermal properties used in this calculation are:

1) Aluminum cladding thermal conductivity = 191 W/m-K, conservatively high value from [5], page 18
2) Fissile fuel matrix (UAl_x) = 14.47 W/m-K, conservatively high based on equation 2.3 from [5], at 300K
3) Aluminum cladding density = 2702 kg/m^3, from [5], page 16
4) Fissile fuel matrix (UAl_x) density = 3680 kg/m^3, from [5], Table 2.5, average density
5) Aluminum cladding specific heat = 1034 J/kg-K, from [5], Table 3.2, mean value at 600K
6) Fissile fuel matrix (UAl_x) specific heat = 708 J/kg-K, from [5], Table 2.4, average value at 600K

Table 3.5-1 presents the composite thermal conductivity, specific heat, and density values for each of the nineteen (19) fuel plates making up the ATR fuel element. These composite values are based on the thermal property values given above and the geometry depicted in Figure 3.5-15.

Thermal Properties for MIT Fuel Plates

Like the ATR fuel, the MIT fuel plates are a composite material consisting of a fissile fuel matrix sandwiched within an aluminum cladding. The thermal properties for the plates making up the MIT fuel element are computed using the same approach described above for the ATR fuel and the data contained in [5] and [13]. The plates have a thickness of 0.08 inches and a width of 2.526 inches. The nominal gap between the plates is 0.078 inches. Since the aluminum cladding contains 110 grooves on each side of the plate, the effective thickness of the cladding is reduced from 0.025 inches to 0.02 inches.

Table 3.5-2 presents the composite thermal conductivity, specific heat, and density values for the fifteen (15) fuel plates making up the MIT fuel element. These composite values are based on the thermal property values provided above for the ATR fuel element and the geometry described in Table 3.5-2 and depicted in Figure 3.5-16.

Thermal Properties for MURR Fuel Plates

The MURR fuel plates are also a composite of a fissile fuel matrix sandwiched within an aluminum cladding. The thermal properties for the MURR fuel element are computed using the

same approach described above for the ATR fuel and the data contained in [5] and [12]. The inner plate has an inner radius of 2.77 inches and an arc length of 1.993 inches, while the outer plate has an inner radius of 5.76 inches and an arc length of 4.342 inches. The nominal gap between the plates is 0.08 inches. The thickness of the aluminum cladding is 0.01 inches.

Table 3.5-3 presents the composite thermal conductivity, specific heat, and density values for the twenty four (24) fuel plates making up the MURR fuel element. These composite values are based on the thermal property values provided above for the ATR fuel element and the geometry described in Table 3.5-3 and depicted in Figure 3.5-17.

Thermal Properties for TRIGA Fuel Element

The cladding thickness for the TRIGA fuel is relatively thin and the fuel's thermal properties are dominated by the homogenous properties for the uranium-zirconium hydride fuel and the graphite materials. As such, composite properties are not required. Instead, the thermal properties listed in Table 3.2-2 for the uranium-zirconium hydride fuel and the graphite are used directly in the thermal model.

Table 3.5-1 – Composite ATR Fuel Plate Thermal Properties

Plate	Plate Thickness, in	UAlx Thickness, in	Axial & Circumferential Conductivity (W/m-K)	Inner radius, in	Outer radius, in	Mean radius, in	Mean density, kg/m^3	Mean specific heat, J/(kg K)
1	0.08	0.05	80.7	3.015	3.095	3.055	3313.3	807.7
2	0.05	0.02	120.4	3.173	3.223	3.198	3093.2	878.9
3	0.05	0.02	120.4	3.301	3.351	3.326	3093.2	878.9
4	0.05	0.02	120.4	3.429	3.479	3.454	3093.2	878.9
5	0.05	0.02	120.4	3.557	3.607	3.582	3093.2	878.9
6	0.05	0.02	120.4	3.685	3.735	3.710	3093.2	878.9
7	0.05	0.02	120.4	3.813	3.863	3.838	3093.2	878.9
8	0.05	0.02	120.4	3.941	3.991	3.966	3093.2	878.9
9	0.05	0.02	120.4	4.069	4.119	4.094	3093.2	878.9
10	0.05	0.02	120.4	4.197	4.247	4.222	3093.2	878.9
11	0.05	0.02	120.4	4.325	4.375	4.350	3093.2	878.9
12	0.05	0.02	120.4	4.453	4.503	4.478	3093.2	878.9
13	0.05	0.02	120.4	4.581	4.631	4.606	3093.2	878.9
14	0.05	0.02	120.4	4.709	4.759	4.734	3093.2	878.9
15	0.05	0.02	120.4	4.837	4.887	4.862	3093.2	878.9
16	0.05	0.02	120.4	4.965	5.015	4.990	3093.2	878.9
17	0.05	0.02	120.4	5.093	5.143	5.118	3093.2	878.9
18	0.05	0.02	120.4	5.221	5.271	5.246	3093.2	878.9
19	0.1	0.07	67.4	5.349	5.449	5.399	3386.6	786.0

Table 3.5-2 – Composite MIT Fuel Plate Thermal Properties

Plate	Plate Thickness, in	UAlx Thickness, in	Axial and Circumferential Conductivity (W/m-K)	Plate Width, in	Mean density, kg/m^3	Mean specific heat, J/(kg K)
1 to 15	0.08*	0.03	115.3	2.314	3121.1	869.3

* - mean plate thickness estimated at 0.07 inches after allowance for ribbing

Table 3.5-3 – Composite MURR Fuel Plate Thermal Properties

Plate	Plate Thickness, in	UAlx Thickness, in	Axial and Circumferential Conductivity (W/m-K)	Inner radius, in	Outer radius, in	Plate Arc Length, in	Mean density, kg/m^3	Mean specific heat, J/(kg K)
1	0.05	0.03	85.1	2.77	2.82	1.993	3288.8	815.1
2	0.05	0.03	85.1	2.9	2.95	2.095	3288.8	815.1
3	0.05	0.03	85.1	3.03	3.08	2.197	3288.8	815.1
4	0.05	0.03	85.1	3.16	3.21	2.300	3288.8	815.1
5	0.05	0.03	85.1	3.29	3.34	2.402	3288.8	815.1
6	0.05	0.03	85.1	3.42	3.47	2.504	3288.8	815.1
7	0.05	0.03	85.1	3.55	3.6	2.606	3288.8	815.1
8	0.05	0.03	85.1	3.68	3.73	2.708	3288.8	815.1
9	0.05	0.03	85.1	3.81	3.86	2.810	3288.8	815.1
10	0.05	0.03	85.1	3.94	3.99	2.912	3288.8	815.1
11	0.05	0.03	85.1	4.07	4.12	3.014	3288.8	815.1
12	0.05	0.03	85.1	4.2	4.25	3.116	3288.8	815.1
13	0.05	0.03	85.1	4.33	4.38	3.218	3288.8	815.1
14	0.05	0.03	85.1	4.46	4.51	3.321	3288.8	815.1
15	0.05	0.03	85.1	4.59	4.64	3.423	3288.8	815.1
16	0.05	0.03	85.1	4.72	4.77	3.525	3288.8	815.1
17	0.05	0.03	85.1	4.85	4.9	3.627	3288.8	815.1
18	0.05	0.03	85.1	4.98	5.03	3.729	3288.8	815.1
19	0.05	0.03	85.1	5.11	5.16	3.831	3288.8	815.1
20	0.05	0.03	85.1	5.24	5.29	3.933	3288.8	815.1
21	0.05	0.03	85.1	5.37	5.42	4.035	3288.8	815.1
22	0.05	0.03	85.1	5.5	5.55	4.137	3288.8	815.1
23	0.05	0.03	85.1	5.63	5.68	4.239	3288.8	815.1
24	0.05	0.03	85.1	5.76	5.81	4.342	3288.8	815.1

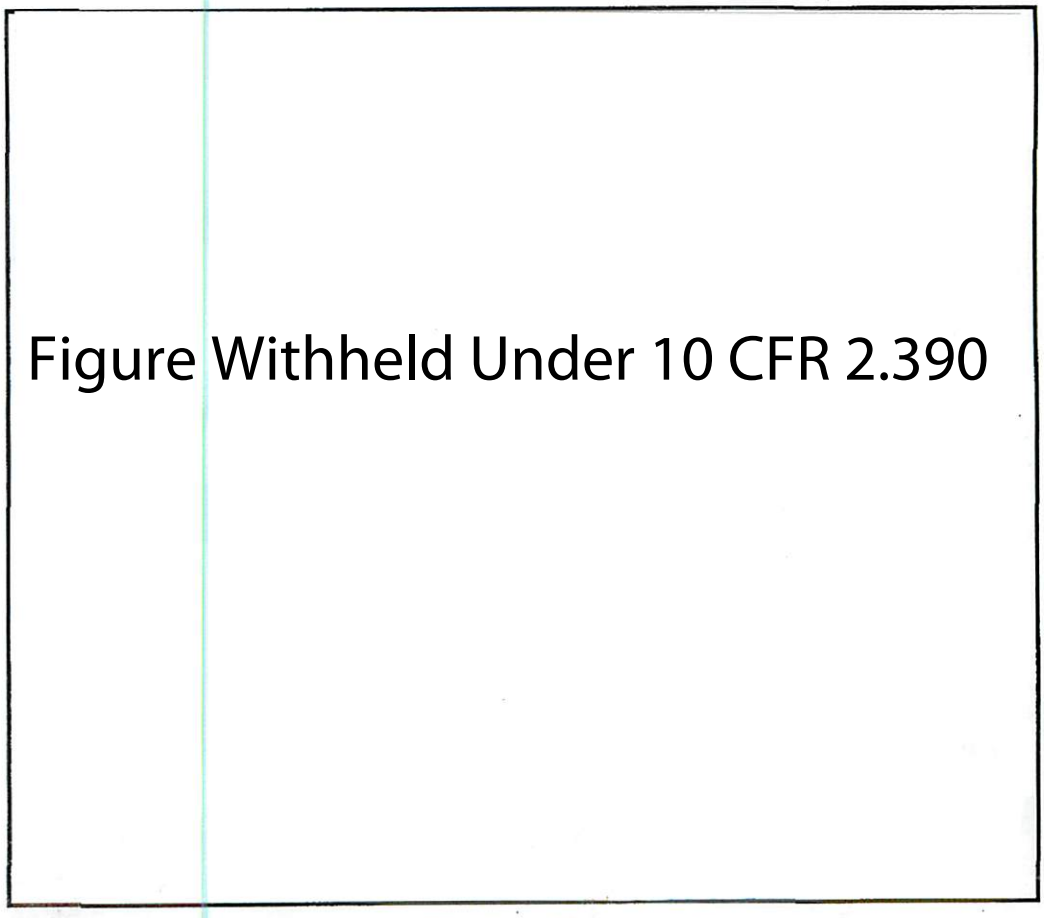

Figure 3.5-15 – ATR Fuel Element Cross Section

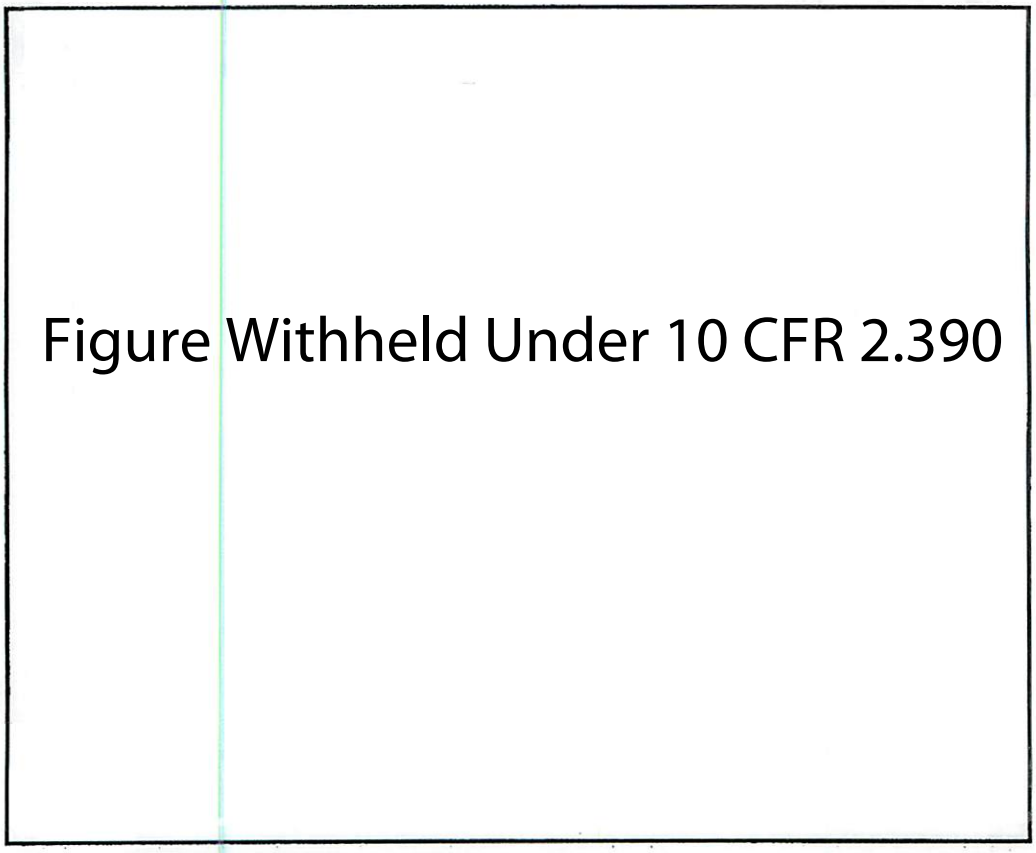

Figure 3.5-16 – MIT Fuel Element Cross Section

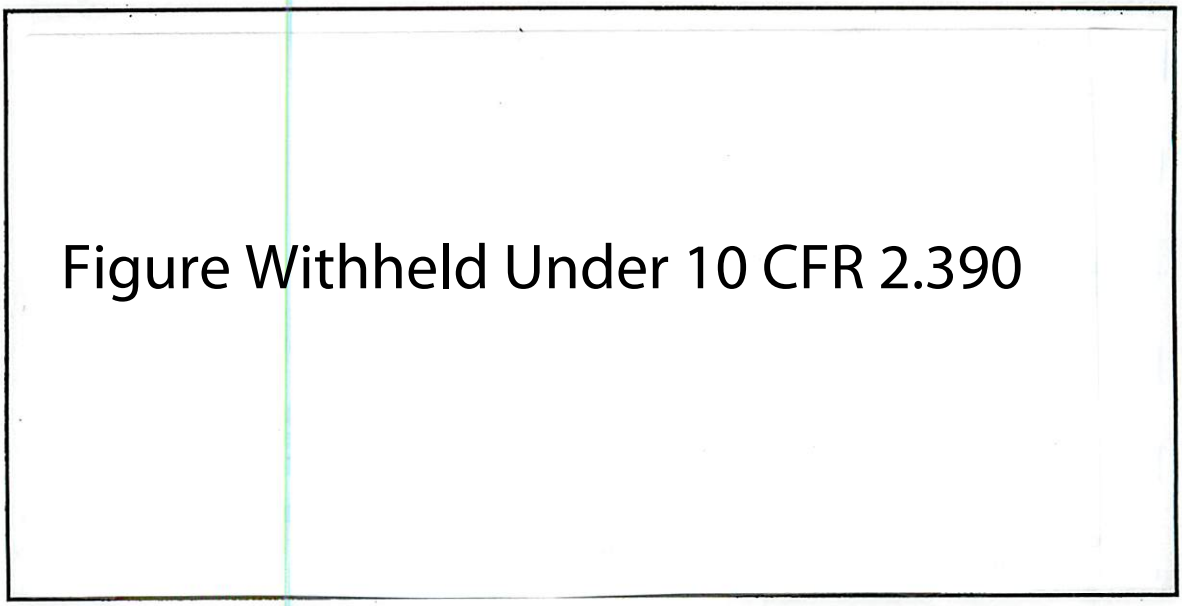

Figure 3.5-17 – MURR Fuel Element Cross Section

3.5.4 'Last-A-Foam' Response under HAC Conditions

The General Plastics LAST-A-FOAM® FR-3700 rigid polyurethane foam [18] used in the impact limiters has been used for numerous transportation packages. The FR-3700 formulation is specially designed to allow predictable impact-absorption performance under dynamic loading, while also providing a significant level of thermal protection under the HAC conditions. Upon exposure to fire temperatures, this proprietary foam decomposes into an intumescent char that swells and tends to fill voids or gaps created by free drop or puncture bar damage. This thermal decomposition absorbs a significant amount of the heat transferred into the foam, which is then expelled from the impact limiters as a high temperature gas. Because the char has no appreciable structural capacity and will not develop unless there is space available, the char will not generate stresses within the adjacent package components. Without available space the pyrolysis gases developed as a result of the charring process will move excess char mass out through the vent ports and prevent its buildup. Only as the charring process continues and space becomes available will the char be retained, filling the available space and plugging holes at the surface of the impact limiters. The thermal decomposition process does not alter or cause a chemical reaction within the adjacent materials.

The mechanisms behind the observed variations in the thermal properties and behavior of the FR-3700 foam at elevated temperatures are varied and complex. A series of fire tests [27 and 28] conducted on 5-gallon cans filled with FR-3700 foam at densities from 6.7 to 25.8 lb/ft^3 helped define the expected performance of the foam under fire accident conditions. Under the referenced fire tests, one end of the test article was subjected to an open diesel fueled burner flame at temperatures of 980 to 1,200°C (1,800 to 2,200 °F) for more than 30 minutes. A thermal shield prevented direct exposure to the burner flame on any surface of the test article other than the hot face. Each test article was instrumented with thermocouples located at various depths in the foam. In addition, samples of the foam were subjected to thermogravimetric analysis (TGA) to determine the thermal decomposition vs. temperature. The exposure temperatures for the TGA tests varied from 70 to 1,500 °F, and were conducted in both air and nitrogen atmospheres. The result for the nitrogen environment (see Figure 3.5-18) is more representative of the low oxygen environment existing within the impact limiter shells encasing the foam. These test results indicate that the following steps occur in the thermal breakdown of the foam under the level of elevated temperatures reached during the HAC fire event:

- Below 250 °F, the variation in foam thermal properties with temperature is slight and reversible. As such, fixed values for specific heat and thermal conductivity are appropriate.
- Between 250 and 500 °F, small variations in foam thermal properties occur as water vapor and non-condensable gases are driven out of the foam. As such, fixed values for specific heat and thermal conductivity are also appropriate for this temperature range. Further, the observed changes are so slight that the same thermal properties used for temperatures below 250 °F may also be used to characterize the thermal performance of the foam between 250 and 500 °F.
- Irreversible thermal decomposition of the foam begins as the temperature rises above 500 °F and increases non-linearly with temperature. Based on the TGA testing (see

Figure 3.5-18), approximately 2/3's of this decomposition occurs over a narrow temperature range centered about 670 °F.

- The decomposition is accompanied by vigorous out-gassing from the foam and an indeterminate amount of internal heat generation. The internal heat generation arises from the gases generated by the decomposition process that are combustible under piloted conditions. However, since the decomposition process is endothermic, the foam will not support combustion indefinitely. Further, the out-gassing process removes a significant amount of heat from the package via mass transport.
- The weight loss due to out-gassing not only has direct affect on the heat flux into the remaining virgin foam, but changes the composition of the resulting foam char since the foam constituents are lost at different rates. This change in composition affects both the specific heat and the thermal conductivity of the foam char layer.
- As temperature continues to rise, the developing char layer begins to take on the characteristics of a gas-filled cellular structure where radiative interchange from one cell surface to another becomes the dominant portion of the overall heat transfer mechanism. This change in heat transfer mechanisms causes the apparent heat conductivity to take on a highly non-linear relationship with temperature.
- Finally, at temperatures above 1,250 °F, the thermal breakdown of the foam is essentially completed and only about 5 to 10% of the original mass is left. In the absence of direct exposure to a flame or erosion by the channeling of the outgas products through the foam, the char layer will be the same or slightly thicker than the original foam depth. This char layer will continue to provide radiative shielding to the underlying foam material.

Since the thermal decomposition of the foam is an endothermic process, the foam is self-extinguishing and will not support a flame once the external flame source is removed. However, the gases generated by the decomposition process are combustible and will burn under piloted conditions. A portion of these generated gases can remain trapped within the charred layer of the foam after the cessation of the HAC fire event and continue to support further combustion, although at a much reduced level, until a sufficient time has passed for their depletion from the cell structure. This extended time period is typically from 15 to 45 minutes.

The sharp transition in the state of the foam noted in Figure 3.5-18 at or about 670 °F can be used to correlate the observed depth of the foam char following a burn test with the occurrence of this temperature level within the foam. The correlation between the foam recession depth and the foam density, as compiled from a series of tests, is expressed by the relation:

$$y = -0.94581 - 11.64 \times \log_{10}(x)$$

where, y = the recession depth, cm

x = foam density (g/cm^3)

Based on this correlation, the recession depth expected for the nominal 9 pcf density foam used in the packaging is estimated to be 3.5 inches. The loss of foam could increase to a depth of approximately 3.8 inches for foam fabricated at the low end of the density tolerance (i.e., 7.65 pcf).

It should be noted that these results assume that the foam is enclosed within a steel shell with surface openings that are approximately 0.3 ft^2 or smaller. The presence of the steel enclosure helps shield the foam from the heat flux of a HAC fire event and helps contain the foam char that is generated. Test results with and without a steel interface between the foam and the heat source indicates that the foam loss could be an additional 1.5 inches for the 7.65 pcf foam if larger face areas are exposed directly to the fire.

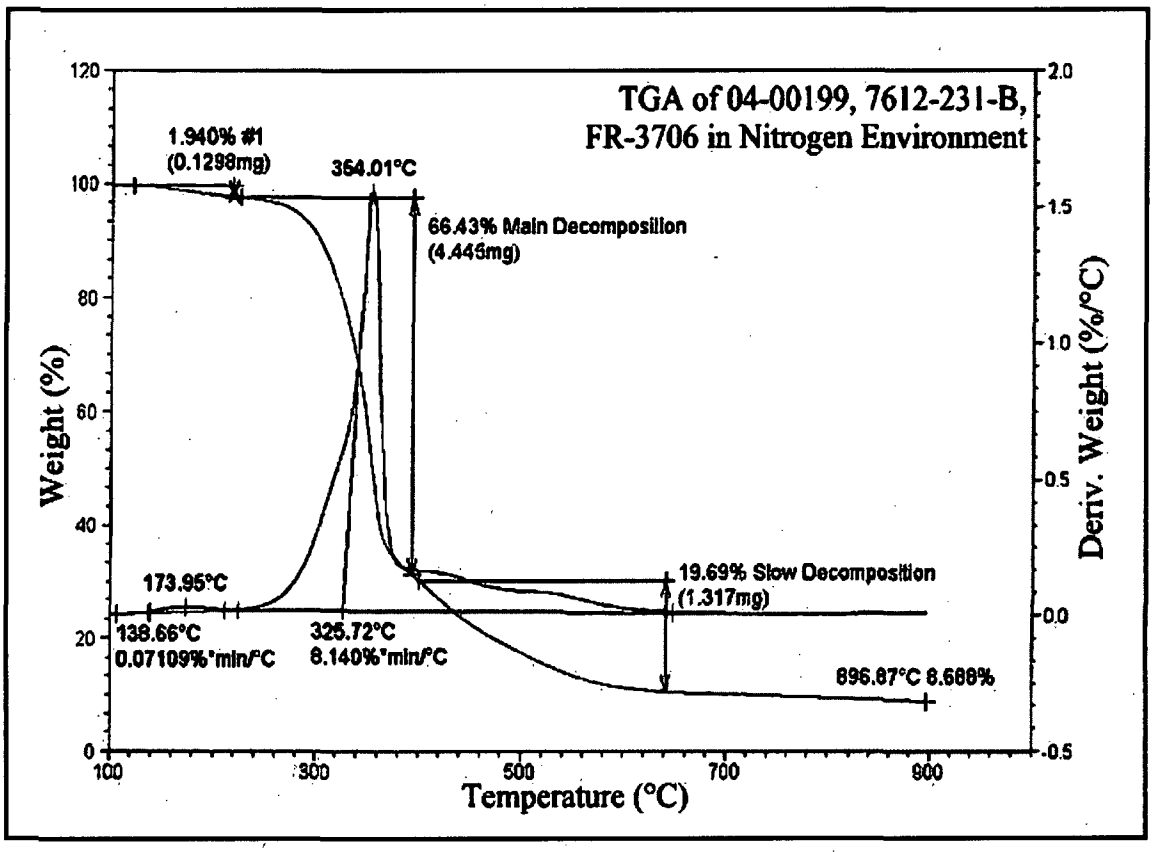

Figure 3.5-18 – TGA Analysis of Foam Decomposition in Nitrogen Environment

4.0 CONTAINMENT

4.1 Description of the Containment System

4.1.1 Containment Boundary

The BRR package provides a single level of leaktight containment, defined as a leakage rate of less than 1×10^{-7} reference cubic centimeters per second (ref–cm^3/s), air, per ANSI N14.5 [1]. The containment boundary of the BRR package consists of the following elements. Unless noted, all elements are made of ASTM Type 304 stainless steel in various product forms. A full description of the packaging is given in Section 1.2.1, *Packaging*.

- The lower massive end structure (including the passage to the drain port)
- The inner cylindrical shell
- The upper massive end structure
- The containment O–ring seal (the inner seal in the closure lid; face–type seal made of butyl elastomer)
- The closure lid
- The vent port in the closure lid (closed using a brass port plug, sealed with a butyl sealing washer)
- The drain port in the lower end structure (closed using a brass port plug, sealed with a butyl sealing washer)

The containment boundary is shown in Figure 4.1-1.

4.1.2 Containment Penetrations

Besides the bolted closure lid, there are two containment penetrations: the vent port, located in the closure lid, and the drain port, located in the lower end structure, as described above. Each penetration is designed and tested to ensure leaktight sealing integrity, i.e., a leakage rate not exceeding 1×10^{-7} ref–cm^3/s, per ANSI N14.5.

4.1.3 Seals

The elastomeric portion of the containment boundary is comprised of a nominally 3/8–inch diameter, O–ring face seal located in the inner groove in the closure lid, and seal washer sealing elements (an O–ring integrated with a stainless steel washer) for the vent and drain ports. The seals are made using a butyl elastomer compound suitable for continuous use between the temperatures of -65 °F and 225 °F [2], and capable of much higher temperatures during the HAC fire case transient. Further discussion of the thermal performance capabilities of the butyl rubber seals is provided in Appendix 2.12.7, *Containment Seal Performance Tests*.

Two O–ring seals are provided in the closure lid: the inner seal is containment, and the outer forms an annular space for leakage rate testing of the containment seal. The leakage rate tests used for various purposes are summarized in Section 4.4, *Leakage Rate Tests for Type B Packages*, and described in detail in Chapter 8, *Acceptance Tests and Maintenance Program.*

The O–ring containment seal is retained in the closure lid using a dovetail groove having a depth of 0.284 ± 0.003 inches, or 0.281 – 0.287 inches. The O–ring has a cross sectional diameter of 0.375 ± 0.007 inches, or 0.368 – 0.382 inches. The minimum compression corresponds to the maximum groove depth and the minimum O–ring cross–sectional diameter:

$$C_{Min} = 100 \times \left(1 - \frac{G_{Max}}{D_{Min}} \right) = 22\%$$

where G_{Max} = 0.287 inches and D_{Min} = 0.368 inches. The maximum compression corresponds to the minimum groove depth and the maximum O–ring cross–sectional diameter:

$$C_{Max} = 100 \times \left(1 - \frac{G_{Min}}{D_{Max}} \right) = 26\%$$

where G_{Min} = 0.281 inches and D_{Max} = 0.382 inches. The Parker O–ring Handbook [7] recommends a minimum compression of 16%. The limit for maximum compression is when the O–ring cross-section, adjusted for maximum temperature, fills the cross sectional area of the dovetail groove. This condition occurs for the BRR package closure O–ring at a compression of 31.2%. The compression range of 22% to 26% will therefore provide satisfactory performance of the O–ring during all NCT and HAC.

4.1.4 Welds

All welds used in the containment boundary are full penetration and volumetrically inspected to ensure structural and containment integrity. The welds joining the inner shell to either end structure are ultrasonically inspected in accordance with the ASME Code, Subsection NB, Article NB–5000, and Section V, Article 4 [4]. The weld joining the inner shell and the lower end structure may be optionally radiograph inspected in accordance with the ASME Code, Subsection NB, Article NB–5000, and Section V, Article 2 [3]. All containment boundary welds are inspected by liquid penetrant inspection on the final pass in accordance with the ASME Code, Subsection NB, Article NB–5000, and Section V, Article 6 [5]. All containment boundary welds are confirmed to be leaktight as discussed in Section 8.1.4, *Fabrication Leakage Rate Tests.*

4.1.5 Closure

The closure lid completes the containment boundary, and is attached to the cask body using (12) 1-8 UNC socket head cap screws tightened to 220 ± 20 ft-lb. As shown in Chapter 2, *Structural Evaluation*, the closure lid cannot become detached by any internal pressure, NCT, or HAC events. The closure lid, including the vent port, is completely covered by the upper impact limiter, which is attached to the cask using eight (8) 1–inch diameter ball lock pins. Similarly, the drain port is covered by the lower impact limiter. Thus, the containment openings cannot be inadvertently opened.

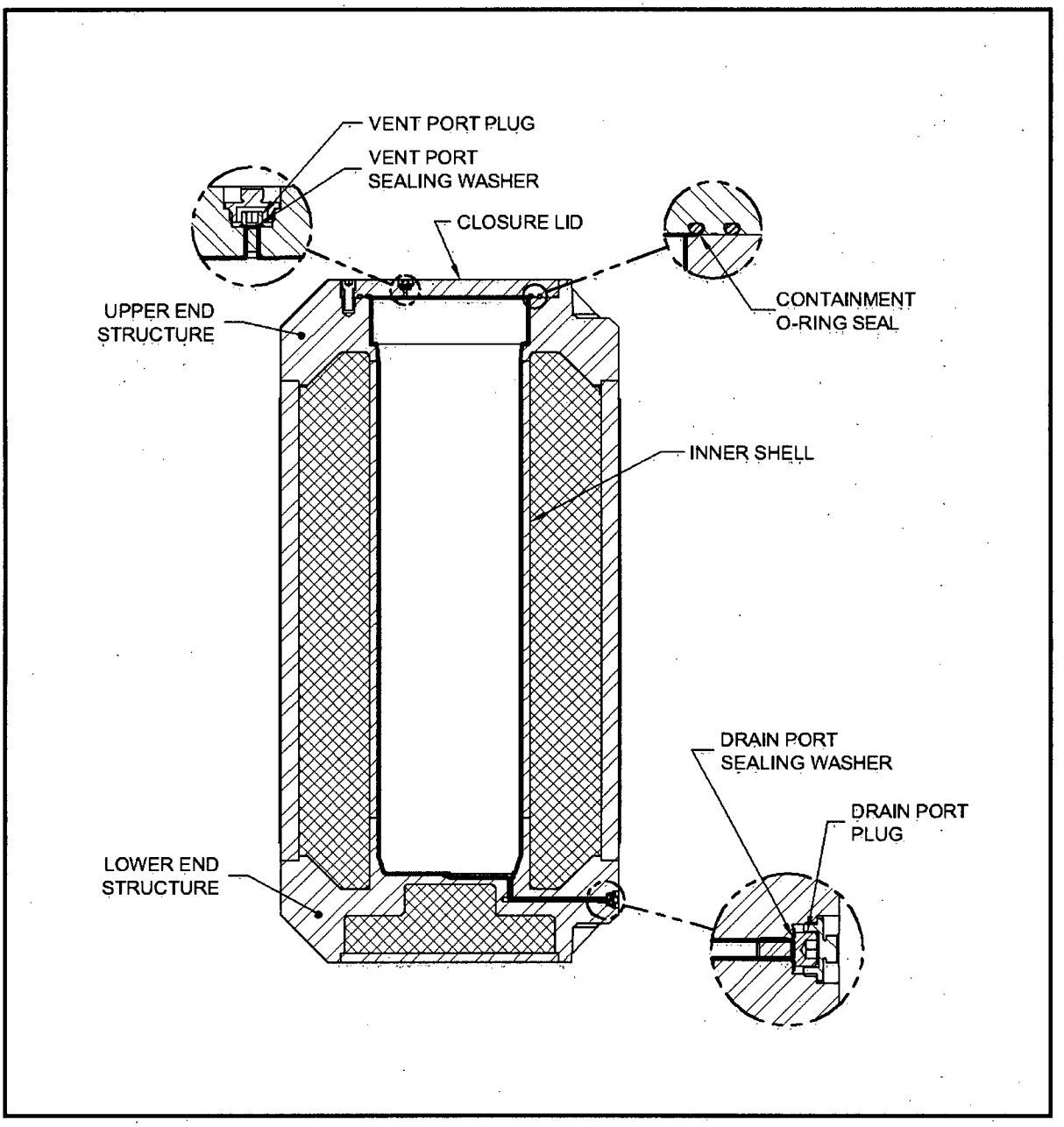

Figure 4.1-1 – BRR Package Containment Boundary

4.2 Containment Under Normal Conditions of Transport

The results of the NCT structural and thermal evaluations presented in Sections 2.6, *Normal Conditions of Transport*, and 3.3, *Thermal Evaluation Under Normal Conditions of Transport*, respectively, demonstrate that there is no release of radioactive materials per the "leaktight" definition of ANSI N14.5 under any of the NCT tests described in 10 CFR §71.71 [6].

4.3 Containment Under Hypothetical Accident Conditions

The results of the HAC structural and thermal evaluations performed in Sections 2.7, *Hypothetical Accident Conditions*, and 3.4, *Thermal Evaluation Under Hypothetical Accident Conditions*, respectively, demonstrate that there is no release of radioactive materials per the "leaktight" definition of ANSI N14.5 under any of the hypothetical accident condition tests described in 10 CFR §71.73.

4.4 Leakage Rate Tests for Type B Packages

4.4.1 Fabrication Leakage Rate Tests

During fabrication, the containment boundary is leakage rate tested as described in Section 8.1.4, *Fabrication Leakage Rate Tests*. The fabrication leakage rate tests are consistent with the guidelines of Section 7.3 of ANSI N14.5. This leakage rate test verifies the containment integrity of the BRR packaging to a leakage rate not to exceed 1×10^{-7} ref–cm^3/s, air.

4.4.2 Maintenance/Periodic Leakage Rate Tests

Annually, or at the time of damaged containment seal replacement or sealing surface repair, the containment O–ring seal and the vent port and drain port sealing washers are leakage rate tested as described in Section 8.2.2, *Maintenance/Periodic Leakage Rate Tests*. The maintenance/periodic leakage rate tests are consistent with the guidelines of Section 7.4 of ANSI N14.5. This test verifies the sealing integrity of the containment seals to a leakage rate not to exceed 1×10^{-7} ref–cm^3/s, air.

4.4.3 Preshipment Leakage Rate Tests

Prior to shipment of the loaded BRR package, the containment O–ring seal and the vent port and drain port sealing washers are leakage rate tested per Section 8.2.2, *Maintenance/Periodic Leakage Rate Tests*. The preshipment leakage rate tests are consistent with the guidelines of Section 7.6 of ANSI N14.5. This test verifies the sealing integrity of the containment seals to a leakage rate not to exceed 1×10^{-7} ref–cm^3/s, air.

4.5 Appendix

4.5.1 References

1. ANSI N14.5–1997, *American National Standard for Radioactive Materials – Leakage Tests on Packages for Shipment*, American National Standards Institute (ANSI), Inc.
2. Rainier Rubber Company, Seattle, WA.
3. American Society of Mechanical Engineers (ASME) Boiler and Pressure Vessel Code, Section III, *Rules for Construction of Nuclear Facility Components*, Division 1 – Subsection NB, *Class 1 Components*, and Section V, *Nondestructive Examination*, Article 2, *Radiographic Examination*, 2007 Edition.
4. American Society of Mechanical Engineers (ASME) Boiler and Pressure Vessel Code, Section III, *Rules for Construction of Nuclear Facility Components*, Division 1 – Subsection NB, *Class 1 Components*, and Section V, *Nondestructive Examination*, Article 4, *Ultrasonic Examination Methods for Welds*, 2007 Edition.
5. American Society of Mechanical Engineers (ASME) Boiler and Pressure Vessel Code, Section III, *Rules for Construction of Nuclear Facility Components*, Division 1 – Subsection NB, *Class 1 Components*, and Section V, *Nondestructive Examination*, Article 6, *Liquid Penetrant Examination*, 2007 Edition.
6. Title 10, Code of Federal Regulations, Part 71 (10 CFR 71), *Packaging and Transportation of Radioactive Material*, 01–01–08 Edition.
7. Parker O–ring Handbook, ORD–5700, Parker-Hannifin Corporation, Cleveland, OH, © 2007.

5.0 SHIELDING EVALUATION

The Battelle Energy Alliance (BEA) Research Reactor (BRR) Package is used to transport spent fuel from a variety of research reactors, including the University of Missouri Research Reactor (MURR), Massachusetts Institute of Technology Research Reactor (MITR-II), Advanced Test Reactor (ATR), and various types of Training, Research, Isotope General Atomics (TRIGA) reactors. The following analyses demonstrate that the BRR Package complies with the external radiation requirements of 10 CFR §71.47 [1]. MCNP5 v1.30 [2] is used to compute the dose rates.

5.1 Description of Shielding Design

5.1.1 Design Features

The principal design features are a lead-filled shield plug, lead-filled side wall, and lead-filled bottom. The top plug consists of approximately 9.5-in lead, with a 1-in stainless steel bottom plate, and 0.5-in stainless steel top plate. The lid is constructed of stainless steel 2-in thick. The lead in the side wall of the cask is 8-in thick. The inner steel shell is 1-in thick, and the outer stainless steel shell is 2-in thick. The cask bottom consists of 7.7-in of lead through the centerline, with a 1-in stainless steel bottom cover plate, and approximately 1.2-in stainless steel inner forging.

The fuel is positioned within one of four custom-designed baskets. The baskets maintain their geometry under normal conditions of transport (NCT) and hypothetical accident conditions (HAC), as demonstrated in Section 2.7.1.5, *Fuel Basket Stress Analysis*, thereby maintaining the location of the source.

5.1.2 Summary Table of Maximum Radiation Levels

Although the dose rates are relatively low and non-exclusive use transportation could be justified, because the cask is heavy and only one cask will be transported per vehicle, exclusive use dose rate limits are applied.

Maximum NCT and HAC dose rates are reported in Table 5.1-1. The fuel type associated with each dose rate is provided in the table. Because the geometry of the source, basket design, and source strength vary widely between the fuel types, no one fuel type may be considered bounding at all dose rate locations.

The cask is transported in a vertical orientation in an open vehicle. Because the transport vehicle is open, the dose rate limit is 200 mrem/hr at both the package and vehicle surfaces. The vehicle is assumed to be 8 feet wide, and the vehicle side surface is the projection at this distance. The top and bottom vehicle surfaces are assumed to correspond to the top and bottom of the impact limiters, although the vehicle does not have a top because it is open. The 2 m dose rate is computed 2 m from the vehicle side, while the occupied location (i.e., the driver) is computed 25 feet from the centerline of the cask.

Dose rates are very low. Under NCT, the maximum package surface dose rate is 12.9 mrem/hr, the maximum dose rate 2 m from the vehicle surface is 0.3 mrem/hr, and the dose rate in the occupied location is 0.06 mrem/hr. Under HAC, the maximum dose rate at 1 m from the package is 2.8 mrem/hr.

Table 5.1-1 – Summary of Maximum Total Dose Rates (Exclusive Use)

NCT	Package Surface (mrem/hr)			Vehicle Surface (mrem/hr)		
Fuel→	MITR-II	MITR-II	MURR	MITR-II	MITR-II	MURR
Radiation	Top	Side	Bottom	Top	Side	Bottom
Gamma	9.7	7.9	3.63	9.7	3.7	3.63
Neutron	0.2	5.0	0.02	0.2	0.1	0.02
Total	9.9	12.9	3.7	9.9	3.8	3.7
Limit	200	200	200	200	200	200

NCT	2 m from Vehicle Surface (mrem/hr)			Occupied Location (mrem/hr)
Fuel→	NA	MITR-II	NA	MITR-II
Radiation	Top	Side	Bottom	Side
Gamma	NA	0.2	NA	0.042
Neutron	NA	0.1	NA	0.015
Total	NA	0.3	NA	0.06
Limit	10	10	10	2

HAC	1 m from Package Surface (mrem/hr)		
Fuel→	MITR-II	MITR-II	MURR
Radiation	Top	Side	Bottom
Gamma	2.7	2.23	1.5
Neutron	0.1	0.12	0.01
Total	2.8	2.4	1.5
Limit	1000	1000	1000

5.2 Source Specification

A neutron and gamma source term is developed for each of the four fuel types. The source terms for MURR, MITR-II, and ATR are developed using the TRITON sequence of SCALE6 [3]. The TRIGA source is derived from nuclide activities obtained from INEL-96/0482 [4].

5.2.1 Gamma Source

5.2.1.1 MURR Fuel

The MURR gamma source term is generated by the TRITON sequence of SCALE6. TRITON is a control module that coordinates program flow between the SCALE6 modules involved in the depletion sequence, primarily NEWT and ORIGEN-S.

The TRITON sequence uses a predictor-corrector approach. The two-dimensional discreet ordinates module NEWT calculates the burnup-dependent flux distribution across the fuel element, which is collapsed to three groups for input to the ORIGEN-S depletion module. The first NEWT calculation is performed using the 238-group ENDF/B-VII cross-section library. This flux distribution is then used to collapse the 238-group cross-section library to 49 groups to accelerate subsequent NEWT calculations. Therefore, the 49-group library is problem-dependent. The fuel is depleted over a specified time interval, and the depleted mixture is then used as input to the subsequent NEWT flux calculation. The number of time steps is determined by the user-defined input. One library generation per fuel cycle is the default, although more steps may be requested to improve accuracy. A more detailed discussion of the predictor-corrector approach of the TRITON sequence may be found in Section T.1.2.3 of the TRITON user's manual [3]. An annotated TRITON input file is included in Section 5.5.3.1, *TRITON Input File*. A discussion of this input file follows.

The two-dimensional NEWT model of the MURR fuel element has been simplified compared to the actual fuel element geometry. The MURR fuel element has 24 curved plates, although these plates are modeled as flat in NEWT. Only half of the fuel element is modeled, taking credit for symmetry. In the actual fuel element, the arc length of the fuel meat is different for each plate. To simplify the NEWT model, one-half the average fuel meat arc length is modeled for all 24 plates. Therefore, it is necessary to define only one fuel plate, and then repeat this fuel plate in a 1x24 array. All relevant data used to develop the TRITON model is shown in Table 5.2-1. The NEWT model geometry is shown in Figure 5.2-1.

The nominal fuel meat arc length for each plate is provided in Table 6.9-3 of Chapter 6, *Criticality Evaluation*. Based on these nominal arc lengths, the average fuel meat arc length is 2.882-in. The nominal fuel meat thickness is 0.02-in, and the nominal plate thickness is 0.05-in. The nominal channel thickness between plates is 0.08-in, so the nominal pitch is 0.05+0.08 = 0.13-in. These parameters are used as input both in the NEWT model and the LATTICECELL card.

Three materials are modeled; fuel, cladding, and moderator. The number densities of the fuel are computed based on the fuel loading and fuel meat volume. The density of the fuel meat is estimated using the equation listed in Table 6.2-5 of Chapter 6, *Criticality Evaluation*, using the

known density of U-235. Aluminum and water are modeled as pure. Temperatures for the fuel, cladding, and water during reactor operation are typical values for this reactor.

The MURR fuel element has a fuel loading of 775.0 ± 7.8 g U-235. Two TRITON models are developed, one for the minimum fuel loading (767.2 g U-235), and a second for the maximum fuel loading (782.8 g U-235). The U-235 nominal enrichment is 93%. The balance of uranium is modeled as U-238. The fuel is burned in 21 cycles. The first 20 cycles are 7 days in duration, and the final cycle is 4 days in duration, giving a total irradiation time of 144 days. The total core power is 10.0 MW, with 8 fuel elements, so the average element power is 1.25 MW. A peak fuel element could have a power greater than 1.25 MW for any particular cycle, but because no fuel element is ever maintained at the peak power throughout its entire life, modeling an average value of 1.25 MW is conservative. For an element power of 1.25 MW, the total burnup is 180 MWD. Power is input to TRITON in units of MW/MTU. Two weeks of cooling is assumed between each cycle. The source is allowed to cool 180 days after reactor shutdown.

The fuel cycle is modeled as an extreme case of the MURR fuel cycle. Unlike many other research reactors, MURR does not use a once-through fuel cycle. Each fuel element is cycled in and out of the core several times before reaching the final discharge burnup. Typically, a given fuel element is irradiated in several 6.2 to 6.5-day periods with varying cooling (non-irradiation) times in between the irradiation periods. For this calculation, the fuel assembly is irradiated in 7.0-day periods in a one-week-in and two-week-out pattern until the fuel is discharged. This overestimates the source term since MURR fuel elements generally remain outside the core for several weeks at a time during their active life and are never cycled in and out of the core continuously until discharge. Therefore, the irradiation parameters utilized result in a source term that bounds any expected MURR fuel element.

The OPUS module of SCALE6 is used to extract key data from the output, including decay heat, U-235 mass, plutonium activity, and the source term. Note that all TRITON output uses a basis of 1 MTU because the specific power must be input in units of MW/MTU. Therefore, the results must be multiplied by the fuel loading (in MTU) of the fuel element to obtain the desired results for a single fuel element.

The gamma source term for both the maximum and minimum fuel loadings are nearly identical (within 0.02%), although the source term computed for the minimum fuel loading is slightly higher. The MURR gamma source computed with the minimum fuel loading is summarized in Table 5.2-3. Note that the MURR basket may transport up to eight fuel elements.

A representative axial burnup distribution is provided in Table 5.2-4. This distribution is the ratio of the burnup in each segment to the average burnup.

Key output data are summarized in Table 5.2-2. The fuel depletion may be computed based on the initial and final U-235 mass. The initial U-235 mass is 767.2 g, and the final U-235 mass is 530.4 g, or a depletion of 30.9%. The decay heat at a decay time of 180 days is 147.6 W.

5.2.1.2 MITR-II Fuel

The MITR-II gamma source term is generated by the TRITON sequence in the same manner as MURR fuel. Data used to develop the TRITON model is summarized in Table 5.2-1, and the NEWT model for MITR-II is shown in Figure 5.2-2. An actual MITR-II fuel element has a trapezoidal design, although the fuel is modeled in NEWT as a simple rectangle for simplicity.

The MITR-II fuel element has a loading of 510.0 +3/-10 g U-235. Two TRITON models are developed, one for the minimum fuel loading (500.0 g U-235), and a second for the maximum fuel loading (513.0 g U-235). The U-235 nominal enrichment is 93%. The balance of uranium is modeled as U-238.

The fuel is burned in six cycles, with 7 days between cycles. The first 5 cycles have an irradiation time of 120 days, and the last cycle has an irradiation time of 60 days, for a total irradiation time of 660 days. The average fuel element power is 0.25 MW for a 6.0 MW reactor with 24 fuel elements. A peak fuel element could have a power greater than 0.25 MW for any particular cycle, but because no fuel element is ever maintained at the peak power throughout its entire life, modeling an average value of 0.25 MW is conservative. Therefore, for an element power of 0.25 MW, the burnup is 165 MWD. The irradiation time is highly conservative because the MITR-II reactor typically operates on a monthly cycle, and operates only 300 days per year. The source is allowed to cool 120 days after reactor shutdown.

The MITR-II gamma source is summarized in Table 5.2-3. Consistent with the MURR gamma source, the source is slightly larger using the minimum fuel loading. Note that the MITR-II basket may transport up to 8 fuel elements.

The axial burnup distribution is provided in Table 5.2-5. This distribution is the ratio of the burnup in each segment to the average burnup. A symmetric distribution is utilized. Because the widths of the distribution are not constant (the end segments are half the width of the remaining segments), the distribution input to MCNP must be divided by 2 for the end regions, as indicated in the last column in the table.

Key output data are summarized in Table 5.2-2. The fuel depletion may be computed based on the initial and final U-235 mass. The initial U-235 mass is 500.0 g, and the final U-235 mass is 280.6 g, or a depletion of 43.9%. The decay heat at a decay time of 120 days is 142.5 W.

5.2.1.3 ATR Fuel

The ATR gamma source term is generated by the TRITON sequence in the same manner as MURR and MITR-II fuel. Data used to develop the TRITON model is summarized in Table 5.2-1, and the NEWT model for ATR is shown in Figure 5.2-3. An ATR fuel element is similar in geometry to a MURR fuel element, although an ATR fuel element has 19 fuel plates instead of 24. The NEWT model uses the same base assumption as the MURR model that the plates may be modeled as flat using the average half-width of the fuel meat. The average fuel meat arc length is 2.65-in (see Table 6.9-1 in Chapter 6, *Criticality Evaluation*).

There are two general classes of ATR fuel element, XA and YA. The XA fuel element has a fresh fuel loading of 1,075 ± 10 g U–235. The XA fuel element is further subdivided into fuel element types 7F, 7NB, 7NBH. In the 7F fuel element, all 19 fuel plates are loaded with enriched uranium in an aluminum matrix with the eight outer plates (1 through 4 and 16 through 19) containing boron as a burnable poison. The fuel element 7NB contains no burnable poison. The 7NBH fuel element is similar to the 7NB fuel element except that it contains one or two borated plates. The YA fuel element is identical to the 7F fuel element except that plate 19 of the YA fuel element is an aluminum alloy plate containing neither uranium fuel nor boron burnable poison. The YA fuel element has a fresh fuel loading of 1,022.4 ± 10 g U–235.

ATR fuel has an additional complexity that each fuel plate has different uranium number densities. The U-235 number densities in plates 5 through 15 are approximately constant, although the U-235 number densities in plates 1 through 4 and 16 through 19 are reduced. In the NEWT models, all 19 plates are assigned the same number densities for simplicity, although the total fuel loading is preserved. This level of detail is sufficient to generate a source term for shielding applications, especially since that the ATR fuel element is homogenized in the MCNP shielding model.

Both the XA type 7NB and 7F fuel elements are modeled in TRITON. The B-10 loading of the type 7F element is 660 mg (which has been conservatively rounded up to 700 mg), and for simplicity is distributed evenly throughout all 19 plates rather than only on the eight outer plates. The 7NBH element is bounded by the 7F element. The XA element bounds the YA element because the fission density (fissions/cm^3) limit is the same for both fuel types, and the type XA element has a larger fuel volume than the type YA element.

Fuel plate 1 is nominally 0.080-in thick, fuel plates 2 through 18 are nominally 0.050-in thick, and fuel plate 19 is nominally 0.100-in thick. In the TRITON models, 0.050-in is used for all plates for simplicity. The fuel meat is nominally 0.02-in thick for all 19 plates. Channels 2 through 10 have a nominal width of 0.078-in, while channels 11 through 19 have a nominal width of 0.077-in. The channel width is modeled at 0.078-in between all plates for simplicity. Therefore, the pitch is 0.05+0.078 = 0.128-in.

Three TRITON models are developed:

- Type 7NB, minimum fuel loading (1065.0 g U-235),
- Type 7NB, maximum fuel loading (1085.0 g U-235),
- Type 7F, minimum fuel loading (1065.0 g U-235),

The U-235 nominal enrichment is 93%. The balance of uranium is modeled as U-238.

The burnup parameters are selected to bound the highest burned ATR fuel element ever generated. This element had a starting U-235 loading of 1075 g, and a final U-235 loading of 457 g, or a depletion of 57.5%. The fuel is burned in one continuous cycle for 48 days to achieve approximately the same level of depletion of the highest burned ATR element. A bounding element power of 10 MW is utilized, for a total burnup of 480 MWD[1]. The source is allowed to cool 1670 days after reactor shutdown.

The fuel cycle modeled is an extreme case of the ATR fuel cycle. The ATR reactor consists of 5 lobes of 8 fuel elements each, and the maximum lobe power is 60 MW (total reactor power is limited to 250 MW). Therefore, the average power in a maximum power lobe is 7.5 MW, although the maximum fuel element power may be in the range from 8 to 9 MW. A fuel element power of 10 MW is conservatively modeled. Likewise, a typical cycle length is in the range from 49 to 56 days, while 48 days is modeled. To completely burn a fuel element would typically require a minimum of three cycles, and any down time between cycles has been conservatively ignored in the calculation.

[1] The element burnup of 480 MWD should not be a limit for licensing purposes because the element burnup is typically not known in units of MWD. ATR staff compute and report the final U-235 mass within an element.

The ATR gamma source is summarized in Table 5.2-3. Note that the ATR basket may transport up to eight fuel elements.

The axial burnup distribution provided in Table 5.2-6 is simply assumed based upon a peak of 1.45 at the axial center. This distribution is the ratio of the burnup in each segment to the average burnup. The distribution is divided over 10 segments of equal width over the fuel length of 48-in (121.92 cm).

Key output data are summarized in Table 5.2-2. The fuel depletion may be computed based on the initial and final U-235 mass. The initial U-235 mass is 1065.0 g, and the final U-235 mass is 440.5 g, or a depletion of 58.6%. The decay heat at a decay time of 1670 days is 29.8 W.

5.2.1.4 TRIGA Fuel

The TRIGA fuel gamma source term is derived from information in INEL-96/0482 [4]. This report provides detailed activity values for 145 key isotopes as a function of burnup and decay time for four different TRIGA fuel types. These four fuel types are included in Section 1.2.2, *Contents*:

- Type 101 = aluminum-clad standard
- Type 103 = stainless steel-clad standard
- Type 109 = High-enrichment Fuel Life Improvement Program (FLIP)
- Type 117 = Low-enrichment Fuel Life Improvement Program (FLIP-LEU-I)

Key parameters for the four fuel types are summarized in Table 5.2-7. Decay times range from discharge to 20 years. Note that the minimum decay time reported in this table has been selected to be the minimum for transportation purposes.

The models used to generate the source are described in [4]. The TRIGA fuel is modeled with an irradiation time of 4 years. TRIGA reactors tend to run only sporadically rather than continuously, and TRIGA fuel elements often have residence times exceeding 10 years. Therefore, the source is conservative.

For shielding calculations, a bounding source term is selected. The Type 109 fuel has by far the largest burnup of the four candidate TRIGA fuels and hence results in the largest source. It is desired to set a minimum decay time of 1 year for the two higher-burnup fuels (Type 109 and 117) to allow many of the short-lived daughters to decay. For the two standard fuels, a much shorter 28 day decay time is stipulated. It may be demonstrated that the Type 109 fuel is bounding simply by comparing key isotopes (e.g., Co-60, Sr-90, Cm-244, etc.) in the activity tables provided in [4].

A fifth fuel type is included in Section 1.2.2, *Contents*, Type 203 (8.5 wt.% instrumented, stainless steel clad), which is simply a longer, instrumented version of Type 103. The source term for this fuel type is not specifically provided in [4]. However, the source for a Type 203 fuel element would be comparable to a Type 103 element, and the Type 103 element is well-bounded by the high-burnup Type 109 fuel element utilized in the shielding calculations.

However, source term data that could be utilized directly in MCNP are not provided in [4]. Rather, these activities are input into SCALE6 (ORIGEN-S) to generate a suitable source term

that may be used in shielding computations. The source information from Table F.14 of [4] at discharge is input to ORIGEN-S, and then decayed to 1 year. The gamma source for TRIGA fuel is summarized in Table 5.2-3. Note that the TRIGA basket holds 19 fuel elements.

No axial burnup profile is provided for TRIGA fuel, and a flat distribution is utilized.

5.2.2 Neutron Source

The neutron sources are extracted from the same output files that define the gamma sources, as described in Section 5.2.1, *Gamma Source*. The neutron source for MURR, MITR-II, ATR, and TRIGA are presented in Table 5.2-8. The neutron sources presented are the combined spontaneous fission and (α,n) components. Aluminum in the fuel matrix is used as the target nucleus to generate the (α,n) source for the MURR, MITR-II, and ATR fuels. For the TRIGA fuels, no (α,n) target nuclides are present in the fuel matrix. By default, ORIGEN-S utilizes oxygen as a target nucleus if no other target nuclides are present. To be conservative, the (α,n) source with an oxygen target is included in the total for TRIGA, although the actual (α,n) source would be effectively zero because there is no applicable target nuclide in the fuel matrix. This assumption results in an additional conservatism of 9% in the neutron source for the TRIGA fuels.

The neutron sources for MURR, MITR-II, and ATR are extracted from the minimum fuel loading models, consistent with the gamma sources. However, while the fuel loading had essentially no effect on the gamma source, the neutron source is noticeably larger when the minimum fuel loading is utilized. For these fuels, the increase in neutron source strength when using the minimum fuel loading rather than maximum fuel loading is approximately 1 to 3%.

The neutron sources for MURR, MITR-II, ATR, and TRIGA fuel are input with the same axial distribution provided in Section 5.2.1, *Gamma Source*.

Table 5.2-1 – TRITON Input and Supporting Data (MURR, MITR-II, ATR)

Parameter	MURR(-)	MURR(+)	MITR-II(-)	MITR-II(+)	ATR(-)①	ATR(+)
U-235 loading (g)	767.2	782.8	500.0	513.0	1065.0	1085.0
Fuel meat temperature (K)	358.0	358.0	341.0	341.0	378.0	378.0
Fuel cladding temp. (K)	355.2	355.2	338.0	338.0	372.4	372.4
Water temp. (K)	327.4	327.4	323.0	323.0	340.8	340.8
Water density (g/cm^3)	0.983	0.983	0.9968	0.9968	0.9786	0.9786
Fuel meat width (in)	2.88	2.88	2.08	2.08	2.65	2.65
Fuel meat thickness (in)	0.02	0.02	0.03	0.03	0.02	0.02
Fuel plate thickness (in)	0.05	0.05	0.08②	0.08	0.05	0.05
Fuel plate pitch (in)	0.13	0.13	0.158	0.158	0.128	0.128
Active fuel length (in)	24.0	24.0	22.375	22.375	48.0	48.0
Number of fuel plates	24	24	15	15	19	19
Fuel Meat Volume (cm^3)	544.1	544.1	342.5	342.5	792.6	792.6
U density (g/cm^3)	1.52	1.55	1.57	1.61	1.44	1.47
U-235 density (g/cm^3)	1.41	1.44	1.46	1.50	1.34	1.37
U-238 density (g/cm^3)	0.1061	0.1083	0.1099	0.1127	0.1011	0.1030
Al density (g/cm^3)	2.25	2.25	2.24	2.23	2.26	2.26
UAlx+Al density (g/cm^3)	3.77	3.79	3.81	3.84	3.71	3.73
N U-235 (atom/b-cm)	3.6124E-03	3.6859E-03	3.7399E-03	3.8371E-03	3.4426E-03	3.5072E-03
N U-238 (atom/b-cm)	2.6847E-04	2.7393E-04	2.7794E-04	2.8517E-04	2.5584E-04	2.6065E-04
N Al (atom/b-cm)	5.0239E-02	5.0110E-02	5.0015E-02	4.9844E-02	5.0538E-02	5.0425E-02
U mass (g)	824.9	841.7	537.6	551.6	1145.2	1166.7
U mass (MTU)	8.2495E-04	8.4172E-04	5.3763E-04	5.5161E-04	1.1452E-03	1.1667E-03
Element power (MW)	1.25	1.25	0.25	0.25	10.0	10.0
Sp. Power (MW/MTU)	1515.3	1485.1	465.0	453.2	8732.4	8571.4
Irradiation time (D)	144.0	144.0	660.0	660.0	48.0	48.0
Cycles (#)	21	21	6	6	1	1
Decay time (D)	180	180	120	120	1670	1670
Burnup (MWD)	180.0	180.0	165.0	165.0	480.0	480.0
Burnup (MWD/MTU)	218,196	213,848	306,900	299,123	419,155	411,429

①Data in this column is for the model without B-10. For the model including B-10, the B-10 number density is 5.3115E-05 atoms/b-cm. The nominal B-10 loading in an ATR Type 7F assembly is 660 mg. This value has been conservatively rounded up to 700 mg.

②The grooves present in MITR-II cladding have been neglected.

Table 5.2-2 – TRITON Output Data (MURR, MITR-II, ATR)

Parameter	MURR(-)①	MURR(+)	MITR-II(-)	MITR-II(+)
Initial U-235 (g)	**767.2**	782.8	**500.0**	513.0
Final U-235 (g)	**530.4**	545.8	**280.6**	293.2
Depleted mass (g)	**236.8**	237.0	**219.4**	219.8
Depletion (%)	**30.9%**	30.3%	**43.9%**	42.8%
Element decay heat (W)	**147.6**	147.6	**142.5**	142.5
Parameter	**ATR(-)**	**ATR(+)**	**ATR(-) with B-10**	--
Initial U-235 (g)	1065.0	1085.0	**1065.0**	--
Final U-235 (g)	440.8	460.1	**440.5**	--
Depleted mass (g)	624.2	624.9	**624.5**	--
Depletion (%)	58.6%	57.6%	**58.6%**	--
Element decay heat (W)	29.8	29.8	**29.8**	--

①Bounding analysis values in boldface.

Table 5.2-3 – Gamma Source Terms

	MURR	MITR-II	ATR	TRIGA
Upper Energy Bin (MeV)	Gamma Source (γ/s)	Gamma Source (γ/s)	Gamma Source (γ/s)	Gamma Source (γ/s)
4.50E-02①	2.576E+14	2.343E+14	5.575E+13	2.573E+13
1.00E-01	9.423E+13	8.380E+13	1.973E+13	9.352E+12
2.00E-01	9.441E+13	9.049E+13	1.527E+13	8.658E+12
3.00E-01	1.976E+13	1.756E+13	3.897E+12	1.952E+12
4.00E-01	1.478E+13	1.304E+13	2.881E+12	1.498E+12
6.00E-01	4.237E+13	5.917E+13	1.445E+13	7.684E+12
8.00E-01	4.328E+14	4.460E+14	5.736E+13	1.928E+13
1.00E+00	7.534E+12	1.117E+13	5.941E+12	3.454E+12
1.33E+00	3.040E+12	3.308E+12	1.387E+12	8.832E+12
1.66E+00	1.786E+12	2.576E+12	5.689E+11	2.637E+12
2.00E+00	2.304E+11	2.013E+11	3.490E+10	2.716E+10
2.50E+00	2.171E+12	1.795E+12	2.387E+11	2.099E+11
3.00E+00	8.765E+09	3.290E+10	1.346E+09	1.065E+09
4.00E+00	4.661E+08	6.118E+08	1.061E+08	8.208E+07
5.00E+00	9.414E+01	7.015E+02	7.644E+02	2.045E+03
6.50E+00	3.740E+01	2.802E+02	3.051E+02	8.196E+02
8.00E+00	7.270E+00	5.473E+01	5.955E+01	1.606E+02
1.00E+01	1.582E+00	1.195E+01	1.300E+01	3.407E+01
Total	9.707E+14	9.634E+14	1.775E+14	8.932E+13
Number of Fuel Elements in Basket	8	8	8	19
Basket Total	7.766E+15	7.707E+15	1.420E+15	1.697E+15

①The lower energy bound for this group is 0.01 MeV.

Table 5.2-4 – Axial Burnup Distribution, MURR

Distance from Bottom of Fuel Element (cm)	Axial Burnup Distribution
5	0.872
10	0.939
15	1.132
20	1.233
25	1.367
30	1.358
35	1.308
40	1.233
45	1.023
50	0.679
55	0.486
60	0.369

Table 5.2-5 – Axial Burnup Distribution, MITR-II

Distance from Bottom of Fuel Element (cm)	Axial Burnup Distribution	MCNP Input
2.368	0.999	0.500
4.736	0.788	0.394
9.472	0.788	0.788
14.208	0.901	0.901
18.944	1.042	1.042
23.680	1.140	1.140
28.416	1.253	1.253
33.152	1.267	1.267
37.888	1.112	1.112
42.624	1.028	1.028
47.360	0.901	0.901
52.096	0.774	0.774
54.464	0.802	0.401
56.833	0.999	0.500

Table 5.2-6 – Axial Burnup Distribution, ATR

Distance from Bottom of Fuel Element (cm)	Axial Burnup Distribution
12.19	0.50
24.38	0.70
36.58	1.00
48.77	1.30
60.96	1.45
73.15	1.45
85.34	1.30
97.54	1.00
109.73	0.70
121.92	0.50

Table 5.2-7 – TRIGA Fuel Parameters

Fuel Type	Enrichment (%)	Maximum U-235 depletion (%)	Maximum Burnup (MWD/MTU)	Minimum Decay Time
Type 101 (Aluminum-clad standard)	20.0	22.42	36,953	28 days
Type 103/203 (Stainless steel-clad standard)	20.0	20.72	34,111	28 days
Type 109 (FLIP)	70.0	59.74	339,368	1 year
Type 117 (FLIP-LEU-I)	20.0	43.81	75,415	1 year

Table 5.2-8 – Neutron Source Term

	MURR	MITR-II	ATR	TRIGA
Upper Energy Bin (MeV)	Neutron Source (n/s)	Neutron Source (n/s)	Neutron Source (n/s)	Neutron Source (n/s)
1.000E-08①	6.449E-09	4.868E-08	1.201E-08	7.233E-08
3.000E-08	7.938E-09	6.084E-08	3.617E-08	1.283E-07
5.000E-08	8.240E-09	6.354E-08	4.933E-08	1.547E-07
1.000E-07	2.361E-08	1.828E-07	1.652E-07	4.866E-07
2.250E-07	7.635E-08	5.933E-07	5.993E-07	1.703E-06
3.250E-07	7.588E-08	5.906E-07	6.239E-07	1.748E-06
4.140E-07	7.688E-08	5.988E-07	6.430E-07	1.802E-06
8.000E-07	4.171E-07	3.250E-06	3.556E-06	9.942E-06
1.000E-06	2.611E-07	2.035E-06	2.254E-06	6.247E-06
1.125E-06	1.772E-07	1.381E-06	1.534E-06	4.233E-06
1.300E-06	2.632E-07	2.052E-06	2.284E-06	6.318E-06
1.855E-06	1.351E-05	1.000E-04	8.317E-06	2.276E-05
3.059E-06	3.703E-05	2.741E-04	2.319E-05	6.128E-05
1.068E-05	2.487E-04	1.837E-03	2.809E-04	6.377E-04
2.902E-05	2.430E-03	1.040E-02	1.047E-02	2.622E-03
1.013E-04	1.556E-02	6.678E-02	6.686E-02	1.909E-02
5.830E-04	1.850E-01	7.886E-01	8.143E-01	2.893E-01
3.035E-03	2.194E+00	9.182E+00	9.925E+00	3.385E+00
1.503E-02	2.700E+01	1.127E+02	1.204E+02	3.705E+01
1.111E-01	8.508E+02	3.446E+03	3.766E+03	7.566E+02
4.076E-01	5.625E+03	2.377E+04	2.328E+04	4.304E+03
9.072E-01	1.323E+04	5.727E+04	5.285E+04	9.353E+03
1.423E+00	1.235E+04	5.086E+04	5.203E+04	9.709E+03
1.827E+00	8.372E+03	3.444E+04	3.576E+04	6.981E+03
3.012E+00	7.363E+03	3.685E+04	2.753E+04	1.626E+04
6.376E+00	5.001E+02	4.004E+03	4.327E+03	1.357E+04
2.000E+01	4.587E+01	3.817E+02	4.356E+02	1.207E+03
Total	4.837E+04	2.111E+05	2.001E+05	6.218E+04
Number of Fuel Elements in Basket	8	8	8	19
Basket Total	3.869E+05	1.689E+06	1.601E+06	1.181E+06

①The lower energy bound for this group is 1.0E-11 MeV.

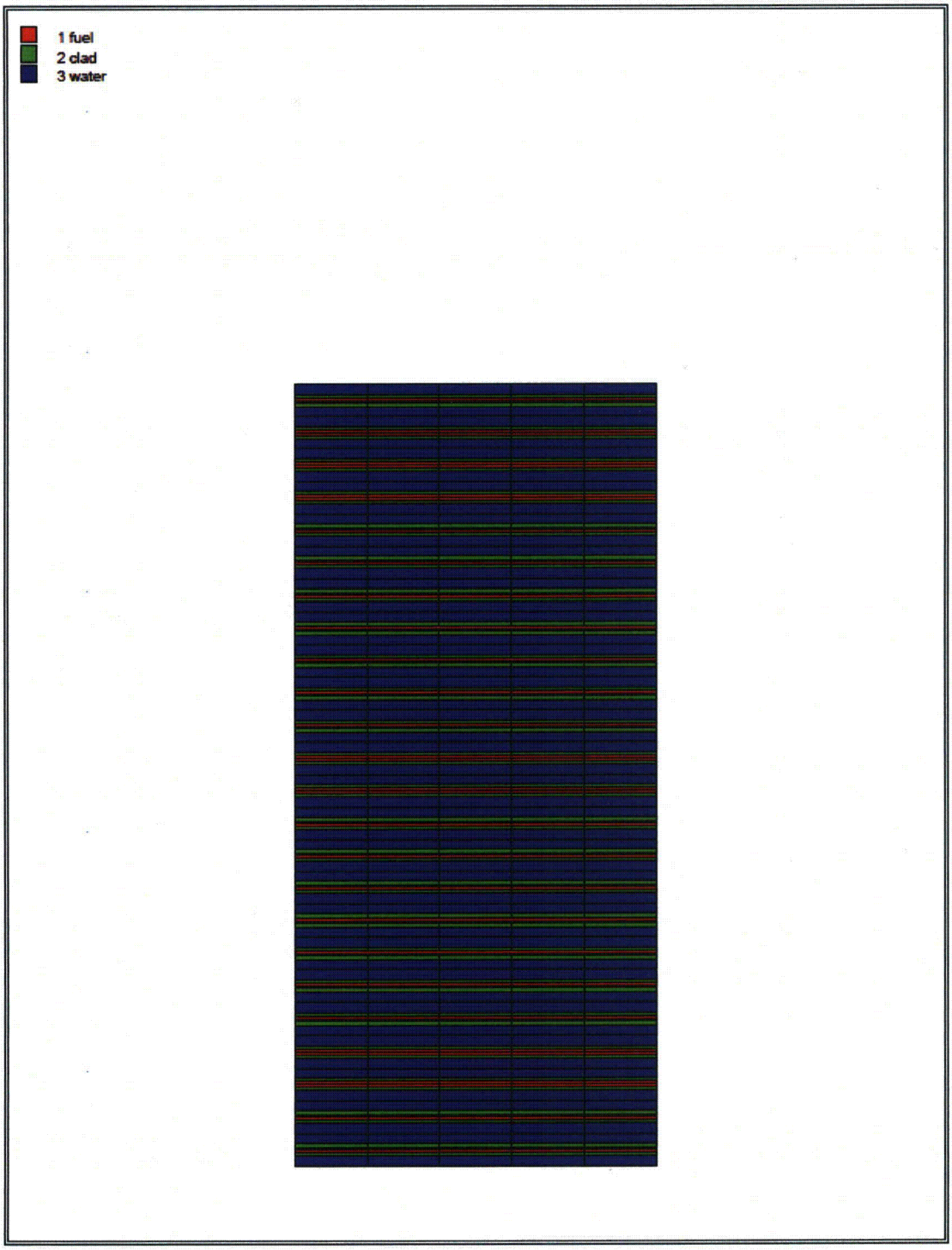

Figure 5.2-1 – NEWT Model for MURR

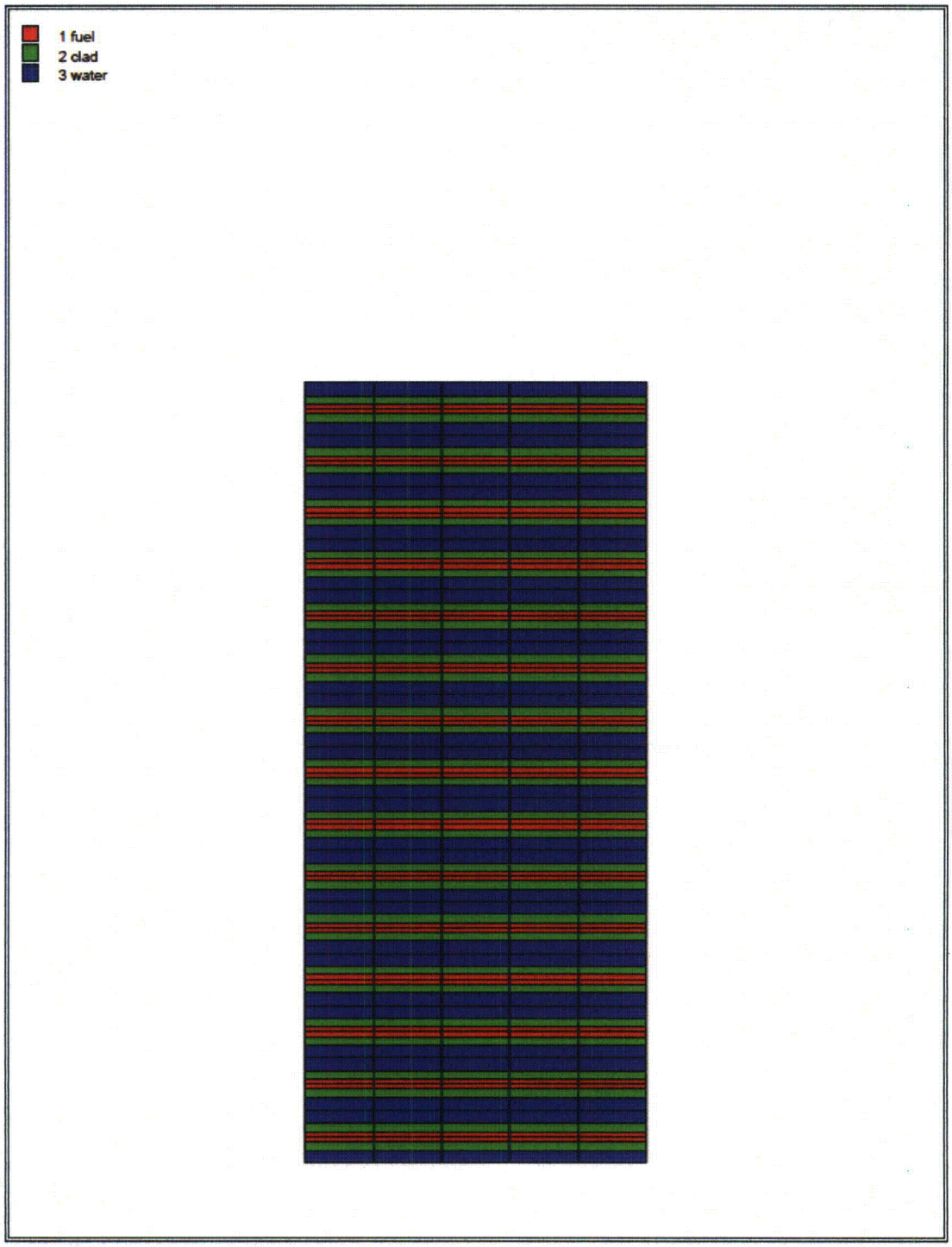

Figure 5.2-2 – NEWT Model for MITR-II

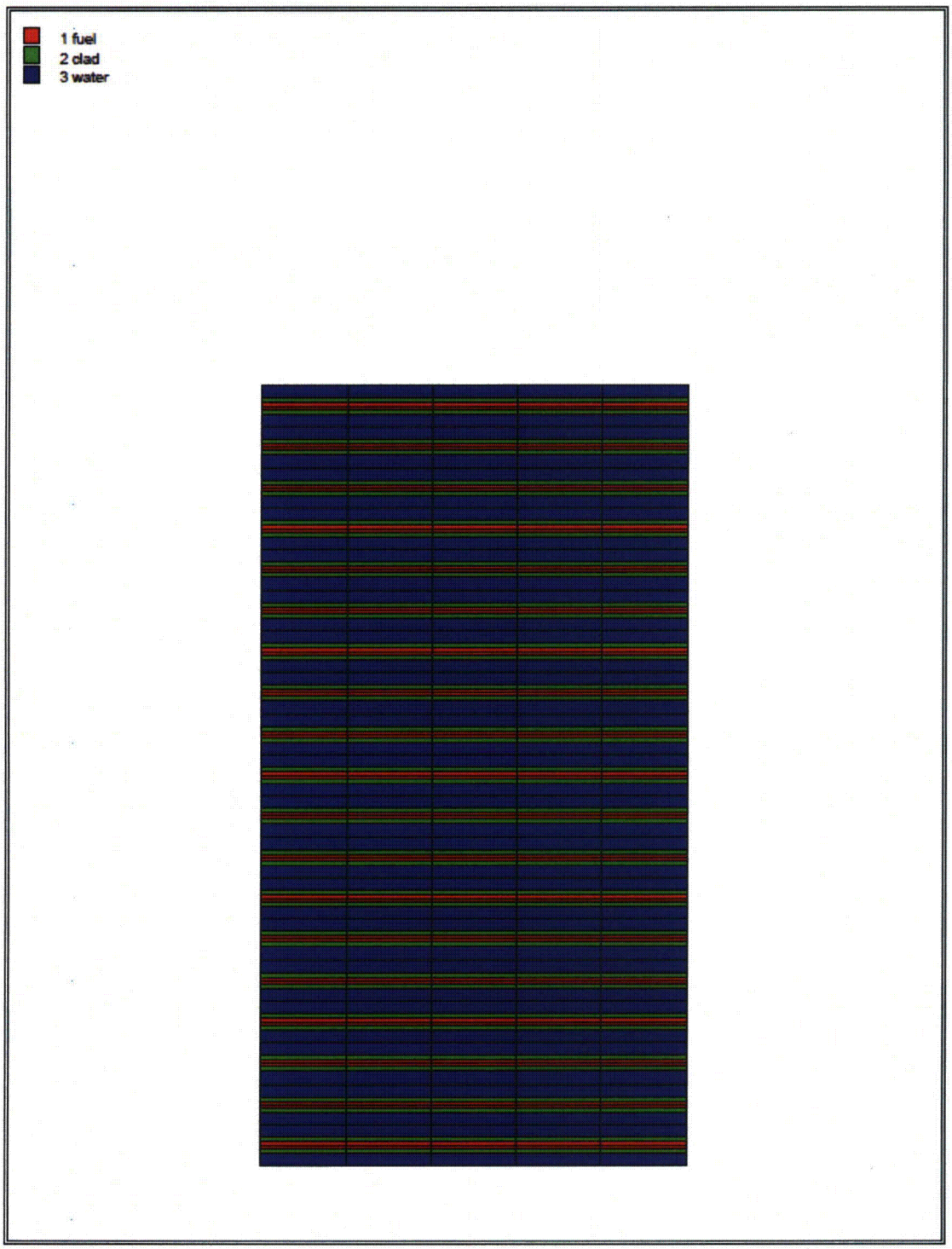

Figure 5.2-3 – NEWT Model for ATR

5.3 Shielding Model

5.3.1 Configuration of Source and Shielding

All relevant design features of the BRR Package are modeled in three-dimensions in MCNP, as shown in Figure 5.3-1. The key dimensions relevant to the MCNP model are summarized in Table 5.3-1 and are obtained from Section 1.3.3, *Packaging General Arrangement Drawings*. Minor details are not included in this table but may be inferred from the drawings.

Some differences exist between the as-modeled and packaging general arrangement drawing dimensions, as shown in Table 5.3-1. Most differences are small and may be neglected. The only notable differences are the outer diameter of the impact limiters, and the diameter of lead at the bottom of the cask. The outer diameter of the impact limiters is modeled at a reduced diameter of 72.0-in, which is conservative because the dose rate tally location is brought closer to the source. Also, the lead diameter in the cask bottom is modeled at 9.75-in rather than 10.3-in, which is conservative for shielding.

To simplify model preparation and add conservatism, the impact limiters are modeled simply as air, neglecting the impact limiter foam and outer steel shell. The "impact limiter air" is modeled with a different material number than the other air regions to more clearly illustrate the location of the impact limiters (see Figure 5.3-1), although the composition is unchanged. Credit is taken for the distance provided by the impact limiters, although the impact limiters are modeled simply as cylinders without the conical regions.

An axial lead slump of 1.18-in (see Section 2.7.1.2, *End Drop*) is modeled at the top of the cask. This slump represents the maximum expected slump due to lead shrinkage and a drop event. Also, an additional 0.0625-in radial lead shrinkage is assumed.

Each fuel element type is transported in its own unique basket. Key geometrical parameters for the four basket designs are summarized in Table 5.3-2. The inner cavity region of the MITR-II basket is modeled as a cylinder with the largest possible diameter to minimize shielding, as the actual geometry is complex. The inner cutout is also conservatively neglected for the top plate of the MITR-II basket. These simplifications are expected to have a negligible impact on the results. As with the cask, this table shows both the actual and as-modeled dimensions. Most differences are within round-off and may be neglected. For the TRIGA basket, the final cavity length is longer than the as-modeled dimension, although this has no effect on the results because the fuel elements are modeled shifted upward to the bottom of the shield plug. The baskets and source are also shown graphically in Figure 5.3-2 and Figure 5.3-3.

Because the MURR, MITR-II, and ATR fuels are geometrically complex, the fuel elements are homogenized over the active length of the fuel and distributed across the width of each basket compartment. Fuel element homogenization is a standard practice utilized to simplify complex source geometry and has little effect on the final results. Basic fuel dimensions used in the homogenization calculation are summarized in Table 5.3-3. These fuel dimensions are not modeled explicitly in MCNP.

For the TRIGA fuel, the fuel is a simple cylindrical design. Therefore, the TRIGA fuel elements are modeled explicitly, and the source is distributed over the fuel pellets. Basic geometrical data

for the modeled TRIGA fuel is summarized in Table 5.3-3. For the TRIGA fuel, the Type 109 fuel is modeled, as this fuel type results in the largest source.

Because each basket is custom designed for each fuel type, there is little space for axial shifting of the fuel elements. Of course, because the cask is transported in a vertical orientation, the fuel elements would simply rest on the bottom of the basket support plate during NCT. However, because it is desired to use the same MCNP models for both NCT and HAC, the fuel is modeled near the top of the cavity in each model. Modeling the fuel near the lid places the source in the closest proximity to the interface between the lid and cask side, where the lead concentration is at a minimum. Note that in actual practice, the active fuel region will never be up against the cask lid because of the offset due to the fuel element support structures (end caps, nozzles, etc.).

Table 5.3-3 provides both the active fuel length and total overall length of each fuel element. If it is assumed that the active fuel is centered within the fuel element, the minimum distance between the active fuel and cask lid may be estimated. In all models, the distance between the top of the active fuel and bottom of the cask lid is less than or equal to this minimum distance. The minimum estimated and modeled distances from the top of the active fuel to the bottom of the lid are listed below.

- MURR: 4.25-in estimated, 4.00-in modeled
- MITR-II: 1.945-in estimated, 0.54-in modeled
- ATR: 1.5-in estimated, 0.54-in modeled
- TRIGA: 6.95-in estimated, 2.6-in modeled

NCT dose rates are tallied at the package surface (i.e., surface of cask body and impact limiters), surface of the vehicle (the vehicle is assumed to be 8 feet wide), 2 m from the surface of the vehicle, and in the occupied location of the vehicle driver (assumed to be 25 feet from the cask centerline.) Details of the tally locations, with figures, are provided with the results in Section 5.4.4, *External Radiation Levels*.

Because the impact limiters are modeled as air, both NCT and HAC dose rates may be computed from a single MCNP model. Under HAC, tallies are measured 1 m from the surface of the package. In the radial direction, this distance is measured from the surface of the cask, so any radial impact limiter crush does not impact the dose rate location. In the axial direction, because an end drop results in a maximum crush of 10.5-in, as shown in Appendix 2.12.5, *Impact Limiter Performance Evaluation*, Table 2.12.5-13, a bounding crush of 12-in is applied at each end. The 1 m tally surface is measured from the hypothetical crushed end of the impact limiter, although the impact limiter crush is not modeled explicitly (since the impact limiter is modeled simply as air). It is demonstrated in Section 2.7.1.5, *Fuel Basket Stress Analysis* that the baskets remain intact after a drop event, and therefore the baskets may be modeled as undamaged for both NCT and HAC.

5.3.2 Material Properties

As indicated in Section 5.3.1, *Configuration of Source and Shielding*, homogenized fuel number densities are utilized in the MURR, MITR-II, and ATR fuel models. For nominal fuel meat and cladding thicknesses, the total mass of U-235, U-238, and aluminum is estimated for each fuel

element. For this computation, all structural aluminum is ignored, and the width of the plates is treated as equal to the width of the fuel matrix for simplicity. These assumptions result in a conservative underestimate of the aluminum mass. These masses are distributed over the volume of each basket over the active fuel length. The basket compartment volumes are computed based on the dimensions provided in Table 5.3-2. The homogenized data are summarized in Table 5.3-4, and homogenized number densities are provided in Table 5.3-5. Note that the number densities of all three fuel types are quite similar, as all three fuel types are aluminum plate fuel.

The TRIGA fuel composition is provided in Table 5.3-6 and is based on 196 g uranium, 2,060 g zirconium, H/Zr ratio of 1.6, and U-235 enrichment of 70%. The composition of stainless steel cladding utilized is taken from the SCALE material library [5] and is provided in Table 5.3-7. The zirconium rod in the center of the active fuel is modeled as pure with a density of 6.5 g/cm^3 [6]. The graphite reflectors in the TRIGA fuel elements are modeled as air.

The baskets are manufactured out of stainless steel, and the cask is constructed of stainless steel and lead. The stainless steel composition and density utilized in the MCNP models are provided in Table 5.3-7. Lead is modeled as pure with a density of 11.35 g/cm^3 [6].

Void spaces are filled with dry air. The composition is obtained from SCALE material library [5] and is provided in Table 5.3-8.

Table 5.3-1 – Key Cask Model Dimensions

Item	Dimension (in)
Cask Radial	
Cask inner diameter	16.0
Cask inner steel thickness	1.0
Cask lead thickness	8.0, modeled as 7.9375
Cask lead radial shrinkage gap (assumed)	0.0625
Cask outer steel thickness	2.0
Cask outer diameter (w/o heat shield)	38.0
Cask to heat shield gap	0.105
Heat shield thickness	0.105
Upper and lower impact limiter diameter	78.0, modeled as 72.0
Cask Axial Top	
Shield plug bottom plate thickness	1.0
Shield plug lead thickness	9.7, modeled as 9.58
Shield plug top plate thickness	0.5
Shield plug overall height	11.2, modeled as 11.08
Shield plug vent pipe inner diameter (schedule 40S)	0.824
Lid thickness	2.0
Upper impact limiter thickness at centerline	21.2
Overall height (including impact limiters)	119.5
Cask Axial Bottom	
Bottom outer plate thickness	1.0
Bottom lead thickness at centerline	7.7, modeled as 7.72
Bottom casting inner thickness (after machining)	1.1, modeled as 1.22
Bottom lead major diameter	23.7
Bottom lead minor diameter	10.3, modeled as 9.75
Drain hole diameter	0.5
Lower impact limiter thickness at centerline	21.2

Table 5.3-2 – Key Basket Model Dimensions

Item	Dimension (in)
MURR Basket	
Overall height	53.45
Cavity length	33.13
Support plate thickness	0.375
Compartment separator width	1.0
Shell outer diameter	15.63
Shell thickness	0.25
Inner tube outer diameter	7.9, modeled as 7.938
Inner tube inner diameter	7.0
MITR-II Basket	
Overall height	53.45
Cavity length	26.88
Support plate thickness	0.5
Inner Diameter	Complex, modeled as 9.45
Outer Diameter	15.63
Compartment perpendicular width	2.7
Distance, cutout to center	4.8
ATR Basket	
Overall height	53.45
Cavity length	51.38, modeled as 51.37
Support plate thickness	0.5
Compartment separator width	0.375
Shell outer diameter	13.5
Shell thickness	0.25
Inner tube outer diameter	7.2
Inner tube inner diameter	6.5
TRIGA Basket	
Overall height	53.45
Cavity length	48.0, modeled as 46.42
Support plate thickness (after machining)	0.3, modeled as 0.25
Tube outer diameter	2.0
Tube wall thickness	0.12, modeled as 0.11
Inner row position diameter	6.5
Outer row position diameter	11.5

Table 5.3-3 – Key Fuel Dimensions

Item	Dimension (in)
MURR①	
Nominal active fuel length	24
Overall length	32.5
Nominal cladding thickness	0.015
Nominal fuel matrix thickness	0.02
Nominal fuel matrix width	variable
MITR-II①	
Nominal active fuel length	22.375
Overall length	26.265
Nominal cladding thickness	0.025
Nominal fuel matrix thickness	0.03
Nominal fuel matrix width	2.076
ATR①	
Nominal active fuel length	48
Overall length	51
Nominal cladding thickness (plate 1 / plates 2 – 18, plate 19)	0.03 / 0.015 / 0.04
Nominal fuel matrix thickness	0.02
Nominal fuel matrix width	variable
TRIGA (Type 109)	
Active fuel length	15
Overall length	28.9
Fuel pellet outer diameter	1.44
Fuel pellet inner diameter	0.25
Cladding outer diameter	1.48
Cladding thickness	0.02
Top reflector length	2.6
Top bottom reflector length	3.7
Zirconium rod diameter	0.225

①The fuel dimensions for MURR, MITR-II, and ATR are used in the homogenization calculations, but are not modeled explicitly.

Table 5.3-4 – Homogenized Fuel Data

Parameter	MURR	MITR-II	ATR
U-235 (g)	785	515	1200
U-238 (g)	50.1	32.9	76.6
Al (g)	3353.1	2311.9	5414.5
Compartment volume (cm^3)	4884.2	3018.3	8192.0

Table 5.3-5 – Homogenized Fuel Number Densities (atom/b-cm)

Isotope	MURR	MITR-II	ATR
U-235	4.1178E-04	4.3716E-04	3.7531E-04
U-238	2.5952E-05	2.7552E-05	2.3653E-05
Al	1.5322E-02	1.7095E-02	1.4752E-02
Total	1.5760E-02	1.7560E-02	1.5151E-02

Table 5.3-6 – TRIGA Fuel Number Densities (atom/b-cm)

Isotope	TRIGA
H	5.6041E-02
Zr	3.5025E-02
U-235	9.0406E-04
U-238	3.8442E-04
Total	9.2354E-02

Table 5.3-7 – SS304 Composition

Component	Wt.%
C	0.08
Si	1.0
P	0.045
Cr	19.0
Mn	2.0
Fe	68.375
Ni	9.5
Density (g/cm^3)	7.94

Table 5.3-8 – Air Composition

Component	Wt.%
N	76.508
O	23.4793
C	0.0126
Density (g/cm^3)	0.0012

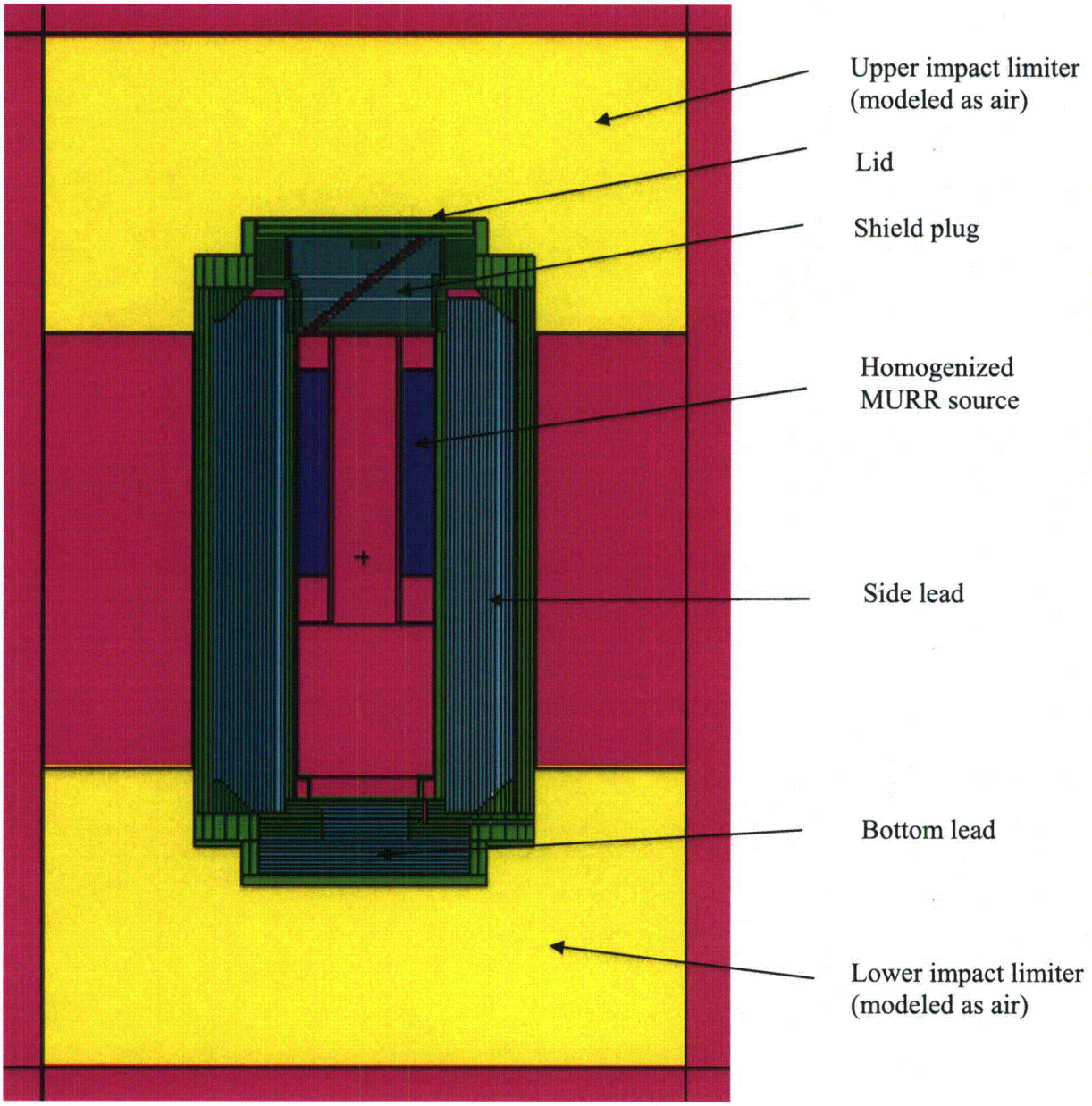

Figure 5.3-1 – Shielding Model

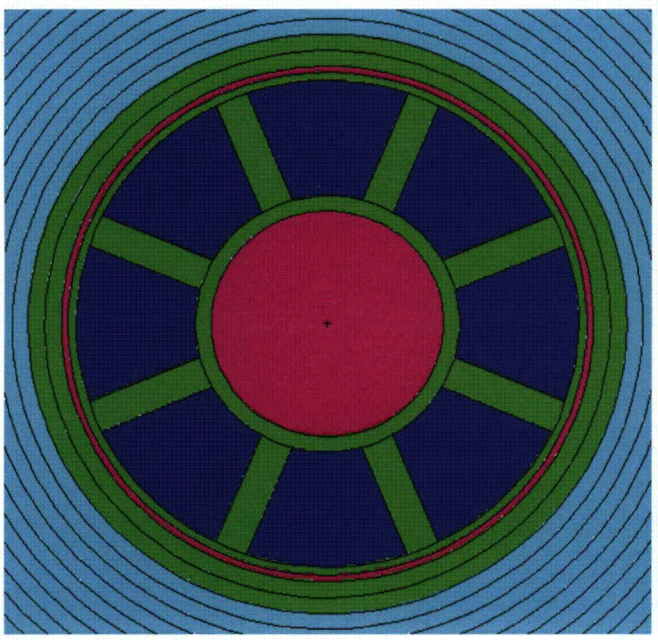

MURR

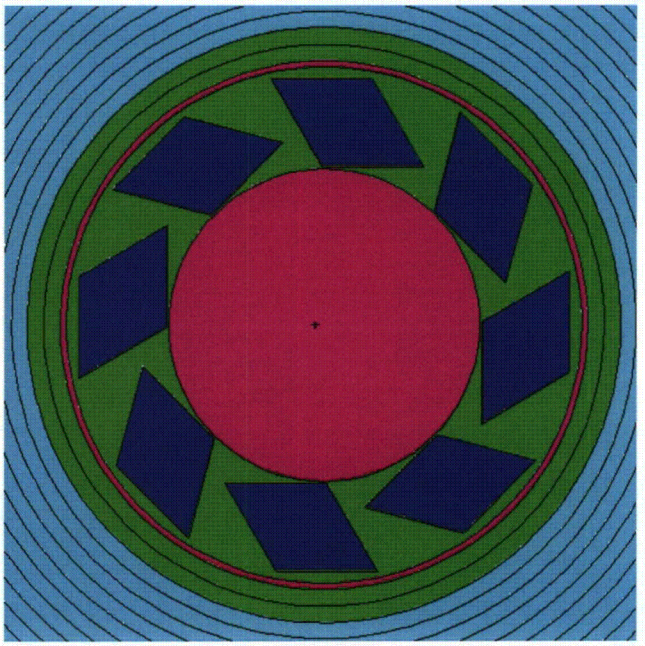

MITR-II

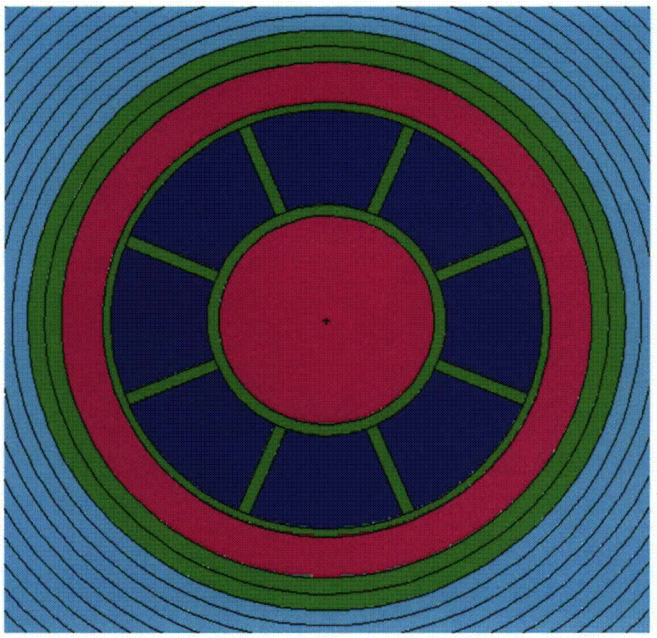

ATR

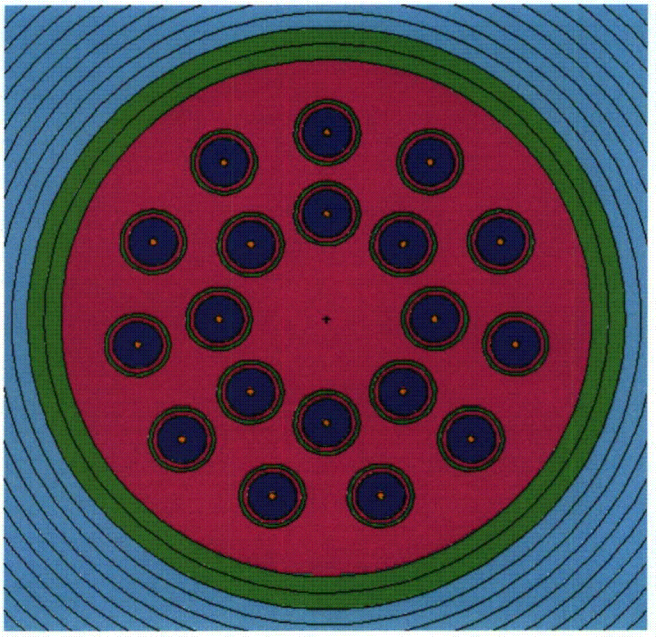

TRIGA

Figure 5.3-2 – Basket Models (cross section)

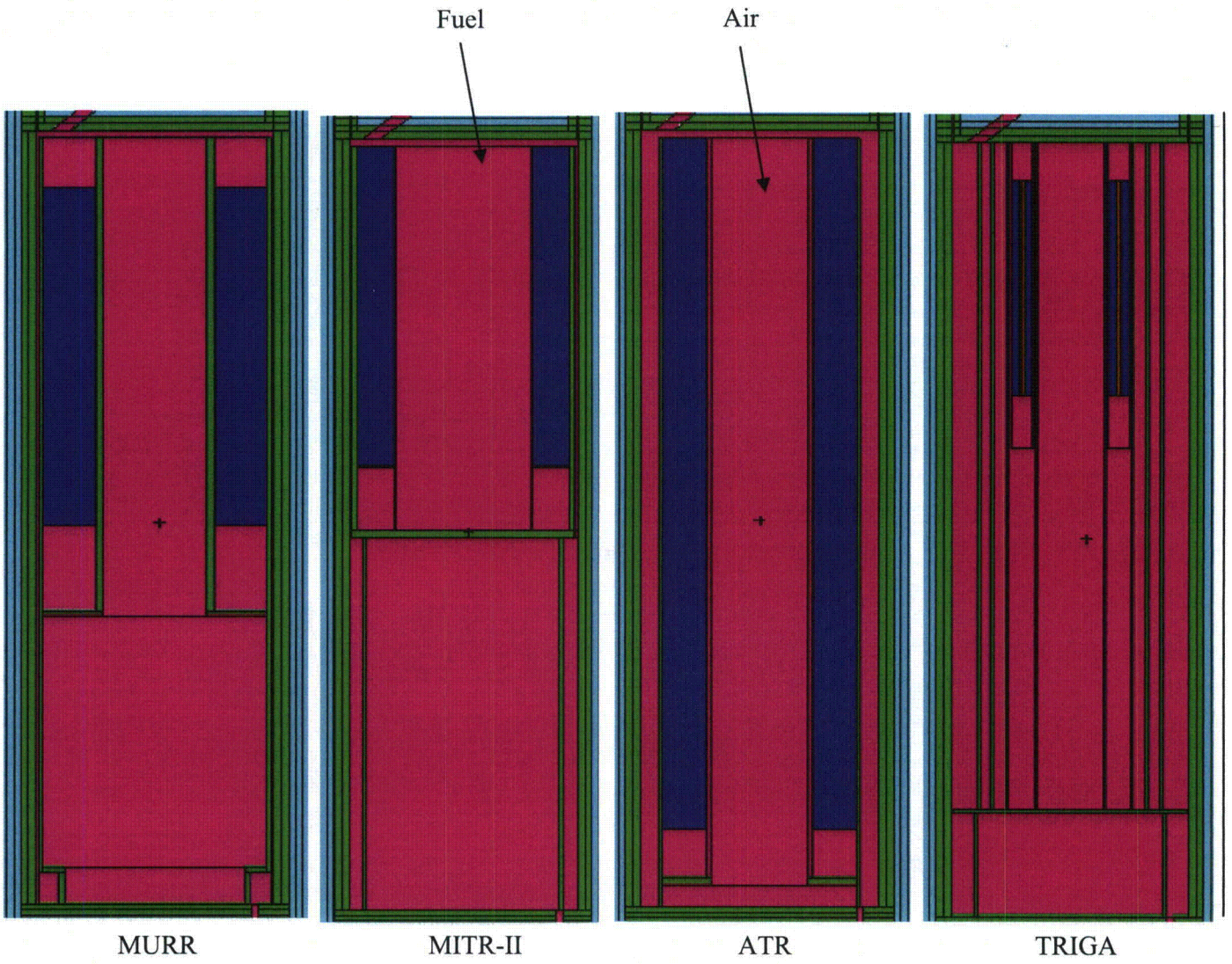

Figure 5.3-3 – Basket Models (axial)

5.4 Shielding Evaluation

5.4.1 Methods

The dose rates are computed using the MCNP5 v1.30 computer program [2]. All relevant package features are modeled in three-dimensions. For simplicity, the impact limiters are modeled simply as air, although the outer surfaces of the impact limiters are treated as the outer surfaces of the package when computing surface dose rates at the ends of the package. It is assumed that under HAC the impact limiters remain attached and suffer 12-in axial crush on each end, and the same MCNP model is used to compute both NCT and HAC dose rates. This approach is reasonable, because no shielding credit is taken for the impact limiters, other than distance.

Separate models are developed for neutron and gamma radiation. For MURR, MITR-II, and ATR fuel, the fuel plates are homogenized and fill the basket cavities. Homogenization is performed to simplify the source description. For the TRIGA fuel, because the fuel is a simple cylinder, the fuel is modeled explicitly, and the source is distributed over the fuel matrix. Note that subcritical neutron multiplication is handled automatically by MCNP.

Little clearance is available in any of the designs for axial shifting of the fuel. Because the fuel is positioned by the baskets closer to the lid end, to maximize the dose rates at the impact limiter surface, the fuel is modeled as shifted to the top of the cavity. Distance credit is taken for non-fuel structural material, such as the graphite reflectors in the TRIGA fuel.

In general, secondary gammas generated by neutron capture are not computed, as there is no hydrogenous neutron shielding material. Secondary gamma dose rates are computed only for the TRIGA fuel because hydrogen is included in the fuel matrix. However, even for the TRIGA fuel, the secondary gamma dose rate is essentially zero, because the secondary gammas are generated inside the cask, and are then attenuated in the shield.

In all cases, dose rates are computed on segmented surfaces so that the maximum dose rates may be located. Neutron and gamma surface fluxes are computed by MCNP, and converted to dose rates using flux-to-dose rate conversion factors (see Section 5.4.3, *Flux-to-Dose Rate Conversion*). Side dose rates are averaged over the circumference of the cylindrical tallies.

5.4.2 Input and Output Data

A sample input file (gamma source, MITR-II fuel) is included in Section 5.5.3.2, *MCNP Input File*. The input file may be compared against the gamma sources in table Table 5.2-3 and gamma axial distribution in Table 5.2-5 to verify proper model setup. Model geometry and material descriptions may be verified by inspection of the supplied input file.

The results are highly converged for all dose rate locations of interest. In the models with a gamma source, the materials are split into thin layers, and the importance of each layer is increased away from the source. In the models with a neutron source, the importances are all set to the same value, as there is no neutron shield. Statistical uncertainties are typically in the range of 2-3%.

5.4.3 Flux-to-Dose Rate Conversion

ANSI/ANS-6.1.1-1977 flux-to-dose rate conversion factors are used in this analysis. These are obtained from the MCNP User's Manual [2], Tables H.1 and H.2, although these values have been converted to provide results in mrem/hr rather than rem/hr. These conversion factors are provided in Table 5.4-1.

5.4.4 External Radiation Levels

A total of eight input files are developed to compute the NCT and HAC dose rates. A gamma and neutron model is developed for each of the four sources. The files are itemized as follows, where N refers to neutron modeling and G refers to gamma modeling:

- MURR fuel: MURR_N2, MURR_G2
- MITR-II fuel: MIT_N3, MIT_G3
- ATR fuel: ATR_N2, ATR_G2
- TRIGA fuel: TRIGA_NG2, TRIGA_G2

For exclusive use transport, the following 10 CFR 71.47 dose rates must be met:

- Maximum NCT cask surface dose rate of 200 mrem/hr. The higher 1000 mrem/hr limit is not claimed because the vehicle will be open. The dose rate limit applies at the outer surface of the heat shield, and the outer surface of the impact limiters. These results are summarized in Table 5.4-2 and Table 5.4-3. See also Figure 5.4-1 and Figure 5.4-2 for a graphical depiction of the tally locations.
- Maximum NCT vehicle surface dose rate of 200 mrem/hr. This limit is somewhat redundant because it is the same as the cask surface limit, and the cask surface dose rates are always higher than the vehicle surface dose rates. In this case, the vehicle surface is projected, because the actual vehicle will be open. It is assumed the vehicle is 8 ft wide, and the cask is laterally centered on the vehicle. These results are summarized in Table 5.4-4. See also Figure 5.4-3 and Figure 5.4-4 for a graphical depiction of the tally locations.
- Maximum NCT dose rate 2 m from the vehicle surface of 10 mrem/hr. These results are summarized in Table 5.4-4. See also Figure 5.4-3 and Figure 5.4-4 for a graphical depiction of the tally locations.
- Maximum NCT dose rate in any occupied location of 2 mrem/hr. The only occupied location is the driver of the vehicle, which is assumed to be 25 ft from the centerline of the cask. These results are summarized in Table 5.4-5. See also Figure 5.4-3 and Figure 5.4-4 for a graphical depiction of the tally location.
- Maximum HAC dose rate of 1000 mrem/hr 1 m from the surface of the cask. As the impact limiters will remain attached under HAC, the end dose rates are computed 1 m from the ends of the impact limiters, assuming 12-in crush on each end. In the radial direction, the dose rates are computed 1 m from the heat shield. These results are summarized in Table 5.4-6 and Table 5.4-7. See also Figure 5.4-3, Figure 5.4-4, and Figure 5.4-5 for a graphical depiction of the tally locations

Dose rates are not constant along the side of the cask. The dose rate is typically at a maximum next to the active fuel, and becomes lower away from this region. Therefore, it is customary to segment the tallies into small regions in order to capture the maximum dose rate. On the side surface of the cask, the tally is divided into 12 equal segments 10.7 cm wide (see Figure 5.4-1). On the cylindrical sides of the impact limiters, the tally is divided into 5 equal segments 17.6 cm wide (see Figure 5.4-2). On the upper and lower impact limiter surfaces, the tally is divided into 9 concentric rings of width 10.2 cm (see Figure 5.4-2).

For the four side tallies (vehicle surface, 2 m from vehicle surface, occupied location, and 1 m HAC), the tallies are segmented into 15 segments 20.3 cm wide (see Figure 5.4-3 and Figure 5.4-4). In addition, the side dose rates above and below the impact limiter surfaces are also reported, although these tallies are approximately 70 cm wide.

The HAC 1 m tallies from the top and bottom of the impact limiters are divided into 11 segments, up to 1 m radially from the surface of the thermal shield (see Figure 5.4-5).

The dose rates reported in the following tables are the summed gamma and neutron dose rates. Dose rates are presented for each of the four fuel types. The maximum cask surface dose rate is 12.9 mrem/hr (limit = 200 mrem/hr). The maximum vehicle surface dose rate is 3.8 mrem/hr (limit = 200 mrem/hr). The maximum dose rate 2 m from the surface of the vehicle is 0.3 mrem/hr (limit = 10 mrem/hr), and the maximum dose rate at the occupied location is 0.06 mrem/hr (limit = 2 mrem/hr). Therefore, all of the NCT dose rates are met with large margins.

Note that the maximum dose rate on the vehicle surface occurs at location 1 (see Figure 5.4-4), which is actually above the upper impact limiter. The dose rate is peaking in this region rather than beside the source because the gamma shielding is greatly reduced in the "corners" of the cask. Also, the modeled lead slump in this region could be contributing to this effect.

The maximum HAC dose rate 1 m from the cask is 2.8 mrem/hr (limit = 1000 mrem/hr), and occurs at measured from the top at location 11, for the reasons cited in the previous paragraph. Clearly, the HAC dose rate limit is met with a large margin.

The detailed results from the MITR-II fuel, including statistical uncertainties, are reported in Section 5.5.2, *Detailed MITR-II Results*. MITR-II is selected for this detailed presentation because it results in the largest cask surface dose rate.

Table 5.4-1 – Flux-to-Dose Rate Conversion Factors

E (MeV)	Neutron Factors (mrem/hr)/(n/cm^2/s)	E (MeV)	Neutron Factors (mrem/hr)/(n/cm^2/s)
2.50E-08	3.67E-03	0.5	9.26E-02
1.00E-07	3.67E-03	1.0	1.32E-01
1.00E-06	4.46E-03	2.5	1.25E-01
1.00E-05	4.54E-03	5.0	1.56E-01
1.00E-04	4.18E-03	7.0	1.47E-01
0.001	3.76E-03	10.0	1.47E-01
0.01	3.56E-03	14.0	2.08E-01
0.1	2.17E-02	20.0	2.27E-01
E (MeV)	**Gamma Factors (mrem/hr)/(γ/cm^2/s)**	**E (MeV)**	**Gamma Factors (mrem/hr)/(γ/cm^2/s)**
0.01	3.96E-03	1.4	2.51E-03
0.03	5.82E-04	1.8	2.99E-03
0.05	2.90E-04	2.2	3.42E-03
0.07	2.58E-04	2.6	3.82E-03
0.1	2.83E-04	2.8	4.01E-03
0.15	3.79E-04	3.25	4.41E-03
0.2	5.01E-04	3.75	4.83E-03
0.25	6.31E-04	4.25	5.23E-03
0.3	7.59E-04	4.75	5.60E-03
0.35	8.78E-04	5.0	5.80E-03
0.4	9.85E-04	5.25	6.01E-03
0.45	1.08E-03	5.75	6.37E-03
0.5	1.17E-03	6.25	6.74E-03
0.55	1.27E-03	6.75	7.11E-03
0.6	1.36E-03	7.5	7.66E-03
0.65	1.44E-03	9.0	8.77E-03
0.7	1.52E-03	11.0	1.03E-02
0.8	1.68E-03	13.0	1.18E-02
1.0	1.98E-03	15.0	1.33E-02

Table 5.4-2 – NCT Cask Side Total Dose Rates (mrem/hr)

Location	MURR	MITR-II	ATR	TRIGA
1	2.2	8.2	2.1	6.7
2	5.0	11.3	2.9	9.9
3	8.5	12.9	3.6	10.7
4	10.9	12.4	4.2	9.1
5	11.1	10.0	4.7	5.8
6	9.0	6.4	4.9	3.1
7	5.2	3.4	4.8	1.8
8	2.1	1.9	4.5	1.1
9	0.7	1.2	4.0	0.7
10	0.3	0.8	3.3	0.5
11	0.2	0.6	2.5	0.4
12	0.1	0.4	1.8	0.3
Max	11.1	**12.9**	4.9	10.7
Limit = 200 mrem/hr				

Table 5.4-3 – NCT Impact Limiter Total Dose Rates (mrem/hr)

	Upper Impact Limiter Side				Lower Impact Limiter Side			
Location	**MURR**	**MITR-II**	**ATR**	**TRIGA**	**MURR**	**MITR-II**	**ATR**	**TRIGA**
1	2.0	8.0	0.5	6.1	0.2	0.3	0.6	0.2
2	1.4	5.5	0.5	4.4	0.1	0.2	0.4	0.1
3	0.9	3.2	0.4	2.7	0.2	0.2	0.5	0.1
4	0.7	2.3	0.5	1.8	0.3	0.3	0.6	0.1
5	1.0	2.3	0.6	1.8	0.3	0.2	0.6	0.1
Max	2.0	**8.0**	0.6	6.1	0.3	0.3	**0.6**	0.2
	Upper Impact Limiter Horizontal				**Lower Impact Limiter Horizontal**			
Location	**MURR**	**MITR-II**	**ATR**	**TRIGA**	**MURR**	**MITR-II**	**ATR**	**TRIGA**
1	1.4	4.3	0.3	2.1	3.5	2.7	0.7	0.3
2	1.5	4.5	0.3	2.3	3.7	3.0	0.7	0.4
3	2.0	5.4	0.4	2.8	2.8	2.2	0.6	0.3
4	2.1	5.7	0.4	3.1	1.8	1.6	0.5	0.2
5	1.7	5.5	0.4	3.5	1.1	0.9	0.4	0.1
6	1.6	5.6	0.4	3.9	0.6	0.5	0.4	0.1
7	1.8	6.5	0.5	4.8	0.4	0.3	0.4	0.1
8	2.3	8.5	0.6	6.8	0.3	0.3	0.5	0.1
9	2.3	9.9	0.6	7.2	0.3	0.2	0.5	0.1
Max	2.3	**9.9**	0.6	7.2	**3.7**	3.0	0.7	0.4
Limit = 200 mrem/hr								

Table 5.4-4 – NCT Vehicle Side and 2 m Total Dose Rates (mrem/hr)

	Vehicle Side				2 m from Vehicle Side			
Location	**MURR**	**MITR-II**	**ATR**	**TRIGA**	**MURR**	**MITR-II**	**ATR**	**TRIGA**
1	1.0	3.8	0.3	2.9	0.1	0.3	0.1	0.2
2	0.7	2.6	0.3	2.0	0.2	0.3	0.1	0.2
3	0.6	1.9	0.3	1.5	0.2	0.3	0.1	0.2
4	0.6	1.5	0.3	1.2	0.2	0.3	0.1	0.2
5	0.7	1.5	0.4	1.2	0.2	0.3	0.1	0.2
6	1.2	1.8	0.6	1.4	0.2	0.3	0.1	0.2
7	1.7	2.1	0.7	1.5	0.3	0.3	0.1	0.2
8	1.9	2.0	0.9	1.4	0.3	0.3	0.1	0.2
9	1.6	1.6	0.9	1.0	0.3	0.3	0.1	0.2
10	1.1	1.1	0.8	0.7	0.2	0.3	0.1	0.2
11	0.6	0.7	0.7	0.4	0.2	0.2	0.1	0.2
12	0.3	0.4	0.6	0.3	0.2	0.2	0.1	0.1
13	0.2	0.3	0.4	0.2	0.2	0.2	0.1	0.1
14	0.1	0.2	0.3	0.1	0.1	0.2	0.1	0.1
15	0.2	0.2	0.3	0.1	0.1	0.1	0.1	0.1
16	0.2	0.2	0.4	0.1	0.1	0.1	0.1	0.1
17	0.2	0.1	0.3	0.05	0.1	0.1	0.1	0.1
Max	1.9	**3.8**	0.9	2.9	0.3	**0.3**	0.1	0.2
	Limit = 200 mrem/hr				Limit = 10 mrem/hr			

Table 5.4-5 – NCT Occupied Location Total Dose Rates (mrem/hr)

Location	MURR	MITR-II	ATR	TRIGA
1	0.04	0.06	0.02	0.04
2	0.04	0.06	0.02	0.04
3	0.04	0.06	0.02	0.04
4	0.04	0.06	0.02	0.04
5	0.04	0.06	0.02	0.04
6	0.05	0.06	0.02	0.04
7	0.05	0.05	0.02	0.04
8	0.04	0.05	0.02	0.04
9	0.04	0.05	0.02	0.04
10	0.04	0.05	0.02	0.04
11	0.04	0.05	0.02	0.04
12	0.04	0.05	0.02	0.03
13	0.04	0.05	0.02	0.03
14	0.04	0.05	0.02	0.03
15	0.04	0.04	0.02	0.03
16	0.04	0.04	0.02	0.03
17	0.03	0.04	0.02	0.03
Max	0.05	**0.06**	0.02	0.04
Limit = 2 mrem/hr				

Table 5.4-6 – HAC 1 m Side Total Dose Rates (mrem/hr)

Location	MURR	MITR-II	ATR	TRIGA
1	0.6	2.4	0.2	1.7
2	0.4	1.4	0.2	1.1
3	0.4	1.2	0.2	0.9
4	0.5	1.1	0.3	0.9
5	0.6	1.2	0.4	0.9
6	0.9	1.3	0.4	1.0
7	1.2	1.4	0.5	1.0
8	1.3	1.4	0.6	1.0
9	1.1	1.1	0.6	0.8
10	0.9	0.9	0.6	0.6
11	0.6	0.6	0.5	0.4
12	0.4	0.4	0.4	0.3
13	0.2	0.3	0.3	0.2
14	0.2	0.2	0.3	0.1
15	0.1	0.2	0.2	0.1
16	0.1	0.2	0.2	0.1
17	0.1	0.1	0.2	0.1
Max	1.3	**2.4**	0.6	1.7
Limit = 1000 mrem/hr				

Table 5.4-7 – HAC 1 m End Total Dose Rates (mrem/hr)

	Upper Impact Limiter				Lower Impact Limiter			
Location	MURR	MITR-II	ATR	TRIGA	MURR	MITR-II	ATR	TRIGA
1	0.6	1.8	0.1	1.0	1.4	1.1	0.3	0.1
2	0.7	1.8	0.1	1.0	1.5	1.2	0.3	0.1
3	0.8	2.1	0.1	1.2	1.3	1.0	0.2	0.1
4	0.8	2.1	0.1	1.2	1.0	0.8	0.2	0.1
5	0.8	2.2	0.1	1.2	0.8	0.7	0.2	0.1
6	0.7	2.1	0.1	1.3	0.6	0.6	0.2	0.1
7	0.7	2.0	0.1	1.3	0.5	0.4	0.2	0.1
8	0.6	2.0	0.1	1.3	0.3	0.3	0.1	0.05
9	0.6	2.0	0.1	1.4	0.3	0.2	0.1	0.04
10	0.6	2.3	0.2	1.7	0.2	0.1	0.1	0.03
11	0.8	2.8	0.2	2.3	0.1	0.1	0.2	0.04
Max	0.8	**2.8**	0.2	2.3	**1.5**	1.2	0.3	0.1
Limit = 1000 mrem/hr								

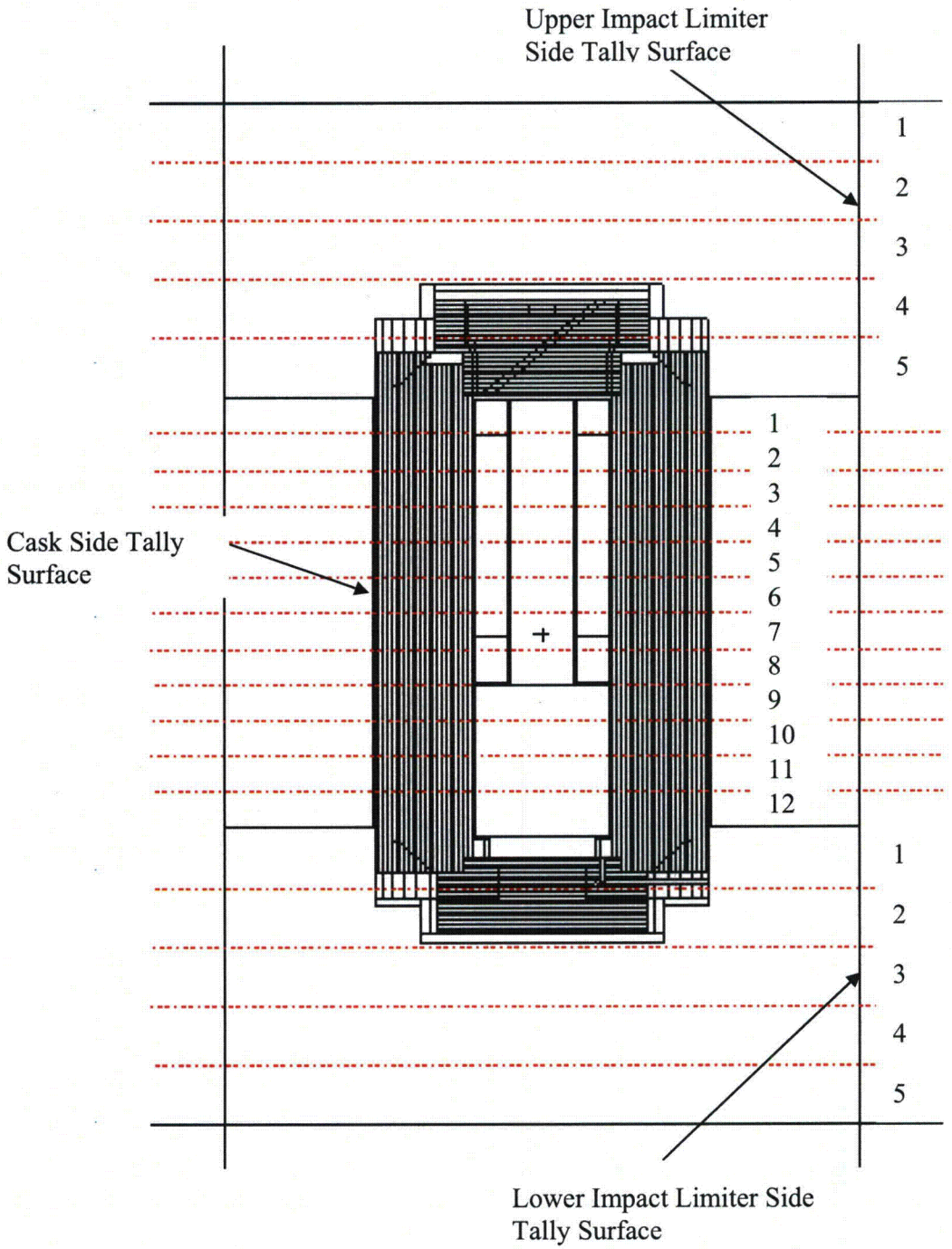

Note: All tallies are circumferential.

Figure 5.4-1 – Cask/Impact Limiter Side Tally Segmentations

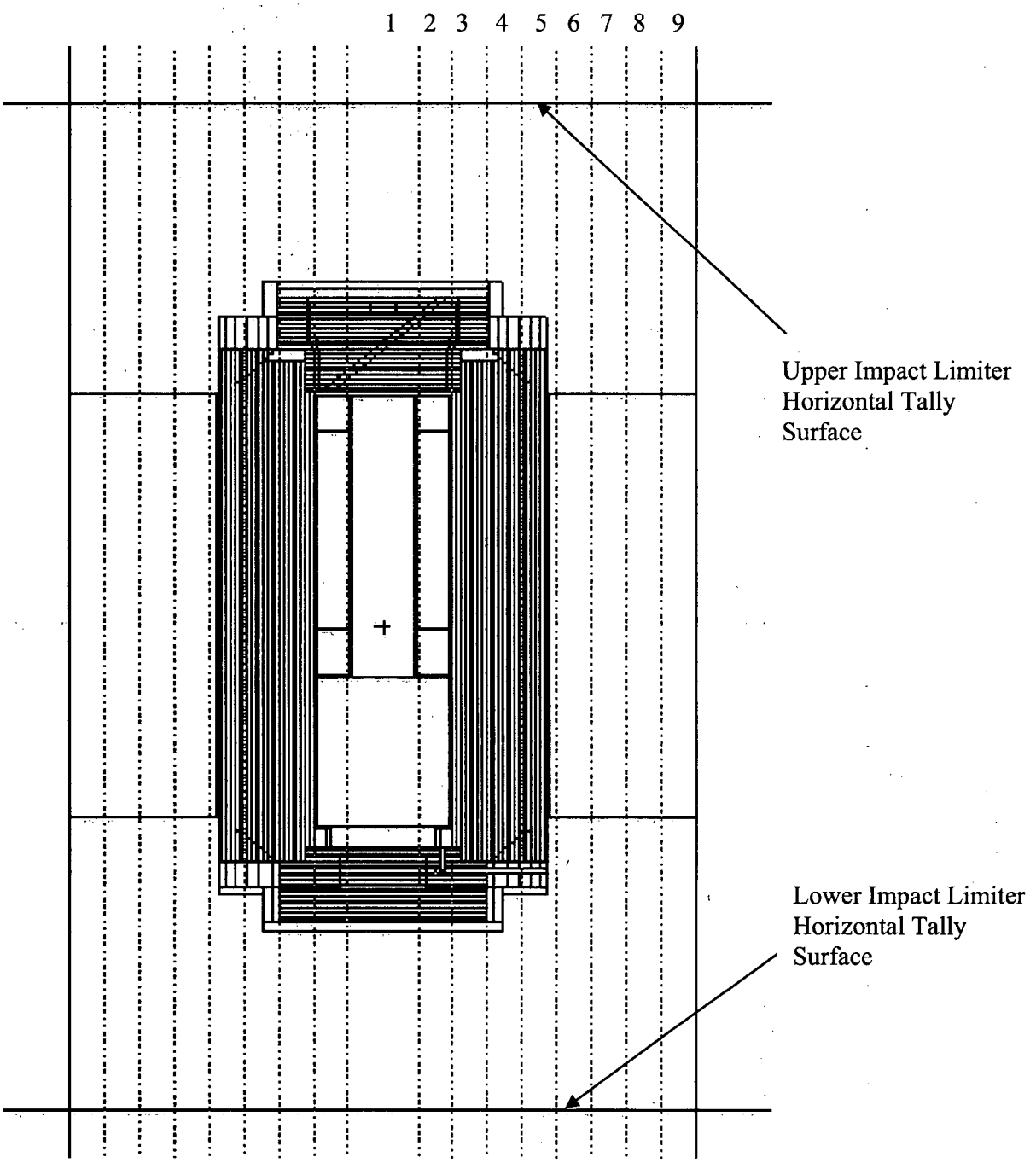

Figure 5.4-2 – Impact Limiter Horizontal Tally Segmentations

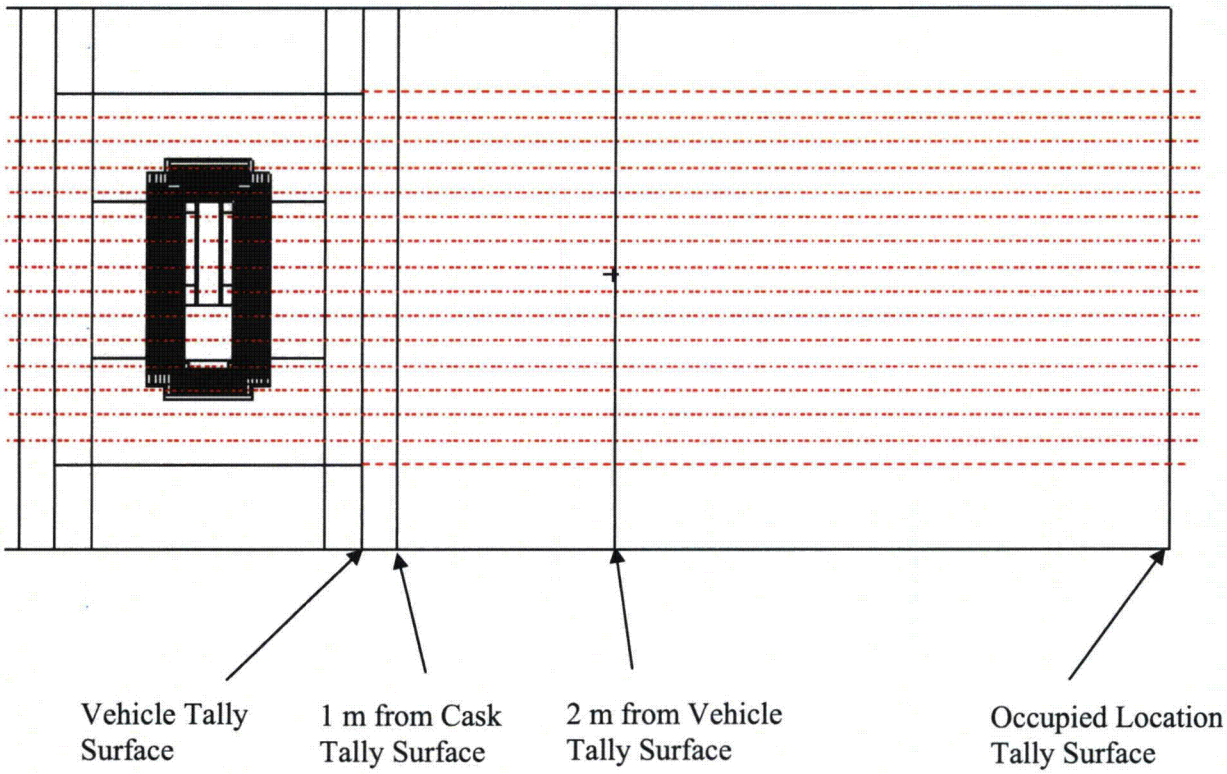

Note: All tallies are circumferential.

Figure 5.4-3 – Side Tally Locations

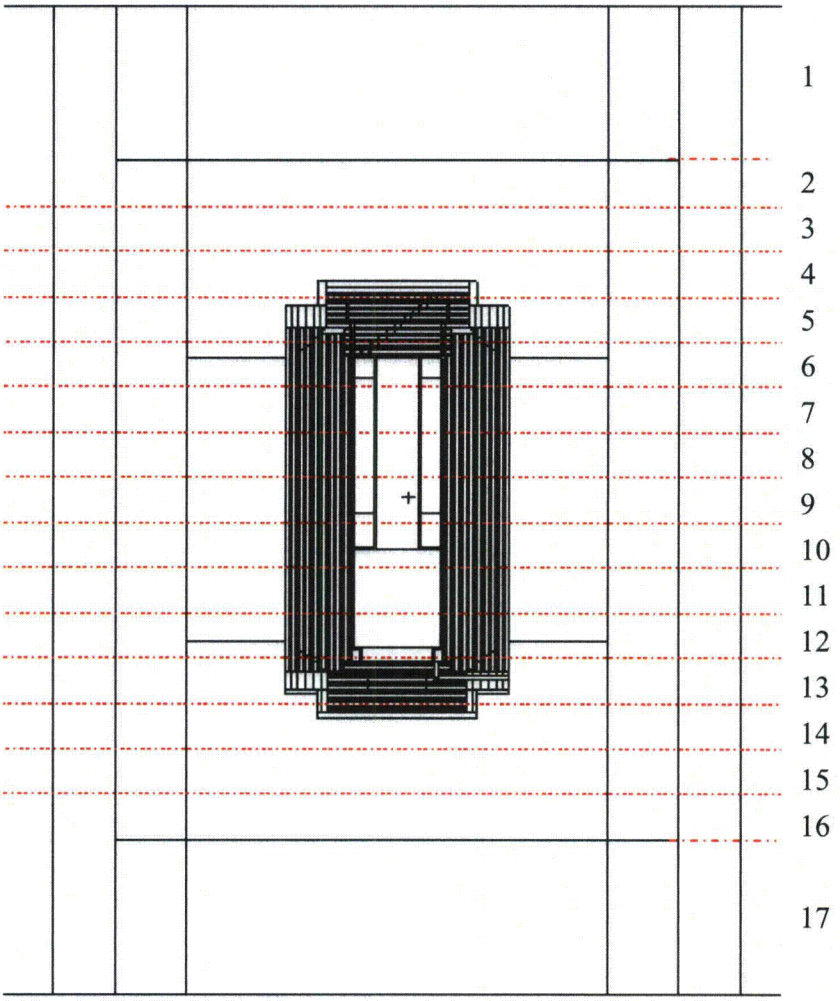

Note: All tallies are circumferential.

Figure 5.4-4 – Side Tally Segmentations (excluding cask surface)

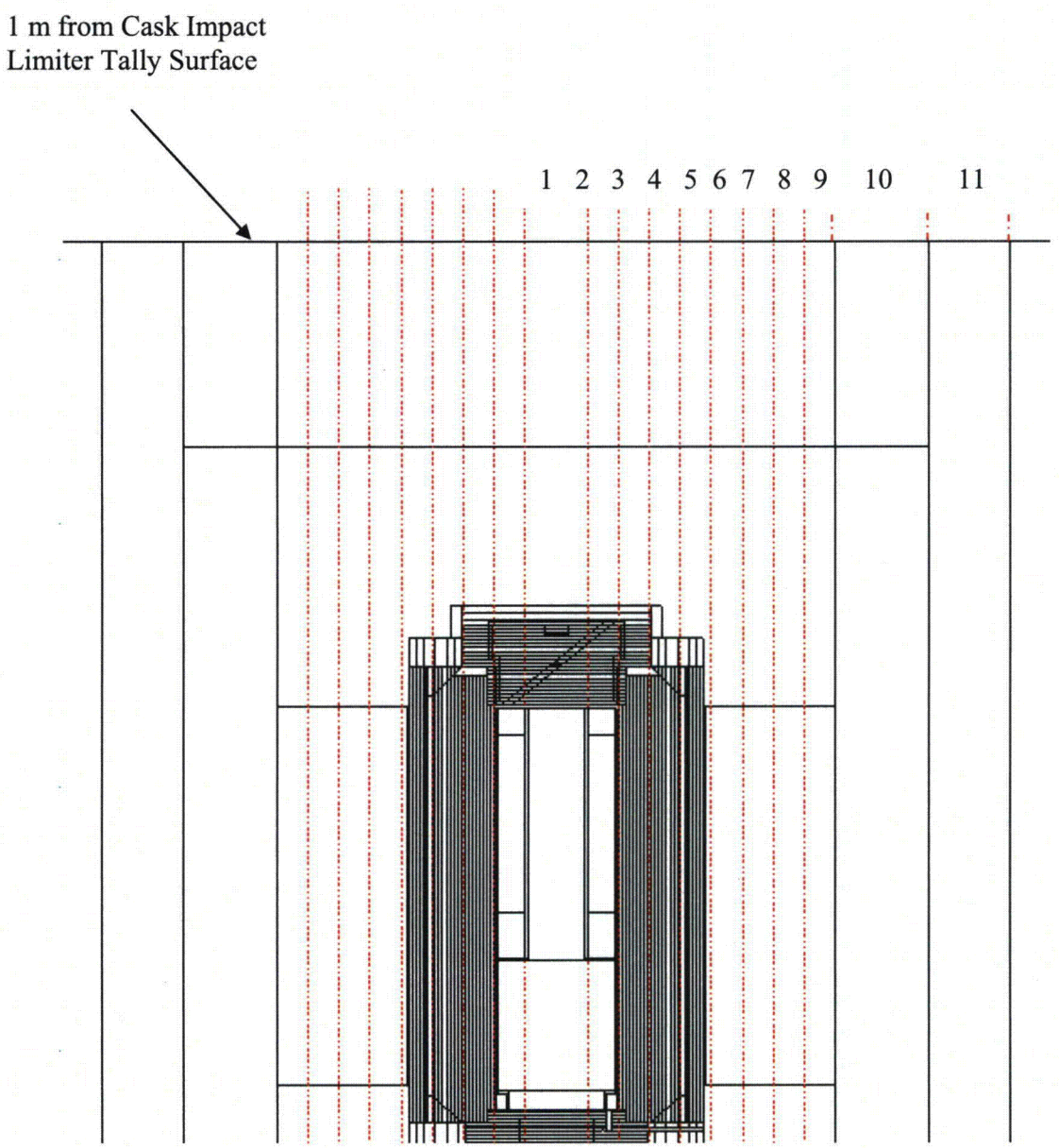

Figure 5.4-5 – HAC 1 m End Tally Segmentations

5.5 Appendices

5.5.1 References

1. Title 10, Code of Federal Regulations, Part 71 (10 CFR 71), Packaging and Transportation of Radioactive Material, 1–1–09 Edition.
2. MCNP5, "*MCNP – A General Monte Carlo N-Particle Transport Code, Version 5; Volume II: User's Guide*," LA-CP-03-0245, Los Alamos National Laboratory, April 2003. MCNP5 is distributed by the Radiation Safety Information Computational Center (www-rsicc.ornl.gov), Release C00710MNYCP02 (Windows PC).
3. *SCALE: A Modular Code System for Performing Standardized Computer Analyses for Licensing Evaluations*, ORNL/TM-2005/39, Version 6, Vols. I-III, January 2009.
4. JW Sterbentz, *Radionuclide Mass Inventory, Activity, Decay Heat, and Dose Rate Parametric Data for TRIGA Spent Nuclear Fuels*, INEL-96/0482, Idaho National Engineering Laboratory, March 1997.
5. *Standard Composition Library*, ORNL/TM-2005/39, Version 6, Vol. III, Section M8, January 2009.
6. *Nuclides and Isotopes, Chart of the Nuclides, Fifteenth Edition*, General Electric Co. and KAPL, Inc., 1996.

5.5.2 Detailed MITR-II Results

The following tables provide the detailed results for MITR-II fuel, because this fuel is limiting on the side of the cask.

Table 5.5-1 – MITR-II NCT Cask Side Dose Rates (mrem/hr)

Location	Gamma	σ	Neutron	σ	Total	σ
1	4.6	0.6%	3.6	0.1%	8.2	0.3%
2	6.8	0.5%	4.6	0.04%	11.3	0.3%
3	7.9	0.4%	5.0	0.04%	12.9	0.3%
4	7.6	0.5%	4.8	0.04%	12.4	0.3%
5	5.9	0.5%	4.1	0.1%	10.0	0.3%
6	3.2	0.7%	3.2	0.1%	6.4	0.3%
7	1.1	1.0%	2.3	0.1%	3.4	0.3%
8	0.3	1.7%	1.6	0.1%	1.9	0.3%
9	0.1	2.8%	1.1	0.1%	1.2	0.2%
10	0.03	4.1%	0.8	0.1%	0.8	0.2%
11	0.01	5.0%	0.6	0.1%	0.6	0.1%
12	0.004	5.7%	0.4	0.1%	0.4	0.1%

Table 5.5-2 – MITR-II NCT Impact Limiter Dose Rates (mrem/hr)

Location	Gamma	σ	Neutron	σ	Total	σ
Upper Impact Limiter Side						
1	7.7	1.4%	0.2	0.1%	8.0	1.3%
2	5.2	1.0%	0.3	0.1%	5.5	0.9%
3	2.8	0.8%	0.4	0.1%	3.2	0.7%
4	1.7	0.5%	0.6	0.1%	2.3	0.4%
5	1.5	0.4%	0.8	0.04%	2.3	0.2%
Lower Impact Limiter Side						
1	0.1	2.6%	0.2	0.1%	0.3	0.6%
2	0.1	2.1%	0.1	0.1%	0.2	0.6%
3	0.1	2.6%	0.1	0.2%	0.2	1.4%
4	0.2	3.0%	0.1	0.2%	0.3	2.2%
5	0.2	3.9%	0.1	0.2%	0.2	3.0%
Upper Impact Limiter Horizontal						
1	3.9	3.0%	0.4	0.3%	4.3	2.7%
2	4.1	2.8%	0.4	0.2%	4.5	2.6%
3	5.0	2.4%	0.4	0.1%	5.4	2.2%
4	5.4	2.2%	0.3	0.1%	5.7	2.0%
5	5.2	2.0%	0.3	0.1%	5.5	1.9%
6	5.3	1.8%	0.3	0.1%	5.6	1.7%
7	6.2	1.5%	0.2	0.1%	6.5	1.5%
8	8.3	2.7%	0.2	0.1%	8.5	2.6%
9	9.7	2.6%	0.2	0.1%	9.9	2.6%
Lower Impact Limiter Horizontal						
1	2.6	1.7%	0.1	0.7%	2.7	1.6%
2	2.9	1.7%	0.1	0.4%	3.0	1.7%
3	2.2	1.6%	0.1	0.3%	2.2	1.5%
4	1.5	1.5%	0.1	0.3%	1.6	1.4%
5	0.9	1.5%	0.1	0.3%	0.9	1.4%
6	0.5	1.5%	0.05	0.3%	0.5	1.3%
7	0.3	1.7%	0.05	0.3%	0.3	1.5%
8	0.2	3.5%	0.05	0.3%	0.3	2.9%
9	0.2	4.8%	0.05	0.2%	0.2	3.8%

Table 5.5-3 – MITR-II NCT Vehicle Surface Dose Rates (mrem/hr)

Location	Gamma	σ	Neutron	σ	Total	σ
1	3.7	1.5%	0.1	0.1%	3.8	1.5%
2	2.4	1.0%	0.2	0.1%	2.6	0.9%
3	1.6	0.8%	0.3	0.1%	1.9	0.6%
4	1.2	0.5%	0.4	0.1%	1.5	0.4%
5	1.1	0.3%	0.5	0.04%	1.5	0.2%
6	1.2	0.3%	0.6	0.04%	1.8	0.2%
7	1.4	0.3%	0.7	0.03%	2.1	0.2%
8	1.3	0.3%	0.7	0.03%	2.0	0.2%
9	1.0	0.3%	0.6	0.04%	1.6	0.2%
10	0.6	0.4%	0.5	0.04%	1.1	0.2%
11	0.3	0.4%	0.4	0.1%	0.7	0.2%
12	0.1	0.4%	0.3	0.1%	0.4	0.1%
13	0.1	1.4%	0.2	0.1%	0.3	0.4%
14	0.1	1.2%	0.1	0.1%	0.2	0.4%
15	0.1	2.0%	0.1	0.1%	0.2	0.9%
16	0.1	2.5%	0.1	0.1%	0.2	1.5%
17	0.1	2.8%	0.04	0.1%	0.1	2.0%

Table 5.5-4 – MITR-II NCT 2 m Vehicle Surface Dose Rates (mrem/hr)

Location	Gamma	σ	Neutron	σ	Total	σ
1	0.2	0.6%	0.1	0.04%	0.3	0.5%
2	0.2	0.4%	0.1	0.1%	0.3	0.3%
3	0.2	0.4%	0.1	0.1%	0.3	0.3%
4	0.2	0.3%	0.1	0.1%	0.3	0.2%
5	0.2	0.3%	0.1	0.1%	0.3	0.2%
6	0.2	0.3%	0.1	0.1%	0.3	0.2%
7	0.2	0.3%	0.1	0.1%	0.3	0.2%
8	0.2	0.3%	0.1	0.1%	0.3	0.2%
9	0.2	0.3%	0.1	0.1%	0.3	0.2%
10	0.2	0.3%	0.1	0.1%	0.3	0.2%
11	0.2	0.4%	0.1	0.1%	0.2	0.2%
12	0.1	0.4%	0.1	0.1%	0.2	0.2%
13	0.1	0.5%	0.1	0.1%	0.2	0.3%
14	0.1	0.4%	0.1	0.1%	0.2	0.2%
15	0.1	0.4%	0.1	0.1%	0.1	0.2%
16	0.1	0.4%	0.1	0.1%	0.1	0.2%
17	0.04	0.5%	0.04	0.1%	0.1	0.2%

Table 5.5-5 – MITR-II NCT Occupied Location Dose Rates (mrem/hr)

Location	Gamma	σ	Neutron	σ	Total	σ
1	0.042	0.4%	0.014	0.1%	0.056	0.3%
2	0.042	0.4%	0.015	0.1%	0.057	0.3%
3	0.042	0.4%	0.015	0.1%	0.057	0.3%
4	0.042	0.4%	0.015	0.1%	0.057	0.3%
5	0.042	0.4%	0.015	0.1%	0.057	0.3%
6	0.041	0.4%	0.015	0.1%	0.056	0.3%
7	0.040	0.4%	0.015	0.1%	0.055	0.3%
8	0.039	0.4%	0.015	0.1%	0.054	0.3%
9	0.038	0.4%	0.015	0.1%	0.053	0.3%
10	0.037	0.4%	0.015	0.1%	0.052	0.3%
11	0.036	0.4%	0.015	0.1%	0.051	0.3%
12	0.035	0.6%	0.015	0.1%	0.049	0.4%
13	0.033	0.4%	0.014	0.1%	0.048	0.3%
14	0.031	0.4%	0.014	0.1%	0.046	0.3%
15	0.030	0.4%	0.014	0.1%	0.044	0.3%
16	0.028	0.4%	0.014	0.1%	0.042	0.3%
17	0.024	0.3%	0.013	0.1%	0.037	0.2%

Table 5.5-6 – MITR-II HAC 1 m Side Dose Rates (mrem/hr)

Location	Gamma	σ	Neutron	σ	Total	σ
1	2.2	1.6%	0.1	0.1%	2.4	1.5%
2	1.2	0.8%	0.2	0.1%	1.4	0.7%
3	0.9	0.6%	0.2	0.1%	1.2	0.5%
4	0.8	0.5%	0.3	0.1%	1.1	0.3%
5	0.8	0.3%	0.3	0.04%	1.2	0.2%
6	0.9	0.3%	0.4	0.04%	1.3	0.2%
7	1.0	0.3%	0.4	0.04%	1.4	0.2%
8	0.9	0.3%	0.4	0.04%	1.4	0.2%
9	0.7	0.3%	0.4	0.04%	1.1	0.2%
10	0.5	0.3%	0.4	0.04%	0.9	0.2%
11	0.3	0.4%	0.3	0.1%	0.6	0.2%
12	0.2	0.4%	0.2	0.1%	0.4	0.2%
13	0.1	0.9%	0.2	0.1%	0.3	0.3%
14	0.1	0.7%	0.1	0.1%	0.2	0.3%
15	0.1	1.2%	0.1	0.1%	0.2	0.5%
16	0.1	1.8%	0.1	0.1%	0.2	0.8%
17	0.1	2.6%	0.05	0.1%	0.1	1.6%

Table 5.5-7 – MITR-II HAC Impact Limiter 1m End Dose Rates (mrem/hr)

Location	Gamma	σ	Neutron	σ	Total	σ
1 m from Upper Impact Limiter						
1	1.7	2.2%	0.1	0.5%	1.8	2.0%
2	1.7	2.1%	0.1	0.3%	1.8	1.9%
3	1.9	1.9%	0.1	0.2%	2.1	1.8%
4	2.0	1.9%	0.1	0.2%	2.1	1.8%
5	2.0	1.8%	0.1	0.2%	2.2	1.7%
6	2.0	1.7%	0.1	0.2%	2.1	1.6%
7	1.9	1.7%	0.1	0.2%	2.0	1.6%
8	1.9	1.7%	0.1	0.2%	2.0	1.6%
9	1.9	1.6%	0.1	0.2%	2.0	1.5%
10	2.2	1.5%	0.1	0.1%	2.3	1.4%
11	2.7	1.6%	0.1	0.1%	2.8	1.5%
1 m from Lower Impact Limiter						
1	1.1	2.4%	0.03	1.2%	1.1	2.4%
2	1.2	2.1%	0.03	0.7%	1.2	2.1%
3	1.0	1.9%	0.03	0.6%	1.0	1.8%
4	0.8	1.7%	0.02	0.5%	0.8	1.6%
5	0.7	1.6%	0.02	0.4%	0.7	1.6%
6	0.5	1.6%	0.02	0.4%	0.6	1.6%
7	0.4	1.6%	0.02	0.4%	0.4	1.5%
8	0.3	1.5%	0.02	0.4%	0.3	1.4%
9	0.2	1.5%	0.02	0.3%	0.2	1.3%
10	0.1	1.7%	0.03	0.2%	0.1	1.4%
11	0.1	2.7%	0.03	0.1%	0.1	1.9%

5.5.3 Sample Input Files

5.5.3.1 TRITON Input File

A sample TRITON input file for MURR is included. The file is annotated to aid in understanding the input.

Adding parm=weight instructs TRITON to collapse the 238-group ENDF/B-VII data library to a 49-group library for use in the NEWT calculations. The first NEWT calculation is performed with 238 groups, but all subsequent NEWT calculations use the collapsed library to accelerate the run time.

```
=t-depl          parm=weight
MURR Fuel Model
```

```
v7-238
read comp
'Fuel
u-235  1  0  3.6124e-3        358.0 end
u-238  1  0  2.6847e-4        358.0 end
al     1  0  5.0239e-2        358.0 end
'Cladding
al     2                 1.0  355.2 end
'Water
h2o    3  den=0.983      1.0  327.4 end
end comp
```

The pitch, fuel meat thickness, and cladding thickness are specified.

```
read celldata
latticecell symmslabcell   pitch=0.3302 3 fueld=0.0508 1 cladd=0.127  2  end
end celldata
```

Depletion is to be carried out only in material 1 (aluminum cladding has negligible depletion and is neglected). The negative sign means that the total power is to be normalized to the fuel mixture region only. If a positive sign were entered, the power would be normalized across the entire fuel element model (including cladding and water). Due to small amounts of power generated by the cladding and water as a result of (n,γ) reactions, normalizing the power over the entire assembly results in less than the specified power in the fuel itself.

The power is specified in units of MW/MTU. BURN is the number of days at power, while DOWN is the number of days between cycles. NLIB is the number of data libraries to be generated for each burnup specification. Increasing the value of NLIB increases the accuracy (and length) of the calculation, although in this case the days at power are relatively short and one library per cycle is sufficient.

```
read depletion -1 end depletion
read burndata
power=1515.3 burn=7  down=14     nlib=1 end
power=1515.3 burn=7  down=14     nlib=1 end
power=1515.3 burn=7  down=14     nlib=1 end
power=1515.3 burn=7  down=14     nlib=1 end
power=1515.3 burn=7  down=14     nlib=1 end
power=1515.3 burn=7  down=14     nlib=1 end
power=1515.3 burn=7  down=14     nlib=1 end
power=1515.3 burn=7  down=14     nlib=1 end
power=1515.3 burn=7  down=14     nlib=1 end
power=1515.3 burn=7  down=14     nlib=1 end
power=1515.3 burn=7  down=14     nlib=1 end
power=1515.3 burn=7  down=14     nlib=1 end
power=1515.3 burn=7  down=14     nlib=1 end
power=1515.3 burn=7  down=14     nlib=1 end
power=1515.3 burn=7  down=14     nlib=1 end
power=1515.3 burn=7  down=14     nlib=1 end
power=1515.3 burn=7  down=14     nlib=1 end
power=1515.3 burn=7  down=14     nlib=1 end
power=1515.3 burn=7  down=14     nlib=1 end
power=1515.3 burn=7  down=14     nlib=1 end
power=1515.3 burn=4  down=180    nlib=1 end
end burndata
```

Because of the size of the output file, extracting data from the output could be tedious. OPUS is simply a tool used to extract output, which appears at the end of the file. Five different quantities are requested: (1) power, (2) mass of U-235, (3) curies of the plutonium isotopes, (4) neutron source, and (5) gamma source. MATL=0 means to extract data from all depleted materials in the problem, which in this case is simply material 1. It is specified only once and applies to all five requested quantities. Note that all output is for a basis of 1 MTU. Output must be converted to a single fuel element by multiplying by the MTU of the element.

```
read opus
 units=watts
 matl=0 end
new case
 units=gram symnuc=u-235 end
new case
 units=curie symnuc=pu-238 pu-239
 pu-240 pu-241 pu-242 end
new case
 units=particles/s typarams=nspectrum
new case
 units=particles/s typarams=gspectrum
end opus
```

The NEWT model is specified as a 1x24 array of flat plates, each half the width of an average fuel plate. Each plate has a 5x2 mesh. The default mesh applied to global unit 2 is not used, because it is completely overridden by the mesh applied to unit 1. Reflective boundary conditions are placed on all 4 sides of the fuel element model.

```
' NEWT model
read model
MURR fuel element
read parm
 drawit=yes run=yes
end parm
read materials
  mix=1  pn=1   com='fuel'  end
  mix=2  pn=1   com='clad'  end
  mix=3  pn=1   com='water' end
end materials
read geom
unit 1
 cuboid  10  3.6606 0.0 0.1905 0.1397
 cuboid  20  3.6606 0.0 0.2286 0.1016
 cuboid  30  3.6606 0.0 0.3302 0.0
 media   1  1  10
 media   2  1  20 -10
 media   3  1  30 -20
 boundary 30 5 2
global unit 2
 cuboid 10  3.6606 0.0 7.9248 0.0
 media  3 1 10
 array  1 10 place 1 1 0.0 0.0
 boundary 10
end geom
read array
 ara=1 nux=1 nuy=24 typ=cuboidal fill
 1 1 1 1 1  1 1 1 1 1  1 1 1 1 1  1 1 1 1 1  1 1 1 1 end fill
end array
read bounds all=refl end bounds
```

```
end model
' End of NEWT model
end
```

5.5.3.2 MCNP Input File

A sample input file is provided for the MITR-II fuel with a gamma source (filename MIT_G3).

```
BRRC
c
c lateral cask wall including Pb shield
c
10  4   -7.94     100 -157   1 -2          imp:p=1       $ SS inner shell split
11  4   -7.94     100 -157   2 -3          imp:p=2       $ SS inner shell split
12  8  -11.35     103 -133   3 -4          imp:p=4       $ Pb gamma shield split
13  8  -11.35     103 -133   4 -5          imp:p=8       $ Pb gamma shield split
14  8  -11.35     103 -133   5 -6          imp:p=16      $ Pb gamma shield split
15  8  -11.35     103 -133   6 -7          imp:p=32      $ Pb gamma shield split
16  8  -11.35     103 -133   7 -8          imp:p=64      $ Pb gamma shield split
17  8  -11.35     103 -133   8 -801        imp:p=128     $ Pb gamma shield split
18  8  -11.35     103 -133   801 -9        imp:p=200     $ Pb gamma shield split
19  4   -7.94     103 300    9 -10         imp:p=256     $ SS
20  4   -7.94     301 -132   9 -10         imp:p=256     $ SS
21  8  -11.35     -300 -301 -133  9 -10    imp:p=256     $ Pb gamma shield split
22  4   -7.94     103 300    10 -11        imp:p=512     $ SS
23  4   -7.94     301 -132   10 -11        imp:p=512     $ SS
24  8  -11.35     -300 -133  10 -11        imp:p=512     $ Pb gamma shield split
25  4   -7.94     103 300    11 -12        imp:p=1024    $ SS
26  4   -7.94     301 -132   11 -12        imp:p=1024    $ SS
27  8  -11.35     -300 -133 -301 11 -12    imp:p=1024    $ Pb gamma shield split
28  4   -7.94     103 300    12 -13        imp:p=2048    $ SS
29  4   -7.94     301 -132   12 -13        imp:p=2048    $ SS
30  8  -11.35     -300 -301  12 -13        imp:p=2048    $ Pb gamma shield split
31  4   -7.94     103 300    13 -14        imp:p=4096    $ SS
32  4   -7.94     301 -132   13 -14        imp:p=4096    $ SS
33  8  -11.35     -300 -301  13 -14        imp:p=4096    $ Pb gamma shield split
34  4   -7.94     103 300    14 -15        imp:p=8192    $ SS
35  4   -7.94     301 -132   14 -15        imp:p=8192    $ SS
36  8  -11.35     -300 -301  14 -15        imp:p=8192    $ Pb gamma shield split
37  4   -7.94     103 300    15 -16        imp:p=1.6e4   $ SS
38  4   -7.94     301 -132   15 -16        imp:p=1.6e4   $ SS
39  8  -11.35     -300 -301  15 -16        imp:p=1.6e4   $ Pb gamma shield split
40  4   -7.94     103 300    16 -17        imp:p=3.2e4   $ SS
41  4   -7.94     301 -132   16 -17        imp:p=3.2e4   $ SS
42  8  -11.35     -300 -301  16 -17        imp:p=3.2e4   $ Pb gamma shield split
43  4   -7.94     103 -101   17 -18        imp:p=6.4e4   $ SS
44  4   -7.94     102 -132   17 -18        imp:p=6.4e4   $ SS
45  8  -11.35     101 -102   17 -18        imp:p=6.4e4   $ Pb gamma shield split
46  4   -7.94     103 -101   18 -19        imp:p=1.3e5   $ SS
47  4   -7.94     102 -132   18 -19        imp:p=1.3e5   $ SS
48  8  -11.35     101 -102   18 -19        imp:p=1.3e5   $ Pb gamma shield split
49  4   -7.94     103 -101   19 -20        imp:p=2.6e5   $ SS
50  4   -7.94     102 -132   19 -20        imp:p=2.6e5   $ SS
51  1 -0.0012     101 -102   19 -20        imp:p=1.3e5   $ radial gap (Pb shrinkage
1/16")
52  1 -0.0012     133 -132   3 -301        imp:p=256     $ top axial gap (Pb shrinkage
1/4")
53  4   -7.94     3 -36 132 -152           imp:p=512
54  4  -7.94      103 -132   20 -21        imp:p=2.6e5   $ SS outer shell split
55  4  -7.94      103 -132   21 -22        imp:p=5.2e5   $ SS outer shell split
56  4  -7.94      103 -132   22 -23        imp:p=1.0e6   $ SS outer shell split
57  4  -7.94      103 -132   23 -24        imp:p=2.1e6   $ SS outer shell split
58  1 -0.0012     201 -200   24 -25        imp:p=2.1e6   $ air gap thermal shield
59  4  -7.94      201 -200   25 -26        imp:p=2.1e6   $ SS shell over thermal gap
c
c  cask body bottom including Pb shield
c
```

```
100  4   -7.94     104 -100 -3     #174       imp:p=1       $ SS axial split bottom cask
101  4   -7.94    -104 105  -3     #174       imp:p=2       $ SS axial split bottom cask
102  4   -7.94    -105 106  -3     #174       imp:p=4       $ SS axial split bottom cask
104  8  -11.35    -106 103  -27               imp:p=8       $ Bottom cask Pb split
105  4   -7.94    -106 103  -3 27 #174       imp:p=8       $ SS split bottom cask
106  8  -11.35    -103 108  -27               imp:p=16      $ bottom cask Pb split
107  8  -11.35    -108 109  -27               imp:p=32      $ bottom cask Pb split
108  8  -11.35    -109 110  -27               imp:p=64      $ bottom cask Pb split
109  8  -11.35    -110 111  -27               imp:p=128     $ bottom cask Pb split
110  8  -11.35    -111 112  -27               imp:p=256     $ bottom cask Pb split
111  8  -11.35    -112 113  -27               imp:p=512     $ bottom cask Pb split
112  8  -11.35    -113 115  -27               imp:p=1024    $ bottom cask Pb split
113  8  -11.35    115 -114  27 -33            imp:p=1024    $ radius of first  gap (Pb
shrinkage)
c
120  4  -7.94  108 -103   27 -801 #174        imp:p=16       $ SS split bottom cask
121  4  -7.94  109 -108   27 -801 #174        imp:p=32       $ SS split bottom cask
122  4  -7.94  110 -109   27 -801 #174 #175   imp:p=64       $ SS split bottom cask
123  4  -7.94  111 -110   27 -801 #175        imp:p=128      $ SS split bottom cask
124  4  -7.94  112 -111   27 -801             imp:p=256      $ SS split bottom cask
125  4  -7.94  113 -112   27 -801             imp:p=512      $ SS split bottom cask
126  4  -7.94  114 -113   27 -801             imp:p=1024     $ SS split bottom cask
128  4  -7.94  -103 114   801 -10 #175        imp:p=1024     $ SS radial split bottom
cask
129  4  -7.94  -103 114   10 -13  #175        imp:p=2048     $ SS radial split bottom
cask
130  4  -7.94  -103 114   13 -16  #175        imp:p=1.6e4    $ SS radial split bottom
cask
131  4  -7.94  -103 114   16 -20  #175        imp:p=1.3e4    $ SS radial split bottom
cask
132  4  -7.94  -103 114   20 -22  #175        imp:p=5.2e4    $ SS radial split bottom
cask
133  4  -7.94  -103 114   22 -24  #175        imp:p=2.1e6    $ SS radial split bottom
cask
c
141  8  -11.35    -115 116  -33               imp:p=2048     $ bottom cask Pb split
142  8  -11.35    -116 117  -33               imp:p=4096     $ bottom cask Pb split
143  8  -11.35    -117 118  -33               imp:p=8192     $ bottom cask Pb split
144  8  -11.35    -118 119  -33               imp:p=1.6e4    $ bottom cask Pb split
145  8  -11.35    -119 120  -33               imp:p=3.3e4    $ bottom cask Pb split
146  8  -11.35    -120 121  -33               imp:p=6.6e4    $ bottom cask Pb split
147  8  -11.35    -121 122  -33               imp:p=1.3e5    $ bottom cask Pb split
148  8  -11.35    -122 123  -33               imp:p=2.6e5    $ bottom cask Pb split
149  8  -11.35    -123 125  -33               imp:p=5.2e5    $ bottom cask Pb split
c
170  4  -7.94     -114 125  33 -10            imp:p=5.2e5    $ SS radial split bottom cask
171  4  -7.94     -114 125  10 -35            imp:p=1e6      $ SS radial split bottom cask
172  4  -7.94     -114 126  35 -24            imp:p=2.1e6    $ SS shoulder
173  4  -7.94     -125 127  -35               imp:p=1e6      $ SS bottom  plate (1")
174  1  -0.0012    309 -100 -306              imp:p=32       $ vertical drain hole 95
175  1  -0.0012   -307 308 -24  #174          imp:p=1024     $ horizontal drain hole 96
c
c   cask body top
c
201  4  -7.94  -134 145   41 -36              imp:p=1.3e5    $ SS tapered interface with
shield plug
202  4  -7.94  -145 146   41 -36              imp:p=6.6e4    $ SS tapered interface with
shield plug
203  4  -7.94  -146 147   41 -36              imp:p=3.3e4    $ SS tapered interface with
shield plug
204  4  -7.94  -147 148   41 -36              imp:p=1.6e4    $ SS tapered interface with
shield plug
205  4  -7.94  -148 149   41 -36              imp:p=8192     $ SS tapered interface with
shield plug
206  4  -7.94  -149 150   41 -36              imp:p=4096     $ SS tapered interface with
shield plug
```

```
207  4  -7.94   -150 151    302 -36          imp:p=2048     $ SS tapered interface with
shield plug
208  4  -7.94   -151 152    302 -36          imp:p=1024     $ SS tapered interface with
shield plug
209  4  -7.94   -152 153    302 -3           imp:p=512      $ SS tapered interface with
shield plug
210  4  -7.94   -153 154    302 -3           imp:p=256      $ SS tapered interface with
shield plug
211  4  -7.94   155 -154     1 -3            imp:p=128      $ SS  interface with  shield
plug
212  4  -7.94   1551 -155    1 -3            imp:p=64       $ SS  interface with  shield
plug
213  4  -7.94   1552 -1551   1 -3            imp:p=32       $ SS  interface with  shield
plug
214  4  -7.94   1553 -1552   1 -3            imp:p=16       $ SS  interface with  shield
plug
215  4  -7.94   1554 -1553   1 -3            imp:p=8        $ SS  interface with  shield
plug
216  4  -7.94   1555 -1554   1 -3            imp:p=4        $ SS  interface with  shield
plug
217  4  -7.94   156 -1555    1 -3            imp:p=2        $ SS  interface with  shield
plug
218  4  -7.94   157 -156     1 -3            imp:p=1        $ SS  interface with  shield
plug
c
223  4  -7.94   -138 132    36 -11           imp:p=2.6e5    $ SS radial split
224  4  -7.94   -138 132    11 -13           imp:p=5.2e5    $ SS radial split
225  4  -7.94   -138 132    13 -16           imp:p=1.04e6   $ SS radial split
226  4  -7.94   -138 132    16 -20           imp:p=2.1e6    $ SS radial split
227  4  -7.94   -138 132    20 -22           imp:p=4.2e6    $ SS radial split
228  4  -7.94   -138 132    22 -24           imp:p=8.4e6    $ SS radial split
c
230  4  -7.94   137 -136   -37               imp:p=4.2e6    $ SS top closure lid split
231  4  -7.94   -135 136   -37               imp:p=8.4e6    $ SS top closure lid split
232  1 -0.0012 -135 137    37  -36           imp:p=8.4e6    $ radial gap at lid
233  4  -7.94   138 -135    36  -35           imp:p=4.2e6    $ cask body
c
240  4  -7.94   134 -143   -36  41            imp:p=2.6e5     $ cask body top
241  4  -7.94   143 -142   -36  41            imp:p=5.2e5     $ cask body top
242  4  -7.94   142 -140   -36  41            imp:p=1e6       $ cask body top
243  4  -7.94   140 -137   -36  41            imp:p=2.1e6     $ cask body top
c
c
c shield plug
c
300  4  -7.94     140 -141 -40 161           imp:p=2.1e6    $ SS top shield plug
301  1  -0.0012  -137 141 -41                 imp:p=2.1e6    $ axial gap at top of shield
plug
302  1  -0.0012   140 -141  40 -41           imp:p=2.1e6    $ radial gap at top of shield
plug
303  8  -11.35   -140 142 -43 46 161         imp:p=1e6      $ shield plug Pb split (no
radial gap)
304  4  -7.94    -140 142 43 -40             imp:p=1e6      $ SS top shield plug
305  1  -0.0012  -140 142 40 -41             imp:p=1e6      $ gap split
306  4  -7.94    -140 142 -46                imp:p=1e6      $ SS rod center
307  8  -11.35   -142 143 -43 46 161         imp:p=5.2e5    $ shield plug Pb split
308  4  -7.94    -142 143 43 -40             imp:p=5.2e5    $ SS top shield plug
309  1  -0.0012  -142 143 40 -41             imp:p=5.2e5    $ gap split
310  4  -7.94    -142 143 -46                imp:p=5.2e5    $ SS rod center
311  4  -7.94    -143 1431 -46               imp:p=2.6e5    $ SS rod center
312  8  -11.35   -143 134 -43 #311 161       imp:p=2.6e5    $ shield plug Pb split
313  4  -7.94    -143 134 43 -40             imp:p=2.6e5    $ SS top shield plug
314  1  -0.0012  -143 134 40 -41             imp:p=2.6e5    $ gap split
315  8  -11.35   -134 145 -43 161           imp:p=1.3e5    $ shield plug Pb split
316  4  -7.94    -134 145 43 -40             imp:p=1.3e5    $ SS top shield plug
317  1  -0.0012  -134 145 40 -41             imp:p=1.3e5    $ gap split
318  8  -11.35   -145 146 -43 161           imp:p=6.6e4    $ shield plug Pb split
```

```
319  4  -7.94     -145 146 43 -40            imp:p=6.6e4   $ SS top shield plug
320  1  -0.0012   -145 146 40 -41            imp:p=6.6e4   $ gap split
321  8  -11.35    -146 147 -43 161           imp:p=3.3e4   $ shield plug Pb split
322  4  -7.94     -146 147 43 -40            imp:p=3.3e4   $ SS top shield plug
323  1  -0.0012   -146 147 40 -41            imp:p=3.3e4   $ gap split
324  8  -11.35    -147 148 -43 161           imp:p=1.6e4   $ shield plug Pb split
325  4  -7.94     -147 148 43 -40            imp:p=1.6e4   $ SS top shield plug
326  1  -0.0012   -147 148 40 -41            imp:p=1.6e4   $ gap split
327  8  -11.35    -148 149 -43 161           imp:p=8192    $ shield plug Pb split
328  4  -7.94     -148 149 43 -40            imp:p=8192    $ SS top shield plug
329  1  -0.0012   -148 149 40 -41            imp:p=8192    $ gap split
330  8  -11.35    (-149 150 -45 161):(160 -149 45 -43) imp:p=4096  $ shield plug Pb
split
331  4  -7.94     -149 150 43 -40            imp:p=4096    $ SS top shield plug
332  1  -0.0012   -149 150 40 -41            imp:p=4096    $ gap split
333  4  -7.94     -160 150 45 -43            imp:p=4096    $ SS ring at seating surface
334  8  -11.35    -150 151 -45  161          imp:p=2048    $ shield plug Pb split
335  4  -7.94     -150 151 45  -303          imp:p=2048    $ SS top shield plug
336  1  -0.0012   -150 151 303 -302          imp:p=2048    $ gap split
337  8  -11.35    -151 152 -45  161          imp:p=1024    $ shield plug Pb split
338  4  -7.94     -151 152 45  -303          imp:p=1024    $ SS top shield plug
339  1  -0.0012   -151 152 303 -302          imp:p=1024    $ gap split
340  8  -11.35    -152 153 -45  161          imp:p=512     $ shield plug Pb split
341  4  -7.94     -152 153 45  -303          imp:p=512     $ SS top shield plug
342  1  -0.0012   -152 153 303 -302          imp:p=512     $ gap split
343  8  -11.35    -153 154 -45  161          imp:p=256     $ shield plug Pb split
344  4  -7.94     -153 154 45  -303          imp:p=256     $ SS top shield plug
345  1  -0.0012   -153 154 303 -302          imp:p=256     $ gap split
346  8  -11.35    -154 155 -45 161           imp:p=128     $ shield plug Pb split
347  4  -7.94     -154 155 45 -44            imp:p=128     $ SS
348  1 -0.0012   -154 155 44 -1              imp:p=128     $ gap split
350  8  -11.35    -155 1551 -45 161          imp:p=64      $ shield plug Pb split
351  4  -7.94     -155 1551 45 -44           imp:p=64      $ SS
352  1 -0.0012   -155 1551 44 -1            imp:p=64      $ gap split
353  8  -11.35    -1551 1552 -45 161         imp:p=32      $ shield plug Pb split
354  4  -7.94     -1551 1552 45 -44          imp:p=32      $ SS
355  1 -0.0012   -1551 1552 44 -1           imp:p=32      $ gap split
356  8  -11.35    -1552 1553 -45 161         imp:p=16      $ shield plug Pb split
357  4  -7.94     -1552 1553 45 -44          imp:p=16      $ SS
358  1 -0.0012   -1552 1553 44 -1           imp:p=16      $ gap split
359  8  -11.35    -1553 1554 -45 161         imp:p=8       $ shield plug Pb split
360  4  -7.94     -1553 1554 45 -44          imp:p=8       $ SS
361  1 -0.0012   -1553 1554 44 -1           imp:p=8       $ gap split
362  8  -11.35    -1554 1555 -45 161         imp:p=4       $ shield plug Pb split
363  4  -7.94     -1554 1555 45 -44          imp:p=4       $ SS
364  1 -0.0012   -1554 1555 44 -1           imp:p=4       $ gap split
365  4  -7.94     -1555 156 -45 161          imp:p=2       $ shield plug ss
366  4  -7.94     -1555 156 45 -44           imp:p=2       $ SS
367  1 -0.0012   -1555 156 44 -1           imp:p=2       $ gap split
368  4  -7.94    -156 157 -44 161           imp:p=1       $ SS bottom shield plug
369  1 -0.0012  -156 157 44 -1             imp:p=1       $ gap split
370  1 -0.0012  157 -156 -161              imp:p=1       $ plug drain
371  1 -0.0012  156 -1555 -161             imp:p=2       $ plug drain
372  1 -0.0012  1555 -1554 -161            imp:p=4       $ plug drain
373  1 -0.0012  1554 -1553 -161            imp:p=8       $ plug drain
374  1 -0.0012  1553 -1552 -161            imp:p=16      $ plug drain
375  1 -0.0012  1552 -1551 -161            imp:p=32      $ plug drain
376  1 -0.0012  1551 -155 -161             imp:p=64      $ plug drain
377  1 -0.0012  155  -154 -161             imp:p=128     $ plug drain
378  1 -0.0012  154  -153 -161             imp:p=256     $ plug drain
379  1 -0.0012  153  -152 -161             imp:p=512     $ plug drain
380  1 -0.0012  152  -151 -161             imp:p=1024    $ plug drain
381  1 -0.0012  151  -150 -161             imp:p=2048    $ plug drain
382  1 -0.0012  150  -149 -161             imp:p=4096    $ plug drain
383  1 -0.0012  149  -148 -161             imp:p=8192    $ plug drain
384  1 -0.0012  148  -147 -161             imp:p=1.6e4   $ plug drain
385  1 -0.0012  147  -146 -161             imp:p=3.3e4   $ plug drain
```

```
386  1 -0.0012  146  -145 -161              imp:p=6.6e4   $ plug drain
387  1 -0.0012  145  -134 -161              imp:p=1.3e5   $ plug drain
388  1 -0.0012  134  -143 -161              imp:p=2.6e5   $ plug drain
389  1 -0.0012  143  -142 -161              imp:p=5.2e5   $ plug drain
390  1 -0.0012  142  -140 -161              imp:p=1e6     $ plug drain
391  1 -0.0012  140  -141 -161              imp:p=2.1e6   $ plug drain
c
999   0      -1 100 -157     fill=1(22) imp:p=1 $ insert basket
c
c placeholders for IL and outside air volumes
c
400  3 -0.0012   (200 24 -50 -202):
                 (138 -202 -24 35) :(-202 135 -35)  imp:p=8.4e6   $ placeholder for
upper IL
401  3 -0.0012   (-201 24 203 -50):
                 (-24 -126 203 35):(-127 203 -24)   imp:p=4.2e6   $ placeholder for
lower IL
c
402  1 -0.0012   201 -200 -50 26                    imp:p=4.2e6   $ lateral cask outer
air
403  1 -0.0012   50  -540 203 -202                  imp:p=4.2e6   $ outer air
404  1 -0.0012   -203 211 -50                       imp:p=4.2e6   $ bottom outer air
405  1 -0.0012   -203 211 50 -540                   imp:p=4.2e6   $ bottom outer air
406  1 -0.0012   202 -210 -50                       imp:p=8.4e6   $ outer air
407  1 -0.0012   202 -210 50 -540                   imp:p=8.4e6   $ outer air
408  1 -0.0012   211 -210 540 -543                 imp:p=4.2e6   $ outer air
409  1 -0.0012   211 -210 543 -541                 imp:p=4.2e6   $ outer air
410  1 -0.0012   211 -210 541 -542                 imp:p=4.2e6   $ outer air
c
1000  1 -0.0012   (542:-211:210) -999              imp:p=4.2e6
1001  0           999                              imp:p=0
c
c      Universe 1: Basket
c
600     0 630 -631 633 -632 680 -681 fill=5 u=1 imp:p=1 $ basket loc. 1
601     like 600 but trcl=2                              u=1 imp:p=1 $ basket location
2
602     like 600 but trcl=3                              u=1 imp:p=1 $ basket location
3
603     like 600 but trcl=4                              u=1 imp:p=1 $ basket location
4
604     like 600 but trcl=5                              u=1 imp:p=1 $ basket location
5
605     like 600 but trcl=6                              u=1 imp:p=1 $ basket location
6
606     like 600 but trcl=7                              u=1 imp:p=1 $ basket location
7
607     like 600 but trcl=8                              u=1 imp:p=1 $ basket location
8
620     4 -7.94        680 -681 687 -683 #600 #601 #602 #603
                       #604 #605 #606 #607              u=1 imp:p=1 $ inside basket
630     1 -0.0012      681                              u=1 imp:p=1 $ above basket
631     4 -7.94        682 -680 -683                    u=1 imp:p=1 $ support plate
632     4 -7.94        684 -685 -682                    u=1 imp:p=1 $ basket bottom
633     1 -0.0012      -684 -682                        u=1 imp:p=1
634     1 -0.0012      682 -680 683                     u=1 imp:p=1
635     1 -0.0012      685 -682                         u=1 imp:p=1
636     1 -0.0012      680 -681 -687                    u=1 imp:p=1 $ inner air
637     1 -0.0012      680 -681 683                     u=1 imp:p=1 $ annular air
c
c       Universe 2: Fuel
c
700      2  1.7560E-02   686          u=2     imp:p=1   $ fuel
701      1  -0.0012      -686         u=2     imp:p=1   $ air around fuel
c
c       Universe 5: Fuel Shifted (for source purposes)
c
```

```
500      0    991 -992 fill=2(1.7413 15.5236 0) u=5 imp:p=1

c
c ***** cylindrical cask surfaces
c
1     cz   20.32         $ cask inner surface cavity wall radius
2     cz   21.59         $ split of cavity wall (1/2")
3     cz   22.86         $ outside inner shell radius
4     cz   24.06         $ gamma shield split
5     cz   25.26         $ gamma shield split
6     cz   26.46         $ gamma shield split
7     cz   27.66         $ gamma shield split
8     cz   28.86         $ gamma shield split
801     cz   30.06       $ gamma shield split
9     cz   31.2801       $ gamma shield split ***
10    cz   32.4725       $ gamma shield split
11    cz   33.6725       $ gamma shield split
12    cz   34.8725       $ gamma shield split
13    cz   36.0725       $ gamma shield split
14    cz   37.2725       $ gamma shield split
15    cz   38.4725       $ gamma shield split
16    cz   39.6725       $ gamma shield split
17    cz   40.8051       $ gamma shield split ***
18    cz   41.9975       $ gamma shield split
19     cz   43.02125     $ outer gamma shield (Pb shrinkage surface - 1/16")
20     cz   43.18        $ cask inner surface outer wall
21     cz   44.45        $ split  outer wall (1/2")
22     cz   45.72        $ split  outer wall (1/2")
23     cz   46.99        $ split  outer wall (1/2")
24     cz   48.26        $ cask outer surface outer wall
25     cz   48.5267      $ air gap ( 0.105 ")
26     cz   48.7934      $ thermal shield outer surface
27     cz   12.3825      $ bottom lead sheet cavity (small)
c 28     cz   12.1285      $ radial gap due to lead shrinkage (1/10")
c
c 29     cz   14.0825      $ SS split  bottom cask
c 30     cz   15.7825      $ SS split  bottom cask
c 31     cz   17.4825      $ SS split  bottom cask
c
33     cz   30.099       $ bottom lead sheet cavity (large)
c 34     cz   30.32125     $ bottom cask second  radial gap surface due to lead
shrinkage
35     cz   34.6837      $ bottom and top cask SS outer surface
36     cz   31.115       $ top cask inner cavity for closure lid
37     cz   30.7975      $ closure lid radius
c
40     cz   22.1361      $ shield plug - SS outer radius(upper cylindrical region)
41     cz   22.3901      $ shield plug cavity
c 42     cz   19.15        $ shield plug SS inner radius at seating (item 7)
43     cz   21.1836      $ shield plug- SS inner radius (upper cylindrical region)
44     cz   20.066       $ shield plug - SS outer radius (lower cylindrical region)
45     cz   18.796       $ shield plug - SS inner radius (lower cylindrical region)
46     cz    3.81        $  SS bar at center of shield plug
c
50     cz   91.44        $ outer radius of impact limiter
c
c  tally surfaces
c
c 51     cz   800          $ problem  radial delimiter
c
c **** Horizontal  planes
c
100    pz  -0.6426     $  bottom of cask inner cavity
101    pz  4.445       $  horizontal surface for lateral gamma shield
102    pz  139.7       $  horizontal surface at top of  lateral gamma shield +3"
103    pz  -5.08       $  horizontal surface at bottom of lateral gamma shield
c
```

```
104     pz  -1.5        $  SS bottom cask split
105     pz  -2.54       $  SS bottom cask split
106     pz  -3.7338     $  bottom cask interface of SS - shrinkage gap
c 107    pz  -3.9878     $  bottom cask - lower horizontal surface of lead shrinkage
gap (1/10")
108     pz  -6          $  bottom cask - Pb split
109     pz  -6.845      $  bottom cask - Pb split
110     pz  -8.045      $  bottom cask - Pb split
111     pz  -9.245      $  bottom cask - Pb split
112     pz  -10.445     $  bottom cask - Pb split
113     pz  -11.645     $  bottom cask - Pb split
114     pz  -12.7       $  bottom cask - Pb split
115     pz  -12.954     $  bottom cask - lower horizontal surface of lead shrinkage gap
(1/10")
116     pz  -14.154     $  bottom cask - Pb split
117     pz  -15.354     $  bottom cask - Pb split
118     pz  -16.554     $  bottom cask - Pb split
119     pz  -17.754     $  bottom cask - Pb split
120     pz  -18.954     $  bottom cask - Pb split
121     pz  -20.154     $  bottom cask - Pb split
122     pz  -21.354     $  bottom cask - Pb split
123     pz  -22.554     $  bottom cask - Pb split
125     pz  -23.3426    $  bottom cask - lower Pb surface
126     pz  -14.9352    $  bottom cask - SS outer surface (shoulder)
127     pz  -25.8826    $  bottom cask - SS outer surface
c
c 131    pz  144.3736    $  horizontal surface at cask body top
132     pz 149.225      $  horizontal surface at top of  lateral Pb shield cavity
133     pz  146.2278    $  top surface of lateral Pb shield after drop (1.12")
134     pz  159.7152    $  cask body top outer surface (shoulder)
135     pz  170.0276    $  top surface of closure lid
136     pz  167.4876    $  SS split in top lid
137     pz  164.9476    $  seating surface for top lid
138     pz  159.0802
c
140     pz  163.3728    $  shield plug Pb top surface
141     pz  164.6428    $  shield plug top surface
142     pz  162.1536    $  shield plug Pb split surface
143     pz  160.8836    $  shield plug Pb split surface
1431    pz  160.6296    $  surface for SS rod (surface 141- 1.5")
c 144    pz  159.6136    $  shield plug Pb split surface
145     pz  158.3436    $  shield plug Pb split surface
146     pz  157.0736    $  shield plug Pb split surface
147     pz  155.8036    $  shield plug Pb split surface
148     pz  154.5336    $  shield plug Pb split surface
149     pz  153.2636    $  shield plug Pb split surface
150     pz  151.7396    $  shield plug Pb split surface - modified
151     pz  150.7236    $  shield plug Pb split surface
152     pz  149.4536    $  shield plug Pb split surface
153     pz  148.1836    $  shield plug Pb split surface
154     pz  146.7104    $  shield plug Pb split surface - modified
155     pz  145.3896    $  new Pb split
1551     pz  144.1196   $  new Pb split
1552     pz  142.8496   $  new Pb split
1553     pz  141.5796   $  new Pb split
1554     pz  140.3096   $  new Pb split
1555     pz  139.0396   $  bottom plug steel
156     pz  137.7696    $  SS surface at shield plug bottom -modified
157     pz  136.4996    $  bottom surface of shield plug -modified
160     pz  153.0096    $  upper SS surface at seating ring -new
161  20  cz  1.04648     $  pipe in shield plug
c
c  surfaces for IL
c
200     pz  135.9916    $  upper interface IL with thermal shield
201     pz    8.1534    $  lower interface IL with thermal shield
202     pz  223.8756    $  upper surface of top impact limiter
```

```
203    pz  -79.7306   $  bottom surface of bottom impact limiter
c
210    pz  293.3956   $  HAC upper surface
211    pz  -149.2506  $  HAC lower surface
c
c various conical surfaces
c
300    kz -36.3601 1 1          $ tapered surface at bottom of lateral gamma shield
301    kz  180.5051 1 -1        $  tapered surface at top of lateral gamma shield
302    kz -143.9353 0.00489 1    $ tapered surface at cask top tapered cavity
303    kz -140.2468 0.00489 1    $ tapered surface at shield plug (SS)
c 304    kz -220.38 0.00275 1  $ tapered surface at shield plug (gap)
c 305    kz -122.0849 0.00489 1   $ tapered surface at shield plug (lead surface)
c
c bottom drain
c
306    c/z  17.145 0 0.635      $ vertical cylinder for bottom drain
307    c/x  0  -7.5184 0.635    $ horizontal cylinder for bottom drain
308    px  15.24                $ start of horizontal bottom drain
309    pz  -7.94                $ depth of vertical drain
c
540   cz  121.92   $ surface of vehicle  (4 ft=121.92 cm from BRRC centerline)
541   cz  321.92   $ 2 m from vehicle surface
542   cz  762.0    $ driver (25 ft=7.62m) from BRRC centerline)
543   cz  148.7934 $ 1m for HAC
c
c    basket surfaces
c
630   1   py -3.3909
631   1   py  3.3909
632   1   p  -1.7321 -1 0  6.7818 $ left basket inner bound
633   1   p  -1.7321 -1 0 -6.7818 $ right basket inner bound
c
680   pz  67.4878 $ top of plate
681   pz  135.763 $ top of fuel (22.375")
682   pz  66.2178 $ bottom of plate
683   cz  19.8501 $ OR of basket
684   cz  17.145
685   cz  17.78
686   pz  78.9305
687   cz  12      $ IR of basket
c
c horizontal surfaces for segmentation
c
701   pz  18.8
702   pz  29.5
703   pz  40.1
704   pz  50.8
705   pz  61.4
706   pz  72.1
707   pz  82.7
708   pz  93.4
709   pz  104.0
710   pz  114.7
711   pz  125.3
c
720   pz 153.6  $ top IL
721   pz 171.1
722   pz 188.7
723   pz 206.3
c
740   pz -62.2  $ bottom IL
741   pz -44.6
742   pz -27.0
743   pz -9.4
c
c cylindrical surfaces for segmentation
```

```
c
760   cz 10.2
761   cz 20.3
762   cz 30.5
763   cz 40.6
764   cz 50.8
765   cz 61.0
766   cz 71.1
767   cz 81.3
c
770   pz -59.5
771   pz -39.2
772   pz -19.0
773   pz  1.2
774   pz  21.5
775   pz  41.7
776   pz  62.0
777   pz  82.2
778   pz  102.4
779   pz  122.7
780   pz  142.9
781   pz  163.2
782   pz  183.4
783   pz  203.6
c
991   pz -1000
992   pz  1000
999   sz 100 1000

c     ***************************************************************
c      Dry air;  density = 0.0012 g/cm^3
c
c     ***************************************************************/
m1     7014  -76.508
       8016  -23.4793
       6000  -0.0126
c     ***************************************************************
c      Homogenized fuel;  atomic density = 1.7560E-02 atoms/(barn*cm)
c
c     ***************************************************************
m2    92235  4.3716E-04
      92238  2.7552E-05
      13027  1.7095E-02
c     ***************************************************************
c      Dry air;  density = 0.0012 g/cm^3
c
c     ***************************************************************
m3     7014  -76.508
       8016  -23.4793
       6000  -0.0126
c     ***************************************************************
c       SS304;   Density = 7.94 g/cm^3
c     ***************************************************************
m4     6012   -0.08
       14000  -1.0
       15000  -0.045
       24000  -19
       25000  -2
       26000  -68.375
       28000  -9.5
c     ***************************************************************
c     Lead; Density = 11.35 g/cm^3
c     ***************************************************************
m8     82000   1.0  $ lead
c
mode p
sdef cel=d1 rad=d2 ext=d3 erg=d10  axs=0 0 1 pos=0 0 78.9305 wgt=7.707E+15
```

```
si1     L  999:600:500:700 999:601:500:700 999:602:500:700
           999:603:500:700 999:604:500:700 999:605:500:700
           999:606:500:700 999:607:500:700
sp1     1 1 1 1  1 1 1 1
si2     7.0
#       si3     sp3     $ fuel axial dist
        0       0
        2.368   0.500
        4.736   0.394
        9.472   0.788
        14.208  0.901
        18.944  1.042
        23.680  1.140
        28.416  1.253
        33.152  1.267
        37.888  1.112
        42.624  1.028
        47.360  0.901
        52.096  0.774
        54.464  0.401
        56.833  0.500
#       si10    sp10
        H         D
        0         0
        1.00E-02  0
        4.50E-02  2.343E+14
        1.00E-01  8.380E+13
        2.00E-01  9.049E+13
        3.00E-01  1.756E+13
        4.00E-01  1.304E+13
        6.00E-01  5.917E+13
        8.00E-01  4.460E+14
        1.00E+00  1.117E+13
        1.33E+00  3.308E+12
        1.66E+00  2.576E+12
        2.00E+00  2.013E+11
        2.50E+00  1.795E+12
        3.00E+00  3.290E+10
        4.00E+00  6.118E+08
        5.00E+00  7.015E+02
        6.50E+00  2.802E+02
        8.00E+00  5.473E+01
        1.00E+01  1.195E+01
c          Total  9.634E+14
c        Total*8  7.707E+15
c
c       ansi/ans-6.1.1-1977 flux-to-dose, photons (mrem/hr)/(p/cm**2/s)
de0         0.01    0.03    0.05    0.07    0.10    0.15    0.20    0.25    0.30
            0.35    0.40    0.45    0.50    0.55    0.60    0.65    0.70    0.80
            1.00    1.40    1.80    2.20    2.60    2.80    3.25    3.75    4.25
            4.75    5.00    5.25    5.75    6.25    6.75    7.50    9.00    11.0
            13.0    15.0
df0         3.96-3 5.82-4 2.90-4 2.58-4 2.83-4 3.79-4 5.01-4 6.31-4 7.59-4
            8.78-4 9.85-4 1.08-3 1.17-3 1.27-3 1.36-3 1.44-3 1.52-3 1.68-3
            1.98-3 2.51-3 2.99-3 3.42-3 3.82-3 4.01-3 4.41-3 4.83-3 5.23-3
            5.60-3 5.80-3 6.01-3 6.37-3 6.74-3 7.11-3 7.66-3 8.77-3 1.03-2
            1.18-2 1.33-2
c
c     Tallies
c
FC2       Radial doses at contact (between IL on heat shield)
F2:p      26
FS2      -701 -702 -703 -704 -705 -706 -707 -708 -709 -710 -711
c
FC12      Radial doses at top side IL surface
F12:p     50
FS12     -200 -720 -721 -722 -723 -202
```

```
c
FC22     Radial doses at bottom side IL surface
F22:p    50
FS22    -203 -740 -741 -742 -743 -201
c
FC32     Doses at top limiter horizontal surface
F32:p    202
FS32     -760 -761 -762 -763 -764 -765 -766 -767 -50
c
FC42     Doses at bottom limiter horizontal surface
F42:p    203
FS42     -760 -761 -762 -763 -764 -765 -766 -767 -50
c
FC52     Doses at vehicle surface (4 ft from BRRC centerline)
F52:p    540
FS52     -203 -770 -771 -772 -773 -774 -775 -776 -777 -778
         -779 -780 -781 -782 -783 -202
c
FC62     Doses at 2m from vehicle surface
F62:p    541
FS62     -203 -770 -771 -772 -773 -774 -775 -776 -777 -778
         -779 -780 -781 -782 -783 -202
c
FC72     Doses at driver seat (25 ft from BRRC centerline)
F72:p    542
FS72     -203 -770 -771 -772 -773 -774 -775 -776 -777 -778
         -779 -780 -781 -782 -783 -202
c
FC82     HAC Doses at 1 m side
F82:p    543
FS82     -203 -770 -771 -772 -773 -774 -775 -776 -777 -778
         -779 -780 -781 -782 -783 -202
c
FC92     HAC Doses at 1m top
F92:p    210
FS92     -760 -761 -762 -763 -764 -765 -766 -767 -50 -540 -543
c
FC102    HAC Doses at 1m bottom
F102:p   211
FS102    -760 -761 -762 -763 -764 -765 -766 -767 -50 -540 -543
c
c   TRCL definitions
c
*tr1     1.7413 15.5236 0                          $ wedge 1
*tr2     0 0 0          45 135 90 45 45 90         $ wedge 2(8)
*tr3     0 0 0          90 180 90 0  90 90         $ wedge 3(7)
*tr4     0 0 0         135 225 90 45 135 90        $ wedge 4(6)
*tr5     0 0 0         180 90 90 90 180 90         $ wedge 5
*tr6     0 0 0         135 45 90 225 135 90        $ wedge 6
*tr7     0 0 0         90 0 90 180 90 90           $ wedge 7
*tr8     0 0 0         45 45 90 135 45 90          $ wedge 8
*tr20    0 0 150.022 50 90 140 90 0 90 40 90 50   $ pipe
*tr22    0 0 -0.6426
c
prdmp    j j 1 2
ctme     3600
phys:p   4j 1
```

6.0 CRITICALITY EVALUATION

The Battelle Energy Alliance (BEA) Research Reactor (BRR) package is used to transport spent fuel from a variety of research reactors, including the University of Missouri Research Reactor (MURR), Massachusetts Institute of Technology Research Reactor (MITR-II), Advanced Test Reactor (ATR), and various types of Training, Research, Isotope General Atomics (TRIGA) reactors. The following analyses demonstrate that the BRR package complies with the requirements of 10 CFR 71.55 and 71.59. Based on the analysis, the Criticality Safety Index (CSI), per 10 CFR 71.59, is 0.

6.1 Description of Criticality Design

6.1.1 Design Features

Each fuel type has a unique basket that is used to properly position the fuel within the cask cavity. These baskets limit the number of fuel elements that may be shipped at a given time, and also control the spacing between the fuel elements. No poisons are utilized in the package. The separation provided by the packaging is sufficient to maintain criticality safety.

6.1.2 Summary Table of Criticality Evaluation

The upper subcritical limit (USL) for ensuring that the package is acceptably subcritical, as determined in Section 6.8, *Benchmark Evaluations*, is:

$$USL = 0.9209$$

The package is considered to be acceptably subcritical if the computed k_{safe} (k_s), which is defined as $k_{effective}$ (k_{eff}) plus twice the statistical uncertainty (σ), is less than or equal to the USL, or:

$$k_s = k_{eff} + 2\sigma \leq USL$$

The USL is determined on the basis of a benchmark analysis and incorporates the combined effects of code computational bias, the uncertainty in the bias based on both benchmark-model and computational uncertainties, and an administrative margin. The results of the benchmark analysis indicate that the USL is adequate to ensure subcriticality of the package.

The packaging design is shown to meet the requirements of 10 CFR 71.55(b). No credit is taken for fuel element burnup in any models. In the single package normal conditions of transport (NCT) models, credit is taken for the leaktight performance of the cask, while in the single package hypothetical accident condition (HAC) models, water is modeled in all cavities at the density in which reactivity is maximized. For the aluminum plate fuels (MURR, MITR-II, ATR), the most reactive credible configuration is utilized by maximizing the gap between the fuel plates. Maximizing this gap maximizes the moderation and hence the reactivity because the system is undermoderated. In all single package models, 12-in of water reflection is utilized.

Infinite reflection is utilized in both NCT and HAC array models. In the HAC array cases, internal and external water moderation is selected to optimize the reactivity.

The maximum results of the criticality calculations for each of the four fuel element types are summarized in Table 6.1-1. The maximum calculated k_s is 0.807, which occurs for the HAC array case for MURR fuel. The maximum reactivity is less than the USL of 0.9209. The most reactive MITR-II, ATR, and TRIGA cases are well below the USL.

Note that the TRIGA fuel is significantly more reactive than the aluminum plate fuel types under NCT. This is because hydrogen is included in the TRIGA fuel matrix, providing some moderation. However, the reactivity of the NCT TRIGA cases is still very low.

6.1.3 Criticality Safety Index

An infinite number of packages is used in the array calculations for both NCT and HAC. Therefore, the criticality safety index per 10 CFR 71.59 is 0.

Table 6.1-1 – Summary of Criticality Evaluation

Normal Conditions of Transport (NCT)				
	MURR	**MITR-II**	**ATR**	**TRIGA**
Case	k_s	k_s	k_s	k_s
Single Unit Maximum	0.085	0.058	0.088	**0.417**
Infinite Array Maximum	0.197	0.144	0.234	**0.539**
Hypothetical Accident Conditions (HAC)				
	MURR	**MITR-II**	**ATR**	**TRIGA**
Case	k_s	k_s	k_s	k_s
Single Unit Maximum	**0.761**	0.525	0.685	0.709
Infinite Array Maximum	**0.807**	0.563	0.697	0.720
USL = 0.9209				

6.2 Fissile Material Contents

Four different spent fuel types are allowed contents: MURR, MITR-II, ATR, and TRIGA. For criticality control purposes, all fuel is modeled as fresh, and the information provided in this section pertains to fresh fuel.

6.2.1 MURR Fuel Element

The package can accommodate up to eight MURR fuel elements. Each MURR element contains up to 782.8 g U-235, with an enrichment of 93 ± 1 wt.%. This fuel loading and enrichment is bounded by modeling 785 g U-235 and 94% enrichment. The weight percents of the remaining uranium isotopes are 1.2 wt.% U-234, 0.7 wt.% U-236, and 5.0-7.0 wt.% U-238. Each fuel element contains 24 curved fuel plates. Fuel plate 1 has the smallest radius, while fuel plate 24 has the largest radius, as shown in Figure 6.2-1. The fuel "meat" is a mixture of uranium metal and aluminum, while the cladding and structural materials are an aluminum alloy.

The relevant fuel element information is summarized in Figure 6.2-2. Each fuel plate is nominally 0.05-in thick, with a thickness tolerance of ±0.002-in. The fuel meat is nominally 0.02-in thick, and the cladding is nominally 0.015-in thick. The plate cladding material is aluminum. Fuel element side plates are fabricated of ASTM B 209, aluminum alloy 6061-T6 or 6061-T651. These fuel element side plates have a minimum thickness of 0.145-in. The average measured channel spacing between fuel plates, over the entire fuel element, is less than or equal to 0.088-in.

The midpoint radii of the fuel plates are treated as fixed quantities, and are computed based on nominal dimensions. However, the channel width is modeled at the maximum average value of 0.088-in between all plates in all final (i.e., non-parametric) fuel element models. To achieve this channel width between all fuel plates, the cladding is modeled with a reduced thickness of 0.011-in, or a total plate thickness of 0.042-in. This plate thickness is impossible to achieve in actual practice because it is below the allowable minimum plate thickness of 0.048-in.

The arc length of the fuel meat changes from plate to plate. Reference minimum fuel meat arc length and inner radius dimensions for each plate are provided on Figure 6.2-2. The active fuel length ranges from 23.25-in to 24.75-in.

It is necessary to determine the number densities of the fuel meat, which are the same for all fuel plates. To determine the number densities of the fuel meat, it is first necessary to compute the volume of the fuel meat. The volume of the fuel meat for each plate is the maximum arc length of the meat (nominal + 0.065-in) multiplied by the nominal active fuel length (24.0-in) and meat thickness (0.02-in). The active fuel length and meat thickness are modeled at nominal values in all final (i.e., non-parametric) fuel element models, and the use of these dimensions is justified in Section 6.9.2, *Parametric Evaluations to Determine the Most Reactive Fuel Geometries*. It is demonstrated in Section 6.9.2.2, *MURR Fuel Parametric Evaluation*, that reactivity increases with increasing meat arc length. The results of the fuel meat volume computations for all 24 plates are provided in Table 6.2-1 for maximum fuel arc length.

The U-235 gram density for each fuel plate is computed by dividing the U-235 mass by the total volume, or 785 g/556.4 cm^3 = 1.41 g/cm^3. The fuel itself is a mixture of UAl_x and aluminum.

An equation that relates the U-235 density to the overall fuel meat density for ATR fuel is presented in Table 6.2-5. Because ATR and MURR fuel are of the same type, the fuel density equation shown in Table 6.2-5 is also used to develop the MURR fuel matrix density. Using this equation, the total density of the fuel matrix is computed to be approximately 3.77 g/cm^3.

From the fuel volumes, U-235 gram densities, and total mixture densities provided, the number densities for the fuel region may be computed. These number densities are provided in Table 6.2-2. The U-235 weight percent is modeled at 94%. Representative weight percents of 0.6% and 0.35% are utilized for U-234 and U-236, respectively, and the balance (5.05%) is modeled as U-238.

6.2.2 MITR-II Fuel Element

The package can accommodate up to 11 MITR-II fuel elements. Each MITR-II element contains up to 513 g U-235, with an enrichment of 93 ± 1 wt.%. This fuel loading and enrichment is bounded by modeling 515 g U-235 and 94% enrichment. The weight percents of the remaining uranium isotopes are 1.2 wt.% U-234, 0.7 wt.% U-236, and 5.0-7.0 wt.% U-238. Each fuel element contains 15 flat fuel plates, as shown in Figure 6.2-3. The fuel "meat" is a mixture of uranium metal and aluminum, while the cladding and structural materials are an aluminum alloy.

The relevant fuel element information is summarized in Figure 6.2-4. Each fuel plate is nominally 0.08-in thick, with a thickness tolerance of ±0.003-in. The fuel meat is nominally 0.03-in thick, and the cladding is nominally 0.025-in thick. The plate cladding material is aluminum. Fuel element side plates are fabricated of ASTM B 209, aluminum alloy 6061-T6. These fuel element side plates have a nominal thickness of 0.188-in. The channel width between the plates is 0.078 ± 0.004-in. These tolerances represent average and not localized channel width. For an actual fuel element, the channel width may exceed these tolerances in localized areas.

The maximum and minimum active fuel lengths and maximum and minimum active fuel widths may be computed based the dimensions on Figure 6.2-4:

- Maximum active fuel length = (23.0+0.01)-2(0.125) = 22.76-in
- Minimum active fuel length = (23.0-0.01)-2(0.5) = 21.99-in
- Maximum active fuel width = 2.531 – 2(0.18) = 2.171-in
- Minimum active fuel width = 2.521 – 2(0.27) = 1.981-in.

The nominal active fuel length may be estimated as the average of the maximum and minimum values, or 22.375-in.

It is necessary to determine the number densities of the fuel meat, which are the same for all fuel plates. To determine the number densities of the fuel meat, it is first necessary to compute the volume of the fuel meat. The volume of the fuel meat for each plate is the maximum width of the meat (2.171-in) multiplied by the active fuel length (22.375-in) and meat thickness (0.03-in). The active fuel length and meat thickness are modeled at nominal values in all final (i.e., non-parametric) fuel element models, and the use of these dimensions is justified in Section 6.9.2, *Parametric Evaluations to Determine the Most Reactive Fuel Geometries*. It is demonstrated in

Section 6.9.2.3, *MITR-II Fuel Parametric Evaluation*, that reactivity increases with increasing meat width. The total meat volume is therefore (15)(0.03)(22.375)(2.171)(2.54^3) = 358.2 cm^3.

The centerlines of the fuel plates are treated as fixed quantities, and are computed based on nominal dimensions. However, the channel width is modeled at the maximum average value between all plates in all final (i.e., non-parametric) fuel element models. The average measured channel spacing between fuel plates, over the entire fuel element, is less than or equal to 0.082-in. The fuel plates also have grooves a maximum of 0.012-in deep cut into the surface of the fuel plates to increase heat transfer. Because the grooves cover approximately half the surface area of the cladding, half of the groove depth (i.e., 0.006-in) is removed from each cladding plate, increasing the effective channel width to 0.094-in. A channel width of 0.094-in is modeled in all non-parametric cases. To achieve this channel width between all fuel plates, the cladding is artificially reduced to a thickness of 0.017-in, or a total plate thickness of 0.064-in.

The U-235 gram density for each fuel plate is computed by dividing the U-235 mass by the total volume, or 515 g/358.2 cm^3 = 1.44 g/cm^3. The fuel itself is a mixture of UAl_x and aluminum. An equation that relates the U-235 density to the overall fuel meat density for ATR fuel is presented in Table 6.2-5. Because ATR and MITR-II fuel are of the same type, the fuel density equation shown in Table 6.2-5 is also used to develop the MITR-II fuel matrix density. Therefore, using this equation, the total density of the fuel matrix is computed to be approximately 3.79 g/cm^3.

From the fuel volumes, U-235 gram densities, and total mixture densities provided, the number densities for the fuel region may be computed. These number densities are provided in Table 6.2-3. The U-235 weight percent is modeled at 94%. Representative weight percents of 0.6% and 0.35% are utilized for U-234 and U-236, respectively, and the balance (5.05%) is modeled as U-238.

6.2.3 ATR Fuel Element

The package can accommodate up to eight ATR fuel elements. Each element contains up to 1085 g U-235, with an enrichment of 93 ± 1 wt.%. This fuel loading and enrichment is bounded by modeling 1200 g U-235 and 94% enrichment. The weight percents of the remaining uranium isotopes are 1.2 wt.% U-234 (max), 0.7 wt.% U-236 (max), and 5.0-7.0 wt.% U-238. Each fuel element contains 19 curved fuel plates. Fuel plate 1 has the smallest radius, while fuel plate 19 has the largest radius, as shown in Figure 6.2-5. The fuel "meat" is a mixture of uranium metal and aluminum, while the cladding and structural material are an aluminum alloy.

The relevant fuel element details are summarized on Figure 6.2-6. Fuel plate 1 is nominally 0.080-in thick, fuel plates 2 through 18 are nominally 0.050-in thick, and fuel plate 19 is nominally 0.100-in thick. The plate thickness tolerance is +0.000/-0.002-in for all plates. The fuel meat is nominally 0.02-in thick for all 19 plates. The plate cladding material is aluminum ASTM B 209, 6061-0. Fuel element side plates are fabricated of ASTM B 209, aluminum alloy 6061-T6 or 6061-T651. These fuel element side plates have a minimum thickness of 0.182-in. Channels 2 through 10 have an average width of 0.078 ± 0.007-in, while channels 11 through 19 have an average width of 0.077 +0.008/-0.006-in. The average measured channel spacing between fuel plates, over the entire fuel element, is less than or equal to 0.085-in.

The midpoint radii of the fuel plates are treated as fixed quantities, and are computed based on nominal dimensions. However, the channel width is modeled at the maximum average value of 0.085-in between all plates in all final (i.e., non-parametric) fuel element models. To achieve this channel width between all fuel plates, the cladding thickness is artificially reduced by 0.0035-in. Such a scenario is impossible to achieve in actual practice because it would result in overall plate thicknesses below the allowed minimum value.

The arc length of the fuel meat changes from plate to plate. This arc length varies based on the distance from the edge of the fuel meat to the fuel element side plate, as defined for each plate on Figure 6.2-6. This dimension is 0.245-in (max)/0.145-in (min) for fuel plates 1 and 19, 0.145-in (max)/0.045-in (min) for fuel plates 2 through 17, and 0.165-in (max)/0.065-in (min) for fuel plate 18. The smaller this dimension, the larger the arc length of the fuel meat.

The active fuel length varies between a minimum of 47.245-in (= 49.485 – 2*1.12) and a maximum of 48.775-in (= 49.515 – 2*0.37) for all fuel plates.

It is demonstrated in Section 6.9.2.1, *ATR Fuel Parametric Evaluation*, that reactivity increases with increasing meat arc length. Therefore, the arc length is modeled at the maximum value. To determine the number densities of the fuel meat, it is first necessary to compute the volume of the fuel meat. The volume of the fuel meat for each plate is the maximum arc length of the meat multiplied by the fuel length (48-in) and meat thickness (0.02-in). The fuel length and meat thickness are treated as fixed quantities in all fuel element models, and the use of these dimensions is justified in Section 6.9.2.1.

The fuel meat volume for each of the 19 fuel plates is provided in Table 6.2-4. The mass of U-235 per plate utilized in the analysis is also provided in Table 6.2-4. The U-235 gram density for each fuel plate is also computed. Note that the U-235 gram density is higher in the inner plates compared to the outer plates.

The fuel itself is a mixture of UAl_x and aluminum. The density of this mixture is proportional to the U-235 gram density, as shown in Table 6.2-5. These data are perfectly linear, and a linear fit of the data is $\rho_2 = 0.8733\rho_1 + 2.5357$, where ρ_2 is the total gram density of the mixture, and ρ_1 is the gram density of the U-235 in the mixture. This equation is used to compute the total mixture gram density provided as the last column in Table 6.2-4.

From the fuel volumes, U-235 gram densities, and total mixture densities provided, the number densities for the fuel region of each fuel plate may be computed. These number densities are provided in Table 6.2-6. The U-235 weight percent is modeled at 94%. Representative weight percents of 0.6% and 0.35% are utilized for U-234 and U-236, respectively, and the balance (5.05%) is modeled as U-238.

6.2.4 TRIGA Fuel Element

The package can accommodate up to 19 TRIGA fuel elements. While many different types of TRIGA fuel elements have been fabricated over the past 40 years, only five specific TRIGA fuel element types are considered in this analysis:

1. 8 wt.% uranium, aluminum clad (General Atomics catalog number 101)
2. 8.5 wt.% uranium, stainless steel clad (General Atomics catalog number 103)

3. 8.5 wt.% uranium, stainless steel clad, high enriched uranium (General Atomics catalog number 109)
4. 20 wt.% uranium, stainless steel clad (General Atomics catalog number 117)
5. 8.5 wt.% uranium, instrumented, stainless steel clad (General Atomics catalog number 203)

The fuel matrix of a TRIGA fuel element consists of a mixture of uranium and zirconium hydride. Therefore, the TRIGA elements contain hydrogen moderator material. Detailed fuel characteristics for the five TRIGA fuel element types are summarized in Table 6.2-7. A schematic of a typical stainless steel clad fuel element is shown in Figure 6.2-8.

TRIGA fuel elements consist of a central active fuel region with graphite axial reflectors above and below the active fuel. Type 101 and 103 TRIGA fuel manufactured prior to 1964 utilizes thin samarium trioxide discs between the active fuel and graphite reflectors. Type 109, 117, and 203 TRIGA fuel utilizes a thin molybdenum disc between the active fuel and lower reflector rather than samarium trioxide. The samarium trioxide discs act a as a burnable poison and are conservatively omitted from the models. The molybdenum disc is only 0.031-in thick and has essentially no effect on the reactivity, as demonstrated in Section 6.9.2.4, *TRIGA Fuel Parametric Evaluation*. For this reason, the molybdenum disc is also omitted from the models.

For all TRIGA fuel elements with the exception of Type 101, a solid zirconium rod with an outer diameter of 0.225-in is placed along the active fuel length in the center of the fuel pellet. It is assumed that the inner diameter of the fuel pellet is 0.25-in to allow a small clearance between the rod and the fuel.

The fuel elements are modeled in detail from the bottom of the bottom reflector to the top of the top reflector. The end cap regions are neglected for simplicity. The graphite reflectors are modeled at the same diameter as the fuel pellets for simplicity, although the actual graphite reflectors have a slightly smaller diameter, as shown in Table 6.2-7. The Type 109 and 117 fuel elements contain erbium poison, although this poison is conservatively ignored in the criticality models.

The number densities within the TRIGA fuel elements are computed based upon the information in Table 6.2-7. Because the masses of U-235 and uranium are provided, the uranium number densities in the fuel may be computed based on the known volumes. The uranium is treated as a mix of only U-235 and U-238 for simplicity. The zirconium number density is computed based on the zirconium mass provided, and the hydrogen number density is computed based upon the H/Zr ratio. The fuel number densities for the five fuel types are summarized in Table 6.2-8.

Table 6.2-1 – MURR Fuel Volume Computation (maximum arc length)

Plate	Midpoint Radius (cm)	Fuel Arc (cm)	Volume① (cm^3)
1	7.0993	4.5034	13.9460
2	7.4295	4.7625	14.7484
3	7.7597	5.0216	15.5507
4	8.0899	5.2832	16.3608
5	8.4201	5.5423	17.1632
6	8.7503	5.8014	17.9655
7	9.0805	6.0604	18.7678
8	9.4107	6.3195	19.5701
9	9.7409	6.5786	20.3724
10	10.0711	6.8377	21.1747
11	10.4013	7.0968	21.9770
12	10.7315	7.3558	22.7793
13	11.0617	7.6149	23.5816
14	11.3919	7.8765	24.3918
15	11.7221	8.1356	25.1941
16	12.0523	8.3947	25.9964
17	12.3825	8.6538	26.7987
18	12.7127	8.9129	27.6011
19	13.0429	9.1719	28.4034
20	13.3731	9.4310	29.2057
21	13.7033	9.6901	30.0080
22	14.0335	9.9492	30.8103
23	14.3637	10.2083	31.6126
24	14.6939	10.4699	32.4228
Total			556.4024

① Volume is computed as Fuel Arc*Active Fuel Height*Fuel Thickness, where Active Fuel Height = 24-in (60.96 cm) and Fuel Thickness = 0.02-in (0.0508 cm).

Table 6.2-2 – MURR Fuel Number Densities (maximum arc length)

Isotope	Number Density (atom/b-cm)
U-234	2.3171E-05
U-235	3.6147E-03
U-236	1.3402E-05
U-238	1.9174E-04
Al	5.0596E-02
Total	5.4439E-02

Table 6.2-3 – MITR-II Fuel Number Densities (maximum meat width)

Isotope	Number Density (atom/b-cm)
U-234	2.3613E-05
U-235	3.6835E-03
U-236	1.3657E-05
U-238	1.9539E-04
Al	5.0481E-02
Total	5.4398E-02

Table 6.2-4 – ATR Fuel Element Volume and Gram Densities (maximum arc length)

Plate	Fuel Meat Arc Length (cm)	Fuel Meat Volume (cm^3)	U-235 Mass Per Plate (g)	U-235 density, ρ_1 (g/cm^3)	Total UAl_x + Al Density, ρ_2 (g/cm^3)
1	4.2247	26.2	27.1	1.04	3.44
2	5.0209	31.1	32.5	1.04	3.45
3	5.2764	32.7	43.2	1.32	3.69
4	5.5319	34.3	45.1	1.32	3.69
5	5.7873	35.8	58.2	1.62	3.95
6	6.0427	37.4	60.9	1.63	3.96
7	6.2982	39.0	63.6	1.63	3.96
8	6.5536	40.6	66.3	1.63	3.96
9	6.8090	42.2	69.0	1.64	3.96
10	7.0644	43.8	71.7	1.64	3.97
11	7.3198	45.3	74.3	1.64	3.97
12	7.5752	46.9	77.0	1.64	3.97
13	7.8306	48.5	79.7	1.64	3.97
14	8.0860	50.1	82.4	1.64	3.97
15	8.3414	51.7	85.2	1.65	3.98
16	8.5968	53.2	71.4	1.34	3.71
17	8.8521	54.8	73.6	1.34	3.71
18	9.0058	55.8	60.1	1.08	3.48
19	8.9039	55.1	58.7	1.06	3.47
Total	--	824.5	1200.0	--	--

Table 6.2-5 – ATR Fuel Density Equation

U-235 Density (g/cm^3) ρ_1	Total Fuel Density (g/cm^3) ρ_2
1.00	3.409
1.30	3.671
1.60	3.933
Linear Fit: $\rho_2 = 0.8733\rho_1 + 2.5357$	

Table 6.2-6 – ATR Fuel Number Densities (maximum arc length)

Plate	U-234 (atom/b-cm)	U-235 (atom/b-cm)	U-236 (atom/b-cm)	U-238 (atom/b-cm)	Aluminum (atom/b-cm)	Total (atom/b-cm)
1	1.7026E-05	2.6560E-03	9.8475E-06	1.4089E-04	5.2187E-02	5.5010E-02
2	1.7156E-05	2.6763E-03	9.9226E-06	1.4196E-04	5.2153E-02	5.4998E-02
3	2.1711E-05	3.3869E-03	1.2557E-05	1.7966E-04	5.0974E-02	5.4574E-02
4	2.1618E-05	3.3724E-03	1.2503E-05	1.7889E-04	5.0998E-02	5.4583E-02
5	2.6648E-05	4.1571E-03	1.5413E-05	2.2051E-04	4.9696E-02	5.4115E-02
6	2.6746E-05	4.1724E-03	1.5470E-05	2.2132E-04	4.9670E-02	5.4106E-02
7	2.6790E-05	4.1791E-03	1.5495E-05	2.2168E-04	4.9659E-02	5.4102E-02
8	2.6830E-05	4.1854E-03	1.5518E-05	2.2201E-04	4.9649E-02	5.4098E-02
9	2.6867E-05	4.1911E-03	1.5539E-05	2.2232E-04	4.9639E-02	5.4095E-02
10	2.6901E-05	4.1965E-03	1.5559E-05	2.2260E-04	4.9630E-02	5.4092E-02
11	2.6933E-05	4.2015E-03	1.5577E-05	2.2287E-04	4.9622E-02	5.4089E-02
12	2.6963E-05	4.2061E-03	1.5595E-05	2.2311E-04	4.9614E-02	5.4086E-02
13	2.6990E-05	4.2105E-03	1.5611E-05	2.2334E-04	4.9607E-02	5.4083E-02
14	2.7017E-05	4.2145E-03	1.5626E-05	2.2356E-04	4.9600E-02	5.4081E-02
15	2.7077E-05	4.2239E-03	1.5661E-05	2.2406E-04	4.9585E-02	5.4075E-02
16	2.2037E-05	3.4377E-03	1.2746E-05	1.8235E-04	5.0889E-02	5.4544E-02
17	2.2037E-05	3.4377E-03	1.2745E-05	1.8235E-04	5.0889E-02	5.4544E-02
18	1.7683E-05	2.7586E-03	1.0228E-05	1.4633E-04	5.2016E-02	5.4949E-02
19	1.7487E-05	2.7279E-03	1.0114E-05	1.4470E-04	5.2067E-02	5.4967E-02

Table 6.2-7 – TRIGA Fuel Characteristics

Parameter	Type 101	Type 103	Type 109	Type 117	Type 203
General Description	8 wt.% aluminum clad	8.5 wt.% stainless steel clad	8.5 wt.% stainless steel clad, HEU	20 wt.% stainless steel clad	8.5 wt.% instrumented stainless steel clad
Active Fuel Length (in)	14	15	15	15	15
Fuel Pellet OD (in)	1.41	1.44	1.44	1.44	1.44
U (wt.% in fuel)	8.0	8.5	8.5	20	8.5
U (g)	180	195	196	504	195
U-235 (wt.% in U)	20	20	70	20	20
U-235 (g)	36	39	137	101	39
H/Zr	1.0	1.7	1.6	1.6	1.7
Erbium (wt.%)	0	0	1.3	0.5	0
Zirconium Rod Length (in)	n/a	15.0	15.0	15.0	15.0
Overall Rod Length (in)	28.37	28.90	28.90	29.68	45.25
Cladding OD (in)	1.48	1.48	1.48	1.48	1.48
Cladding Thickness (in)	0.03	0.02	0.02	0.02	0.02
Graphite Reflector Length Top/Bottom (in)	4.0 / 4.0①	2.6 / 3.7	2.6 / 3.7	2.6 / 3.7	3.1 / 3.4
Graphite Reflector OD (in)	1.4	1.4	1.4	1.4	1.4
Molybdenum Disc (Y/N)	No	Yes	Yes	Yes	Yes
Samarium Trioxide Disc (Y/N)	Yes (prior to 1964)	Yes (prior to 1964)	No	No	No
Zr Fuel Matrix Mass (g)	2,070	2,088	2,060	2,060	2,088

Notes:

①Graphite reflector dimensions provided for an active fuel length of 14-in. If the active fuel length is reduced, the top and bottom reflectors increase equally in length, and the overall column stackup of fuel and reflector remains fixed at 22-in.

Table 6.2-8 – TRIGA Fuel Number Densities

Isotope	Type 101 (atom/b-cm)	Type 103/203 (atom/b-cm)	Type 109 (atom/b-cm)	Type 117 (atom/b-cm)
H	3.8146E-02	6.0352E-02	5.6041E-02	5.6041E-02
Zr	3.8146E-02	3.5501E-02	3.5025E-02	3.5025E-02
U-235	2.5748E-04	2.5736E-04	9.0406E-04	6.6650E-04
U-238	1.0169E-03	1.0164E-03	3.8442E-04	2.6258E-03
Total	7.7566E-02	9.7128E-02	9.2354E-02	9.4358E-02

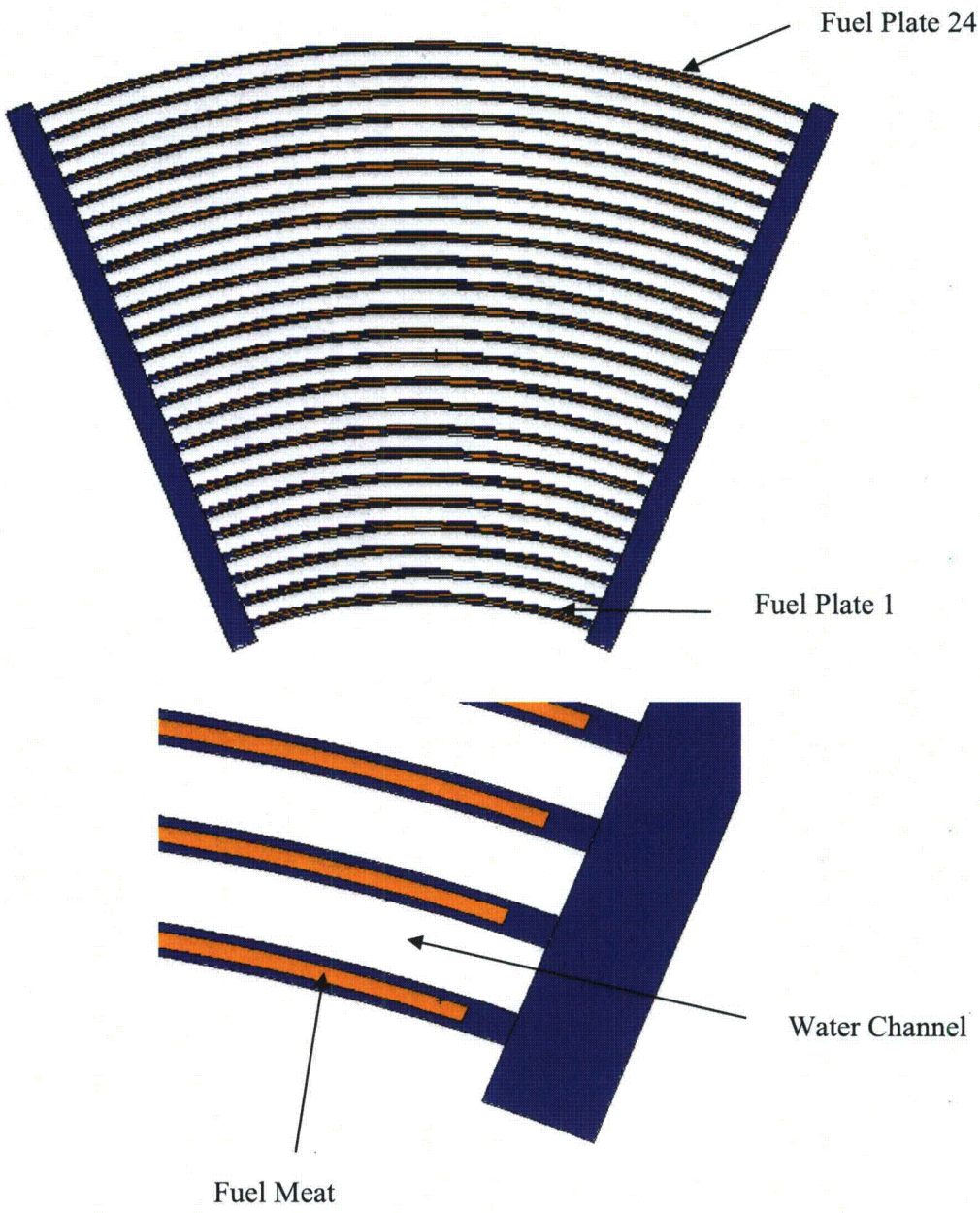

Figure 6.2-1 – MURR Fuel Element Model

Figure Withheld Under 10 CFR 2.390

Figure 6.2-2 – MURR Fuel Element Details

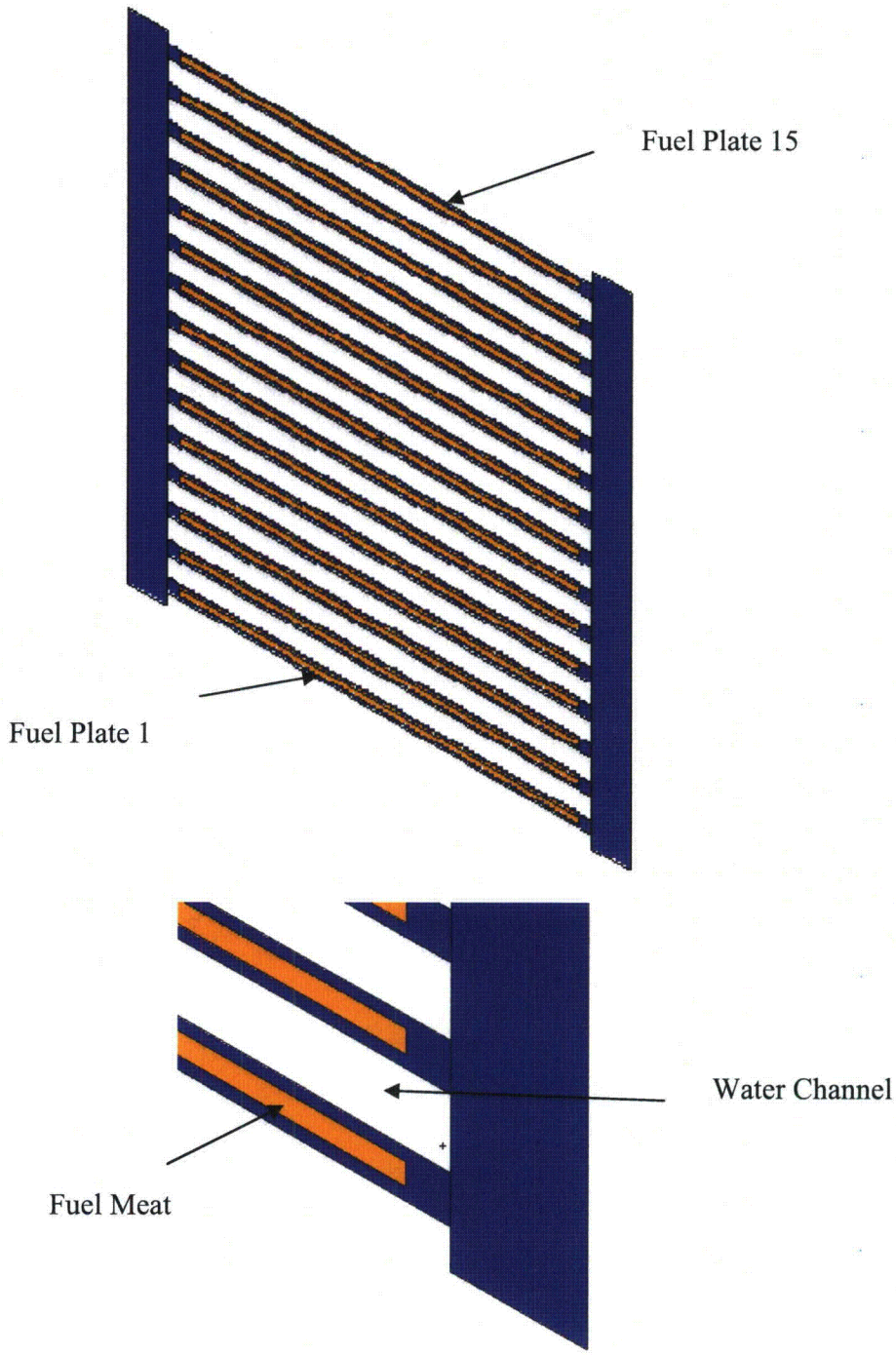

Figure 6.2-3 – MITR-II Fuel Element Model

Figure Withheld Under 10 CFR 2.390

Figure 6.2-4 – MITR-II Fuel Element Details

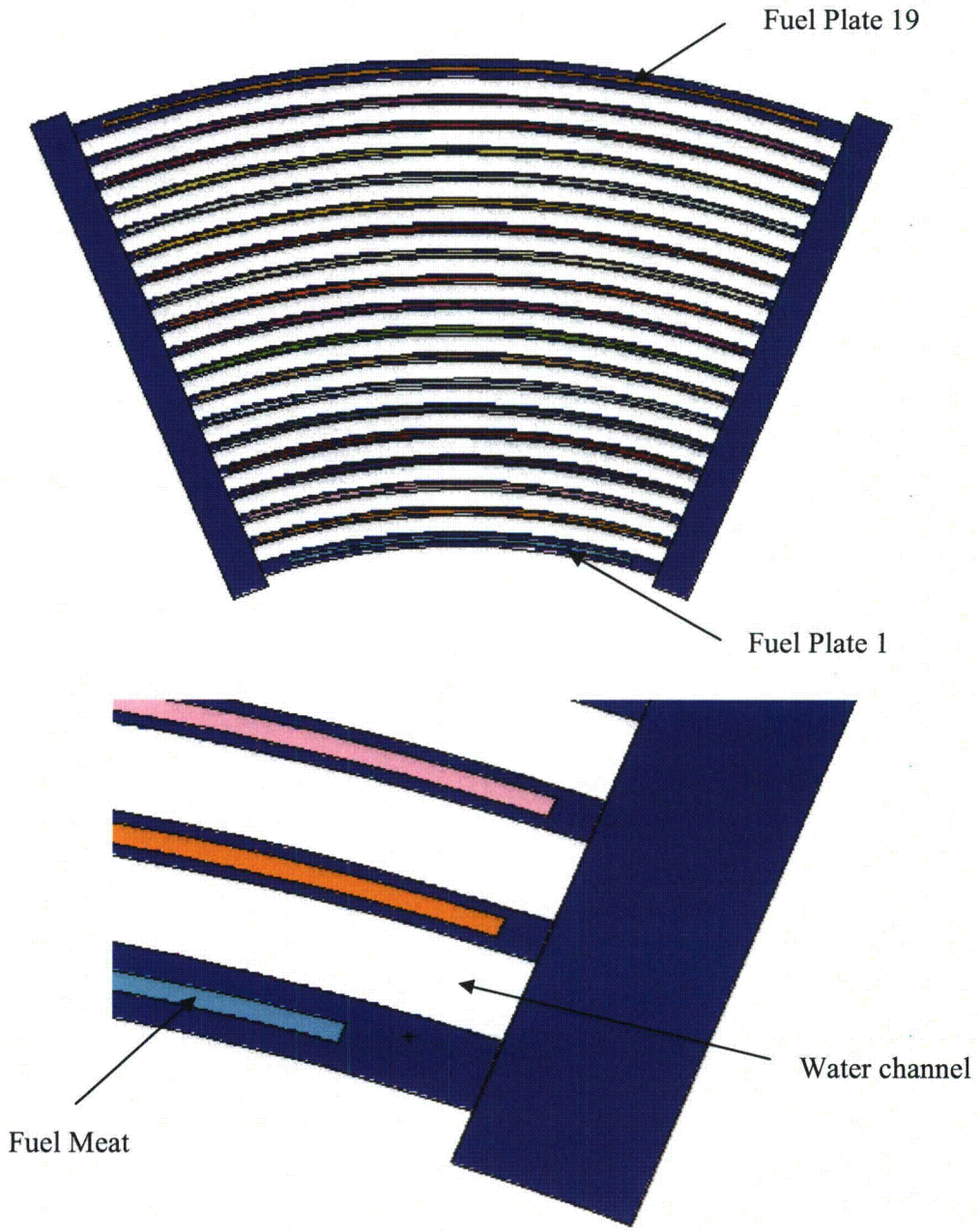

Figure 6.2-5 – ATR Fuel Element Model

Figure Withheld Under 10 CFR 2.390

Figure 6.2-6 – ATR Fuel Element Details

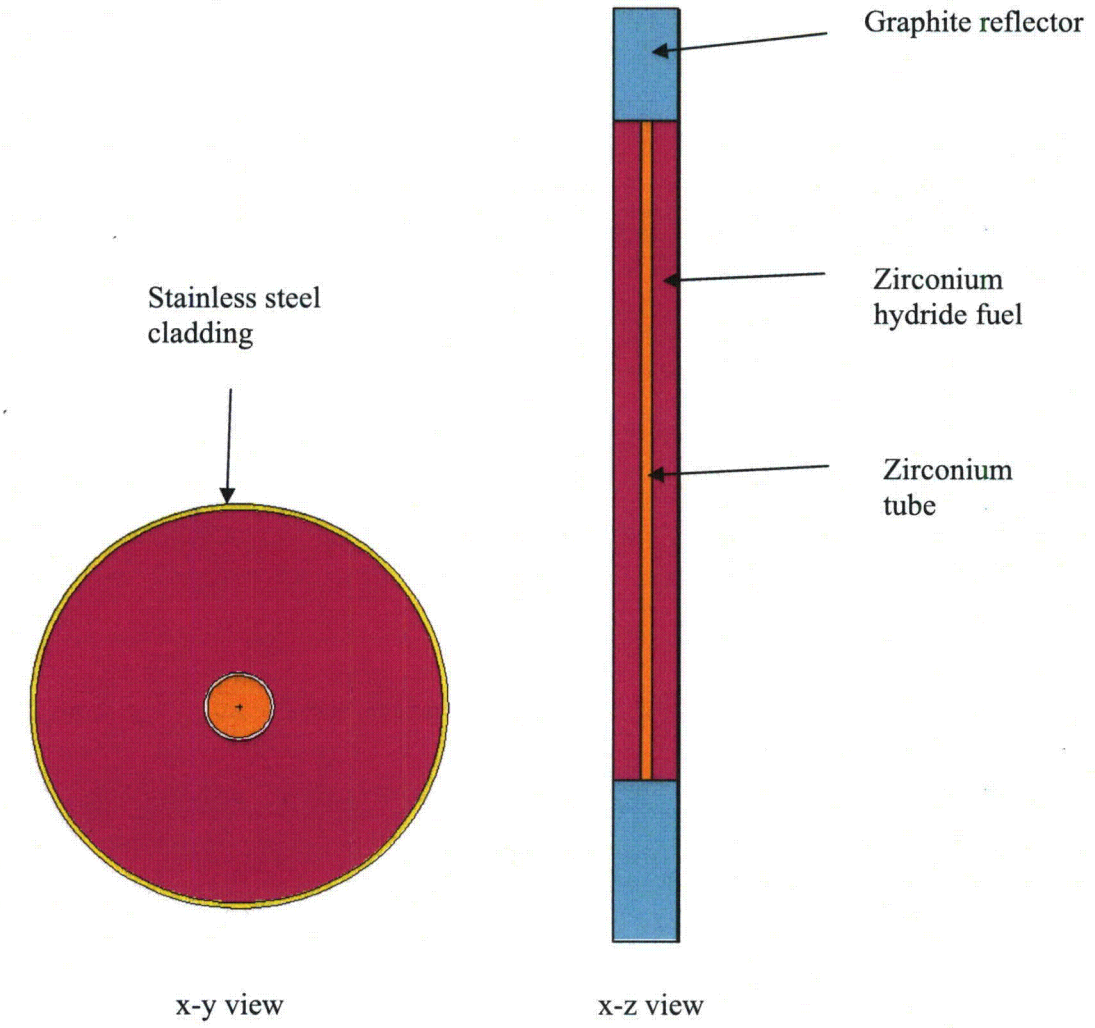

Figure 6.2-7 – Stainless Steel Clad TRIGA Fuel Element (Type 109)

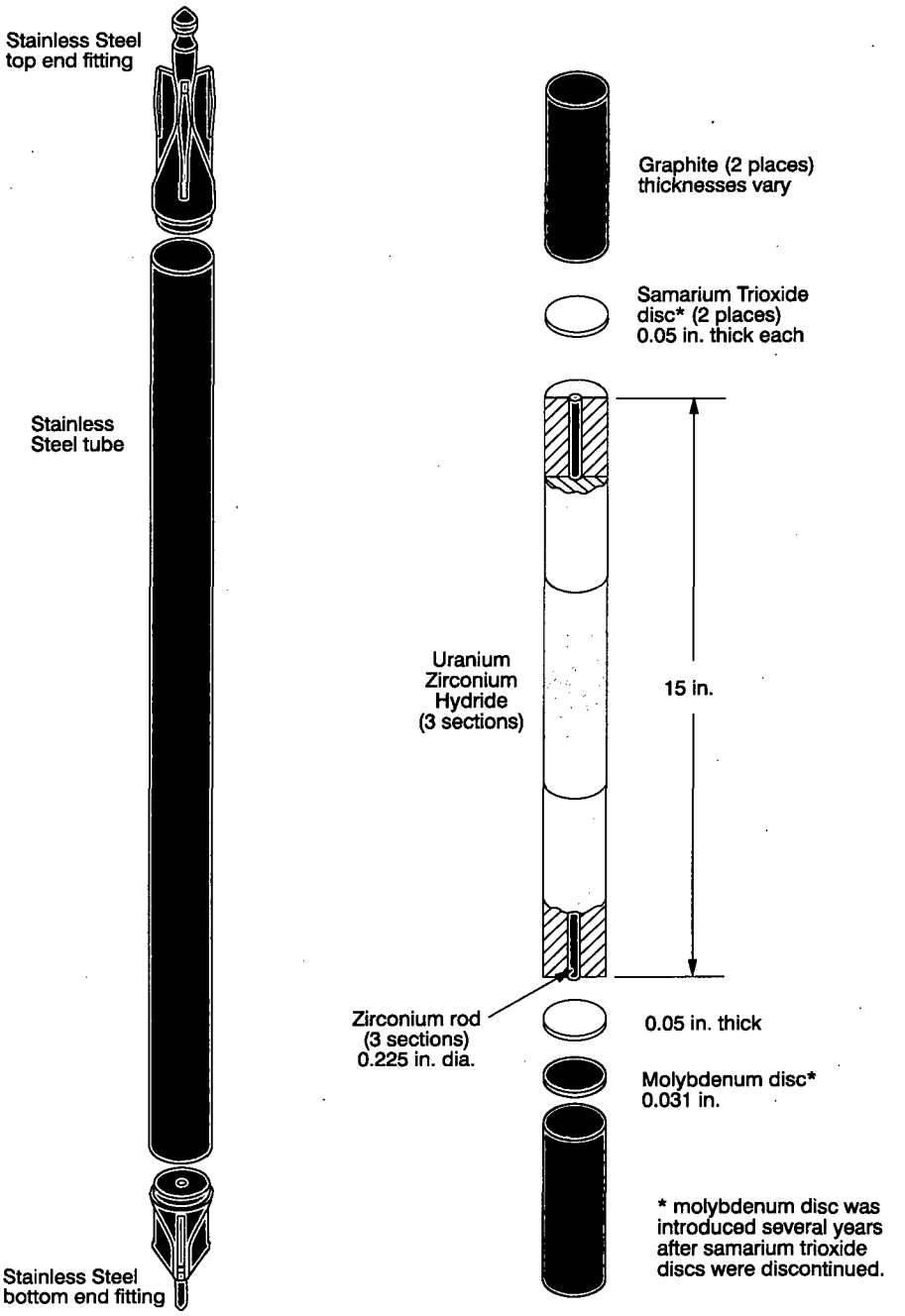

Figure 6.2-8 – Typical Stainless Steel Clad TRIGA Fuel Element

6.3 General Considerations

6.3.1 Model Configuration

The BRR cask is modeled using conservative simplifying assumptions. The impact limiters are not modeled, and in the single package cases the cask is reflected with 12-in of water. In the array cases, removing the impact limiters conservatively minimizes the separation between the packages and increases the reactivity. The cask body itself is simply modeled as cylinders of steel-lead-steel without modeling the minor cask details, as these minor details have a negligible effect on the system reactivity.

The modeled cask geometry is shown in Figure 6.3-1, and the key model dimensions are provided in Table 6.3-1. Cask dimensions are based on the drawings in Section 1.3.3, *Packaging General Arrangement Drawings*. Note that the cask model in the upper region is simply representative of the shield plug thicknesses and that the 2-in thick steel lid is not included in the model, thereby bring the casks closer together in the array configuration.

Each fuel type has its own unique basket design. The baskets are modeled in sufficient detail to capture the relevant criticality effects, which are primarily of interest near the active fuel region. The key basket dimensions are included in Table 6.3-2, and x-y and x-z views of the four basket designs are provided in Figure 6.3-2 and Figure 6.3-3, respectively. Basket dimensions are based on the drawings in Section 1.3.3, *Packaging General Arrangement Drawings*. Note that the axial and radial fuel positions shown in these figures do not reflect the most reactive configurations, which is determined in Section 6.4, *Single Package Evaluation.*

Minor differences exist between the as-modeled and packaging general arrangement drawing dimensions, as shown in Table 6.3-1 and Table 6.3-2. These differences are small and are within the uncertainty of the Monte Carlo method and may therefore be neglected.

The baskets are modeled as undamaged in all NCT and HAC models. The baskets have been shown to be elastic in all accident scenarios and maintain their geometry (see Section 2.7.1.5, *Fuel Basket Stress Analysis*). The fuel is also modeled as undamaged in all models (with end structures conservatively removed), as it has also been demonstrated that the fuel maintains its structural integrity during accident conditions (see Section 2.7.1.6, *Fuel Impact Deformation*).

In the NCT cases, credit is taken for the leaktight nature of the package, and the cask cavity is modeled as dry (void). Although the package has been shown to be leaktight under accident conditions, in the HAC cases, water is conservatively modeled in the cask cavity at the density that maximizes reactivity. If it is assumed that water is free to flow throughout the cask cavity and fuel elements (as the baskets are designed to drain freely), the moderator water density between the fuel plates may be modeled at the same value as the water density between the fuel elements. This assumption is utilized in all MCNP criticality models. However, it has been shown that when an ATR fuel element is removed from a spent fuel pool and allowed to drip dry, a small volume of water remains between the fuel plates due to the surface tension in the thin channels between the fuel plates. Because the quantity of residual water is relatively small, any minor surface tension effects have been neglected in the MCNP modeling. In addition, no models are developed in which the cask is partially filled with water with some fuel elements

uncovered (such as might be the case if the cask were on its side in an accident), because this scenario would be less reactive due to lack of moderation in the uncovered fuel elements.

In the array cases, a close-packed hexagonal array is modeled by adding a hexagonal reflective boundary condition. The water density between the casks in the array is adjusted to determine the most reactive condition.

6.3.2 Material Properties

The fuel meat compositions are provided in Table 6.2-2, Table 6.2-3, Table 6.2-6, and Table 6.2-8 for MURR, MITR-II, ATR, and TRIGA fuel, respectively. For all fuels, aluminum structural material is modeled as pure aluminum with a density of 2.7 g/cm^3.

The TRIGA fuel contains materials not found in the aluminum plate fuels, such as stainless steel, graphite, and zirconium. For the stainless steel clad TRIGA fuel, the composition of stainless steel utilized is the standard composition provided in the SCALE material library [4] and is provided in Table 6.3-3. For the TRIGA fuels that contain a zirconium rod in the center of the fuel element, the zirconium is modeled as pure with a density of 6.5 g/cm^3. The graphite reflectors in the TRIGA fuel elements is modeled as pure graphite with a density of 1.6 g/cm^3. The density is obtained from the TRIGA benchmark experiments (IEU-COMP-THERM-003) listed in the *International Handbook of Evaluated Criticality Benchmark Experiments* [3]. The molybdenum disc is omitted in most models, but when present is modeled as pure molybdenum with a density of 10.22 g/cm^3. The material properties of the remaining packaging and moderating materials are described as follows.

The inner and outer tubes of the package are constructed from stainless steel 304. The standard compositions for stainless steel 304 are obtained from the SCALE material library [4], which is a standard set accepted for use in criticality analyses. The stainless steel composition and density utilized in the MCNP models are provided in Table 6.3-3.

Water is modeled with a density ranging up to 1.0 g/cm^3 and the chemical formula H_2O.

6.3.3 Computer Codes and Cross-Section Libraries

MCNP5 v1.30 is used for the criticality analysis [1]. All cross sections utilized are at room temperature (293.6 K). The uranium isotopes utilize preliminary ENDF/B-VII cross section data that are considered by Los Alamos National Laboratory to be more accurate than ENDF/B-VI cross sections. ENDF/B-V cross sections are utilized for chromium, nickel, iron, and lead because natural composition ENDF/B-VI cross sections are not available for these elements. The remaining isotopes utilize ENDF/B-VI cross sections. Titles of the cross sections utilized in the models have been extracted from the MCNP output (when available) and provided in Table 6.3-4. The S(α,β) card LWTR.60T is used to simulate hydrogen bound to water in all models. For the TRIGA models only, the S(α,β) cards H/ZR.60T and ZR/H.60T are used to simulate hydrogen and zirconium in zirconium hydride, respectively.

All cases are run with 2500 neutrons per generation for 250 generations, skipping the first 50. The 1-sigma uncertainty is approximately 0.001 for the HAC cases, and somewhat less for the NCT cases.

6.3.4 Demonstration of Maximum Reactivity

The reactivities of the NCT single package and array cases are small (<0.6) because the package is leaktight and no water is present in the package cavity. The TRIGA fuel is the most reactive under NCT because hydrogen moderator is included in the zirconium hydride fuel matrix, although the reactivity is still relatively low.

Under HAC, water is allowed to enter the package cavity at the density that maximizes reactivity. For the plate fuels, the system is always the most reactive when full-density water is utilized because the system is undermoderated. For the TRIGA fuel, optimum reactivity is achieved for a reduced water density (0.6 or 0.7 g/cm^3). All four fuels show an increase in reactivity when the fuel is axially shifted to the top of the cavity, as this configuration maximizes reflection from the lead in the shield plug. All four fuels also show an increase in reactivity when the fuel elements are moved to the radial center of the package. For the MITR-II fuel, which has an inner and outer row of fuel elements, reactivity is maximized by moving the inner row outward and the outer row inward, which decreases the distance between the fuel elements.

For the array cases, a hexagonal reflective boundary condition is placed around the cask, simulating a hexagonal lattice. The water density between the packages is varied between 0 and 1.0 g/cm^3, and the array reactivities (both NCT and HAC) are maximized with no water between the packages.

It has been demonstrated in the structural analysis that the baskets and fuel elements maintain their structural integrity during accident condition. Therefore, no damaged basket or fuel models are developed.

The MURR fuel is the most reactive, with $k_s = 0.807$ (Case D1), which is below the USL of 0.9209 (see Table 6.1-1). The MITR-II, ATR, and TRIGA configurations are less reactive than MURR.

Table 6.3-1 – Key Cask Model Dimensions

Item	Dimension (in)
Cask Radial	
Cask inner diameter	16.0
Cask inner steel thickness	1.0
Cask lead thickness	8.0
Cask outer steel thickness	2.0
Cask outer diameter (w/o heat shield)	38.00
Cask Axial Top	
Shield plug bottom plate thickness	1.0
Shield plug lead thickness	9.7, modeled as 9.58
Shield plug top plate thickness	0.5
Shield plug overall height	11.2, modeled as 11.08
Cask Axial Bottom	
Bottom outer plate thickness	1.0
Bottom lead thickness at centerline	7.7, modeled as 7.72
Bottom casting inner thickness (after machining)	1.1, modeled as 1.22

Table 6.3-2 – Key Basket Model Dimensions

Item	Dimension (in)
MURR Basket	
Compartment separator width	1.0
Shell outer diameter	15.63
Shell thickness	0.25
Inner tube outer diameter	7.9, modeled as 7.938
Inner tube inner diameter	7.0
MITR-II Basket	
Compartment perpendicular width	2.7
Inner Diameter	Complex, modeled as 9.45
Outer Diameter	15.63
Distance, cutout to center	4.8
ATR Basket	
Compartment separator width	0.375
Shell outer diameter	13.5
Shell thickness	0.25
Inner tube outer diameter	7.2
Inner tube inner diameter	6.5
TRIGA Basket	
Tube outer diameter	2.0
Tube wall thickness	0.12, modeled as 0.11
Inner row position diameter	6.5
Outer row position diameter	11.5

Table 6.3-3 – SS304 Composition

Component	Wt.%
C	0.08
Si	1.0
P	0.045
Cr	19.0
Mn	2.0
Fe	68.375
Ni	9.5
Density (g/cm^3)	7.94

Table 6.3-4 – Cross Section Libraries Utilized

Isotope/Element	Cross Section Label (from MCNP output)
1001.62c	1-h-1 at 293.6K from endf-vi.8 njoy99.50
6000.66c	6-c-0 at 293.6K from endf-vi.6 njoy99.50
8016.62c	8-o-16 at 293.6K from endf-vi.8 njoy99.50
13027.62c	13-al-27 at 293.6K from endf-vi.8 njoy99.50
14000.60c	14-si-nat from endf/b-vi
15031.66c	15-p-31 at 293.6K from endf-vi.6 njoy99.50
17000.66c	17-cl-0 at 293.6K from endf-vi.0 njoy99.50
24000.50c	njoy
25055.62c	25-mn-55 at 293.6K from endf/b-vi.8 njoy99.50
26000.55c	njoy
28000.50c	njoy
40000.66c	40-zr-0 at 293.6K from endf-vi.1 njoy99.50
82000.50c	njoy
92234.69c	92-u-234 at 293.6K from t16 u234la4 njoy99.50
92235.69c	92-u-235 at 293.6K from t16 u235la9d njoy99.50
92236.69c	92-u-236 at 293.6K from t16 u236la2d njoy99.50
92238.69c	92-u-238 at 293.6K from t16 u238la8h njoy99.50

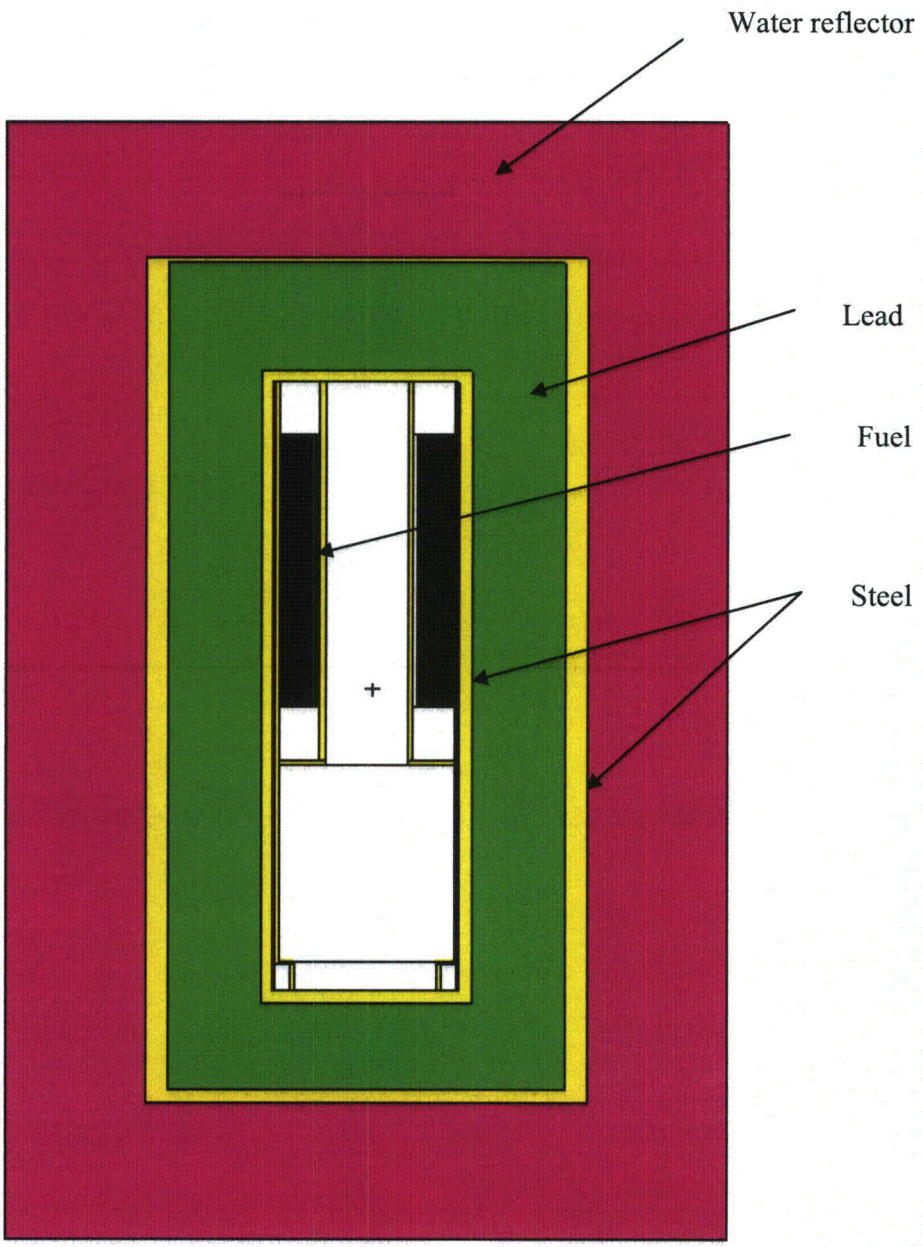

Figure 6.3-1 – NCT Single Package Model (x-z view)

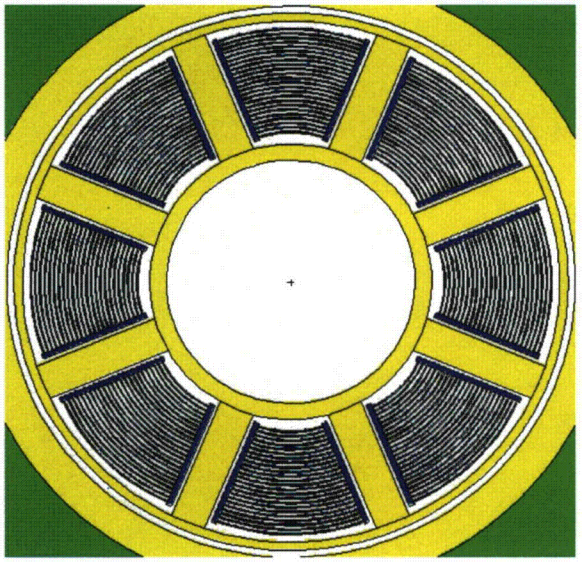

MURR

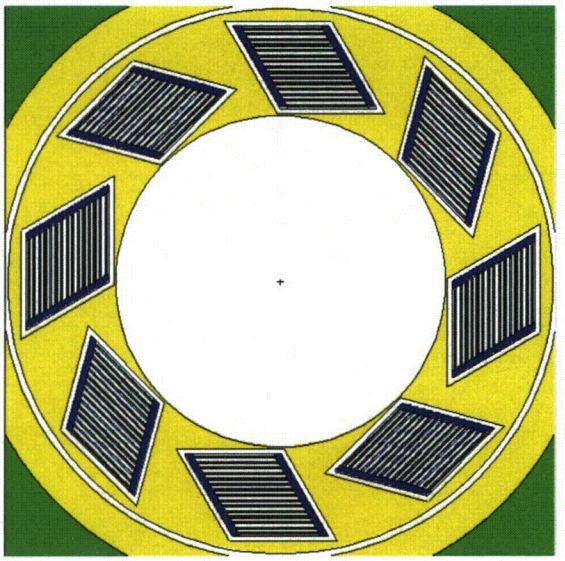

MITR-II

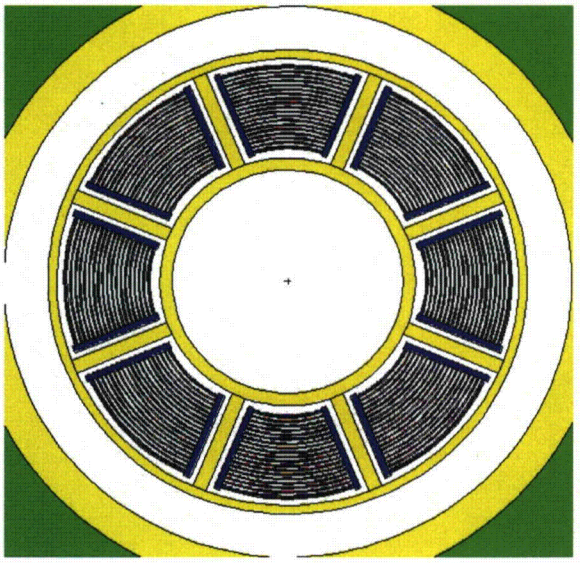

ATR

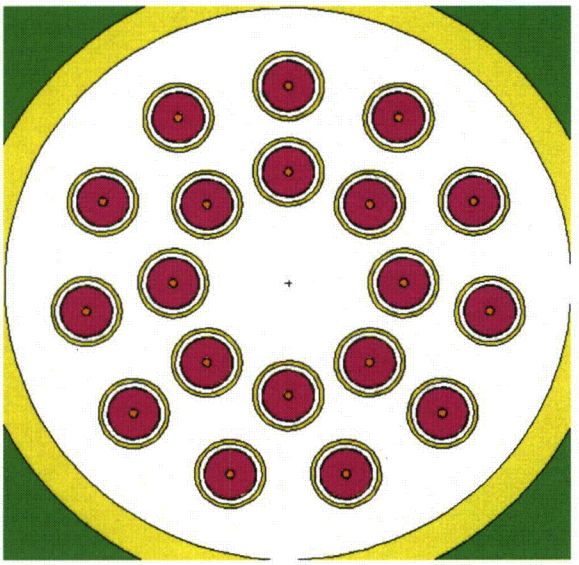

TRIGA

Figure 6.3-2 – Basket Models (x-y view)

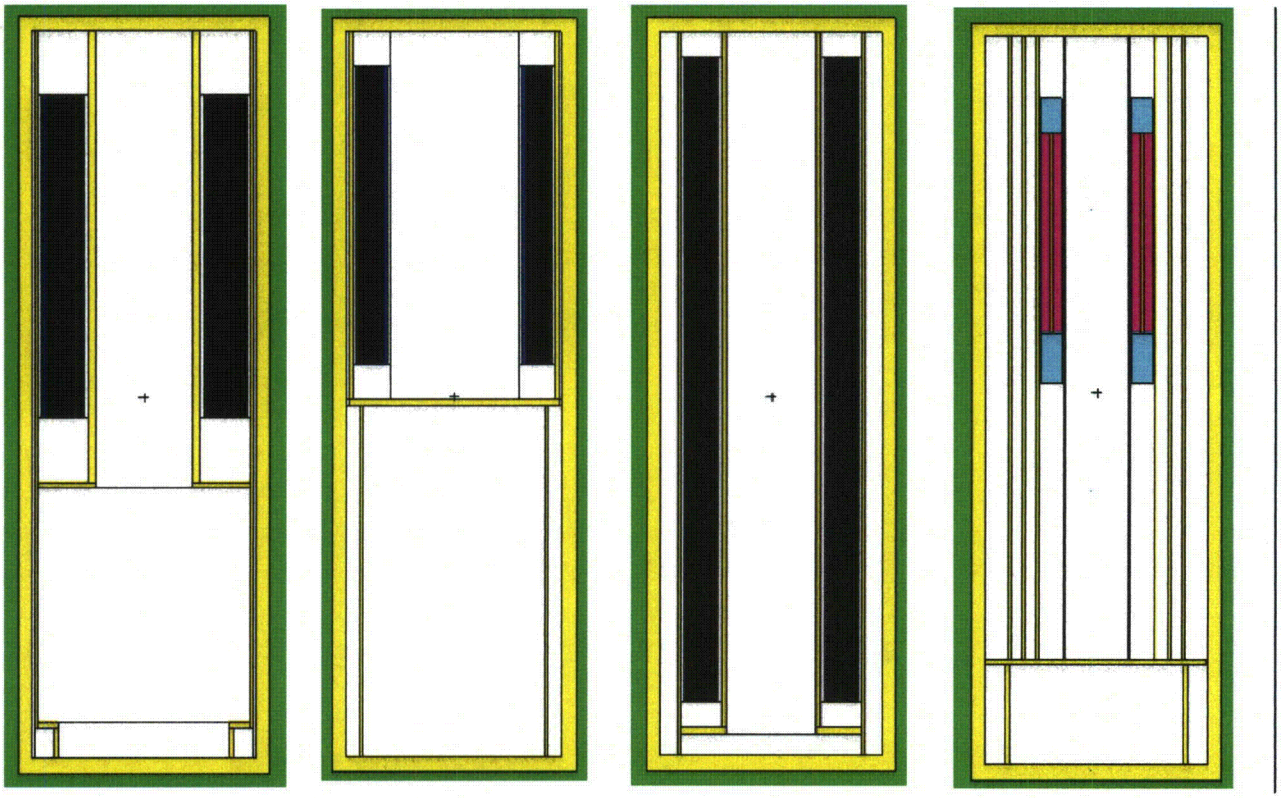

Figure 6.3-3 – Basket Models (x-z view)

6.4 Single Package Evaluation

6.4.1 Configuration

6.4.1.1 NCT Single Package Configuration

The geometry of the NCT single package configuration is discussed in Section 6.3.1, *Model Configuration*. The fuel element geometry is consistent with the most reactive fuel element models, including tolerances, as determined in Section 6.9.2, *Parametric Evaluations to Determine the Most Reactive Fuel Geometries*. For the TRIGA fuels, it is demonstrated in Section 6.9.2.4, *TRIGA Fuel Parametric Evaluation*, that the HEU fuel type (Type 109) is the most reactive of the five TRIGA fuel types under consideration. Therefore, all TRIGA models use this fuel type.

MURR

The MURR results are listed in Table 6.4-1 as Cases A1 through A3. In Case A1, the active fuel region is centered both axially and laterally within the basket compartments. In Case A2, all fuel elements are moved within the basket compartments towards the radial center. In Case A3, the fuel elements are moved radially inward (like Case A2) and shifted axially to the top of the package. In actual practice, it would not be possible to shift the active fuel all the way to the top due to the presence of the end fittings. This configuration is the most reactive, as reflection from the package shield plug is maximized. Therefore, Case A3 is the most reactive, with k_s = 0.08545. Clearly, the reactivity of unmoderated MURR fuel is very low.

MITR-II

The MITR-II results are listed in Table 6.4-1 as Cases A10 through A13. In Case A10, the active fuel region is centered both axially and laterally within the basket compartments. In Case A11, the fuel elements are moved within the basket compartments towards the radial center. In Case A12, the fuel elements are pushed to the radial center of the package and shifted axially to the top of the package. In actual practice, it would not be possible to shift the active fuel all the way to the top due to the presence of the end fittings. Case A13 is the same as Case A12 except the fuel elements are shifted radially outward rather than radially inward. The reactivity of all four cases is rather similar. Case A12 is the most reactive, with k_s = 0.05836. Clearly, the reactivity of unmoderated MITR-II fuel is very low.

ATR

The ATR results are listed in Table 6.4-1 as Cases A20 through A22. In Case A20, the active fuel region is centered both axially and laterally within the basket compartments. In Case A21, all fuel elements are moved within the basket compartments towards the radial center. In Case A22, the fuel elements are moved radially inward (like Case A21) and shifted axially to the top of the package. All three configurations have similar reactivities, although Case A22 is the most reactive, with k_s = 0.08849. Clearly, the reactivity of unmoderated ATR fuel is very low.

TRIGA

The TRIGA results are listed in Table 6.4-1 as Cases A30 through A33. In Case A30, the fuel elements are laterally centered in the basket compartments, and the fuel elements are offset from the package lid. In Case A31, the fuel elements are moved within the basket tubes towards the radial center. In Case A32, the outer row of elements are moved radially inward, and the inner row is moved radially outward. Comparing Cases A30 through A32, Case A31 is the most reactive. In Case A33, the fuel elements are moved radially inward (like Case A31) and shifted axially to the top of the package. In actual practice, it would not be possible to shift the active fuel all the way to the top due to the end fittings. This configuration is the most reactive, as reflection from the package shield plug is maximized. Therefore, Case A33 is the most reactive, with $k_s = 0.41671$. Clearly, the reactivity of unmoderated TRIGA fuel is very low and is significantly less than the USL, although the unmoderated TRIGA fuel results in the highest reactivity compared to the other fuel types (MURR, MITR-II and ATR).

6.4.1.2 HAC Single Package Configuration

The HAC single package configurations are similar to the NCT single package configurations except that water is allowed inside the package at the most reactive density.

MURR

The MURR results are summarized in Table 6.4-2 as Cases B1 through B5. In Cases B1 through B3, the package cavity is flooded with full-density water. In Case B1, the active fuel is centered both laterally and axially within the basket compartments. In Case B2, the active fuel is moved within the basket compartments towards the radial center. In Case B3, the radial configuration from Case B2 is maintained, and the fuel elements are shifted upward to the maximum possible extent, maximizing reflection from the shield plug. Case B3 is the most reactive of the three configurations examined.

In Cases B4 and B5, the configuration of Case B3 is modified so that the basket/fuel element water density is reduced to 0.8 and 0.9 g/cm^3, respectively. Because the MURR fuel is undermoderated, reducing the water density will reduce the reactivity. As expected, the reactivity for Case B4 and B5 drops rapidly as the water density is reduced. Therefore, Case B3 is the most reactive, with $k_s = 0.76124$.

MITR-II

The MITR-II results are summarized in Table 6.4-2 as Cases B20 through B27. In Cases B20 through B25, the package cavity is flooded with full-density water. In Case B20, the active fuel is centered both laterally and axially within the basket compartments. In Case B21, the active fuel is pushed to the radial center of the package, and the reactivity increases. In Case B22, the radial configuration from Case B21 is maintained, and the fuel elements are pushed upward to the maximum possible extent, maximizing reflection from the lid. In Case B23, the fuel is pushed radially outward but shifted upward as in Case B22. Case B22 is the most reactive of the four configurations examined, although the reactivity effect of the axial shifting is small.

In Cases B25 and B26, the reactivity effect of the basket inner cavity radius is examined. The inner cavity of the basket has an irregular shape that is approximated as a cylinder with a radius of 12.0 cm, which is the largest radius that does not interfere with the fuel element cavity cell

descriptions. Cases B25 and B26 are the same as Case B20 except this radius is modeled as 11.0 and 11.5 cm, respectively. Reactivity decreases as the radius decreases, indicating that modeling with the largest possible radius of 12.0 cm is conservative.

In Cases B26 and B27, the configuration of Case B22 is modified so that the basket water density is reduced to 0.8 and 0.9 g/cm^3, respectively. Because the fuel elements and basket are free to drain, reducing the water density in the basket also reduces the water density between the fuel plates. Because the MITR-II fuel is undermoderated, reducing the water density will reduce the reactivity. As expected, the reactivity for Case B26 and B27 drops rapidly as the water density is reduced.

Therefore, Case B22 is the most reactive, with $k_s = 0.52490$.

ATR

The ATR results are summarized in Table 6.4-2 as Cases B40 through B44. In Cases B40 through B42, the package cavity is fully flooded with full-density water. In Case B40, the fuel elements are centered both axially and laterally within the basket compartments. In Case B41, the fuel elements are moved within the basket compartments towards the radial center. In Case B42, the fuel is also shifted axially to the top of the package in addition to be moved toward the radial center. Comparing these three cases, Case B42 is the most reactive, although the reactivities are somewhat similar.

In Cases B43 and B44, the configuration of Case B42 is modified so that the basket/fuel element water density is reduced to 0.8 and 0.9 g/cm^3, respectively. Because the ATR fuel is undermoderated, reducing the water density will reduce the reactivity. As expected, the reactivity for Case B43 and B44 drops rapidly as the water density is reduced. Therefore, Case B42 is the most reactive, with $k_s = 0.68525$.

TRIGA

The TRIGA results are summarized in Table 6.4-2 as Cases B60 through B70. In Cases B60 through B64, the package cavity is fully flooded with full-density water. In Case B60, the fuel elements are laterally centered within the basket tubes, at an arbitrary distance away from the package lid. In Case B61, the fuel elements are moved within the basket tubes towards the radial center, and the reactivity increases. In Case B62, the outer row is moved radially inward and the inner row is moved radially outward. Cases B63 and B64 are essentially repeats of Cases B60 and B61, respectively, except that the fuel elements are shifted upward until the top of the graphite reflector touches the bottom of the shield plug. Comparing these five cases, Case B64 is the most reactive. Therefore, the remaining HAC single package cases utilize this configuration (i.e., fuel elements moved to the radial center, shifted up to the maximum extent.)

In Cases B65 through B70, the configuration of Case B64 is modified so that the water density inside of the basket is allowed to vary between 0.4 and 0.9 g/cm^3. The reactivity peaks at a density of 0.7 g/cm^3 and then decreases with decreasing density. The maximum reactivity occurs for Case B68, with $k_s = 0.70869$.

6.4.2 Results

Following are the tabulated results for the single package cases. The most reactive configurations are listed in boldface.

Table 6.4-1 – NCT Single Package Results

Case ID	Filename	k_{eff}	σ	k_s (k+2σ)
MURR				
A1	NS_MURR	0.08167	0.00023	0.08213
A2	NS_MURR_IN	0.08152	0.00022	0.08196
A3	**NS_MURR_INUP**	**0.08499**	**0.00023**	**0.08545**
MITR-II				
A10	NS_MIT2	0.05655	0.00015	0.05685
A11	NS_MIT2_IN	0.05709	0.00016	0.05741
A12	**NS_MIT2_INUP**	**0.05808**	**0.00014**	**0.05836**
A13	NS_MIT2_OUTUP	0.05762	0.00016	0.05794
ATR				
A20	NS_ATR	0.08689	0.00024	0.08737
A21	NS_ATR_IN	0.08759	0.00025	0.08809
A22	**NS_ATR_INUP**	**0.08797**	**0.00026**	**0.08849**
TRIGA				
A30	NS_TRIGA	0.39557	0.00089	0.39735
A31	NS_TRIGA_IN	0.40299	0.00092	0.40483
A32	NS_TRIGA_INOUT	0.40078	0.00092	0.40262
A33	**NS_TRIGA_INUP**	**0.41493**	**0.00089**	**0.41671**

Table 6.4-2 – HAC Single Package Results

Case ID	Filename	Water Density (g/cm^3)	k_{eff}	σ	k_s (k+2σ)
MURR					
B1	HS_MURR	1.0	0.75395	0.00115	0.75625
B2	HS_MURR_IN	1.0	0.75287	0.00123	0.75533
B3	**HS_MURR_INUP**	**1.0**	**0.75898**	**0.00113**	**0.76124**
B4	HS_MURR_C080INUP	0.8	0.69306	0.00108	0.69522
B5	HS_MURR_C090INUP	0.9	0.72871	0.00118	0.73107
MITR-II					
B20	HS_MIT2_W100	1.0	0.50737	0.00107	0.50951
B21	HS_MIT2_W100IN	1.0	0.52143	0.00111	0.52365
B22	**HS_MIT2_W100INUP**	**1.0**	**0.52284**	**0.00103**	**0.52490**
B23	HS_MIT2_W100OUTUP	1.0	0.49263	0.00103	0.49469
B24	HS_MIT2_W100INUP_R11	1.0	0.48905	0.00107	0.49119
B25	HS_MIT2_W100INUP_R11P5	1.0	0.49907	0.00095	0.50097
B26	HS_MIT2_W080INUP	0.8	0.48751	0.00096	0.48943
B27	HS_MIT2_W090INUP	0.9	0.50573	0.00102	0.50777
ATR					
B40	HS_ATR	1.0	0.67992	0.00113	0.68218
B41	HS_ATR_IN	1.0	0.68013	0.00110	0.68233
B42	**HS_ATR_INUP**	**1.0**	**0.68279**	**0.00123**	**0.68525**
B43	HS_ATR_C080INUP	0.8	0.64718	0.00105	0.64928
B44	HS_ATR_C090INUP	0.9	0.66179	0.00106	0.66391
TRIGA					
B60	HS_TRIGA_W100	1.0	0.66788	0.00108	0.67004
B61	HS_TRIGA_W100IN	1.0	0.69115	0.00097	0.69309
B62	HS_TRIGA_W100INOUT	1.0	0.67398	0.00098	0.67594
B63	HS_TRIGA_W100UP	1.0	0.66998	0.00112	0.67222
B64	HS_TRIGA_W100INUP	1.0	0.69348	0.00106	0.69560
B65	HS_TRIGA_W040INUP	0.4	0.67497	0.00119	0.67735
B66	HS_TRIGA_W050INUP	0.5	0.69534	0.00124	0.69782
B67	HS_TRIGA_W060INUP	0.6	0.70552	0.00104	0.70760
B68	**HS_TRIGA_W070INUP**	**0.7**	**0.70661**	**0.00104**	**0.70869**
B69	HS_TRIGA_W080INUP	0.8	0.70510	0.00099	0.70708
B70	HS_TRIGA_W090INUP	0.9	0.70164	0.00106	0.70376

6.5 Evaluation of Package Arrays under Normal Conditions of Transport

6.5.1 Configuration

In the NCT array configurations, the most reactive NCT single package configuration for each fuel type determined in Section 6.4.1.1, *NCT Single Package Configuration*, is utilized. A hexagonal reflective surface is added around the package, as shown in Figure 6.5-1. This simulates a close-packed infinite hexagonal array of packages. The reflective boundary is also present on the top and bottom surfaces.

Five cases are run for each fuel type. The initial case is simply the most reactive NCT single package case with reflective boundary conditions and no water between the packages. In the remaining four cases, the water density between the packages is varied between 0.25 and 1.0 g/cm^3. In each case, the reactivity is maximized with no water between the packages.

The results are summarized in Table 6.5-1. Cases C1 through C5 are for MURR, Cases C10 through C14 are for MITR-II, Cases C20 through C24 are for ATR, and Cases C30 through C34 are for TRIGA. Of the four fuel types considered, the TRIGA fuel Case C30 with no water between the packages is the most reactive, with $k_s = 0.53939$. TRIGA fuel is significantly more reactive than the other fuels because hydrogen is included in the fuel matrix.

6.5.2 Results

The results for the NCT array cases are provided in the following table. The most reactive configuration for each fuel type is listed in boldface.

Table 6.5-1 – NCT Array Results

Case ID	Filename	External Water Density (g/cm^3)	k_{eff}	σ	k_s ($k+2\sigma$)
MURR					
C1	**NA_MURR_INUP**	**0**	**0.19604**	**0.00037**	**0.19678**
C2	NA_MURR_W025INUP	0.25	0.12467	0.00031	0.12529
C3	NA_MURR_W050INUP	0.50	0.11327	0.00029	0.11385
C4	NA_MURR_W075INUP	0.75	0.10858	0.00026	0.10910
C5	NA_MURR_W100INUP	1.0	0.10606	0.00027	0.10660
MITR-II					
C10	**NA_MIT2_W000**	**0**	**0.14305**	**0.00028**	**0.14361**
C11	NA_MIT2_W025	0.25	0.09091	0.00027	0.09145
C12	NA_MIT2_W050	0.50	0.08283	0.00021	0.08325
C13	NA_MIT2_W075	0.75	0.07970	0.00022	0.08014
C14	NA_MIT2_W100	1.0	0.07704	0.00021	0.07746
ATR					
C20	**NA_ATR_INUP**	**0**	**0.23274**	**0.00041**	**0.23356**
C21	NA_ATR_W025INUP	0.25	0.13567	0.00032	0.13631
C22	NA_ATR_W050INUP	0.50	0.12103	0.00031	0.12165
C23	NA_ATR_W075INUP	0.75	0.11473	0.00029	0.11531
C24	NA_ATR_W100INUP	1.0	0.11116	0.00028	0.11172
TRIGA					
C30	**NA_TRIGA_INUP**	**0**	**0.53733**	**0.00103**	**0.53939**
C31	NA_TRIGA_W025INUP	0.25	0.46130	0.00099	0.46328
C32	NA_TRIGA_W050INUP	0.50	0.44977	0.00096	0.45169
C33	NA_TRIGA_W075INUP	0.75	0.44506	0.00096	0.44698
C34	NA_TRIGA_W100INUP	1.0	0.43997	0.00094	0.44185

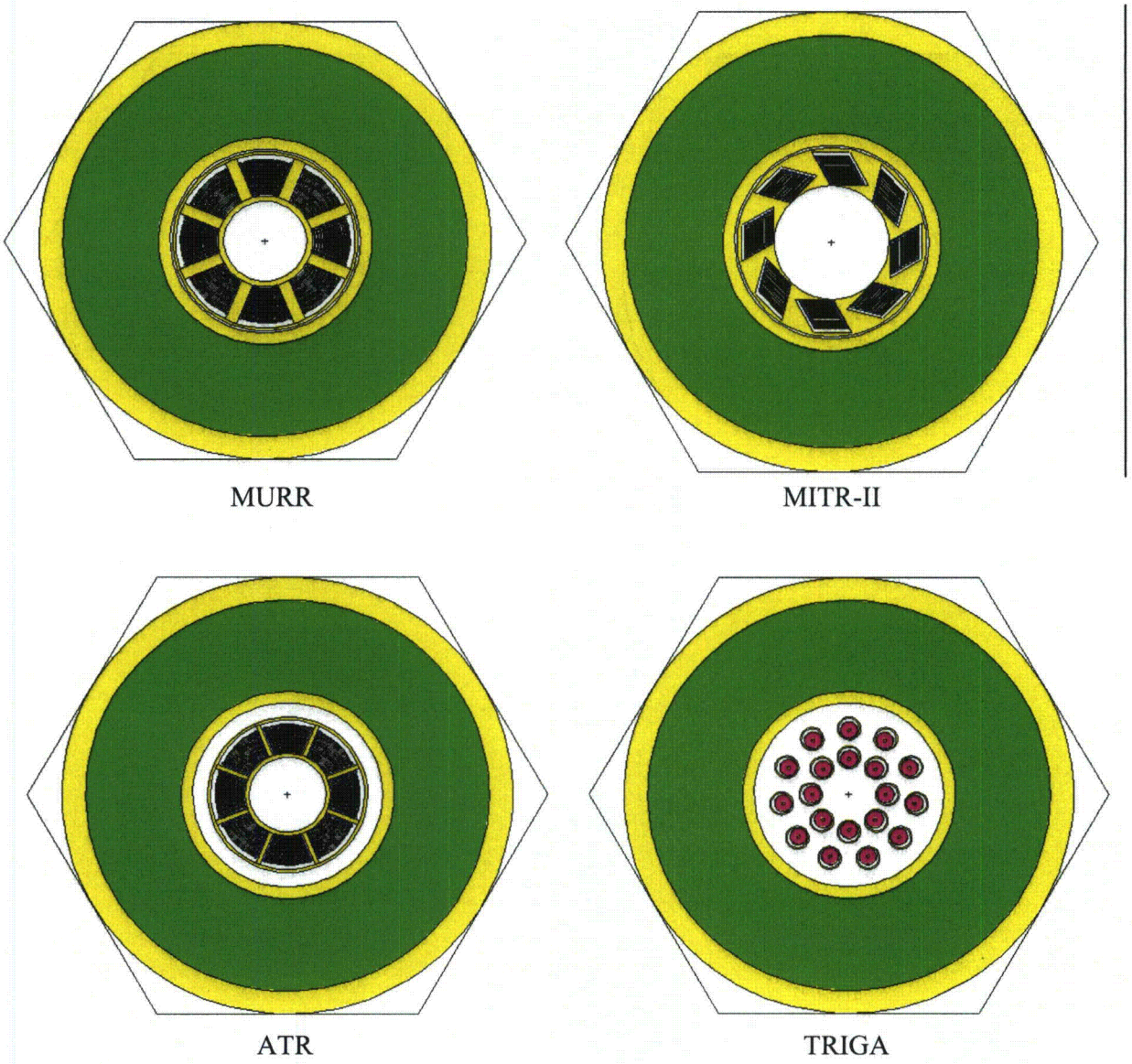

Figure 6.5-1 – NCT Array Geometry

6.6 Package Arrays under Hypothetical Accident Conditions

6.6.1 Configuration

In the HAC array configuration, an infinite hexagonal array of packages is modeled in the same manner as the NCT array. Various internal moderation conditions are examined, as well as various moderation conditions between packages.

MURR

The MURR results are reported in Table 6.6-1. In Case D1, the fuel elements are moved radially inward and shifted to the top of the package, which was determined to be the most reactive single package orientation. The package cavity is flooded with full-density water, and void is modeled between the packages.

In Cases D2 and D3, the configuration of Case D1 is modified so that all water inside the cavity is treated as variable density (0.8 and 0.9 g/cm^3, respectively). Because the water density between the fuel plates is reduced in this configuration, moderation is decreased and the reactivity decreases.

In Cases D4 through D7, the most reactive case (Case D1) is run with variable water density between the packages. The reactivity decreases when water is added to this region. Therefore, Case D1 is the most reactive, with $k_s = 0.80658$. Note that this is also the most reactive case of the four fuel types examined.

MITR-II

The MITR-II results are reported in Table 6.6-2. In Case D20, the fuel elements are pushed radially inward and shifted to the top of the package, which was determined to be the most reactive single package orientation. The package cavity is flooded with full-density water, and void is modeled between the packages.

In Cases D21 and D22, the configuration of Case D20 is modified so that all water inside the cavity is treated as variable density (0.8 and 0.9 g/cm^3, respectively). Because the water density between the fuel plates is reduced in this configuration, moderation is decreased and the reactivity decreases.

In Cases D23 through D26, the most reactive case (Case D20) is run with variable water density between the packages. The reactivity decreases when water is added to this region. Therefore, Case D20 is the most reactive, with $k_s = 0.56307$.

ATR

The ATR results are reported in Table 6.6-3. In Case D40, the fuel elements are moved radially inward and shifted to the top of the package, which was determined to be the most reactive single package orientation. The package cavity is flooded with full-density water, and void is modeled between the packages.

In Cases D41 and D42, the configuration of Case D40 is modified so that all water inside the cavity is treated as variable density (0.8 and 0.9 g/cm^3, respectively). Because the water density

between the fuel plates is reduced in this configuration, moderation is decreased and the reactivity decreases.

In Cases D43 through D46, the most reactive case (Case D40) is run with variable water density between the packages. The reactivity decreases when water is added to this region. Therefore, Case D40 is the most reactive, with $k_s = 0.69739$.

TRIGA

The TRIGA results are reported in Table 6.6-4. In all models, the fuel elements are moved radially inward and axially shifted to the top of the cask, which was determined to be the most reactive single package orientation. It is expected that the most reactive condition will occur at a reduced internal water density, consistent with the single package TRIGA results. Therefore, in Cases D60 through D67, the cavity water density is varied from 0.3 to 1.0 g/cm^3, while void is modeled external to the package. The maximum reactivity occurs for Case D63, which has a water density of 0.6 g/cm^3.

In Cases D68 through D71, the internal water density is modeled at 0.6 g/cm^3 (Case D63 configuration) while the external water density is varied between 0.25 and 1.0 g/cm^3. The reactivity decreases when water is modeled between the packages. Therefore, Case D63 is the most reactive, with $k_s = 0.72039$.

6.6.2 Results

Following are the tabulated results for the HAC array cases. The most reactive configuration in each series is listed in boldface.

Table 6.6-1 – HAC Array Results, MURR

Case ID	Filename	Internal Water Density (g/cm^3)	External Water Density (g/cm^3)	k_{eff}	σ	k_s (k+2σ)
D1	**HA_MURR**	**1.0**	**0**	**0.80428**	**0.00115**	**0.80658**
D2	HA_MURR_C080	0.8	0	0.74913	0.00111	0.75135
D3	HA_MURR_C090	0.9	0	0.77692	0.00116	0.77924
D4	HA_MURR_W025	1.0	0.25	0.77495	0.00125	0.77745
D5	HA_MURR_W050	1.0	0.50	0.77403	0.00106	0.77615
D6	HA_MURR_W075	1.0	0.75	0.77030	0.00115	0.77260
D7	HA_MURR_W100	1.0	1.0	0.76810	0.00131	0.77072

Table 6.6-2 – HAC Array Results, MITR-II

Case ID	Filename	Internal Water Density (g/cm^3)	External Water Density (g/cm^3)	k_{eff}	σ	k_s (k+2σ)
D20	**HA_MIT2**	**1.0**	**0**	**0.56103**	**0.00102**	**0.56307**
D21	HA_MIT2_C080	0.8	0	0.53082	0.00099	0.53280
D22	HA_MIT2_C090	0.9	0	0.54724	0.00106	0.54936
D23	HA_MIT2_W025	1.0	0.25	0.54199	0.00096	0.54391
D24	HA_MIT2_W050	1.0	0.50	0.53616	0.00096	0.53808
D25	HA_MIT2_W075	1.0	0.75	0.53278	0.00111	0.53500
D26	HA_MIT2_W100	1.0	1.0	0.53347	0.00105	0.53557

Table 6.6-3 – HAC Array Results, ATR

Case ID	Filename	Internal Water Density (g/cm^3)	External Water Density (g/cm^3)	k_{eff}	σ	k_s (k+2σ)
D40	**HA_ATR**	**1.0**	**0**	**0.69505**	**0.00117**	**0.69739**
D41	HA_ATR_C080	0.8	0	0.66976	0.00104	0.67184
D42	HA_ATR_C090	0.9	0	0.68206	0.00109	0.68424
D43	HA_ATR_W025	1.0	0.25	0.68753	0.00115	0.68983
D44	HA_ATR_W050	1.0	0.50	0.68575	0.00111	0.68797
D45	HA_ATR_W075	1.0	0.75	0.68528	0.00106	0.68740
D46	HA_ATR_W100	1.0	1.0	0.68342	0.00110	0.68562

Table 6.6-4 – HAC Array Results, TRIGA

Case ID	Filename	Internal Water Density (g/cm^3)	External Water Density (g/cm^3)	k_{eff}	σ	k_s ($k+2\sigma$)
D60	HA_TRIGA_W0C030	0.3	0	0.68281	0.00107	0.68495
D61	HA_TRIGA_W0C040	0.4	0	0.70304	0.00102	0.70508
D62	HA_TRIGA_W0C050	0.5	0	0.71234	0.00113	0.71460
D63	**HA_TRIGA_W0C060**	**0.6**	**0**	**0.71827**	**0.00106**	**0.72039**
D64	HA_TRIGA_W0C070	0.7	0	0.71592	0.00107	0.71806
D65	HA_TRIGA_W0C080	0.8	0	0.71130	0.00109	0.71348
D66	HA_TRIGA_W0C090	0.9	0	0.70455	0.00107	0.70669
D67	HA_TRIGA_W0C100	1.0	0	0.69737	0.00112	0.69961
D68	HA_TRIGA_W025C060	0.6	0.25	0.70793	0.00125	0.71043
D69	HA_TRIGA_W050C060	0.6	0.50	0.70781	0.00097	0.70975
D70	HA_TRIGA_W075C060	0.6	0.75	0.70655	0.00110	0.70875
D71	HA_TRIGA_W100C060	0.6	1.0	0.70660	0.00105	0.70870

6.7 Fissile Material Packages for Air Transport

This section is not applicable, because air transport is not claimed.

6.8 Benchmark Evaluations

The Monte Carlo computer program MCNP5 v1.30 is utilized for this benchmark analysis [1]. MCNP has been used extensively in criticality evaluations for several decades and is considered a standard in the industry.

The ORNL USLSTATS code [2] is used to establish a USL for the analysis. USLSTATS provides a simple means of evaluating and combining the statistical error of the calculation, code biases, and benchmark uncertainties. The USLSTATS calculation uses the combined uncertainties and data to provide a linear trend and an overall uncertainty. Computed multiplication factors, k_{eff}, for the package are deemed to be adequately subcritical if the computed value of k_s is less than or equal to the USL as follows:

$$k_s = k_{eff} + 2\sigma \leq USL$$

The USL includes the combined effects of code bias, uncertainty in the benchmark experiments, uncertainty in the computational evaluation of the benchmark experiments, and an administrative margin. This methodology has accepted precedence in establishing criticality safety limits for transportation packages complying with 10 CFR 71.

6.8.1 Applicability of Benchmark Experiments

The four fuel types analyzed fall into two distinct categories (1) high-enriched aluminum plate fuel, which includes MURR, MITR-II, and ATR, and (2) zirconium hydride (TRIGA) fuel. A separate benchmark analysis is performed for these two categories. The critical experiment benchmarks are selected from the *International Handbook of Evaluated Criticality Safety Benchmark Experiments* [3] based upon their similarity to the packaging and contents.

6.8.1.1 Aluminum Plate Fuel

The important selection parameters are high-enriched uranium plate-type fuel with a thermal spectrum. Thirty-five (35) benchmarks that meet these criteria are selected from the *Handbook*. The titles for all utilized experiments are listed in Table 6.8-1. Note that the benchmark from experiment set HEU-MET-THERM-022 is for the Advanced Test Reactor itself, so the fuel configuration in this benchmark is essentially the same as the ATR fuel modeled in the packaging analysis.

Ideally, benchmarks would be limited to those with a fuel matrix of UAl_x and aluminum, aluminum cladding, and no absorbers, consistent with the aluminum plate fuel criticality models. Experiment set HEU-COMP-THERM-022 consists of 11 benchmark experiments that utilize UO_2 powder sintered with stainless steel, and stainless steel cladding. Experiments 1 through 5 (Cases BA1 through BA5) do not utilize control rods, while experiments 6 through 11 (Cases BA6 through BA11) utilize boron control rods. Experiment set HEU-MET-THERM-006 consists of 23 benchmark experiments. The first 16 experiments are directly applicable (Cases BA12 through BA27), although experiments 17 and 18 (Cases BA28 and BA29) utilize thin cadmium sheets, and experiments 19 through 23 (Cases BA30 through BA34) utilize uranium in solution in addition to the fuel plates. HEU-MET-THERM-022 (Case BA35) is a detailed model of the ATR core using explicit ATR fuel elements very similar to the ATR fuel element model

utilized in the criticality analysis. However, this full-core model necessarily contains absorber materials. Despite the presence of absorbers, because this benchmark utilizes ATR fuel, it is considered directly applicable to the plate fuel criticality analysis.

Therefore, of these 35 benchmarks, 17 benchmarks are directly applicable, while 18 benchmarks are applicable to a lesser degree. To compensate for the benchmarks that are not directly applicable, trending will be performed both on all 35 benchmark experiments and on the subset of 17 directly applicable benchmark experiments. The USL selected is the minimum of both benchmark sets.

6.8.1.2 TRIGA Fuel

The important selection parameters are high-enriched (70%) zirconium hydride fuel with a thermal spectrum. No directly applicable benchmark experiments are available in the *Handbook*, although the *Handbook* does contain two intermediate-enriched (20%) TRIGA benchmarks. The available TRIGA benchmarks are for an entire Mark II core and hence contain absorber materials as well as a graphite reflector. While the BRR package TRIGA criticality analysis does not contain absorbers, these experiments are utilized because they represent the most similar available benchmarks.

Because a sample set of two benchmarks is not of sufficient size to obtain a statistical distribution, additional benchmarks are selected to supplement the two available TRIGA benchmarks. As zirconium hydride fuel contains moderator embedded in the fuel matrix, 10 high-enriched (93%) and 9 low-enriched (10%) uranium solution benchmarks are also utilized to simulate fuel intimately mixed with moderator. Therefore, a total of 21 benchmarks are utilized for benchmarking of TRIGA fuel. These 21 benchmarks are divided into three groups for trending: (1) all 21 benchmarks, (2) a subset of the 10 HEU benchmarks and two TRIGA benchmarks, and (3) a subset of the 9 LEU benchmarks and two TRIGA benchmarks. The USL selected is the minimum of all three benchmark sets.

6.8.2 Bias Determination

The USL is calculated by application of the USLSTATS computer program [2]. USLSTATS receives as input the k_{eff} as calculated by MCNP, the total 1-σ uncertainty (combined benchmark and MCNP uncertainties), and a trending parameter.

The uncertainty value, σ_{total}, assigned to each case is a combination of the benchmark uncertainty for each experiment, σ_{bench}, and the Monte Carlo uncertainty associated with the particular computational evaluation of the case, σ_{MCNP}, or:

$$\sigma_{total} = (\sigma_{bench}^2 + \sigma_{MCNP}^2)^{½}$$

These values are input into the USLSTATS program in addition to the following parameters, which are the values recommended by the USLSTATS user's manual [2]:

- P, proportion of population falling above lower tolerance level = 0.995 (note that this parameter is required input but is not utilized in the calculation of USL Method 1)
- 1-γ, confidence on fit = 0.95

- α, confidence on proportion P = 0.95 (note that this parameter is required input but is not utilized in the calculation of USL Method 1)
- Δk_m, administrative margin used to ensure subcriticality = 0.05.

These data are followed by triplets of trending parameter value, computed k_{eff}, and uncertainty for each case. A confidence band analysis is performed on the data for each trending parameter using USL Method 1.

6.8.2.1 Aluminum Plate Fuel

Five trending parameters are selected for the aluminum plate fuel: (1) Energy of the Average neutron Lethargy causing Fission (EALF), (2) U-235 number density, (3) channel width, (4) ratio of the number of hydrogen atoms in a unit cell to the number of U-235 atoms in a unit cell (H/U-235), and (5) plate pitch.

The USL generated for each of the trending parameters utilized is provided in Table 6.8-2. All benchmark data used as input to USLSTATS are reported in Table 6.8-4.

Energy of the Average neutron Lethargy causing Fission (EALF)

The EALF is used as the first trending parameter for the benchmark cases. The EALF comparison provides a means to observe neutron spectral dependencies or trends. Over the range of applicability, the minimum USL is 0.9254 for the full benchmark set, and 0.9212 for the subset of directly applicable benchmarks.

The HAC ATR cases that are moderated with full-density water fall within the range of applicability. For reduced water density ATR cases, the EALF sometimes exceeds the range of applicability, although the reactivity drops for these cases. None of the HAC MURR or MITR-II cases fall within the range of applicability, even with full-density water, although the most reactive MURR case is only slightly outside the range of applicability (1.74E-07 MeV for Case D1 versus 1.59E-07 MeV upper range). Because the margin to the USL is large, and the EALF is only slightly outside the range of applicability, this behavior is considered to be acceptable. All of the NCT models for MURR, MITR-II, and ATR fall outside the range of applicability for this parameter. This behavior is expected, because the NCT cases are unmoderated and the EALF is relatively large for these cases. Also, the NCT cases have very low reactivity and are not a concern. Therefore, this parameter is judged to be acceptable for the MURR, MITR-II, and ATR fuels.

U-235 Number Density

The U-235 number density is used as the second trending parameter for the benchmark cases. Over the range of applicability, the minimum USL is 0.9240 for the full benchmark set, and 0.9209 for the subset of directly applicable benchmarks.

The U-235 number densities for the three plate fuels are as follows:

- MURR: 3.65E-03 atom/b-cm
- MITR-II: 3.68E-03 atom/b-cm
- ATR: variable, see Table 6.2-6

This parameter is within the range of applicability for both MURR and MITR-II fuel. For the ATR fuel element model, the U-235 number densities for plates 1 through 4 and 16 through 19 fall within the range of applicability, while the number densities for plates 5 through 15 exceed the range of applicability (maximum value = 4.22E-03 atom/b-cm). The maximum range of applicability is 3.92E-03 atom/b-cm, so range is exceeded only slightly. Also, the average U-235 number density for the fuel element is 3.73E-03 atom/b-cm, which is within the allowable range. Therefore, application of this USL to the ATR criticality models is considered acceptable.

Channel Width

The channel width is used as the third trending parameter for the benchmark cases. Over the range of applicability, the minimum USL is 0.9225 for the full benchmark set, and 0.9209 for the subset of directly applicable benchmarks.

The maximum modeled channel width for the three plate fuels are as follows:

- MURR: 0.088-in
- MITR-II: 0.094-in
- ATR: 0.085-in

The channel width for all three plate type fuels exceeds the maximum channel width of 0.078-in of the benchmark experiments. However, this parameter is only slightly larger than the maximum benchmark experiment channel width, and was maximized in order to maximize model reactivity. Extrapolation of the USL equation (0.9218 – 1.1029E-02*X) to the maximum channel width of 0.094-in yields a USL of 0.9208, which is essentially identical to the non-extrapolated value of 0.9209. Therefore, application of the non-extrapolated USL (0.9209) to the criticality models is considered acceptable.

H/U-235 Atom Ratio

The H/U-235 atom ratio is used as the fourth trending parameter for the benchmark cases. The H/U-235 atom ratio is defined here as the ratio of hydrogen atoms to U-235 atoms in a unit cell. This parameter is computed by the following equation:

NH*C/(NU235*M)

where,

NH is the hydrogen number density

C is the channel width

NU235 is the U-235 number density

M is the fuel meat width

Over the range of applicability, the minimum USL is 0.9257 for the full benchmark set, and 0.9209 for the subset of directly applicable benchmarks.

- MURR: The H/U-235 value may be computed as:

  6.687E-02*0.088/(3.6519E-03*0.02) = 80.6

Therefore, H/U-235 of the MURR models is acceptably within the range of applicability of the benchmarks.

- MITR-II: The H/U-235 atom ratio may be computed as:

  6.687E-02*0.094/(3.6835E-03*0.03) = 56.9

  The minimum H/U-235 atom ratio of the benchmark models is 65.1. Therefore, this parameter is slightly outside the range of the benchmark experiments for the MITR-II fuel, although the difference is so small that this parameter is considered to be acceptable.

- ATR: Using the maximum ATR plate U-235 number density, the H/U-235 value may be computed as:

  6.687E-02*0.085/(4.224E-03*0.02) = 67.3

  Therefore, H/U-235 of the ATR models is acceptably within the range of applicability of the benchmarks.

Pitch

The fuel plate pitch is used as the fifth trending parameter for the benchmark cases. Over the range of applicability, the minimum USL is 0.9225 for the full benchmark set, and 0.9209 for the subset of directly applicable benchmarks.

- MURR: The fuel plate pitch is fixed at 0.13-in for all fuel element models. This pitch falls within the range of the benchmark experiments.
- MITR-II: The fuel plate pitch is fixed at 0.16-in for all fuel element models. The maximum pitch of the benchmark models is 0.128-in, so the pitch in the models exceeds the range of the benchmarks. However, the pitch is directly related to system moderation, and the acceptability of the EALF indicator demonstrates that MCNP is performing acceptably for thermal conditions. Therefore, this parameter is considered to be acceptable.
- ATR: The fuel plate pitch is fixed at 0.128-in for all ATR models (excluding the pitch for plates 1 and 19, which is slightly bigger because these plates are thicker). This pitch falls within the range of the benchmark experiments.

Recommended USL

For the full benchmark set, the minimum USL is 0.9225, while for the subset of directly applicable benchmarks, the USL is 0.9209. Therefore, the USL is trending lower for the subset of directly applicable benchmarks. Note, however, that the average k_{eff} = 0.992 for both the full benchmark set and directly applicable subset. The USL could likely be improved by development of additional benchmark models, but given the large margins to the most reactive case, the lower value (0.9209) is conservatively selected as the USL for this analysis.

6.8.2.2 TRIGA Fuel

Three trending parameters are selected for the TRIGA fuel: (1) Energy of the Average neutron Lethargy causing Fission (EALF), (2) U-235 number density, and (3) ratio of the number of hydrogen atoms to U-235 atoms in the fuel matrix (H/U-235).

The USL generated for each of the trending parameters utilized is provided in Table 6.8-3. All benchmark data used as input to USLSTATS are reported in Table 6.8-5.

Energy of the Average neutron Lethargy causing Fission (EALF)

The EALF is used as the first trending parameter for the benchmark cases. The EALF comparison provides a means to observe neutron spectral dependencies or trends. Over the range of applicability, the minimum USL is 0.9301 for the subset consisting of 10 HEU solution benchmarks and 2 TRIGA benchmarks.

All HAC TRIGA models fall within the range of applicability for this parameter, including the most reactive TRIGA case (Case D63). None of the NCT TRIGA models fall within the range of applicability, although this behavior is expected, because the NCT cases are unmoderated (except for the hydrogen in the fuel matrix). Also, because the NCT cases are much lower in reactivity than the HAC cases, this parameter is considered to be acceptable.

U-235 Number Density

The U-235 number density is used as the second trending parameter for the benchmark cases. Over the range of applicability, the minimum USL is 0.9306 for the subset consisting of 10 HEU solution benchmarks and 2 TRIGA benchmarks.

The U-235 number density in the BRR TRIGA models is 9.0406E-04 atom/b-cm, which is only slightly outside the maximum range of applicability of the benchmark models (EALF = 8.5392E-04 atom/b-cm). Therefore, this parameter is considered acceptable.

H/U-235 Atom Ratio

The H/U-235 atom ratio is used as the third trending parameter for the benchmark cases. Over the range of applicability, the minimum USL is 0.9318 for the subset consisting of 10 HEU solution benchmarks and 2 TRIGA benchmarks. The H/U-235 atom ratio is 62.0, which is only slightly outside the minimum range of applicability of the benchmark models (H/U-235 = 68.2). Therefore, this parameter is considered acceptable.

Recommended USL

The minimum USL of 0.9301 occurs for the EALF parameter over the subset of HEU solution and TRIGA benchmarks. Because the USL for the aluminum plate fuel is lower (0.9209), and only two TRIGA benchmarks are available, the USL of 0.9209 is recommended for use in the TRIGA analysis to add additional margin.

Table 6.8-1 – Benchmark Experiments Utilized

Series	Title
Aluminum Plate Fuel (MURR, MITR-II, ATR)	
HEU-COMP-THERM-022	SPERT III Stainless-Steel-Clad Plate-Type Fuel in Water
HEU-MET-THERM-006	SPERT-D Aluminum-Clad Plate-Type Fuel in Water, Dilute Uranyl Nitrate, or Borated Uranyl Nitrate
HEU-MET-THERM-022	Advanced Test Reactor: Serpentine Arrangement of Highly Enriched Water-Moderated Uranium-Aluminide Fuel Plates Reflected by Beryllium
TRIGA Fuel	
IEU-COMP-THERM-003	TRIGA Mark II Reactor: U(20) – Zirconium Hydride Fuel Rods in Water with Graphite Reflector
HEU-SOL-THERM-001	Minimally Reflected Cylinders of Highly Enriched Solutions of Uranyl Nitrate
LEU-SOL-THERM-003	Full and Truncated Bare Spheres of 10% Enriched Uranyl Nitrate Water Solutions

Table 6.8-2 – USL Results for Aluminum Plate Fuel

Trending Parameter (X)	Minimum USL Over Range of Applicability	Range of Applicability
35 Experiment Set		
EALF (MeV)	0.9254	5.22210E-08 <= X <= 1.58510E-07
U-235 Number Density (atom/b-cm)	0.9240	1.84900E-03 <= X <= 3.92600E-03
Channel width (in)	0.9225	6.45700E-02 <= X <= 7.80000E-02
H/U-235	0.9257	65.100 <= X <= 116.50
Pitch (in)	0.9225	0.12457 <= X <= 0.12800
17 Experiment Set		
EALF (MeV)	0.9212	5.22210E-08 <= X <= 1.58510E-07
U-235 Number Density (atom/b-cm)	0.9209	1.84900E-03 <= X <= 3.92600E-03
Channel width (in)	0.9209	6.45700E-02 <= X <= 7.80000E-02
H/U-235	0.9209	66.0 <= X <= 116.50
Pitch (in)	0.9209	0.12457 <= X <= 0.12800

Table 6.8-3 – USL Results for TRIGA Fuel

Trending Parameter (X)	Minimum USL Over Range of Applicability	Range of Applicability
21 Experiment Set		
EALF (MeV)	0.9320	3.42760E-08 <= X <= 2.95740E-07
U-235 Number Density (atom/b-cm)	0.9331	4.33640E-05 <= X <= 8.53920E-04
H/U-235	0.9350	68.200 <= X <= 1437.5
12 Experiment Set (HEU solution + TRIGA)		
EALF (MeV)	0.9301	4.29310E-08 <= X <= 2.95740E-07
U-235 Number Density (atom/b-cm)	0.9306	1.31030E-04 <= X <= 8.53920E-04
H/U-235	0.9318	68.200 <= X <= 499.40
11 Experiment Set (LEU solution + TRIGA)		
EALF (MeV)	0.9338	3.42760E-08 <= X <= 8.71200E-08
U-235 Number Density (atom/b-cm)	0.9339	4.33640E-05 <= X <= 3.68010E-04
H/U-235	0.9340	150.10 <= X <= 1437.5

Table 6.8-4 – Benchmark Experiment Data for Aluminum Plate Fuel

Case ID	Filename	k	σ_{mcnp}	σ_{bench}	σ_{total}	EALF (MeV)	U-235 (atom/b-cm)	Chanel Width (in)	H/U-235	Pitch (in)
BA1	HCT022_C01	0.98895	0.00060	0.0081	0.0081	9.528E-08	3.3155E-03	0.06457	65.1	0.12457
BA2	HCT022_C02	0.98980	0.00061	0.0081	0.0081	9.665E-08	3.3155E-03	0.06457	65.1	0.12457
BA3	HCT022_C03	0.98985	0.00063	0.0081	0.0081	9.809E-08	3.3155E-03	0.06457	65.1	0.12457
BA4	HCT022_C04	0.98856	0.00060	0.0081	0.0081	9.917E-08	3.3155E-03	0.06457	65.1	0.12457
BA5	HCT022_C05	0.98909	0.00063	0.0081	0.0081	9.587E-08	3.3155E-03	0.06457	65.1	0.12457
BA6	HCT022_C06	0.98902	0.00059	0.0081	0.0081	9.840E-08	3.3155E-03	0.06457	65.1	0.12457
BA7	HCT022_C07	0.98963	0.00056	0.0081	0.0081	9.890E-08	3.3155E-03	0.06457	65.1	0.12457
BA8	HCT022_C08	0.98908	0.00057	0.0081	0.0081	9.951E-08	3.3155E-03	0.06457	65.1	0.12457
BA9	HCT022_C09	0.98840	0.00056	0.0081	0.0081	9.589E-08	3.3155E-03	0.06457	65.1	0.12457
BA10	HCT022_C10	0.98845	0.00060	0.0081	0.0081	9.963E-08	3.3155E-03	0.06457	65.1	0.12457
BA11	HCT022_C11	0.98930	0.00060	0.0081	0.0081	1.001E-07	3.3155E-03	0.06457	65.1	0.12457
BA12	HMT006_C01	0.99240	0.00082	0.0044	0.0045	8.481E-08	1.8490E-03	0.06457	116.5	0.12457
BA13	HMT006_C02	0.99331	0.00088	0.0040	0.0041	7.044E-08	1.8490E-03	0.06457	116.5	0.12457
BA14	HMT006_C03	0.99740	0.00072	0.0040	0.0041	6.338E-08	1.8490E-03	0.06457	116.5	0.12457
BA15	HMT006_C04	0.99282	0.00081	0.0040	0.0041	6.185E-08	1.8490E-03	0.06457	116.5	0.12457
BA16	HMT006_C05	0.99230	0.00079	0.0040	0.0041	5.852E-08	1.8490E-03	0.06457	116.5	0.12457
BA17	HMT006_C06	0.99010	0.00071	0.0040	0.0041	5.615E-08	1.8490E-03	0.06457	116.5	0.12457
BA18	HMT006_C07	0.98783	0.00073	0.0040	0.0041	5.432E-08	1.8490E-03	0.06457	116.5	0.12457
BA19	HMT006_C08	0.98428	0.00076	0.0040	0.0041	5.245E-08	1.8490E-03	0.06457	116.5	0.12457
BA20	HMT006_C09	0.98657	0.00072	0.0040	0.0041	5.222E-08	1.8490E-03	0.06457	116.5	0.12457
BA21	HMT006_C10	0.99885	0.00085	0.0040	0.0041	8.220E-08	1.8490E-03	0.06457	116.5	0.12457
BA22	HMT006_C11	0.98965	0.00081	0.0040	0.0041	6.236E-08	1.8490E-03	0.06457	116.5	0.12457
BA23	HMT006_C12	0.99403	0.00070	0.0040	0.0041	5.415E-08	1.8490E-03	0.06457	116.5	0.12457

(continued)

Table 6.8-4 – Benchmark Experiment Data for Aluminum Plate Fuel (concluded)

Case ID	Filename	k	σ_{mcnp}	σ_{bench}	σ_{total}	EALF (MeV)	U-235 (atom/b-cm)	Chanel Width (in)	H/U-235	Pitch (in)
BA24	HMT006_C13	1.01283	0.00086	0.0040	0.0041	8.231E-08	1.8490E-03	0.06457	116.5	0.12457
BA25	HMT006_C14	0.98495	0.00071	0.0061	0.0061	5.715E-08	1.8490E-03	0.06457	116.5	0.12457
BA26	HMT006_C15	0.98128	0.00077	0.0040	0.0041	5.654E-08	1.8490E-03	0.06457	116.5	0.12457
BA27	HMT006_C16	0.99241	0.00078	0.0040	0.0041	6.330E-08	1.8490E-03	0.06457	116.5	0.12457
BA28	HMT006_C17	0.98934	0.00082	0.0040	0.0041	7.405E-08	1.8490E-03	0.06457	116.5	0.12457
BA29	HMT006_C18	0.99282	0.00087	0.0040	0.0041	8.003E-08	1.8490E-03	0.06457	116.5	0.12457
BA30	HMT006_C19	0.99360	0.00068	0.0040	0.0041	5.243E-08	1.8490E-03	0.06457	113.9	0.12457
BA31	HMT006_C20	0.99275	0.00076	0.0040	0.0041	6.471E-08	1.8490E-03	0.06457	113.7	0.12457
BA32	HMT006_C21	0.99469	0.00077	0.0040	0.0041	6.917E-08	1.8490E-03	0.06457	113.7	0.12457
BA33	HMT006_C22	0.99670	0.00080	0.0040	0.0041	7.407E-08	1.8490E-03	0.06457	113.6	0.12457
BA34	HMT006_C23	1.00132	0.00080	0.0040	0.0041	7.670E-08	1.8490E-03	0.06457	113.5	0.12457
BA35	HMT022_C01	0.99179	0.00013	0.0035	0.0035	1.585E-07	3.9260E-03	0.078	66.0	0.12800

Table 6.8-5 – Benchmark Experiment Data for TRIGA Fuel

Case ID	Filename	k	σ_{mcnp}	σ_{bench}	σ_{total}	EALF (MeV)	U-235 (atom/b-cm)	H/U-235
BT1	HST001_C01	0.99686	0.00068	0.0060	0.0060	8.147E-08	3.4777E-04	181.8
BT2	HST001_C02	0.99418	0.00072	0.0072	0.0072	2.763E-07	8.2771E-04	70.6
BT3	HST001_C03	1.00015	0.00067	0.0035	0.0036	8.014E-08	3.4118E-04	185.7
BT4	HST001_C04	0.99470	0.00069	0.0053	0.0053	2.957E-07	8.5392E-04	68.2
BT5	HST001_C05	0.99727	0.00059	0.0049	0.0049	4.293E-08	1.3103E-04	499.4
BT6	HST001_C06	1.00351	0.00057	0.0046	0.0046	4.450E-08	1.4240E-04	458.8
BT7	HST001_C07	0.99609	0.00071	0.0040	0.0041	7.710E-08	3.2800E-04	193.3
BT8	HST001_C08	0.99648	0.00067	0.0038	0.0039	8.174E-08	3.4777E-04	181.8
BT9	HST001_C09	0.99068	0.00068	0.0054	0.0054	2.954E-07	8.5392E-04	68.2
BT10	HST001_C10	0.99130	0.00055	0.0054	0.0054	4.609E-08	1.5266E-04	427.4
BT11	ICT003_C01	0.99699	0.00052	0.0056	0.0056	8.712E-08	3.6801E-04	150.1
BT12	ICT003_C02	1.00145	0.00052	0.0056	0.0056	8.678E-08	3.6801E-04	150.1
BT13	LST003_C01	0.99485	0.00044	0.0039	0.0039	4.098E-08	7.6403E-05	770.3
BT14	LST003_C02	0.99401	0.00042	0.0042	0.0042	3.921E-08	6.8143E-05	877.6
BT15	LST003_C03	0.99902	0.00041	0.0042	0.0042	3.886E-08	6.7111E-05	897.0
BT16	LST003_C04	0.99249	0.00039	0.0042	0.0042	3.875E-08	6.5820E-05	913.2
BT17	LST003_C05	0.99573	0.00035	0.0048	0.0048	3.593E-08	5.2398E-05	1173.4
BT18	LST003_C06	0.99694	0.00031	0.0049	0.0049	3.564E-08	5.0849E-05	1213.1
BT19	LST003_C07	0.99602	0.00031	0.0049	0.0049	3.554E-08	4.9817E-05	1239.8
BT20	LST003_C08	0.99930	0.00028	0.0052	0.0052	3.447E-08	4.4138E-05	1411.6
BT21	LST003_C09	0.99606	0.00027	0.0052	0.0052	3.428E-08	4.3364E-05	1437.5

6.9 Appendices

6.9.1 References

1. MCNP5, "*MCNP – A General Monte Carlo N-Particle Transport Code, Version 5; Volume II: User's Guide*," LA-CP-03-0245, Los Alamos National Laboratory, April 2003. MCNP5 is distributed by the Radiation Safety Information Computational Center (www-rsicc.ornl.gov), Release C00710MNYCP02 (Windows PC).
2. USLSTATS, "*USLSTATS: A Utility To Calculate Upper Subcritical Limits For Criticality Safety Applications,*" Version 1.4.2, Oak Ridge National Laboratory, April 23, 2003. Note: USLSTATS is described in Appendix C, *User's Manual for USLSTATS V1.0*, in NUREG/CR-6361 *Criticality Benchmark Guide for Light-Water-Reactor Fuel in Transportation and Storage Packages*, March 1997. No new user's manual has been developed for later updates to the program.
3. *International Handbook of Evaluated Criticality Safety Benchmark Experiments*, Nuclear Energy Agency, NEA/NSC/DOC(95)03, September 2006.
4. *Standard Composition Library*, ORNL/TM-2005/39, Version 5, Vol. III, Section M8, April 2005.

6.9.2 Parametric Evaluations to Determine the Most Reactive Fuel Geometries

6.9.2.1 ATR Fuel Parametric Evaluation

A parametric analysis is performed to determine the impacts of various fuel element tolerances on the reactivity. This parametric analysis considers the effects of a number of parameters, such as fuel meat arc length, fuel meat thickness, channel width, and active fuel length.

Because the ATR fuel element is complex, with 19 unique fuel plates and 19 unique fuel material descriptions, performing this parametric study on the actual fuel element geometry would be cumbersome. Rather, the approach utilized is to perform the parametric study on a system of 19 identical flat plates. This geometry mimics the ATR fuel element to determine trends in the data. Note that the reactivity of the 19 flat plate model is not identical to the reactivity of an actual ATR fuel element due to geometrical and material differences, although the trends are the same. The most reactive model variations are then incorporated into the ATR fuel element model.

In the parametric models, 1200 g U-235 is equally distributed between 19 identical flat plates. The base configuration consists of plates with a fuel meat width of 6.7355 cm (the average meat arc length for an ATR fuel element), active fuel height of 48-in, fuel meat thickness of 0.02-in, fuel cladding thickness of 0.015-in (total plate thickness of 0.050-in), and fuel channel thickness of 0.078-in. A total of 12 parametric models are developed, as summarized below.

Case ID	ATR Parametric Study Case Description
P1	Base case
P2	Increase width of fuel meat by 0.1-in
P3	Decrease width of fuel meat by 0.1-in
P4	Increase thickness of fuel meat by 0.002-in
P5	Decrease thickness of fuel meat by 0.002-in
P6	Increase thickness of fuel meat by 0.002-in but decrease the cladding thickness to maintain a nominal plate thickness
P7	Decrease thickness of fuel meat by 0.002-in but increase the cladding thickness to maintain a nominal plate thickness
P8	Increase water channel thickness to maximum of 0.085-in
P9	Increase water channel thickness to maximum of 0.085-in by reducing the cladding thickness
P10	Decrease active fuel length to 47.0-in
P11	Reduce cladding thickness to the minimum value of 0.008-in
P12	Combine cases P2 and P9

The geometry of Case P1 is shown in Figure 6.9-1. The fuel element is reflected by approximately 12-in of water.

In Cases P2 through P12, each case is identical to the base case P1 with the exception of the changes identified in the table above. The pitch, which is the sum of the plate thickness and channel thickness, is treated as a dependant variable and is allowed to vary as the independent parameters are changed. For example, in Case P5, decreasing the thickness of the fuel meat decreases the pitch, although the channel thickness remains constant. The detailed model description of the parametric cases is summarized in Table 6.9-1.

The results of the parametric analysis are summarized in Table 6.9-2. Because the uncertainty in the calculation is ~0.001, a difference of at least 0.002 (2 milli-k, abbreviated mk) between the various cases is required in order to distinguish a real effect from statistical fluctuation. The results indicate a reactivity increase of 4.3 mk for Case P2, when the width of the fuel meat is increased, and a decrease of 5.4 mk for Case P3, when the width of the fuel meat is decreased. Therefore, reactivity increases when the width of the fuel meat is maximized.

The nominal thickness of the fuel meat is 0.02-in. No tolerance on the fuel meat is provided on the fuel fabrication drawings because the fuel plates are fabricated using a rolling process. A thickness tolerance of 0.002-in (±10%) is assumed for computational purposes. In Cases P4 and P5, the fuel meat thickness is adjusted for constant channel thickness and variable pitch, while for Cases P6 and P7 the fuel meat thickness is adjusted for constant plate thickness and nominal pitch. The reactivity fluctuations are within 2 mk in all four cases, and it is concluded that a nominal fuel meat thickness of 0.02-in is acceptable for modeling purposes.

In Case P8, the water channel thickness is increased to the maximum value of 0.085-in (increase in pitch), while in Case P9 the water channel thickness is increased to the maximum by artificially reducing the cladding thickness (nominal pitch). Both cases P8 and P9 show large reactivity gains of 9.6 and 12.9 mk, respectively, indicating that reactivity is maximized when the water channel thickness is maximized.

In Case P10, the active fuel length is reduced to a lower bound value of 47.0-in. The reactivity increase is within statistical fluctuation. It may be inferred that increasing the active fuel length would also result in a reactivity effect within statistical fluctuation.

In Case P11, the cladding thickness is reduced to the minimum value of 0.008-in, and the reactivity increases by 5.5 mk. This reactivity gain is likely due to the more compact geometry, as the pitch reduces considerably. This scenario is not directly applicable to an ATR fuel element because the pitch is fixed by the side plates and such a configuration is not possible.

The only cases that show a statistically significant increase are P2, P8, P9, and P11. In Case P12, the increased fuel meat width of Case P2 and increased channel width of Case P9 are combined. This model geometry bounds Case P8, and Case P11 is incorporated in an approximate manner because the cladding thickness has been reduced to accommodate the larger channel. The reactivity of Case P12 represents an increase of 19.5 mk over base Case P1.

Based on the parametric evaluation, an optimized fuel model is developed with both increased channel width and increased meat arc length. In this model, a nominal pitch is utilized (i.e., the centerline radial locations of the 19 plates are the same in each model, as indicated in Table 6.2-4), and the channel width is increased by removing cladding. This approach is highly conservative, because it is unlikely (if not impossible) to maximize the channel width between each plate. In an actual fuel element, maximizing the channel width between two plates would likely minimize the channel width between the next two plates, as the overall plate thickness is held to a rather tight tolerance.

6.9.2.2 MURR Fuel Parametric Evaluation

A parametric analysis is performed to determine the impacts of various fuel element tolerances on the reactivity. In the parametric analysis for ATR fuel, it is determined that reactivity is maximized by maximizing the arc length of the fuel meat and the channel thickness. Because ATR and MURR are both plate-type and utilize similar enrichments, it is expected that MURR fuel will also experience maximum reactivity with these parameters maximized. Therefore, the parametric analysis considers the effects of only the following parameters: fuel meat arc length/width, channel width, and active fuel length.

The base configuration for MURR consists of plates with a nominal meat arc length/width, nominal active fuel length, and nominal channel width. In each parametric case, the indicated parameter is modified in comparison with the base case. The minimum, nominal, and maximum meat arc lengths are provided in Table 6.9-3. The minimum meat arc lengths are obtained directly from Figure 6.2-2 (see dimension B). The maximum meat arc lengths are computed by subtracting twice the fuel-free width (2*0.115-in) from the maximized plate width (dimension C of Figure 6.2-2 + 0.010-in). The nominal value is computed as the average of the minimum and maximum values. The detailed model description of the parametric cases is summarized in Table 6.9-4. A total of 7 parametric models are developed, as summarized below.

Case ID	MURR Parametric Study Case Description
PM1	Base MURR case
PM2	Decrease active fuel length to minimum value
PM3	Increase active fuel length to maximum value
PM4	Increase channel width to maximum value
PM5	Decrease width of fuel meat to minimum value
PM6	Increase width of fuel meat to maximum value
PM7	Combine cases PM4 and PM6

The geometry of base MURR parametric Case PM1 is shown in Figure 6.9-1. The fuel element is reflected with approximately 12-in of water. Note that, unlike the ATR parametric model, the MURR parametric model is an explicit geometrical representation of the MURR fuel element. Although the ATR and MURR fuel elements appear to be rather similar, because all MURR plates utilize the same fuel number densities and fuel meat to side structure distance, performing the parametric study on the actual geometry for MURR fuel is relatively straightforward.

The results of the parametric analysis are summarized in Table 6.9-5. Because the uncertainty in the calculation is ~0.001, a difference of at least 0.002 (2 milli-k, abbreviated mk) between the various cases is required in order to distinguish a real effect from statistical fluctuation. The variation of the active fuel length has a negligible effect on the results. Also, the fuel shows a positive reactivity increase of 23.8 mk when the fuel meat is widened and the channel width is increased (compare Case PM7 with Case PM1). This result is consistent with the results obtained in the ATR fuel parametric analysis. Therefore, in all MURR fuel models, the fuel is modeled with nominal active fuel length, maximum fuel width, and maximum channel width. The maximum channel width is achieved by artificially reducing the cladding thickness.

6.9.2.3 MITR-II Fuel Parametric Evaluation

A parametric analysis is performed to determine the impacts of various fuel element tolerances on the reactivity. In the parametric analysis for ATR and MURR fuel, it is determined that reactivity is maximized by maximizing the arc length of the fuel meat and the channel thickness. Because ATR, MURR, and MITR-II are all plate-type and utilize similar enrichments, it is expected that MITR-II fuel will also experience maximum reactivity with these parameters maximized. Therefore, the parametric analysis considers the effects of only the following parameters: fuel meat arc length/width, channel width, and active fuel length.

The base configuration for MITR-II consists of plates with a nominal meat arc length/width, nominal active fuel length, and nominal channel width. In each parametric case, the indicated parameter is modified in comparison with the base case. The detailed model description of the parametric cases is summarized in Table 6.9-6. A total of 7 parametric models are developed, as summarized below.

Case ID	MITR-II Parametric Study Case Description
PN1	Base MITR-II case
PN2	Decrease active fuel length to minimum value
PN3	Increase active fuel length to maximum value
PN4	Increase channel width to maximum value
PN5	Decrease width of fuel meat to minimum value
PN6	Increase width of fuel meat to maximum value
PN7	Combine cases PN4 and PN6

The geometry of base MITR-II parametric Case PN1 is shown in Figure 6.9-1. The fuel element is reflected with approximately 12-in of water. Note that, like the MURR parametric model, the MITR-II parametric model is an explicit geometrical representation of the MITR-II fuel element.

The results of the parametric analysis are summarized in Table 6.9-7. Because the uncertainty in the calculation is ~0.001, a difference of at least 0.002 (2 milli-k, abbreviated mk) between the various cases is required in order to distinguish a real effect from statistical fluctuation. The variation of the active fuel length has a negligible effect on the results. Although Case PN2 shows a positive reactivity increase when the active fuel height is reduced, because the increase is less than 2 mk, it is concluded that the increase is simply statistical fluctuation. Also, the fuel shows a positive reactivity increase of 11.0 mk when the fuel meat is widened and the channel width is increased (compare Case PN7 with Case PN1). This result is consistent with the results obtained in the ATR and MURR fuel parametric analyses. Therefore, in all MITR-II fuel models, the fuel is modeled with nominal active fuel length, maximum fuel width, and maximum channel width. The maximum channel width is achieved by artificially reducing the cladding thickness.

6.9.2.4 TRIGA Fuel Parametric Evaluation

For the TRIGA fuels, the objective of the parametric analysis is to select the most reactive fuel type for use in the criticality analysis from the five types under consideration. To select the bounding fuel element type, simple moderated pin cell models with infinite square reflection are developed. The lattice pitch is varied for each model by adjusting the location of the reflective surfaces. The pin cell model for each of the fuel element types is shown in Figure 6.9-2. The pin cell models are based upon the data provided in Table 6.2-7. Note that the Type 203 fuel element is not modeled explicitly, since it is essentially the same as Type 103.

The pin cell results are summarized in Table 6.9-8. The most reactive TRIGA fuel type is Type 109 (Case PT20), which is the HEU fuel element. In these cases, the thin molybdenum disc between the fuel and bottom reflector is omitted. In Case PT23, Case PT20 is run with the molybdenum disc modeled explicitly. The reactivity is slightly less, but within the statistical uncertainty of the method. Therefore, this fuel type (without the molybdenum disc) is used for all TRIGA analysis in this calculation.

Table 6.9-1 – ATR Parametric Analysis Input Data

Parameter	P1	P2	P3	P4	P5	P6
Fuel Arc (cm)	6.7355	6.9895	6.4815	6.7355	6.7355	6.7355
Meat thickness (in)	0.02	0.02	0.02	0.022	0.018	0.022
Active fuel height (in)	48	48	48	48	48	48
Channel (in)	0.078	0.078	0.078	0.078	0.078	0.078
Cladding (in)	0.015	0.015	0.015	0.015	0.015	0.014
Total plate (in)	0.050	0.050	0.050	0.052	0.048	0.050
Pitch (in)	0.128	0.128	0.128	0.130	0.126	0.128
Volume (cm^3)	41.7164	43.2895	40.1432	45.8880	37.5447	45.8880
U-235 (g)	63.2	63.2	63.2	63.2	63.2	63.2
U-235 density (g/cm^3)	1.51	1.46	1.57	1.38	1.68	1.38
UAlx+Al density (g/cm^3)	3.86	3.81	3.91	3.74	4.00	3.74
N U-234	2.4865E-05	2.3962E-05	2.5840E-05	2.2605E-05	2.7628E-05	2.2605E-05
N U-235	3.8789E-03	3.7380E-03	4.0309E-03	3.5263E-03	4.3099E-03	3.5263E-03
N U-236	1.4382E-05	1.3859E-05	1.4945E-05	1.3074E-05	1.5980E-05	1.3074E-05
N U-238	2.0576E-04	1.9828E-04	2.1382E-04	1.8705E-04	2.2862E-04	1.8705E-04
N U-Al	5.0157E-02	5.0391E-02	4.9905E-02	5.0742E-02	4.9442E-02	5.0742E-02
Total	5.4281E-02	5.4365E-02	5.4190E-02	5.4491E-02	5.4024E-02	5.4491E-02

Parameter	P7	P8	P9	P10	P11	P12
Fuel Arc (cm)	6.7355	6.7355	6.7355	6.7355	6.7355	6.9895
Meat thickness (in)	0.018	0.02	0.02	0.02	0.02	0.02
Active fuel height (in)	48	48	48	47	48	48
Channel (in)	0.078	0.085	0.085	0.078	0.078	0.085
Cladding (in)	0.016	0.015	0.0115	0.015	0.008	0.0115
Total plate (in)	0.050	0.050	0.0430	0.050	0.036	0.0430
Pitch (in)	0.128	0.135	0.128	0.128	0.114	0.128
Volume (cm^3)	37.5447	41.7164	41.7164	40.8473	41.7164	43.2895
U-235 (g)	63.2	63.2	63.2	63.2	63.2	63.2
U-235 density (g/cm^3)	1.68	1.51	1.51	1.55	1.51	1.46
UAlx+Al density (g/cm^3)	4.00	3.86	3.86	3.89	3.86	3.81
N U-234	2.7628E-05	2.4865E-05	2.4865E-05	2.5394E-05	2.4865E-05	2.3962E-05
N U-235	4.3099E-03	3.8789E-03	3.8789E-03	3.9615E-03	3.8789E-03	3.7380E-03
N U-236	1.5980E-05	1.4382E-05	1.4382E-05	1.4688E-05	1.4382E-05	1.3859E-05
N U-238	2.2862E-04	2.0576E-04	2.0576E-04	2.1014E-04	2.0576E-04	1.9828E-04
N U-Al	4.9442E-02	5.0157E-02	5.0157E-02	5.0020E-02	5.0157E-02	5.0391E-02
Total	5.4024E-02	5.4281E-02	5.4281E-02	5.4232E-02	5.4281E-02	5.4365E-02

Table 6.9-2 – ATR Parametric Analysis Results

Case ID	Filename	k_{eff}	σ	k_s (k+2σ)	Δ from P1 (mk)
P1	HS_ATR_P1	0.46601	0.00096	0.46793	--
P2	HS_ATR_P2	0.47015	0.00102	0.47219	4.3
P3	HS_ATR_P3	0.46045	0.00102	0.46249	-5.4
P4	HS_ATR_P4	0.46403	0.00101	0.46605	-1.9
P5	HS_ATR_P5	0.46442	0.00111	0.46664	-1.3
P6	HS_ATR_P6	0.46753	0.00105	0.46963	1.7
P7	HS_ATR_P7	0.46683	0.00101	0.46885	0.9
P8	HS_ATR_P8	0.47528	0.00112	0.47752	9.6
P9	HS_ATR_P9	0.47879	0.00100	0.48079	12.9
P10	HS_ATR_P10	0.46704	0.00106	0.46916	1.2
P11	HS_ATR_P11	0.47123	0.00108	0.47339	5.5
P12	**HS_ATR_P12**	**0.48534**	**0.00104**	**0.48742**	**19.5**

Table 6.9-3 – MURR Meat Arc Lengths

Plate	Minimum (in)	Nominal (in)	Maximum (in)
1	1.643	1.708	1.773
2	1.745	1.810	1.875
3	1.847	1.912	1.977
4	1.950	2.015	2.080
5	2.052	2.117	2.182
6	2.154	2.219	2.284
7	2.256	2.321	2.386
8	2.358	2.423	2.488
9	2.460	2.525	2.590
10	2.562	2.627	2.692
11	2.664	2.729	2.794
12	2.766	2.831	2.896
13	2.868	2.933	2.998
14	2.971	3.036	3.101
15	3.073	3.138	3.203
16	3.175	3.240	3.305
17	3.277	3.342	3.407
18	3.379	3.444	3.509
19	3.481	3.546	3.611
20	3.583	3.648	3.713
21	3.685	3.750	3.815
22	3.787	3.852	3.917
23	3.889	3.954	4.019
24	3.992	4.057	4.122

Table 6.9-4 – MURR Parametric Analysis Input Data

Parameter	PM1/PM4	PM2	PM3	PM5	PM6/PM7
Fuel width (in)	nominal	nominal	nominal	nominal-0.065	nominal+0.065
Meat thickness (in)	0.02	0.02	0.02	0.02	0.02
Active fuel height (in)	24	23.25	24.75	24	24
Channel (in)	0.08/0.088	0.08	0.08	0.08	0.08/0.088
Cladding (in)	0.015/0.011	0.015	0.015	0.015	0.015/0.011
Total plate (in)	0.050/0.042	0.050	0.050	0.050	0.050/0.042
Pitch (in)	0.13	0.13	0.13	0.13	0.13
Meat volume (cm3)	544.13	527.13	561.14	531.86	556.40
U-235 mass (g)	785	785	785	785	785
U-235 den (g/cm3)	1.44	1.49	1.40	1.48	1.41
UAlx+Al den (g/cm3)	3.80	3.84	3.76	3.82	3.77
N-234 (atom/b-cm)	2.3694E-05	2.4458E-05	2.2976E-05	2.4241E-05	2.3171E-05
N-235 (atom/b-cm)	3.6962E-03	3.8154E-03	3.5842E-03	3.7815E-03	3.6147E-03
N-236 (atom/b-cm)	1.3704E-05	1.4146E-05	1.3289E-05	1.4020E-05	1.3402E-05
N-238 (atom/b-cm)	1.9607E-04	2.0239E-04	1.9012E-04	2.0059E-04	1.9174E-04
N-Al (atom/b-cm)	5.0460E-02	5.0262E-02	5.0646E-02	5.0319E-02	5.0596E-02
Total (atom/b-cm)	5.4390E-02	5.4319E-02	5.4457E-02	5.4339E-02	5.4439E-02

Table 6.9-5 – MURR Parametric Analysis Results

Case ID	Filename	k_{eff}	σ	k_s (k+2σ)	Δ from PM1 (mk)
PM1	HS_MURR3_P1	0.50645	0.00110	0.50865	--
PM2	HS_MURR3_P2	0.50715	0.00099	0.50913	0.5
PM3	HS_MURR3_P3	0.50612	0.00109	0.50830	-0.3
PM4	HS_MURR3_P4	0.52638	0.00103	0.52844	19.8
PM5	HS_MURR3_P5	0.50314	0.00099	0.50512	-3.5
PM6	HS_MURR3_P6	0.50980	0.00106	0.51192	3.3
PM7	**HS_MURR3_P7**	0.53021	0.00114	0.53249	23.8

Table 6.9-6 – MITR-II Parametric Analysis Input Data

Parameter	PN1/PN4	PN2	PN3	PN5	PN6/PN7
Fuel width (in)	2.076	2.076	2.076	1.981	2.171
Meat thickness (in)	0.03	0.03	0.03	0.03	0.03
Active fuel height (in)	22.375	21.99	22.76	22.375	22.375
Channel (in)	0.090/0.094	0.090	0.090	0.090	0.090/0.094
Cladding (in)	0.019/0.017	0.019	0.019	0.019	0.019/0.017
Total plate (in)	0.068/0.064	0.068	0.068	0.068	0.068/0.064
Pitch (in)	0.158	0.158	0.158	0.158	0.158
Meat volume (cm^3)	342.53	336.64	348.43	326.86	358.21
U-235 mass (g)	515	515	515	515	515
U-235 den (g/cm3)	1.503	1.530	1.478	1.576	1.438
UAlx+Al den (g/cm3)	3.85	3.87	3.83	3.91	3.79
N-234 (atom/b-cm)	2.4693E-05	2.5125E-05	2.4275E-05	2.5877E-05	2.3613E-05
N-235 (atom/b-cm)	3.8521E-03	3.9195E-03	3.7869E-03	4.0368E-03	3.6835E-03
N-236 (atom/b-cm)	1.4282E-05	1.4532E-05	1.4040E-05	1.4967E-05	1.3657E-05
N-238 (atom/b-cm)	2.0433E-04	2.0791E-04	2.0088E-04	2.1413E-04	1.9539E-04
N-Al (atom/b-cm)	5.0202E-02	5.0090E-02	5.0310E-02	4.9895E-02	5.0481E-02
Total (atom/b-cm)	5.4297E-02	5.4257E-02	5.4336E-02	5.4187E-02	5.4398E-02

Table 6.9-7 – MITR-II Parametric Analysis Results

Case ID	Filename	k_{eff}	σ	k_s ($k+2\sigma$)	Δ from PN1 (mk)
PN1	HS_MIT2_P1	0.39975	0.00089	0.40153	
PN2	HS_MIT2_P2	0.40082	0.00093	0.40268	1.1
PN3	HS_MIT2_P3	0.39965	0.00088	0.40141	-0.1
PN4	HS_MIT2_P4	0.40562	0.00105	0.40772	6.2
PN5	HS_MIT2_P5	0.39724	0.00096	0.39916	-2.4
PN6	HS_MIT2_P6	0.40496	0.00087	0.40670	5.2
PN7	**HS_MIT2_P7**	**0.41052**	**0.00098**	**0.41248**	**11.0**

Table 6.9-8 – TRIGA Fuel Pin Cell Results

Case ID	Filename	Pitch (cm)	k_{eff}	σ	k_s (k+2σ)
Type 101 (8 wt.% aluminum clad)					
PT1	C101_P19	0.38	1.38089	0.00099	1.38287
PT2	C101_P22	0.44	1.31512	0.00086	1.31684
PT3	C101_P25	0.50	1.21166	0.00082	1.21330
Type 103/203 (8.5 wt.% stainless steel clad)					
PT10	C103_P19	0.38	1.31017	0.00085	1.31187
PT11	C103_P22	0.44	1.22796	0.00092	1.22980
PT12	C103_P25	0.50	1.13356	0.00080	1.13516
Type 109 (8.5 wt.% stainless steel clad, HEU)					
PT20	**C109_P19**	**0.38**	**1.59214**	**0.00094**	**1.59402**
PT21	C109_P22	0.44	1.55156	0.00095	1.55346
PT22	C109_P25	0.50	1.47780	0.00097	1.47974
PT23	C109_P19M	0.38	1.59058	0.00090	1.59238
Type 117 (20 wt.% stainless steel clad)					
PT30	C117_P19	0.38	1.45689	0.00095	1.45879
PT31	C117_P22	0.44	1.43108	0.00090	1.43288
PT32	C117_P25	0.50	1.36660	0.00093	1.36846

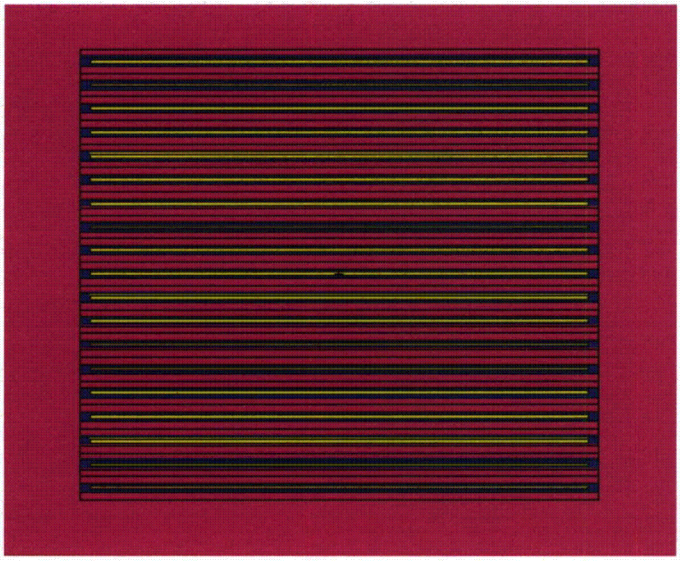

ATR

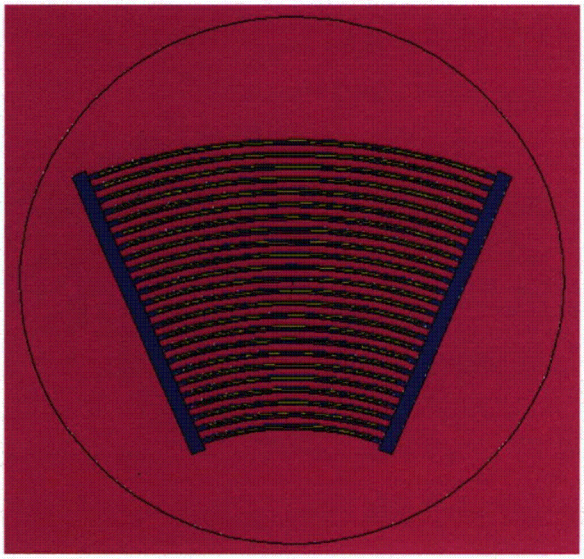

MURR

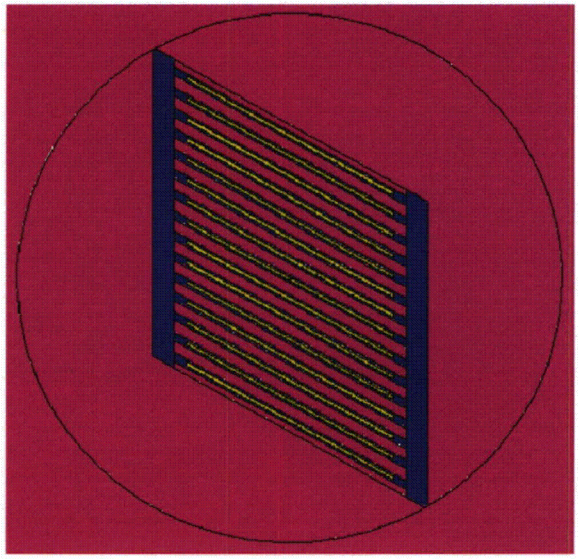

MITR-II

Figure 6.9-1 – ATR, MURR, and MITR-II Base Parametric Models

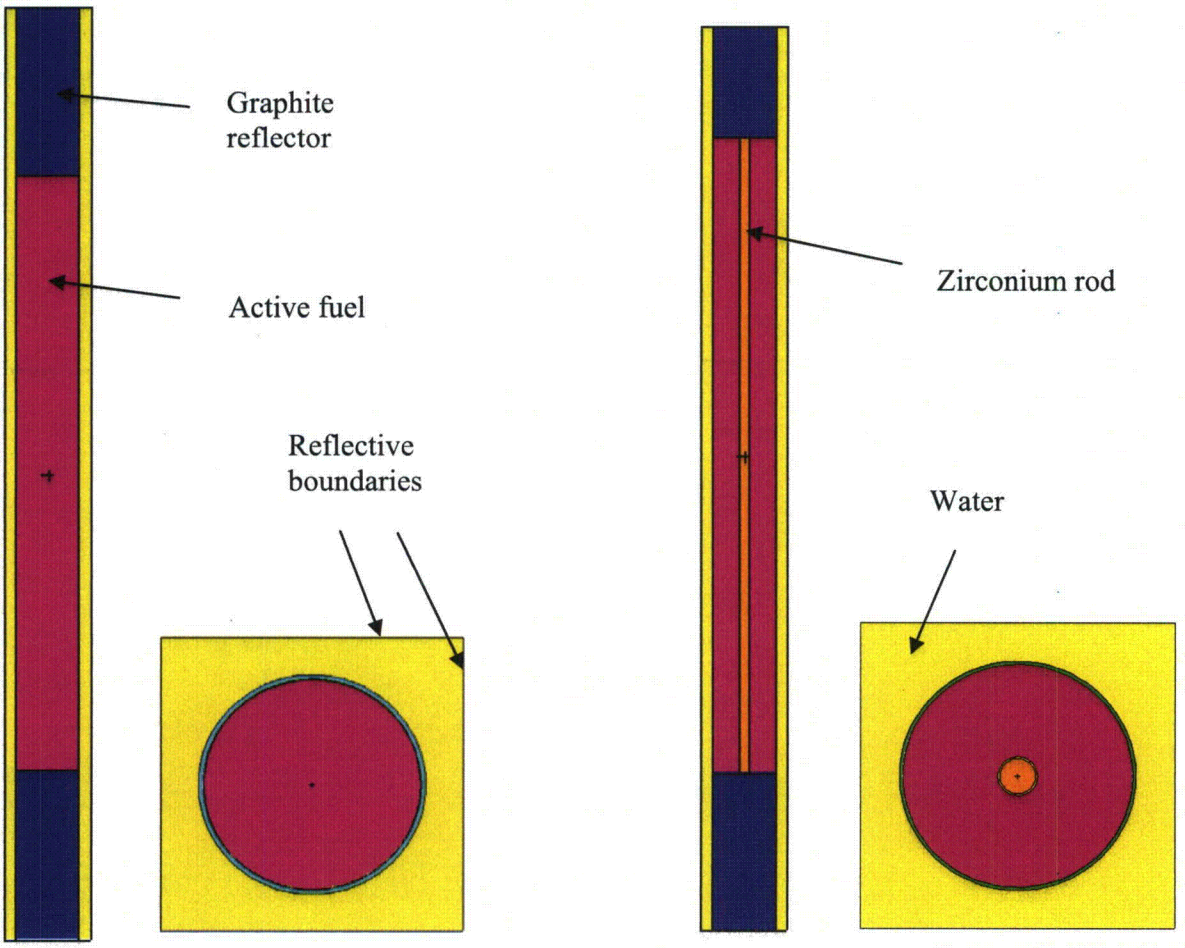

Figure 6.9-2 – TRIGA Pin Cell Models

6.9.3 Sample Input Files

A sample input file is provided for the most reactive case for each of the four fuel types.

MURR Case D1 (HA_MURR)

```
MURR
c
c       Basket
c
300     0          -400 424 -410 fill=6      imp:n=1 $ cavity
c
c       Cask
c
310     4 -7.94    (-424:410:400) 423 -411 -401 imp:n=1 $ inner steel
311     5 -11.35   (-423:411:401) 422 -412 -402 imp:n=1 $ lead
312     4 -7.94    (-422:412:402) 421 -413 -403 imp:n=1 $ outer steel
313     0          (-421:413:403) -405          imp:n=1 $ between
c
999     0                405                    imp:n=0
c
c       Universe 1: MURR Fuel Element (infinitely long)
c
2       3 -2.7          -6 8 9 -10                u=1 imp:n=1 $ left Al piece
4       3 -2.7          -5 7 9 -10                u=1 imp:n=1 $ right Al piece
6       10 5.4439E-02 52 -53 -16 -15              u=1 imp:n=1 $ plate 1
8       3 -2.7          51 -54   -7 -8       #6   u=1 imp:n=1
10      2 -1.0          54 -55   -7 -8            u=1 imp:n=1
12      10 5.4439E-02 56 -57 -16 -15              u=1 imp:n=1 $ plate 2
14      3 -2.7          55 -58   -7 -8       #12  u=1 imp:n=1
16      2 -1.0          58 -59   -7 -8            u=1 imp:n=1
18      10 5.4439E-02 60 -61 -16 -15              u=1 imp:n=1 $ plate 3
20      3 -2.7          59 -62   -7 -8       #18  u=1 imp:n=1
22      2 -1.0          62 -63   -7 -8            u=1 imp:n=1
24      10 5.4439E-02 64 -65 -16 -15              u=1 imp:n=1 $ plate 4
26      3 -2.7          63 -66   -7 -8       #24  u=1 imp:n=1
28      2 -1.0          66 -67   -7 -8            u=1 imp:n=1
30      10 5.4439E-02 68 -69 -16 -15              u=1 imp:n=1 $ plate 5
32      3 -2.7          67 -70   -7 -8       #30  u=1 imp:n=1
34      2 -1.0          70 -71   -7 -8            u=1 imp:n=1
36      10 5.4439E-02 72 -73 -16 -15              u=1 imp:n=1 $ plate 6
38      3 -2.7          71 -74   -7 -8       #36  u=1 imp:n=1
40      2 -1.0          74 -75   -7 -8            u=1 imp:n=1
42      10 5.4439E-02 76 -77 -16 -15              u=1 imp:n=1 $ plate 7
44      3 -2.7          75 -78   -7 -8       #42  u=1 imp:n=1
46      2 -1.0          78 -79   -7 -8            u=1 imp:n=1
48      10 5.4439E-02 80 -81 -16 -15              u=1 imp:n=1 $ plate 8
50      3 -2.7          79 -82   -7 -8       #48  u=1 imp:n=1
52      2 -1.0          82 -83   -7 -8            u=1 imp:n=1
54      10 5.4439E-02 84 -85 -16 -15              u=1 imp:n=1 $ plate 9
56      3 -2.7          83 -86   -7 -8       #54  u=1 imp:n=1
58      2 -1.0          86 -87   -7 -8            u=1 imp:n=1
60      10 5.4439E-02 88 -89 -16 -15              u=1 imp:n=1 $ plate 10
62      3 -2.7          87 -90   -7 -8       #60  u=1 imp:n=1
64      2 -1.0          90 -91   -7 -8            u=1 imp:n=1
66      10 5.4439E-02 92 -93 -16 -15              u=1 imp:n=1 $ plate 11
68      3 -2.7          91 -94   -7 -8       #66  u=1 imp:n=1
70      2 -1.0          94 -95   -7 -8            u=1 imp:n=1
72      10 5.4439E-02 96 -97 -16 -15              u=1 imp:n=1 $ plate 12
```

```
74      3 -2.7          95 -98    -7 -8        #72   u=1 imp:n=1
76      2 -1.0          98 -99    -7 -8             u=1 imp:n=1
78      10 5.4439E-02 100 -101 -16 -15              u=1 imp:n=1 $ plate 13
80      3 -2.7           99 -102   -7 -8        #78   u=1 imp:n=1
82      2 -1.0          102 -103   -7 -8             u=1 imp:n=1
84      10 5.4439E-02 104 -105 -16 -15              u=1 imp:n=1 $ plate 14
86      3 -2.7          103 -106   -7 -8        #84   u=1 imp:n=1
88      2 -1.0          106 -107   -7 -8             u=1 imp:n=1
90      10 5.4439E-02 108 -109 -16 -15              u=1 imp:n=1 $ plate 15
92      3 -2.7          107 -110   -7 -8        #90   u=1 imp:n=1
94      2 -1.0          110 -111   -7 -8             u=1 imp:n=1
96      10 5.4439E-02 112 -113 -16 -15              u=1 imp:n=1 $ plate 16
98      3 -2.7          111 -114   -7 -8        #96   u=1 imp:n=1
100     2 -1.0          114 -115   -7 -8             u=1 imp:n=1
102     10 5.4439E-02 116 -117 -16 -15              u=1 imp:n=1 $ plate 17
104     3 -2.7          115 -118   -7 -8        #102  u=1 imp:n=1
106     2 -1.0          118 -119   -7 -8             u=1 imp:n=1
108     10 5.4439E-02 120 -121 -16 -15              u=1 imp:n=1 $ plate 18
110     3 -2.7          119 -122   -7 -8        #108  u=1 imp:n=1
112     2 -1.0          122 -123   -7 -8             u=1 imp:n=1
114     10 5.4439E-02 124 -125 -16 -15              u=1 imp:n=1 $ plate 19
116     3 -2.7          123 -126   -7 -8        #114  u=1 imp:n=1
118     2 -1.0          126 -127   -7 -8             u=1 imp:n=1
120     10 5.4439E-02 128 -129 -16 -15              u=1 imp:n=1 $ plate 20
122     3 -2.7          127 -130   -7 -8        #120  u=1 imp:n=1
124     2 -1.0          130 -131   -7 -8             u=1 imp:n=1
126     10 5.4439E-02 132 -133 -16 -15              u=1 imp:n=1 $ plate 21
128     3 -2.7          131 -134   -7 -8        #126  u=1 imp:n=1
130     2 -1.0          134 -135   -7 -8             u=1 imp:n=1
132     10 5.4439E-02 136 -137 -16 -15              u=1 imp:n=1 $ plate 22
134     3 -2.7          135 -138   -7 -8        #132  u=1 imp:n=1
136     2 -1.0          138 -139   -7 -8             u=1 imp:n=1
138     10 5.4439E-02 140 -141 -16 -15              u=1 imp:n=1 $ plate 23
140     3 -2.7          139 -142   -7 -8        #138  u=1 imp:n=1
142     2 -1.0          142 -143   -7 -8             u=1 imp:n=1
144     10 5.4439E-02 144 -145 -16 -15              u=1 imp:n=1 $ plate 24
146     3 -2.7          143 -146   -7 -8        #144  u=1 imp:n=1
150     2 -1.0    6:5:-9:10:9 -51 -8 -7:146 -10 -8 -7 u=1 imp:n=1
c
c       Universe 6: Basket
c
600     4  -7.94     600 -601 -620      u=6 imp:n=1 $ bottom
601     4  -7.94     600 -604 620 -621  u=6 imp:n=1 $ bottom
602     4  -7.94     604 -605 620       u=6 imp:n=1 $ shell
603     4  -7.94     602 -604 622 -623  u=6 imp:n=1 $ shelf
604     4  -7.94     602 -603 623       u=6 imp:n=1 $ inner ring
610     2 -1.0      -600 -621          u=6 imp:n=1 $ bottom air
611     2 -1.0      601 -620 -605      u=6 imp:n=1 $ bottom air corner
612     2 -1.0      605                u=6 imp:n=1 $ side and top air
613     2 -1.0      -604 621 -622      u=6 imp:n=1 $ inner air
614     2 -1.0      -602 622           u=6 imp:n=1 $ inner air
615     0           603 -604 623   637 -630 fill=20    u=6 imp:n=1 $ basket loc
1 (top)
616     0           603 -604 623   631 -634 fill=20(2) u=6 imp:n=1 $ basket loc
2
617     0           603 -604 623   635  633 fill=20(3) u=6 imp:n=1 $ basket loc
3
618     0           603 -604 623   637 -632 fill=20(4) u=6 imp:n=1 $ basket loc
4
```

```
619    0           603 -604 623   631 -636 fill=20(5) u=6 imp:n=1 $ basket loc
5
620    0           603 -604 623  -630  635 fill=20(6) u=6 imp:n=1 $ basket loc
6
621    0           603 -604 623  -632 -634 fill=20(7) u=6 imp:n=1 $ basket loc
7
622    0           603 -604 623   633 -636 fill=20(8) u=6 imp:n=1 $ basket loc
8
630    4  -7.94    603 -604 630 -631 623   u=6 imp:n=1 $ web
631    4  -7.94    603 -604 632 -633 623   u=6 imp:n=1 $ web
632    4  -7.94    603 -604 634 -635 623   u=6 imp:n=1 $ web
633    4  -7.94    603 -604 636 -637 623   u=6 imp:n=1 $ web
c
c      Universe 20: MURR fuel element moved +y
c
200    0        -203 24 -25    fill=1(11) u=20 imp:n=1 $ MURR
201    2 -1.0    203:-24:25               u=20 imp:n=1 $ water

5      p  2.4142136 -1 0 -0.13275   $ right Al outer
6      p -2.4142136 -1 0 -0.13275   $ left Al outer
7      p  2.4142136 -1 0 -1.09516   $ right Al inner
8      p -2.4142136 -1 0 -1.09516   $ left Al inner
9      cz 6.858                     $ Al boundary
10     cz 14.884                    $ Al boundary
c
15     p  2.4142136 -1 0 -1.39997   $ plate meat boundary
16     p -2.4142136 -1 0 -1.39997   $ plate meat boundary
c
24     pz  76.1821                  $ bottom of fuel
25     pz  137.1421                 $ top of fuel (24")
c
51     cz 7.0460 $ fuel plate 1
52     cz 7.0739
53     cz 7.1247
54     cz 7.1526
c
55     cz 7.3762 $ fuel plate 2
56     cz 7.4041
57     cz 7.4549
58     cz 7.4828
c
59     cz 7.7064 $ fuel plate 3
60     cz 7.7343
61     cz 7.7851
62     cz 7.8130
c
63     cz 8.0366 $ fuel plate 4
64     cz 8.0645
65     cz 8.1153
66     cz 8.1432
c
67     cz 8.3668 $ fuel plate 5
68     cz 8.3947
69     cz 8.4455
70     cz 8.4734
c
71     cz 8.6970 $ fuel plate 6
72     cz 8.7249
73     cz 8.7757
74     cz 8.8036
```

```
c
75      cz 9.0272 $ fuel plate 7
76      cz 9.0551
77      cz 9.1059
78      cz 9.1338
c
79      cz 9.3574 $ fuel plate 8
80      cz 9.3853
81      cz 9.4361
82      cz 9.4640
c
83      cz 9.6876 $ fuel plate 9
84      cz 9.7155
85      cz 9.7663
86      cz 9.7942
c
87      cz 10.0178 $ fuel plate 10
88      cz 10.0457
89      cz 10.0965
90      cz 10.1244
c
91      cz 10.3480 $ fuel plate 11
92      cz 10.3759
93      cz 10.4267
94      cz 10.4546
c
95      cz 10.6782 $ fuel plate 12
96      cz 10.7061
97      cz 10.7569
98      cz 10.7848
c
99      cz 11.0084 $ fuel plate 13
100     cz 11.0363
101     cz 11.0871
102     cz 11.1150
c
103     cz 11.3386 $ fuel plate 14
104     cz 11.3665
105     cz 11.4173
106     cz 11.4452
c
107     cz 11.6688 $ fuel plate 15
108     cz 11.6967
109     cz 11.7475
110     cz 11.7754
c
111     cz 11.9990 $ fuel plate 16
112     cz 12.0269
113     cz 12.0777
114     cz 12.1056
c
115     cz 12.3292 $ fuel plate 17
116     cz 12.3571
117     cz 12.4079
118     cz 12.4358
c
119     cz 12.6594 $ fuel plate 18
120     cz 12.6873
121     cz 12.7381
122     cz 12.7660
```

```
c
123     cz 12.9896 $ fuel plate 19
124     cz 13.0175
125     cz 13.0683
126     cz 13.0962
c
127     cz 13.3198 $ fuel plate 20
128     cz 13.3477
129     cz 13.3985
130     cz 13.4264
c
131     cz 13.6500 $ fuel plate 21
132     cz 13.6779
133     cz 13.7287
134     cz 13.7566
c
135     cz 13.9802 $ fuel plate 22
136     cz 14.0081
137     cz 14.0589
138     cz 14.0868
c
139     cz 14.3104 $ fuel plate 23
140     cz 14.3383
141     cz 14.3891
142     cz 14.4170
c
143     cz 14.6406 $ fuel plate 24
144     cz 14.6685
145     cz 14.7193
146     cz 14.7472
c
203     cz 100      $ dummy
c
400     cz 20.32    $ IR cask
401     cz 22.86    $ IR lead
402     cz 43.18    $ OR lead
403     cz 48.26    $ OR cask
404     cz 78.74    $ 1 foot water reflector
*405    hex 0 0 -25.25 0 0 190.5355 0 48.27 0
c
410     pz 137.1422 $ bottom of lid
411     pz 139.6822 $ steel
412     pz 164.0154 $ lead
413     pz 165.2854 $ steel
414     pz 195.7654 $ 1 foot water reflector
c
420     pz -55.72   $ 1 foot water reflector
421     pz -25.24   $ bottom of cask
422     pz -22.7    $ steel
423     pz -3.0912  $ lead
424     pz 0        $ steel
c
c    basket surfaces
c
600     cz 15.4432
601     cz 16.3957
602     cz 8.89
603     cz 10.0813
604     cz 19.177
605     cz 19.812
```

```
620      pz 5.715
621      pz 6.6675
622      pz 50.9778
623      pz 51.9303
630 12   px -1.27
631 12   px  1.27
632 12   py -1.27
633 12   py  1.27
634 13   px -1.27
635 13   px  1.27
636 13   py -1.27
637 13   py  1.27

m2       1001.62c  2          $ water
         8016.62c  1
mt2      lwtr.60t
m3       13027.62c 1          $ Al
m4       6000.66c   -0.08     $ SS-304
         14000.60c  -1.0
         15031.66c  -0.045
         24000.50c  -19.0
         25055.62c  -2.0
         26000.55c  -68.375
         28000.50c  -9.5
m5       82000.50c 1          $ Pb
m10      92234.69c 2.3171E-05 $ fuel.
         92235.69c 3.6147E-03
         92236.69c 1.3402E-05
         92238.69c 1.9174E-04
         13027.62c 5.0596E-02
c          total 5.4439E-02
c
*tr2      0 0 0 45 135 90 45 45 90          $ loc 2
*tr3      0 0 0 90 180 90 0 90 90           $ loc 3
*tr4      0 0 0 135 225 90 45 135 90        $ loc 4
*tr5      0 0 0 180 90 90 90 180 90         $ loc 5
*tr6      0 0 0 135 45 90 225 135 90        $ loc 6
*tr7      0 0 0 90 0 90 180 90 90           $ loc 7
*tr8      0 0 0  45 45 90 135 45 90         $ loc 8
*tr11     0 3.4 0                           $ u=20
*tr12     0 0 0 22.5 112.5 90 67.5 22.5 90  $ rotate 22.5 deg
*tr13     0 0 0 67.5 157.5 90 22.5 67.5 90  $ rotate 67.5 deg
c
mode   n
kcode  2500 1.0 50 250
sdef   rad=d1 ext=d2 axs=0 0 1
si1    10 18.5
si2    76 137
```

MITR-II Case D20 (HA_MIT2)

```
MIT
c
c       Basket
c
300      0 630 -631 633 -632 680 -410 fill=5            imp:n=1 $ basket
location 1
301      like 300 but trcl=2                            imp:n=1 $ basket
location 2
```

```
302     like 300 but trcl=3                                  imp:n=1 $ basket
location 3
303     like 300 but trcl=4                                  imp:n=1 $ basket
location 4
304     like 300 but trcl=5                                  imp:n=1 $ basket
location 5
305     like 300 but trcl=6                                  imp:n=1 $ basket
location 6
306     like 300 but trcl=7                                  imp:n=1 $ basket
location 7
307     like 300 but trcl=8                                  imp:n=1 $ basket
location 8
320     4 -7.94        680 -410 687 -683 #300 #301 #302 #303
                       #304 #305 #306 #307                   imp:n=1 $ inside
basket
c 330     2 -1.0         410 -410 -400                        imp:n=1 $ above
basket
331     4 -7.94        682 -680 -683                         imp:n=1 $ support
plate
332     4 -7.94        684 -685 -682 424                     imp:n=1 $ basket
bottom
333     2 -1.0        -684 -682 424                          imp:n=1
334     2 -1.0         682 -680 683 -400                     imp:n=1
335     2 -1.0         685 -682 424 -400                     imp:n=1
336     2 -1.0         680 -410 -687                         imp:n=1 $ inner air
337     2 -1.0         680 -410 683 -400                     imp:n=1 $ annular
air
c
c       Cask
c
410     4 -7.94    (-424:410:400) 423 -411 -401 imp:n=1 $ inner steel
411     5 -11.35   (-423:411:401) 422 -412 -402 imp:n=1 $ lead
412     4 -7.94    (-422:412:402) 421 -413 -403 imp:n=1 $ outer steel
413     0          (-421:413:403) -405          imp:n=1 $ between
c
999     0                405                    imp:n=0
c
c       Universe 1: MIT Fuel Element (infinitely long)
c
10      3 -2.7         10 -11 18 -19            u=1 imp:n=1 $ right Al piece
11      3 -2.7         13 -12 18 -19            u=1 imp:n=1 $ left Al piece
12      2 -1.0         12 -10 18 -50            u=1 imp:n=1
20      10 5.4398E-02  40 -41 70 -90            u=1 imp:n=1 $ plate 1
21      3 -2.7         12 -10 50 -110 #20       u=1 imp:n=1
22      2 -1.0         12 -10 110 -51           u=1 imp:n=1
30      10 5.4398E-02  40 -41 71 -91            u=1 imp:n=1 $ plate 2
31      3 -2.7         12 -10 51 -111 #30       u=1 imp:n=1
32      2 -1.0         12 -10 111 -52           u=1 imp:n=1
40      10 5.4398E-02  40 -41 72 -92            u=1 imp:n=1 $ plate 3
41      3 -2.7         12 -10 52 -112 #40       u=1 imp:n=1
42      2 -1.0         12 -10 112 -53           u=1 imp:n=1
50      10 5.4398E-02  40 -41 73 -93            u=1 imp:n=1 $ plate 4
51      3 -2.7         12 -10 53 -113 #50       u=1 imp:n=1
52      2 -1.0         12 -10 113 -54           u=1 imp:n=1
60      10 5.4398E-02  40 -41 74 -94            u=1 imp:n=1 $ plate 5
61      3 -2.7         12 -10 54 -114 #60       u=1 imp:n=1
62      2 -1.0         12 -10 114 -55           u=1 imp:n=1
70      10 5.4398E-02  40 -41 75 -95            u=1 imp:n=1 $ plate 6
71      3 -2.7         12 -10 55 -115 #70       u=1 imp:n=1
72      2 -1.0         12 -10 115 -56           u=1 imp:n=1
```

```
80       10 5.4398E-02 40 -41 76 -96              u=1 imp:n=1 $ plate 7
81       3 -2.7        12 -10 56 -116 #80         u=1 imp:n=1
82       2 -1.0        12 -10 116 -57             u=1 imp:n=1
90       10 5.4398E-02 40 -41 77 -97              u=1 imp:n=1 $ plate 8
91       3 -2.7        12 -10 57 -117 #90         u=1 imp:n=1
92       2 -1.0        12 -10 117 -58             u=1 imp:n=1
100       10 5.4398E-02 40 -41 78 -98              u=1 imp:n=1 $ plate 9
101       3 -2.7        12 -10 58 -118 #100        u=1 imp:n=1
102       2 -1.0        12 -10 118 -59             u=1 imp:n=1
110       10 5.4398E-02 40 -41 79 -99              u=1 imp:n=1 $ plate 10
111       3 -2.7        12 -10 59 -119 #110        u=1 imp:n=1
112       2 -1.0        12 -10 119 -60             u=1 imp:n=1
120       10 5.4398E-02 40 -41 80 -100             u=1 imp:n=1 $ plate 11
121       3 -2.7        12 -10 60 -120 #120        u=1 imp:n=1
122       2 -1.0        12 -10 120 -61             u=1 imp:n=1
130       10 5.4398E-02 40 -41 81 -101             u=1 imp:n=1 $ plate 12
131       3 -2.7        12 -10 61 -121 #130        u=1 imp:n=1
132       2 -1.0        12 -10 121 -62             u=1 imp:n=1
140       10 5.4398E-02 40 -41 82 -102             u=1 imp:n=1 $ plate 13
141       3 -2.7        12 -10 62 -122 #140        u=1 imp:n=1
142       2 -1.0        12 -10 122 -63             u=1 imp:n=1
150       10 5.4398E-02 40 -41 83 -103             u=1 imp:n=1 $ plate 14
151       3 -2.7        12 -10 63 -123 #150        u=1 imp:n=1
152       2 -1.0        12 -10 123 -64             u=1 imp:n=1
160       10 5.4398E-02 40 -41 84 -104             u=1 imp:n=1 $ plate 15
161       3 -2.7        12 -10 64 -124 #160        u=1 imp:n=1
162       2 -1.0        12 -10 124 -19             u=1 imp:n=1
170       2 -1.0        -13:11:-18:19              u=1 imp:n=1 $ water in pipe
c
c         Universe 5: Element rotated 30 degrees CCW and moved to wedge 1
location outer
c
500       0          -700 24  fill=1(12)     u=5 imp:n=1
501       2 -1.0     -700 -24                u=5 imp:n=1
c 502       2 -1.0     -700 25                 u=5 imp:n=1

10       px  2.5451    $ Al side
11       px  3.0226    $ Al side
12       px -2.5451    $ Al side
13       px -3.0226    $ Al side
18  10   py -3.02768   $ Al bottom
19  10   py 3.02768    $ Al top
c
24       pz  80.3097   $ bottom of fuel
c 25       pz  130.7439 $ top of fuel (22.375")
c
40       px -2.3878 $ meat width (w/2*cos(30))
41       px  2.3878 $ meat width
c
50 10    py -2.89052 $ cladding bottom
51 10    py -2.48920
52 10    py -2.08788
53 10    py -1.68656
54 10    py -1.28524
55 10    py -0.88392
56 10    py -0.48260
57 10    py -0.08128
58 10    py 0.32004
59 10    py 0.72136
60 10    py 1.12268
```

```
61 10    py 1.52400
62 10    py 1.92532
63 10    py 2.32664
64 10    py 2.72796
c
70 10    py -2.84734 $ meat bottom
71 10    py -2.44602
72 10    py -2.04470
73 10    py -1.64338
74 10    py -1.24206
75 10    py -0.84074
76 10    py -0.43942
77 10    py -0.03810
78 10    py 0.36322
79 10    py 0.76454
80 10    py 1.16586
81 10    py 1.56718
82 10    py 1.96850
83 10    py 2.36982
84 10    py 2.77114
c
90 10    py -2.77114 $ meat top
91 10    py -2.36982
92 10    py -1.96850
93 10    py -1.56718
94 10    py -1.16586
95 10    py -0.76454
96 10    py -0.36322
97 10    py 0.03810
98 10    py 0.43942
99 10    py 0.84074
100 10    py 1.24206
101 10    py 1.64338
102 10    py 2.04470
103 10    py 2.44602
104 10    py 2.84734
c
110 10    py -2.72796 $ cladding top
111 10    py -2.32664
112 10    py -1.92532
113 10    py -1.52400
114 10    py -1.12268
115 10    py -0.72136
116 10    py -0.32004
117 10    py 0.08128
118 10    py 0.48260
119 10    py 0.88392
120 10    py 1.28524
121 10    py 1.68656
122 10    py 2.08788
123 10    py 2.48920
124 10    py 2.89052
c
400      cz 20.32 $ IR cask
401      cz 22.86 $ IR lead
402      cz 43.18 $ OR lead
403      cz 48.26 $ OR cask
404      cz 78.74 $ 1 foot water reflector
*405     hex 0 0 -25.25 0 0 190.5355 0 48.27 0
c
```

```
410     pz 137.1422 $ bottom of lid
411     pz 139.6822 $ steel
412     pz 164.0154 $ lead
413     pz 165.2854 $ steel
414     pz 195.7654 $ 1 foot water reflector
c
420     pz -55.72   $ 1 foot water reflector
421     pz -25.24   $ bottom of cask
422     pz -22.7    $ steel
423     pz -3.0912  $ lead
424     pz 0        $ steel
c
c    basket surfaces
c
630   1   py -3.3909
631   1   py  3.3909
632   1   p  -1.7321 -1 0  6.7818 $ left basket inner bound
633   1   p  -1.7321 -1 0 -6.7818 $ right basket inner bound
c
680   pz  67.4878 $ top of plate
682   pz  66.2178 $ bottom of plate
683   cz  19.8501 $ OR of basket
684   cz  17.145
685   cz  17.78
687   cz  12      $ IR of basket
700   cz  1000    $ dummy

m2      1001.62c  2          $ water
        8016.62c  1
mt2     lwtr.60t
m3      13027.62c 1          $ Al
m4      6000.66c   -0.08     $ SS-304
        14000.60c  -1.0
        15031.66c  -0.045
        24000.50c  -19.0
        25055.62c  -2.0
        26000.55c  -68.375
        28000.50c  -9.5
m5      82000.50c 1          $ Pb
m10     92234.69c 2.3613E-05 $ fuel
        92235.69c 3.6835E-03
        92236.69c 1.3657E-05
        92238.69c 1.9539E-04
        13027.62c 5.0481E-02
c           total 5.4398E-02
c
*tr1     1.7413 15.5236 0                      $ wedge 1
*tr2     0 0 0          45 135 90 45 45 90     $ wedge 2(8)
*tr3     0 0 0          90 180 90 0  90 90     $ wedge 3(7)
*tr4     0 0 0         135 225 90 45 135 90    $ wedge 4(6)
*tr5     0 0 0         180 90 90 90 180 90     $ wedge 5
*tr6     0 0 0         135 45 90 225 135 90    $ wedge 6
*tr7     0 0 0         90 0 90 180 90 90       $ wedge 7
*tr8     0 0 0         45 45 90 135 45 90      $ wedge 8
*tr10    0 0 0         30 120 90 60  30 90     $ rotate fuel surfaces 30 deg
CW
*tr12    1.7413 15.15 0   30 60 90 120 30 90  $ rotate 30 CCW
c
mode   n
kcode  2500 1.0 50 250
```

```
sdef   rad=d1 ext=d2 axs=0 0 1
si1    12 20
si2    80 137
```

ATR Case D40 (HA_ATR)

```
ATR
300     0      -400 424 -410 fill=6     imp:n=1 $ cavity
c
c       Cask
c
310     4 -7.94    (-424:410:400) 423 -411 -401 imp:n=1 $ inner steel
311     5 -11.35   (-423:411:401) 422 -412 -402 imp:n=1 $ lead
312     4 -7.94    (-422:412:402) 421 -413 -403 imp:n=1 $ outer steel
313     0          (-421:413:403) -405          imp:n=1 $ between
c
999     0                405                    imp:n=0
c
c       Universe 1: ATR Fuel Element (infinitely long)
c
2       3 -2.7          -6 8 9 -10                u=1 imp:n=1 $ left Al piece
4       3 -2.7          -5 7 9 -10                u=1 imp:n=1 $ right Al piece
6       10 5.5010E-02   52 -53 -14 -13            u=1 imp:n=1 $ plate 1
8       3 -2.7          51 -54   -7 -8       #6   u=1 imp:n=1
10      2 -1.0          54 -55   -7 -8            u=1 imp:n=1
12      11 5.4998E-02   56 -57 -16 -15            u=1 imp:n=1 $ plate 2
14      3 -2.7          55 -58   -7 -8       #12  u=1 imp:n=1
16      2 -1.0          58 -59   -7 -8            u=1 imp:n=1
18      12 5.4574E-02   60 -61 -16 -15            u=1 imp:n=1 $ plate 3
20      3 -2.7          59 -62   -7 -8       #18  u=1 imp:n=1
22      2 -1.0          62 -63   -7 -8            u=1 imp:n=1
24      13 5.4583E-02   64 -65 -16 -15            u=1 imp:n=1 $ plate 4
26      3 -2.7          63 -66   -7 -8       #24  u=1 imp:n=1
28      2 -1.0          66 -67   -7 -8            u=1 imp:n=1
30      14 5.4115E-02   68 -69 -16 -15            u=1 imp:n=1 $ plate 5
32      3 -2.7          67 -70   -7 -8       #30  u=1 imp:n=1
34      2 -1.0          70 -71   -7 -8            u=1 imp:n=1
36      15 5.4106E-02   72 -73 -16 -15            u=1 imp:n=1 $ plate 6
38      3 -2.7          71 -74   -7 -8       #36  u=1 imp:n=1
40      2 -1.0          74 -75   -7 -8            u=1 imp:n=1
42      16 5.4102E-02   76 -77 -16 -15            u=1 imp:n=1 $ plate 7
44      3 -2.7          75 -78   -7 -8       #42  u=1 imp:n=1
46      2 -1.0          78 -79   -7 -8            u=1 imp:n=1
48      17 5.4098E-02   80 -81 -16 -15            u=1 imp:n=1 $ plate 8
50      3 -2.7          79 -82   -7 -8       #48  u=1 imp:n=1
52      2 -1.0          82 -83   -7 -8            u=1 imp:n=1
54      18 5.4095E-02   84 -85 -16 -15            u=1 imp:n=1 $ plate 9
56      3 -2.7          83 -86   -7 -8       #54  u=1 imp:n=1
58      2 -1.0          86 -87   -7 -8            u=1 imp:n=1
60      19 5.4092E-02   88 -89 -16 -15            u=1 imp:n=1 $ plate 10
62      3 -2.7          87 -90   -7 -8       #60  u=1 imp:n=1
64      2 -1.0          90 -91   -7 -8            u=1 imp:n=1
66      20 5.4089E-02   92 -93 -16 -15            u=1 imp:n=1 $ plate 11
68      3 -2.7          91 -94   -7 -8       #66  u=1 imp:n=1
70      2 -1.0          94 -95   -7 -8            u=1 imp:n=1
72      21 5.4086E-02   96 -97 -16 -15            u=1 imp:n=1 $ plate 12
74      3 -2.7          95 -98   -7 -8       #72  u=1 imp:n=1
76      2 -1.0          98 -99   -7 -8            u=1 imp:n=1
78      22 5.4083E-02   100 -101 -16 -15          u=1 imp:n=1 $ plate 13
80      3 -2.7           99 -102   -7 -8     #78  u=1 imp:n=1
```

```
82      2 -1.0          102 -103   -7 -8           u=1 imp:n=1
84      23 5.4081E-02   104 -105 -16 -15           u=1 imp:n=1 $ plate 14
86      3 -2.7          103 -106   -7 -8      #84  u=1 imp:n=1
88      2 -1.0          106 -107   -7 -8           u=1 imp:n=1
90      24 5.4075E-02   108 -109 -16 -15           u=1 imp:n=1 $ plate 15
92      3 -2.7          107 -110   -7 -8      #90  u=1 imp:n=1
94      2 -1.0          110 -111   -7 -8           u=1 imp:n=1
96      25 5.4544E-02   112 -113 -16 -15           u=1 imp:n=1 $ plate 16
98      3 -2.7          111 -114   -7 -8      #96  u=1 imp:n=1
100     2 -1.0          114 -115   -7 -8           u=1 imp:n=1
102     26 5.4544E-02   116 -117 -16 -15           u=1 imp:n=1 $ plate 17
104     3 -2.7          115 -118   -7 -8      #102 u=1 imp:n=1
106     2 -1.0          118 -119   -7 -8           u=1 imp:n=1
108     27 5.4949E-02   120 -121 -18 -17           u=1 imp:n=1 $ plate 18
110     3 -2.7          119 -122   -7 -8      #108 u=1 imp:n=1
112     2 -1.0          122 -123   -7 -8           u=1 imp:n=1
114     28 5.4967E-02   124 -125 -14 -13           u=1 imp:n=1 $ plate 19
116     3 -2.7          123 -126   -7 -8      #114 u=1 imp:n=1
122     2 -1.0          6:5:-9:10:9 -51 -8 -7:126 -10 -8 -7 u=1 imp:n=1
c
c       Universe 6: Basket
c
600     4  -7.94     602 -603 623              u=6 imp:n=1 $ inner ring
601     4  -7.94     602 -604 622 -623         u=6 imp:n=1 $ bottom plate
602     4  -7.94     604 -605                  u=6 imp:n=1 $ outer ring
603     2 -1.0     -604 -622                    u=6 imp:n=1 $ bottom void
604     2 -1.0     -602 622                     u=6 imp:n=1 $ inner void
605     2 -1.0      605                         u=6 imp:n=1 $ inf. water
614     0           603 -604 623   637 -630 fill=20    u=6 imp:n=1 $ basket loc
1 (top)
615     0           603 -604 623   631 -634 fill=20(2) u=6 imp:n=1 $ basket loc
2
616     0           603 -604 623   635  633 fill=20(3) u=6 imp:n=1 $ basket loc
3
617     0           603 -604 623   637 -632 fill=20(4) u=6 imp:n=1 $ basket loc
4
618     0           603 -604 623   631 -636 fill=20(5) u=6 imp:n=1 $ basket loc
5
619     0           603 -604 623  -630  635 fill=20(6) u=6 imp:n=1 $ basket loc
6
620     0           603 -604 623  -632 -634 fill=20(7) u=6 imp:n=1 $ basket loc
7
621     0           603 -604 623   633 -636 fill=20(8) u=6 imp:n=1 $ basket loc
8
630     4  -7.94    603 -604 630 -631 623    u=6 imp:n=1 $ web
631     4  -7.94    603 -604 632 -633 623    u=6 imp:n=1 $ web
632     4  -7.94    603 -604 634 -635 623    u=6 imp:n=1 $ web
633     4  -7.94    603 -604 636 -637 623    u=6 imp:n=1 $ web
c
c       Universe 20: ATR fuel element moved +y
c
200     0        -203 24 -25    fill=1(11) u=20 imp:n=1
201     2 -1.0    203:-24:25               u=20 imp:n=1 $ water

5       p  2.4142136 -1 0 -0.2665911 $ right Al outer
6       p -2.4142136 -1 0 -0.2665911 $ left Al outer
7       p  2.4142136 -1 0 -1.474587  $ right Al inner
8       p -2.4142136 -1 0 -1.474587  $ left Al inner
9       cz 7.52856                   $ Al boundary
10      cz 14.015466                 $ Al boundary
```

```
c
13      p  2.4142136 -1 0 -2.4370013 $ plate 1 & 19 meat
14      p -2.4142136 -1 0 -2.4370013 $ plate 1 & 19 meat
15      p  2.4142136 -1 0 -1.7732672 $ plate 2-17 meat
16      p -2.4142136 -1 0 -1.7732672 $ plate 2-17 meat
17      p  2.4142136 -1 0 -1.9060140 $ plate 18 meat
18      p -2.4142136 -1 0 -1.9060140 $ plate 18 meat
c
24      pz  15.2221                  $ bottom of fuel
25      pz  137.1421                 $ top of fuel (48")
c
51      cz 7.66699 $ fuel plate 1
52      cz 7.7343
53      cz 7.7851
54      cz 7.85241
c
55      cz 8.06831 $ fuel plate 2
56      cz 8.09752
57      cz 8.14832
58      cz 8.17753
c
59      cz 8.39343 $ fuel plate 3
60      cz 8.42264
61      cz 8.47344
62      cz 8.50265
c
63      cz 8.71855 $ fuel plate 4
64      cz 8.74776
65      cz 8.79856
66      cz 8.82777
c
67      cz 9.04367 $ fuel plate 5
68      cz 9.07288
69      cz 9.12368
70      cz 9.15289
c
71      cz 9.36879 $ fuel plate 6
72      cz 9.398
73      cz 9.4488
74      cz 9.47801
c
75      cz 9.69391 $ fuel plate 7
76      cz 9.72312
77      cz 9.77392
78      cz 9.80313
c
79      cz 10.01903 $ fuel plate 8
80      cz 10.04824
81      cz 10.09904
82      cz 10.12825
c
83      cz 10.34415 $ fuel plate 9
84      cz 10.37336
85      cz 10.42416
86      cz 10.45337
c
87      cz 10.66927 $ fuel plate 10
88      cz 10.69848
89      cz 10.74928
90      cz 10.77849
```

```
c
91      cz 10.99439 $ fuel plate 11
92      cz 11.0236
93      cz 11.0744
94      cz 11.10361
c
95      cz 11.31951 $ fuel plate 12
96      cz 11.34872
97      cz 11.39952
98      cz 11.42873
c
99       cz 11.64463 $ fuel plate 13
100      cz 11.67384
101      cz 11.72464
102      cz 11.75385
c
103      cz 11.96975 $ fuel plate 14
104      cz 11.99896
105      cz 12.04976
106      cz 12.07897
c
107      cz 12.29487 $ fuel plate 15
108      cz 12.32408
109      cz 12.37488
110      cz 12.40409
c
111      cz 12.61999 $ fuel plate 16
112      cz 12.6492
113      cz 12.7
114      cz 12.72921
c
115      cz 12.94511 $ fuel plate 17
116      cz 12.97432
117      cz 13.02512
118      cz 13.05433
c
119      cz 13.27023 $ fuel plate 18
120      cz 13.29944
121      cz 13.35024
122      cz 13.37945
c
123      cz 13.59535 $ fuel plate 19
124      cz 13.68806
125      cz 13.73886
126      cz 13.83157
c
203     cz 100       $ dummy
c
400     cz 20.32     $ IR cask
401     cz 22.86     $ IR lead
402     cz 43.18     $ OR lead
403     cz 48.26     $ OR cask
404     cz 78.74     $ 1 foot water reflector
*405    hex 0 0 -25.25 0 0 190.5355 0 48.27 0
c
410     pz 137.1422 $ bottom of lid
411     pz 139.6822 $ steel
412     pz 164.0154 $ lead
413     pz 165.2854 $ steel
414     pz 195.7654 $ 1 foot water reflector
```

```
c
420     pz -55.72    $ 1 foot water reflector
421     pz -25.24    $ bottom of cask
422     pz -22.7     $ steel
423     pz -3.0912   $ lead
424     pz 0         $ steel
c
c    basket surfaces
c
602     cz 8.255
603     cz 9.144
604     cz 16.51
605     cz 17.145
622     pz 4.0132
623     pz 5.2832
c 624     pz 135.763
630 12  px -0.47625
631 12  px  0.47625
632 12  py -0.47625
633 12  py  0.47625
634 13  px -0.47625
635 13  px  0.47625
636 13  py -0.47625
637 13  py  0.47625

m2      1001.62c  2          $ water
        8016.62c  1
mt2     lwtr.60t
m3      13027.62c 1          $ Al
m4      6000.66c   -0.08     $ SS-304
        14000.60c  -1.0
        15031.66c  -0.045
        24000.50c  -19.0
        25055.62c  -2.0
        26000.55c  -68.375
        28000.50c  -9.5
m5      82000.50c 1          $ Pb
m10     92234.69c 1.7026E-05 $ fuel plate 1
        92235.69c 2.6560E-03
        92236.69c 9.8475E-06
        92238.69c 1.4089E-04
        13027.62c 5.2187E-02
c       total     5.5010E-02
m11     92234.69c 1.7156E-05 $ fuel plate 2
        92235.69c 2.6763E-03
        92236.69c 9.9226E-06
        92238.69c 1.4196E-04
        13027.62c 5.2153E-02
c       total     5.4998E-02
m12     92234.69c 2.1711E-05 $ fuel plate 3
        92235.69c 3.3869E-03
        92236.69c 1.2557E-05
        92238.69c 1.7966E-04
        13027.62c 5.0974E-02
c       total     5.4574E-02
m13     92234.69c 2.1618E-05 $ fuel plate 4
        92235.69c 3.3724E-03
        92236.69c 1.2503E-05
        92238.69c 1.7889E-04
        13027.62c 5.0998E-02
```

```
c       total     5.4583E-02
m14     92234.69c 2.6648E-05 $ fuel plate 5
        92235.69c 4.1571E-03
        92236.69c 1.5413E-05
        92238.69c 2.2051E-04
        13027.62c 4.9696E-02
c       total     5.4115E-02
m15     92234.69c 2.6746E-05 $ fuel plate 6
        92235.69c 4.1724E-03
        92236.69c 1.5470E-05
        92238.69c 2.2132E-04
        13027.62c 4.9670E-02
c       total     5.4106E-02
m16     92234.69c 2.6790E-05 $ fuel plate 7
        92235.69c 4.1791E-03
        92236.69c 1.5495E-05
        92238.69c 2.2168E-04
        13027.62c 4.9659E-02
c       total     5.4102E-02
m17     92234.69c 2.6830E-05 $ fuel plate 8
        92235.69c 4.1854E-03
        92236.69c 1.5518E-05
        92238.69c 2.2201E-04
        13027.62c 4.9649E-02
c       total     5.4098E-02
m18     92234.69c 2.6867E-05 $ fuel plate 9
        92235.69c 4.1911E-03
        92236.69c 1.5539E-05
        92238.69c 2.2232E-04
        13027.62c 4.9639E-02
c       total     5.4095E-02
m19     92234.69c 2.6901E-05 $ fuel plate 10
        92235.69c 4.1965E-03
        92236.69c 1.5559E-05
        92238.69c 2.2260E-04
        13027.62c 4.9630E-02
c       total     5.4092E-02
m20     92234.69c 2.6933E-05 $ fuel plate 11
        92235.69c 4.2015E-03
        92236.69c 1.5577E-05
        92238.69c 2.2287E-04
        13027.62c 4.9622E-02
c       total     5.4089E-02
m21     92234.69c 2.6963E-05 $ fuel plate 12
        92235.69c 4.2061E-03
        92236.69c 1.5595E-05
        92238.69c 2.2311E-04
        13027.62c 4.9614E-02
c       total     5.4086E-02
m22     92234.69c 2.6990E-05 $ fuel plate 13
        92235.69c 4.2105E-03
        92236.69c 1.5611E-05
        92238.69c 2.2334E-04
        13027.62c 4.9607E-02
c       total     5.4083E-02
m23     92234.69c 2.7017E-05 $ fuel plate 14
        92235.69c 4.2145E-03
        92236.69c 1.5626E-05
        92238.69c 2.2356E-04
        13027.62c 4.9600E-02
```

```
c       total      5.4081E-02
m24     92234.69c 2.7077E-05 $ fuel plate 15
        92235.69c 4.2239E-03
        92236.69c 1.5661E-05
        92238.69c 2.2406E-04
        13027.62c 4.9585E-02
c       total      5.4075E-02
m25     92234.69c 2.2037E-05 $ fuel plate 16
        92235.69c 3.4377E-03
        92236.69c 1.2746E-05
        92238.69c 1.8235E-04
        13027.62c 5.0889E-02
c       total      5.4544E-02
m26     92234.69c 2.2037E-05 $ fuel plate 17
        92235.69c 3.4377E-03
        92236.69c 1.2745E-05
        92238.69c 1.8235E-04
        13027.62c 5.0889E-02
c       total      5.4544E-02
m27     92234.69c 1.7683E-05 $ fuel plate 18
        92235.69c 2.7586E-03
        92236.69c 1.0228E-05
        92238.69c 1.4633E-04
        13027.62c 5.2016E-02
c       total      5.4949E-02
m28     92234.69c 1.7487E-05 $ fuel plate 19
        92235.69c 2.7279E-03
        92236.69c 1.0114E-05
        92238.69c 1.4470E-04
        13027.62c 5.2067E-02
c       total      5.4967E-02
c
*tr2     0 0 0 45 135 90 45 45 90          $ loc 2
*tr3     0 0 0 90 180 90 0 90 90           $ loc 3
*tr4     0 0 0 135 225 90 45 135 90        $ loc 4
*tr5     0 0 0 180 90 90 90 180 90         $ loc 5
*tr6     0 0 0 135 45 90 225 135 90        $ loc 6
*tr7     0 0 0 90 0 90 180 90 90           $ loc 7
*tr8     0 0 0  45 45 90 135 45 90         $ loc 8
*tr11    0 1.7 0                           $ u=20
*tr12    0 0 0 22.5 112.5 90 67.5 22.5 90  $ rotate 22.5 deg
*tr13    0 0 0 67.5 157.5 90 22.5 67.5 90  $ rotate 67.5 deg
c
mode   n
kcode  2500 1.0 50 250
sdef   rad=d1 ext=d2 axs=0 0 1
si1    9.5 16
si2    15 137
```

TRIGA Case D63 (HA_TRIGA_W0C060)

```
TRIGA
300     0          -400 424 -410  fill=1    imp:n=1 $ cavity
c
c       Cask
c
310     4 -7.94    (-424:410:400) 423 -411 -401 imp:n=1 $ inner steel
311     5 -11.35   (-423:411:401) 422 -412 -402 imp:n=1 $ lead
312     4 -7.94    (-422:412:402) 421 -413 -403 imp:n=1 $ outer steel
313     0          (-421:413:403) -405          imp:n=1 $ between
```

```
c
999     0               405                    imp:n=0
c
c       Universe 1: Basket
c
601     0            601  -611   trcl=1 fill=2     u=1 imp:n=1
602     like 601 but trcl=2                        u=1 imp:n=1
603     like 601 but trcl=3                        u=1 imp:n=1
604     like 601 but trcl=4                        u=1 imp:n=1
605     like 601 but trcl=5                        u=1 imp:n=1
606     like 601 but trcl=6                        u=1 imp:n=1
607     like 601 but trcl=7                        u=1 imp:n=1
608     like 601 but trcl=8                        u=1 imp:n=1
610     like 601 but trcl=9                        u=1 imp:n=1
611     like 601 but trcl=10                       u=1 imp:n=1
612     like 601 but trcl=11                       u=1 imp:n=1
613     like 601 but trcl=12                       u=1 imp:n=1
614     like 601 but trcl=13                       u=1 imp:n=1
615     like 601 but trcl=14                       u=1 imp:n=1
616     like 601 but trcl=15                       u=1 imp:n=1
617     like 601 but trcl=16                       u=1 imp:n=1
618     like 601 but trcl=17                       u=1 imp:n=1
619     like 601 but trcl=18                       u=1 imp:n=1
620     like 601 but trcl=19                       u=1 imp:n=1
625     2 -0.6        601 #601 #602 #603 #604 #605 #606 #607 #608
                     #610 #611 #612 #613 #614 #615 #616 #617
                     #618 #619 #620                u=1 imp:n=1
c 630     0           -600                          u=1 imp:n=1 $ below
basket
631     4 -7.94       600 -601 -602                 u=1 imp:n=1 $ basket plate
632     2 -0.6        600 -601 602                  u=1 imp:n=1
633     4 -7.94       603 -604 -600                 u=1 imp:n=1 $ bottom
support
634     2 -0.6        604 -600                      u=1 imp:n=1
635     2 -0.6       -603 -600                      u=1 imp:n=1
c
c       Universe 2: Fuel in tube
c
650     0            -610  fill=3(0 -0.38 111.488) u=2 imp:n=1 $ inside tube
651     4  -7.94      610                          u=2 imp:n=1 $ tube
c
c       Universe 3: Fuel
c
200     7  -6.5        31 -32 -10     imp:n=1 u=3 $ zirc rod
201     2 -0.6         31 -32 10 -11  imp:n=1 u=3 $ gap
202     1  9.2354E-02 31 -32 11 -20  imp:n=1 u=3 $ fuel
203     6  -1.6        30 -31 -20     imp:n=1 u=3 $ bottom graphite
204     6  -1.6        32 -33 -20     imp:n=1 u=3 $ top graphite
205     4  -7.94       30 -33 20 -22  imp:n=1 u=3 $ cladding
206     2 -0.6         -30:33:22      imp:n=1 u=3 $ inf. water

10      cz 0.28575  $ zirc OR
11      cz 0.3175   $ fuel IR
20      cz 1.8288   $ fuel OR
22      cz 1.8796   $ cladding OR
c
30      pz -28.448  $ bottom graphite
31      pz -19.05   $ bottom fuel
32      pz  19.05   $ top fuel
33      pz  25.654  $ top graphite
```

```
c
400     cz 20.32     $ IR cask
401     cz 22.86     $ IR lead
402     cz 43.18     $ OR lead
403     cz 48.26     $ OR cask
404     cz 78.74     $ 1 foot water reflector
*405    hex 0 0 -25.25 0 0 190.5355 0 48.27 0
c
410     pz 137.1422 $ bottom of lid
411     pz 139.6822 $ steel
412     pz 164.0154 $ lead
413     pz 165.2854 $ steel
414     pz 195.7654 $ 1 foot water reflector
c
420     pz -55.72    $ 1 foot water reflector
421     pz -25.24    $ bottom of cask
422     pz -22.7     $ steel
423     pz -3.0912   $ lead
424     pz 0         $ steel
c
c    basket surfaces
c
600     pz 18.5928       $ bottom of basket support plate
601     pz 19.2278       $ top of basket support plate
602     cz 20.0025       $ bottom plate
603     cz 15.875        $ IR bottom
604     cz 16.51         $ OR bottom
610     cz 2.2606        $ IR inner tube
611     cz 2.54          $ OR inner tube

m1      1001.62c  5.6041E-02 $ fuel
        40000.66c 3.5025E-02
        92235.69c 9.0406E-04
        92238.69c 3.8442E-04
c       Total     9.2354E-02
mt1     h/zr.60t
        zr/h.60t
m2      1001.62c  2          $ water
        8016.62c  1
mt2     lwtr.60t
m4      6000.66c   -0.08     $ SS-304
        14000.60c  -1.0
        15031.66c  -0.045
        24000.50c  -19.0
        25055.62c  -2.0
        26000.55c  -68.375
        28000.50c  -9.5
m5      82000.50c 1          $ Pb
m6      6000.66c  1          $ graphite
mt6     grph.60t
m7      40000.66c  1         $ Zr
c
*tr1      0 -8.255 0  j j j j j j j j j -1
*tr2      0 -8.255 0  45 135 90 45 45 90 j j j -1
*tr3      0 -8.255 0  90 180 90 0 90 90 j j j -1
*tr4      0 -8.255 0  135 225 90 45 135 90 j j j -1
*tr5      0 -8.255 0  180 270 90 90 180 90 j j j -1
*tr6      0 -8.255 0  135 45 90 225 135 90 j j j -1
*tr7      0 -8.255 0  90 0 90 180 90 90 j j j -1
*tr8      0 -8.255 0  45 45 90 135 45 90 j j j -1
```

```
c
*tr9      0 -14.605 0  j j j j j j j j j -1
*tr10     0 -14.605 0  32.7 122.7 90 57.3 32.7 90 j j j -1
*tr11     0 -14.605 0  65.5 155.5 90 24.5 65.5 90 j j j -1
*tr12     0 -14.605 0  98.1 188.1 90 8.1 98.1 90 j j j -1
*tr13     0 -14.605 0  130.8 220.8 90 40.8 130.8 90 j j j -1
*tr14     0 -14.605 0  163.5 253.5 90 73.5 163.5 90 j j j -1
*tr15     0 -14.605 0  163.5 73.5 90 253.5 163.5 90 j j j -1
*tr16     0 -14.605 0  130.8 40.8 90 220.8 130.8 90 j j j -1
*tr17     0 -14.605 0  98.1 8.1 90 188.1 98.1 90 j j j -1
*tr18     0 -14.605 0  65.5 24.5 90 155.5 65.5 90 j j j -1
*tr19     0 -14.605 0  32.7 57.3 90 122.7 32.7 90 j j j -1
c
mode   n
kcode  2500 1.0 50 250
sdef   rad=d1 ext=d2 axs=0 0 1
si1    5.5 16.2
si2    92 130
```

7.0 PACKAGE OPERATIONS

7.1 Procedures for Loading the Package

This section delineates the procedures for loading a payload from the BRR packaging. Hereafter, reference to specific BRR packaging components may be found in Appendix 1.3.3, *Packaging General Arrangement Drawings*.

7.1.1 Preparation for Loading

1. Remove the BRR package tie–down cover from the upper impact limiter.
2. Attach rigging to the upper impact limiter using the three (3) 1/2–13 UNC threaded holes marked as impact limiter lift points.
3. Remove the (8) eight ∅1–inch ball lock pins from each upper impact limiter attachment.
4. Using an overhead crane (or equivalent), lift and remove the upper impact limiter from the cask body.
5. Secure the lift adaptor to the cask body using the four (4) 1– 8UNC bolts. If rigging is used, secure the swivel hoist rings in place using swivel hoist ring 1-8UNC fasteners. Tighten the bolts/fasteners to 220 ±20 ft–lb torque.
6. Remove the (8) eight ∅1–inch ball lock pins from each lower impact limiter attachment.
7. Lift the cask body from the lower impact limiter, and place it on the facility transport equipment.
8. Secure the cask body to the facility transport equipment, and remove the rigging from the lift adaptor.

7.1.2 Loading of Contents

The BRR package is designed to be loaded either in a pool of water (wet) or in a hot cell (dry), as delineated in the following sections.

7.1.2.1 Wet Loading

1. Remove the twelve (12) 1–8UNC socket head cap screws (SHCSs) that retain the closure lid.
2. Install three (3) hoist rings (or equivalent) into the three (3) 1/2–13 UNC threaded holes in the closure lid.
3. Lift and remove the closure lid from the cask body. Store the closure lid in a manner to minimize potential damage to the O–ring seals and sealing surfaces.
4. Install and secure the sealing surface protector to the cask body.
5. Using the center 1/2–13 UNC threaded hole in the shield plug as a lift point, remove the shield plug from the cask body.
6. If not previously installed, install the appropriate fuel basket into the cask body cavity.

7. Remove the drain port dust cover and then the drain port plug. Install an appropriate fitting to the drain port.
8. Using an overhead crane (or equivalent), and attached to the lift adaptor, lift the cask body with the fuel basket from the facility transport equipment and position over the spent fuel pool staging area.
9. Slowly lower the cask body into the pool until the cavity is flooded, and the cask body is secure in the facility fuel loading station.
10. Load a fuel element into each fuel channel in the fuel basket. Up to eight (8) fuel elements may be loaded into the MURR, MITR-II, or ATR baskets. Up to nineteen (19) fuel elements may be loaded into the TRIGA basket.
11. Using the center 1/2–13 UNC threaded hole as a lift point, lower the shield plug into the cask body cavity. Visually verify that the shield plug is properly seated, and reposition if necessary.
12. If required, install the shield plug restraint, or optionally, install the shield plug restraint once the cask body has been raised to the working level.
13. Lift the loaded cask body from the spent fuel pool while spraying exposed portions with clean demineralized water. Perform a radiological survey of the cask body as it is raised out of the pool.
14. Open the drain fitting to drain the pool water from the cavity. Continue draining the cavity until no appreciable water is noted. Optionally, the cavity may be drained after securing the cask body in the facility work area.
15. Close the drain fitting, and remove the connecting plumbing from the drain fitting.
16. Lift the loaded cask body out of the spent fuel pool area and secure it in the facility work area.
17. Remove the sealing surface protector and, if installed, the shield plug restraint from the shield plug and cask body.
18. Remove and discard both main O–ring seals (if present), and clean and inspect the sealing surfaces in the closure lid and the mating surfaces on the cask body. If damage is present which is sufficient to impair containment integrity (scratches or dents, etc.), repair the damaged surfaces per Section 8.2.3.2, *Sealing Area Routine Inspection and Repair.*
19. Install two new (unused) O-rings in the appropriate grooves in the closure lid. As an option, sparingly apply vacuum grease to the O–ring seals and/or sealing surfaces.
20. Install the closure lid on the cask body, using the alignment pin to guide the closure lid into position.
21. Visually inspect the closure SHCSs for wear or damage that could impair their function and, if necessary, replace or repair per the requirements of the drawings in Appendix 1.3.3, *Packaging General Arrangement Drawings.*
22. Install the twelve (12) 1–8UNC SHCSs to secure the closure lid to the cask body. Using a star pattern, tighten the closure SHCSs to 220 ±20 ft–lb torque (lubricated).
23. Remove the vent port dust cover, vent port plug, test port dust cover, and test port plug.
24. Remove the drain port fitting from the drain port.

25. Remove and discard the vent, test, and drain port sealing washers from their respective port plugs (if present), and clean and inspect each sealing surface. If damage is present which is sufficient to impair containment integrity (scratches or dent, etc.), repair the damaged surfaces per Section 8.2.3.2, *Sealing Area Routine Inspection and Repair.*
26. Install the drain port plug and a new (unused) sealing washer in the drain port. Tighten the drain port plug to 20 ±2 ft–lb torque.
27. Using the vent port tool, install the vent port plug with a new (unused) sealing washer. Ensure that the vent port plug is loose enough to allow airflow through the vent port.
28. Install the test port plug and a new (unused) sealing washer in the closure lid approximately finger-tight.
29. Connect a vacuum pump and a shutoff valve to the vent port tool and evacuate the cavity until the internal pressure is 1 – 2 torr. Isolate the vacuum pump from the cask body cavity by closing the shutoff valve and shutting off the vacuum pump, closing the shutoff valve and venting the suction line to atmosphere, or other appropriate means that does not maintain a vacuum on the outlet of the shutoff valve.
30. Monitor the cavity pressure for a minimum of 30 minutes. If the cavity pressure does not exceed 3 torr at the end of the time period, proceed to Step 34.
31. If the pressure exceeds 3 torr, open the port tool to re–pressurize the cask body cavity to atmospheric pressure. Repeat Steps 29 and 30.
32. If after eight (8) hours of vacuum drying with air and the pressure exceeds 3 torr, disconnect the vacuum pump from the vent port tool and connect a source of helium gas.
33. Provide a helium atmosphere inside the cask payload cavity by backfilling with helium gas to a pressure of slightly greater than atmospheric pressure, i.e., +1, -0 psig. Repeat Steps 29 and 30.
34. Disconnect the vacuum pump from the vent port tool and connect a source of helium gas.
35. Provide a helium atmosphere inside the cask payload cavity by backfilling with helium gas to a pressure of slightly greater than atmospheric pressure, i.e., +1, -0 psig.
36. Disconnect the helium gas source from the vent port tool.
37. Using the vent port tool, tighten the vent port plug to 9 ±1 ft–lb torque.
38. Perform leakage rate testing on the containment O-ring seal and the drain and vent port sealing washers per Section 8.2.2.2, *Helium leakage Rate Testing the Main Containment O-ring Seal*, Section 8.2.2.3, *Helium Leakage Rate Testing the Drain Port Sealing Washer*, and Section 8.2.2.4, *Helium Leakage Rate Testing the Vent Port Sealing Washer.*
39. At the conclusion of all leakage rate testing, install the drain port dust cover, the test port dust cover, and vent port dust cover.

7.1.2.2 Dry Loading

Steps 1 – 6 may be performed either inside or outside of the hot cell. A transfer cask may be used in place of the hot cell for this procedure. The cask must remain upright at all times.

1. Remove the twelve (12) 1–8UNC socket head cap screws (SHCSs) that retain the closure lid.
2. Install three (3) hoist rings (or equivalent) into the three (3) 1/2–13 UNC threaded holes in the closure lid.
3. Lift and remove the closure lid from the cask body. Store the closure lid in a manner to minimize potential damage to the O–ring seals and sealing surfaces.
4. Install and secure the sealing surface protector to the cask body.
5. Using the center 1/2–13 UNC threaded hole in the shield plug as a lift point, remove the shield plug from the cask body.
6. If not previously installed, install the appropriate fuel basket into the cask body cavity.
7. If steps 1 – 6 were performed outside of the hot cell, reinstall shield plug in cask.
8. Mate the cask opening with the hot cell. If necessary, place the cask body inside the hot cell.
9. If required, remove the shield plug.
10. Load a fuel element into each fuel channel in the fuel basket. Up to eight (8) fuel elements may be loaded into the MURR, MITR-II, or ATR baskets. Up to nineteen (19) fuel elements may be loaded into the TRIGA basket.
11. Using the center 1/2–13 UNC threaded hole as a lift point and a remote lift adapter, lower the shield plug into the cask body cavity. Visually verify that the shield plug is properly seated, and reposition if necessary.
12. Optionally, install the shield plug restraint.
13. If the cask was placed within the hot cell remove the loaded cask body from the hot cell. Perform a radiological survey of the cask body as it is removed.
14. If the cask was mated to the hot cell, disconnect the cask from the hot cell. Perform a radiological survey of the cask body as it is removed.
15. Remove the sealing surface protector and, if installed, the shield plug restraint from the shield plug and cask body.
16. Remove and discard both main O–ring seals (if present), and clean and inspect the sealing surfaces in the closure lid and the mating surfaces on the cask body. If damage is present which is sufficient to impair containment integrity (scratches or dents, etc.), repair the damaged surfaces per Section 8.2.3.2, *Sealing Area Routine Inspection and Repair*.
17. Install two new (unused) O-rings in the appropriate grooves in the closure lid. As an option, sparingly apply vacuum grease to the O–ring seals and/or sealing surfaces.
18. Install the closure lid on the cask body, using the alignment pin to guide the closure lid into position.
19. Visually inspect the closure SHCSs for wear or damage that could impair their function and, if necessary, replace or repair per the requirements of the drawings in Appendix 1.3.3, *Packaging General Arrangement Drawings*.
20. Install the twelve (12) 1–8UNC SHCSs to secure the closure lid to the cask body. Using a star pattern, tighten the closure SHCSs to 220 ±20 ft–lb torque (lubricated).

21. Remove the vent port dust cover, vent port plug, test port dust cover, and test port plug.
22. Remove the drain port dust cover and drain port plug.
23. Remove and discard the vent, test, and drain port sealing washers from their respective port plugs (if present), and clean and inspect each sealing surface. If damage is present which is sufficient to impair containment integrity (scratches or dent, etc.), repair the damaged surfaces per Section 8.2.3.2, *Sealing Area Routine Inspection and Repair.*
24. Install the drain port plug and a new (unused) sealing washer in the drain port. Tighten the drain port plug to 20 ±2 ft–lb torque.
25. Using the vent port tool, install the vent port plug with a new (unused) sealing washer. Ensure that the vent port plug is loose enough to allow airflow through the vent port.
26. Install the test port plug and a new (unused) sealing washer in the closure lid approximately finger-tight.
27. Connect a vacuum pump and a shutoff valve to the vent port tool and evacuate the cavity until the internal pressure is 1 – 2 torr. Isolate the vacuum pump from the cask body cavity by closing the shutoff valve and shutting off the vacuum pump, closing the shutoff valve and venting the suction line to atmosphere, or other appropriate means that does not maintain a vacuum on the outlet of the shutoff valve.
28. Monitor the cavity pressure for a minimum of 30 minutes. If the cavity pressure does not exceed 3 torr at the end of the time period, proceed to Step 32.
29. If the pressure exceeds 3 torr, open the port tool to re–pressurize the cask body cavity to atmospheric pressure. Repeat Steps 27 and 28.
30. If after eight (8) hours of vacuum drying with air and the pressure exceeds 3 torr, disconnect the vacuum pump from the vent port tool and connect a source of helium gas.
31. Provide a helium atmosphere inside the cask payload cavity by backfilling with helium gas to a pressure of slightly greater than atmospheric pressure, i.e., +1, -0 psig. Repeat Steps 27 and 28.
32. Disconnect the vacuum pump from the vent port tool and connect a source of helium gas.
33. Provide a helium atmosphere inside the cask payload cavity by backfilling with helium gas to a pressure of slightly greater than atmospheric pressure, i.e., +1, -0 psig.
34. Disconnect the helium gas source from the vent port tool.
35. Using the vent port tool, tighten the vent port plug to 9 ±1 ft–lb torque.
36. Perform leakage rate testing on the containment O-ring seal and the drain and vent port sealing washers per Section 8.2.2.2, *Helium leakage Rate Testing the Main Containment O-ring Seal*, Section 8.2.2.3, *Helium Leakage Rate Testing the Drain Port Sealing Washer*, and Section 8.2.2.4, *Helium Leakage Rate Testing the Vent Port Sealing Washer.*
37. At the conclusion of all leakage rate testing, install the drain port dust cover, the test port dust cover, and vent port dust cover.

7.1.3 Preparation for Transport

1. Utilizing the lift adaptor, or optional rigging, lift and lower the cask body into the lower impact limiter that is located on the transport trailer. Ensure that the cask body is aligned with the impact limiter alignment stripe for correct circumferential location.
2. Install the (8) eight ∅1–inch ball lock pins into each lower impact limiter attachment.
3. Remove the (4) four 1 – 8 UNC bolts that attach the lift adaptor to the cask body. Remove the lift adaptor or rigging hardware. The lifting holes may be optionally plugged.
4. Lift and lower the upper impact limiter onto the cask body. Ensure that the upper impact limiter is aligned with the cask body stripe for correct circumferential location.
5. Install the (8) eight ∅1–inch ball lock pins into each upper impact limiter attachment.
6. Install the tamper–indicating device (security seal) in the appropriate upper impact limiter attachment location.
7. Remove the rigging from the upper impact limiter lift points. The lifting holes may be optionally plugged.
8. Install the BRR package tie–down cover over the upper impact limiter, and secure the cover to the semi–trailer using the tie–down attachments. Optionally, install weather seal on bottom impact limiter.
9. Monitor external radiation for each loaded BRR package per the requirements of 49 CFR §173.441.
10. Determine that surface contamination levels for each loaded BRR package is per the requirements of 10 CFR §71.87(i) and 49 CFR §173.443.
11. Determine the transport index for each loaded BRR package per the requirements of 49 CFR §173.403.
12. Complete all necessary shipping papers in accordance with Subpart C of 49 CFR 172 [3].
13. BRR package marking shall be in accordance with 10 CFR §71.85(c) and Subpart D of 49 CFR 172. Package labeling shall be in accordance with Subpart E of 49 CFR 172. Package placarding shall be in accordance with Subpart F of 49 CFR 172.

7.2 Procedures for Unloading the Package

This section delineates the procedures for unloading a payload from the BRR packaging. Hereafter, reference to specific BRR packaging components may be found in Appendix 1.3.3, *Packaging General Arrangement Drawings*.

7.2.1 Receipt of Package from Carrier

1. Remove the BRR package tie–down cover from the upper impact limiter.
2. Verify that the tamper–indicating device (security seal) has not been tampered with or removed.
3. Attach rigging to the upper impact limiter using the three (3) 1/2–13 UNC threaded holes marked as impact limiter lift points.
4. Remove the tamper–indicating device (security seal) and the (8) eight ∅1–inch ball lock pins from each upper impact limiter attachment.
5. Using an overhead crane (or equivalent), lift and remove the upper impact limiter from the cask body.
6. Secure the lift adaptor to the cask body using the (4) four 1– 8UNC bolts. If rigging is used, secure the swivel hoist rings in place using swivel hoist ring 1-8UNC fasteners. Tighten the bolts to 220 ±20 ft–lb.
7. Remove the (8) eight ∅1–inch ball lock pins from each lower impact limiter attachment.
8. Lift the loaded cask body from the lower impact limiter, and place it on the facility transport equipment.
9. Secure the cask body to the facility transport equipment, and remove the rigging from the lift adaptor.

7.2.2 Removal of Contents

The BRR package is designed to be unloaded either in a pool of water (wet) or in a hot cell (dry), as delineated in the following sections. The unloading procedures may require removal of the lift adapter to facilitate gas sampling or other testing. If the lift adapter is removed for this purpose, reinstall per Paragraph 7.2.1, step 6 upon completion of sampling or testing.

7.2.2.1 Wet Unloading

1. Remove the vent port dust cover and connect a vent port tool to the vent port. Connect a gas sampling device to the vent port tool.
2. Loosen and remove the vent port plug using the vent port tool so that a gas sample may be extracted from the cavity .
3. Following verification of no contamination in the gas sample, vent the cavity to atmosphere to equalize cavity pressure.

4. Install three (3) hoist rings (or equivalent) into the three (3) 1/2–13 UNC threaded holes in the closure lid.
5. Remove the twelve (12) 1–8UNC socket head cap screws (SHCSs) that secure the closure lid.
6. Lift and remove the closure lid from the cask body. Store the closure lid in a manner to minimize potential damage to the O–ring seals and sealing surfaces.
7. Install and secure the sealing surface protector to the cask body.
8. Optionally, install the shield plug restraint over the shield plug in the cask body.
9. Remove the drain port dust cover and then the drain port plug. Install an appropriate fitting to the drain port.
10. Using appropriate rigging and an overhead crane (or equivalent) attached to the lift adaptor, lift the loaded cask body from the facility transport equipment and position over the spent fuel pool staging area.
11. If installed, remove the shield plug restraint, or optionally, remove the restraint after the cask body is secured in the facility fuel unloading station.
12. Slowly lower the cask body into the pool until the cavity is flooded, and secure the loaded cask body in the facility fuel unloading station.
13. Using the center 1/2–13 UNC threaded hole in the shield plug as a lift point, remove the shield plug from the cask body.
14. Remove the fuel elements from the basket and place in the facility's receiving station.
15. Using the center 1/2–13 UNC threaded hole as a lift point, lower the shield plug into the cask body cavity. Visually verify that the shield plug is properly seated, and reposition if necessary.
16. Optionally, install the shield plug restraint. The shield plug restraint may be installed once the cask body has been raised to the working level.
17. Lift the cask body from the spent fuel pool while spraying exposed portions with clean demineralized water. Perform a radiological survey of the cask body as it is raised out of the pool.
18. Open the drain fitting to drain the pool water from the cavity. Continue draining the cavity until no appreciable water is noted. Optionally, the cavity may be drained after securing the cask body in the facility work area.
19. Close the drain fitting, and remove the connecting plumbing from the drain fitting.
20. Lift the cask body out of the spent fuel pool area and secure it in the facility work area.
21. Remove the sealing surface protector and, if installed, the shield plug restraint from the shield plug and cask body.
22. Install the closure lid on the cask body, using the alignment pin to guide the closure lid into position.

23. Install the twelve (12) 1–8UNC SHCSs to secure the closure to the cask body. Using a star pattern, tighten the closure SHCSs to 220 ±20 ft–lb torque (lubricated).
24. Install the vent port plug and tighten to 9 ±1 ft–lb torque. Install the vent port dust cover.
25. Install the drain port plug and tighten to 20 ±2 ft–lb torque. Install the drain port dust cover.
26. Assemble the impact limiters onto the package and secure the package to the transport trailer as described in Section 7.1.3, *Preparation for Transport*. A tamper–indicating device is not required.

7.2.2.2 Dry Unloading

Steps 1 – 9 may be performed either inside or outside of the hot cell. A transfer cask may be used in place of the hot cell for this procedure. The cask must remain upright at all times

1. Remove the vent port dust cover and connect a vent port tool to the vent port. Connect a gas sampling device to the vent port tool.
2. Loosen and remove the vent port plug using the vent port tool so that a gas sample may be extracted from the cavity.
3. Following verification of no contamination in the gas sample, vent the cavity to atmosphere to equalize cavity pressure.
4. Install three (3) hoist rings (or equivalent) into the three (3) 1/2–13 UNC threaded holes in the closure lid.
5. Remove the twelve (12) 1–8UNC socket head cap screws (SHCSs) that retain the closure lid.
6. Lift and remove the closure lid from the cask body. Store the closure lid in a manner to minimize potential damage to the O–ring seals and sealing surfaces.
7. Install and secure the sealing surface protector to the cask body.
8. Optionally, install the shield plug restraint over the shield plug in the cask body.
9. Install a remote lift adaptor in the center 1/2–13 UNC threaded hole of the shield plug.
10. Mate the cask opening with the hot cell. If required, place the loaded cask body into the hot cell.
11. Remove the shield plug restraint (if installed) and lift the shield plug from the cask body.
12. Remove the fuel elements from the basket and place in the facility's receiving station.
13. Replace the shield plug into the cask body cavity. Optionally, install the shield plug restraint.
14. Remove or disconnect the unloaded cask body from the hot cell.
15. Remove the remote lift adaptor from the shield plug.
16. Remove the shield plug restraint (if installed) and remove the sealing surface protector.
17. Install the closure lid on the cask body, using the alignment pin to guide the closure lid into position.

18. Install the twelve (12) 1–8UNC SHCSs to secure the closure to the cask body. Using a star pattern, tighten the closure SHCSs to 220 ±20 ft–lb torque (lubricated).
19. Install the vent port plug and tighten to 9 ±1 ft–lb torque. Install the vent port dust cover.
20. If used, install the drain port plug and tighten to 20 ±2 ft–lb torque. Install the drain port dust cover.
21. Assemble the impact limiters onto the package and secure the package to the transport trailer as described in Section 7.1.3, *Preparation for Transport*. A tamper–indicating device is not required.

7.3 Preparation of an Empty Package for Transport

Previously used and empty BRR packagings shall be prepared and transported per the requirements of 49 CFR §173.428.

7.4 Appendix

7.4.1 References

1. Title 10, Code of Federal Regulations, Part 71 (10 CFR 71), *Packaging and Transportation of Radioactive Material*, 01–01–08 Edition.
2. Title 49, Code of Federal Regulations, Part 173 (49 CFR 173), *Shippers–General Requirements for Shipments and Packagings*, 10–01–08 Edition
3. Title 49, Code of Federal Regulations, Part 172 (49 CFR 172), *Hazardous Materials Tables and Hazardous Communications Regulations*, 10–01–08 Edition.

8.0 ACCEPTANCE TESTS AND MAINTENANCE PROGRAM

This section describes the acceptance tests and the maintenance program that shall be used on the BRR package in compliance with Subpart G of 10 CFR 71 [1].

8.1 Acceptance Tests

Per the requirements of 10 CFR §71.85, this section discusses the inspections and tests to be performed prior to first use of the BRR packaging. Acceptance criteria for all inspections and tests are found either on the drawings in Appendix 1.3.3, *Packaging General Arrangement Drawings*, or in the sections that follow. Deviations from requirements will be recorded and dispositioned in accordance with the cognizant quality assurance program.

8.1.1 Visual Inspection and Measurements

Each BRR packaging will be visually inspected and measured to ensure that all of the requirements delineated on the drawings in Appendix 1.3.3, *Packaging General Arrangement Drawings*, are satisfied. This includes but is not limited to such items as materials, physical arrangement of components, quantities, dimensions, welds, and measurements.

8.1.2 Weld Examinations

The locations, types, and sizes of all welds will be identified and recorded to ensure compliance with the drawings in Appendix 1.3.3, *Packaging General Arrangement Drawings*. All welds are subject to visual examination per AWS D1.6 [2]. The welds between the inner containment shell and either end structure, the welds between the outer shell and either end structure, and the longitudinal weld(s) in the outer shell, if any, are examined by ultrasonic inspection in accordance with the ASME Code, Subsection NB, Article NB-5000, and Section V, Article 4 [4]. Optionally, the weld between the inner containment shell and the lower end structure may be examined by radiographic inspection in accordance with the ASME Code, Subsection NB, Article NB-5000, and Section V, Article 2 [3]. All welds on the BRR package, except seal welds, are liquid penetrant inspected on the final pass in accordance with the ASME Code, Subsection N*x*, Article N*x*-5000, and Section V, Article 6 [5]. The appropriate Subsection for the containment welds and outer shell welds is NB; for other cask body welds and the impact limiter shells, NF; and for the fuel baskets, NG.

8.1.3 Structural and Pressure Tests

8.1.3.1 Lifting Device Load Testing

The BRR package does not contain any lifting devices that require load testing.

8.1.3.2 Containment Boundary Pressure Testing

The BRR package containment boundary shall be pressure tested to the greater of 125% of the design pressure per the requirements of ASME Code, Subsection NB, Article NB–6220 [6], or

150% of the maximum normal operating pressure (MNOP), per 10 CFR §71.85(b). Since the MNOP of the BRR package is 10 psig, and the design pressure is 25 psig, the test pressure shall be a minimum of $1.25 \times 25 = 31.25$ psig.

Following pressure testing of the containment boundary, welds directly related to the pressure testing and accessible base material adjacent to the welds shall be visually inspected for plastic deformation or cracking in accordance with AWS D1.6, and liquid penetrant inspected per ASME Code, Subsection NB, Article NB–5000, and Section V, Article 6, as delineated on the drawings in Appendix 1.3.3, *Packaging General Arrangement Drawings*. Indications of cracking or distortion shall be recorded and evaluated in accordance with the cognizant quality assurance program.

Except for the leakage rate testing of the containment body structure prior to lead pour, leakage rate testing per Section 8.1.4, *Fabrication Leakage Rate Tests*, shall be performed after completion of pressure testing to verify package configuration and performance to design criteria.

8.1.4 Fabrication Leakage Rate Tests

This section provides the generalized procedure for fabrication leakage rate testing of the containment vessel boundaries and penetrations during and following the completion of fabrication. Fabrication leakage rate testing shall follow the guidelines of Section 7.3, *Fabrication Leakage Rate Test*, of ANSI N14.5 [7].

Prior to leakage rate testing, internal components that are not permanently affixed to the containment boundary, such as shield plug and spent fuel baskets, shall be removed. For ease of leakage rate testing, the interior surfaces of the containment boundary should be thoroughly cleaned.

Fabrication leakage rate testing shall be performed on the containment boundary. Four separate tests comprise the series. Each test shall meet the acceptance criteria delineated in Section 8.1.4.1, *Fabrication Leakage Rate Test Acceptance Criteria.*

8.1.4.1 Fabrication Leakage Rate Test Acceptance Criteria

1. To be acceptable, each leakage rate test shall demonstrate a "leaktight" leakage rate of 1×10^{-7} reference cubic centimeters per second (ref–cm^3/s), air, or less, per Section 6.3, *Application of Reference Air Leakage Rate (L_R)*, of ANSI N14.5.
2. In order to demonstrate the leaktight leakage rate, the sensitivity of the leakage rate test procedure shall be 5×10^{-8} cm^3/s, air, or less, per Section 8.4, *Sensitivity*, of ANSI N14.5.
3. Failure to meet the stated leakage rate shall be recorded and evaluated in accordance with the cognizant quality assurance program.

8.1.4.2 Helium Leakage Rate Testing the Containment Structure Integrity

Fabrication leakage rate testing of the containment structure integrity is performed in two stages: prior to lead pour, and following lead pour. These two stages are necessitated by the in–situ lead shielding surrounding the cylindrical containment shell between the upper and lower end structures, which would prevent helium gas from reaching the surface of the steel.

8.1.4.2.1 Containment Body Structure (Prior to Lead Pour)

This leakage rate test verifies the leak tightness of the upper and lower end forgings/castings, and the inner shell that comprise the primary metallic containment boundary of the BRR packaging.

1. The fabrication leakage rate test shall be performed following the guidelines of Section A.5.3, *Gas Filled Envelope – Gas Detector*, of ANSI N14.5.
2. The BRR packaging shall be assembled with a test lid and seal in place of the closure lid onto the partially fabricated cask, consisting of the upper and lower end structures, inner containment shell, and outer structural shell.
3. Connect a port tool to the drain port in the lower end forging.
4. Install a helium mass spectrometer leak detector (MSLD) to the port tool. Evacuate through the drain port until the vacuum is sufficient to operate the MSLD.
5. Surround the outer surface of the containment body with an envelope filled with helium gas (99% purity or better) to a minimum concentration of 50%, and to a pressure slightly greater than atmospheric pressure. The final leakage rate shall be adjusted for the helium concentration in the envelope.
6. Perform the helium leakage rate test to the requirements of Section 8.1.4.1, *Fabrication Leakage Rate Test Acceptance Criteria.* If, after repeated attempts, the containment structure fails to pass the leakage rate test, isolate the leak path and, prior to repairing the leak path and repeating the leakage rate test, record on a nonconformance report and disposition prior to final acceptance in accordance with the cognizant quality assurance program.
7. Disconnect the port tool from the drain port in the lower end forging.

8.1.4.2.2 Containment Body Structure (Following Lead Pour)

This leakage rate test verifies the leak tightness of the closure lid, and the final machined configuration of the upper end structure that comprise the balance of the metallic containment boundary of the BRR packaging.

1. The fabrication leakage rate test shall be performed following the guidelines of Section A.5.3, *Gas Filled Envelope – Gas Detector*, of ANSI N14.5.
2. The BRR packaging shall be assembled with the two O–ring seals installed in the closure lid, and the vent and seal test port plugs installed with their associated sealing washers. If not previously tightened, tighten the closure lid bolts to 200 – 240 ft-lb torque (lubricated). Assembly is as shown in Appendix 1.3.3, *Packaging General Arrangement Drawings.*
3. Connect a port tool to the drain port in the lower end of the packaging.
4. Install a helium mass spectrometer leak detector (MSLD) to the port tool. Evacuate through the drain port until the vacuum is sufficient to operate the MSLD.
5. Surround the outer surface of the closure lid and upper end structure with an envelope filled with helium gas (99% purity or better) to a minimum concentration of 50%, and to a pressure slightly greater than atmospheric pressure. The final leakage rate shall be adjusted for the helium concentration in the envelope.

6. Perform the helium leakage rate test to the requirements of Section 8.1.4.1, *Fabrication Leakage Rate Test Acceptance Criteria.* If, after repeated attempts, the containment structure fails to pass the leakage rate test, isolate the leak path and, prior to repairing the leak path and repeating the leakage rate test, record on a nonconformance report and disposition prior to final acceptance in accordance with the cognizant quality assurance program.
7. Remove the port tool and re–install the drain port plug. Tighten to 18 – 22 ft-lb torque.

8.1.4.3 Helium Leakage Rate Testing the Main Containment O–ring Seal

1. The fabrication leakage rate test of the BRR package containment O–ring seal integrity shall be performed following the guidelines of Section A.5.4, *Evacuated Envelope – Gas Detector*, of ANSI N14.5.
2. Assemble the BRR package with the two O–ring seals installed in the closure lid. Ensure the vent and seal test ports are installed with their associated sealing washers. Assembly is as shown in Appendix 1.3.3, *Packaging General Arrangement Drawings.*
3. Utilizing a port tool, attach a vacuum pump and a source of helium gas, in parallel, to the vent port.
4. Close the valve to the source of helium gas and open the valve to the vacuum pump.
5. Utilizing a port tool, rotate the vent port plug to the open position.
6. Evacuate the system to a 90% vacuum or better (≤ 10% ambient atmospheric pressure). Isolate the vacuum pump from the system.
7. Provide a helium atmosphere inside the evacuated cavity by backfilling with helium gas (99% purity or better) to ambient atmospheric pressure (+1 psi, -0 psi).
8. Utilizing the port tool, rotate the vent port plug to the closed position, and remove the helium–contaminated port tool from the vent port.
9. Install a clean (helium–free) port tool into the seal test port.
10. Utilizing appropriate fittings, attach a helium MSLD to the port tool.
11. Utilizing the port tool, rotate the seal test port plug to the open position.
12. Evacuate the cavity between the containment O–ring seal and the test O–ring seal until the vacuum is sufficient to operate the leak detector per the manufacturer's recommendations.
13. Perform the helium leakage rate test to the requirements of Section 8.1.4.1, *Fabrication Leakage Rate Test Acceptance Criteria.* If, after repeated attempts, the BRR package containment O–ring seal fails to pass the leakage rate test, isolate the leak path and, prior to repairing the leak path and repeating the leak test, record on a nonconformance report and disposition prior to final acceptance in accordance with the cognizant quality assurance program.

8.1.4.4 Helium Leakage Rate Testing the Drain Port Sealing Washer

1. The fabrication leakage rate test of the drain port plug containment sealing washer integrity shall be performed following the guidelines of Section A.5.4, *Evacuated Envelope – Gas Detector*, of ANSI N14.5.

2. The BRR package shall be assembled with the two O–ring seals installed on the closure lid. Ensure the vent and seal test port plugs are installed with their associated sealing washers. Assembly is as shown in Appendix 1.3.3, *Packaging General Arrangement Drawings*.
3. Verify the presence of a helium atmosphere below the vent port plug containment sealing washer, as specified above in Steps 3 – 8 of Section 8.1.4.3, *Helium Leakage Rate Testing the Main Containment O–ring Seal*.
4. Install a port tool into the drain port.
5. Utilizing appropriate fittings, attach a helium MSLD to the port tool.
6. Evacuate the cavity above the drain port plug containment sealing washer until the vacuum is sufficient to operate the leak detector per the manufacturer's recommendations.
7. Perform the helium leakage rate test to the requirements of Section 8.1.4.1, *Fabrication Leakage Rate Test Acceptance Criteria*. If, after repeated attempts, the drain port plug containment sealing washer fails to pass the leakage rate test, isolate the leak path and, prior to repairing the leak path and repeating the leak test, record on a nonconformance report and disposition prior to final acceptance in accordance with the cognizant quality assurance program.

8.1.4.5 Helium Leakage Rate Testing the Vent Port Sealing Washer

The fabrication leakage rate test of the vent port sealing washer may also be performed during the leakage rate testing of the metallic containment boundary following lead pour per Section 8.1.4.2.2, *Containment Body Structure (Following Lead Pour)*.

1. The fabrication leakage rate test of the vent port plug containment sealing washer integrity shall be performed following the guidelines of Section A.5.4, *Evacuated Envelope – Gas Detector*, of ANSI N14.5.
2. The BRR package shall be assembled with the two O–ring seals installed on the closure lid. Ensure the vent and seal test port plugs are installed with their associated sealing washers. Assembly is as shown in Appendix 1.3.3, *Packaging General Arrangement Drawings*.
3. Verify the presence of a helium atmosphere below the vent port plug containment sealing washer, as specified above in Steps 3 – 8 of Section 8.1.4.3, *Helium Leakage Rate Testing the Main Containment O–ring Seal*.
4. Install a port tool into the vent port.
5. Utilizing appropriate fittings, attach a helium MSLD to the port tool.
6. Evacuate the cavity above the vent port plug containment sealing washer until the vacuum is sufficient to operate the leak detector per the manufacturer's recommendations.
7. Perform the helium leakage rate test to the requirements of Section 8.1.4.1, *Fabrication Leakage Rate Test Acceptance Criteria*. If, after repeated attempts, the vent port plug containment sealing washer fails to pass the leakage rate test, isolate the leak path and, prior to repairing the leak path and repeating the leak test, record on a nonconformance report and disposition prior to final acceptance in accordance with the cognizant quality assurance program.

8.1.5 Component and Material Tests

8.1.5.1 Polyurethane Foam

This section establishes the requirements and acceptance criteria for installation, inspection, and testing of the rigid, closed-cell, polyurethane foam utilized within the BRR packaging impact limiters.

8.1.5.1.1 Introduction and General Requirements

The polyurethane foam used within the BRR packaging is comprised of a specific "formulation" of foam constituents that, when properly apportioned, mixed, and reacted, produce a polyurethane foam material with physical characteristics consistent with the requirements given in Section 8.1.5.1.2, *Physical Characteristics*. In practice, the chemical constituents are batched into multiple parts (e.g., parts A and B) for later mixing in accordance with a formulation. Therefore, a foam "batch" is considered to be a specific grouping and apportionment of chemical constituents into separate and controlled vats or bins for each foam formulation part. Portions from each batch part are combined in accordance with the foam formulation requirements to produce the liquid foam material for pouring into a component or box. Thus, a foam "pour" is defined as apportioning and mixing the batch parts into a desired quantity for subsequent installation (pouring). Finally, all contiguous pours into a single mold are termed a "bun".

The following sections describe the general requirements for constituent storage, and foam pour and test data records.

8.1.5.1.1.1 Polyurethane Foam Constituent Storage

The foam supplier shall certify that the polyurethane foam constituents have been properly stored prior to use, and that the polyurethane foam constituents have been used within their shelf life.

8.1.5.1.1.2 Impact Limiter Shell Preparation

Prior to installing foam into the impact limiter shells, the interior surfaces of the shells shall be treated with an antibonding agent, such as a paste wax.

8.1.5.1.1.3 Polyurethane Foam Installation

The foam shall be installed while the longitudinal axis of the impact limiter shell is vertical. The walls of the shell where the liquid foam material is to be installed shall be between 55 °F and 95 °F prior to foam installation. Measure and record the shell temperature to an accuracy of ±2 °F prior to foam installation.

In the case of multiple pours into a single impact limiter, the cured level of each pour shall be measured and recorded to an accuracy of ±1 inch.

Measure and record the weight of liquid foam material installed during each pour to an accuracy of ±10 pounds.

All test samples shall be poured into disposable containers at the same time as the actual pour it represents, clearly marking the test sample container with the pour date and a unique pour

identification number. All test samples shall be cut from a larger block to obtain freshly cut faces. Prior to physical testing, each test sample shall be cleaned of superfluous foam dust.

8.1.5.1.1.4 Polyurethane Foam Pour and Test Data Records

A production pour and testing record shall be compiled by the foam supplier during the foam pouring operation and subsequent physical testing. Upon completion of production and testing, the foam supplier shall issue a certification referencing the production record data and test data pertaining to each foamed component. At a minimum, relevant pour and test data shall include:

- formulation, batch, and pour numbers, with foam material traceability, and pour date,
- instrumentation description, serial number, and calibration due date,
- pour and test data (e.g., date, temperature, dimensional, and/or weight measurements, compressive stress, etc., as applicable), and
- technician and Quality Assurance/Quality Control (QA/QC) sign–off.

8.1.5.1.2 Physical Characteristics

The following subsections define the required physical characteristics of the polyurethane foam material.

Testing for the various polyurethane foam physical characteristics is based on a "formulation", "batch", or "pour", as appropriate, as defined in Section 8.1.5.1.1, *Introduction and General Requirements*. The physical characteristics determined for a specific foam formulation are relatively insensitive to small variations in chemical constituents and/or environmental conditions, and therefore include physical testing only for leachable chlorides, thermal conductivity, and specific heat. Similarly, the physical characteristics determined for a batch are only slightly sensitive to small changes in formulation and/or environmental conditions during batch mixing, and therefore include physical testing only for flame retardancy. Finally, the physical characteristics determined for a pour are also only slightly sensitive to small changes in formulation and slightly more sensitive to variations in environmental conditions during pour mixing, and therefore include physical testing for density and compressive stress.

8.1.5.1.2.1 Physical Characteristics Determined for a Foam Formulation

8.1.5.1.2.1.1 Leachable Chlorides

The leachable chloride physical characteristic shall be determined once for a particular foam formulation. If multiple components are to utilize a specific foam formulation, then additional physical testing, as defined below, need not be performed.

1. The leachable chlorides test shall be performed using an ion chromatograph (IC) apparatus. The IC measures inorganic anions of interest (i.e., chlorides) in water. Description of a typical IC is provided in EPA Method 300.0 [8]. The IC shall be calibrated against a traceable reference specimen per the IC manufacturer's operating instructions.
2. One test sample shall be taken from a pour for each foam formulation. The test sample shall be a cube with dimensions of 2.00 ±0.06 in.

3. Place the test sample in a room (ambient) temperature environment (i.e., 68 °F to 86 °F) for sufficient time to thermally stabilize the test sample. Measure and record the room temperature to an accuracy of ±2 °F.
4. Obtain a minimum of 550 mL of distilled or de–ionized water for testing. The test water shall be from a single source to ensure consistent anionic properties for testing control.
5. Obtain a 400 mL, or larger, contaminant free container that is capable of being sealed. Fill the container with 250 ±3 mL of test water. Fully immerse the test sample inside the container for a duration of 72 ±3 hours. If necessary, use an inert standoff to ensure the test sample is completely immersed for the full test duration. Seal the container prior to the 72–hour duration.
6. Obtain a second, identical container to use as a "control". Fill the control container with 250 ±3 mL of the same test water. Seal the control container prior to the 72–hour duration.
7. At the end of the test period, measure and record the leachable chlorides in the test water per the IC manufacturer's operating instructions. The leachable chlorides in the test water shall not exceed one part per million (1 ppm).
8. Should leachable chlorides in the test water exceed 1 ppm, measure and record the leachable chlorides in the test water from the "control" container. The difference in leachable chlorides from the test water and "control" water sample shall not exceed 1 ppm.

8.1.5.1.2.1.2 Thermal Conductivity

1. The thermal conductivity test shall be performed using a heat flow meter (HFM) apparatus. The HFM establishes steady state unidirectional heat flux through a test specimen between two parallel plates at constant but different temperatures. By measurement of the plate temperatures and plate separation, Fourier's law of heat conduction is used by the HFM to automatically calculate thermal conductivity. Description of a typical HFM test method is provided in ASTM C518 [9]. The HFM shall be calibrated against a traceable reference specimen per the HFM manufacturer's operating instructions.
2. Three test samples shall be taken from the sample pour. Each test sample shall be of sufficient size to enable testing per the HFM manufacturer's operating instructions.
3. Place the test samples in a room (ambient) temperature environment (i.e., 68 °F to 86 °F) for sufficient time to thermally stabilize the test samples.
4. Measure and record the necessary test sample parameters as input data to the HFM apparatus per the HFM manufacturer's operating instructions.
5. Perform thermal conductivity testing and record the measured thermal conductivity for each test sample following the HFM manufacturer's operating instructions.
6. Determine and record the average thermal conductivity of the three test samples. The numerically averaged thermal conductivity of the three test samples shall be within the range between 0.17 and 0.25 (BTU–in)/(hr–ft^2–°F).

8.1.5.1.2.1.3 Specific Heat

1. The specific heat test shall be performed using a differential scanning calorimeter (DSC) apparatus. The DSC establishes a constant heating rate and measures the differential heat flow into both a test specimen and a reference specimen. Description of a typical DSC is provided in ASTM E1269 [10]. The DSC shall be calibrated against a traceable reference specimen per the DSC manufacturer's operating instructions.
2. Three test samples shall be taken from the sample pour. Each test sample shall be of sufficient size to enable testing per the DSC manufacturer's operating instructions.
3. Place the test samples in a room (ambient) temperature environment (i.e., 68 °F to 86 °F) for sufficient time to thermally stabilize the test samples.
4. Measure and record the necessary test sample parameters as input data to the DSC per the DSC manufacturer's operating instructions.
5. Perform specific heat testing and record the measured specific heat for each test sample following the DSC manufacturer's operating instructions.
6. Determine and record the average specific heat of the three test specimens. The numerically averaged specific heat of the three test samples shall be within the range between 0.28 and 0.42 $Btu/lb_m–°F$.

8.1.5.1.2.2 Physical Characteristics Determined for a Foam Batch

Polyurethane foam material physical characteristics for flame retardancy shall be determined once for a particular foam batch based on the batch definition in Section 8.1.5.1.1, *Introduction and General Requirements*. If single or multiple components are to utilize a single foam batch, then additional flame retardancy testing, as defined below, need not be performed for each foam pour.

Polyurethane foam shall be tested for flame retardancy as follows:

1. Three test samples shall be taken from a pour from each foam batch. Each test sample shall be a rectangular prism with nominal dimensions of 0.5 inches thick, 3.0 inches wide, and a minimum length of 7.0 inches. In addition, individual sample lengths must not be less than the total burn length observed for the sample when tested.
2. Place the test samples in a room (ambient) temperature environment (i.e., 68 °F to 86 °F) for sufficient time to thermally stabilize the test samples. Measure and record the room temperature to an accuracy of ±2 °F.
3. Measure and record the length of each test sample to an accuracy of ±0.15 in.

4. Install an approximately 3/8–inch, or larger, Bunsen or Tirrill burner inside an enclosure of sufficient size to perform flame retardancy testing. Adjust the burner flame height to 1½ ±1/4 inch. Verify that the burner flame temperature is 1,550 °F, minimum.
5. Support the test sample with the long axis oriented vertically within the enclosure such that the test sample's bottom edge will be 3/4 ±1/8 inch (see adjacent figure) above the top edge of the burner.

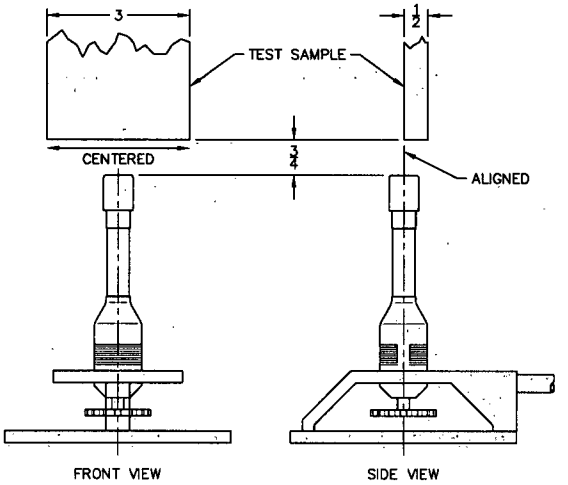

6. Move the burner flame under the test sample for an elapsed time of 60 ±2 seconds. As illustrated, align the burner flame with the front edge of the test sample thickness and the center of the test sample width.
7. Immediately after removal of the test sample from the burner flame, measure and record the following data:
   a. Measure and record, to the nearest second, the elapsed time until flames from the test sample extinguish.
   b. Measure and record, to the nearest second, the elapsed time from the occurrence of drips, if any, until drips from the test sample extinguish.
   c. Measure and record, to the nearest 0.15 inch, the burn length following cessation of all visible burning and smoking.
8. Flame retardancy testing acceptance is based on the following criteria:
   a. The numerically averaged flame extinguishment time of the three test samples shall not exceed fifteen seconds.
   b. The numerically averaged flame extinguishment time of drips from the three test samples shall not exceed three seconds.
   c. The numerically averaged burn length of the three test samples shall not exceed 6.0 in.

8.1.5.1.2.3 Physical Characteristics Determined for a Foam Pour

8.1.5.1.2.3.1 Density

Polyurethane foam material physical characteristic for density shall be determined for each foam pour based on the pour definition in Section 8.1.5.1.1, *Introduction and General Requirements*.

1. Three test samples shall be taken from the foam pour. Each test sample shall be a rectangular prism with minimum nominal dimensions of 1.0 inch thick (T) × 2.0 inch wide (W) × 2.0 inch long (L).

2. Place the test samples in a room (ambient) temperature environment (i.e., 68 °F to 86 °F) for sufficient time to thermally stabilize the test samples. Measure and record the room temperature to an accuracy of ±2 °F.
3. Measure and record the weight of each test sample to an accuracy of ±1 gram.
4. Measure and record the thickness, width, and length of each test sample to an accuracy of ±0.03 in.
5. Determine and record the room temperature density of each test sample utilizing the following formula:

$$\rho_{foam} = \frac{\text{Weight, g}}{453.6\ \text{g/lb}_m} \times \frac{1{,}728\ \text{in}^3/\text{ft}^3}{\text{T} \times \text{W} \times \text{L, in}^3},\ \text{lb}_m/\text{ft}^3$$

6. Determine and record the average density of the three test samples. The numerically averaged density of the three test samples shall be within ±15% of the specified nominal foam density, i.e., within the range of 7.7 to 10.4 lb_m/ft^3 for a nominal 9 lb_m/ft^3 foam.

8.1.5.1.2.3.2 Compressive Stress

1. Three test samples shall be taken from each foam pour. Each test sample shall be a rectangular prism with minimum nominal dimensions of 1.0 inch thick (T) × 2.0 inch wide (W) × 2.0 inch long (L). The thickness dimension shall be the parallel–to–rise direction (for the perpendicular–to–rise direction, see below).
2. Place the test samples in a room (ambient) temperature environment (i.e., 68 °F to 86 °F) for sufficient time to thermally stabilize the test samples. Measure and record the room temperature to an accuracy of ±2 °F.
3. Measure and record the thickness, width, and length of each test sample to an accuracy of ±0.03 inch.
4. Compute and record the surface area of each test sample by multiplying the width by the length (i.e., W × L).
5. Place a test sample in a Universal Testing Machine. Lower the machine's crosshead until it touches the test sample. Set the machine's parameters for the thickness of the test sample.
6. Determine and record the average parallel–to–rise compressive stress of the three test samples from each batch pour for each foam density. As shown in Table 8.1-1, the average parallel–to–rise compressive stress for each foam pour shall be the nominal compressive stress ±15% at strains of 20%, 40%, and 70%.
7. Determine and record the average parallel–to–rise compressive stress of all test samples from each foamed component. As shown in Table 8.1-1, the average parallel–to–rise compressive stress for all foam pours used in a single bun shall be the nominal compressive stress ±10% at strains of 20%, 40%, and 70%.
8. Data for compressive stress in the perpendicular–to–rise direction shall be obtained in an identical manner, using three additional test samples, except that the thickness dimension of the test samples shall be perpendicular to the foam rise direction. As shown in Table 8.1-2, the average perpendicular–to–rise compressive stress for each foam pour shall be the nominal compressive stress ±15% at strains of 20%, 40%, and 70%. As further shown in

Table 8.1-2, the average perpendicular–to–rise compressive stress for all foam pours used in a single bun shall be the nominal compressive stress ±10% at strains of 20%, 40%, and 70%.

8.1.5.2 Butyl Rubber O–rings

Physical characteristics of the butyl rubber containment O–ring seals and sealing washers for the following parameters shall be determined for each lot based on the following acceptance tests. All material shall conform to the following ASTM D2000 [11] designation:

M4AA710 A13 B13 F17 F48 Z Trace Element.

8.1.5.2.1 Durometer

The durometer of each lot of the butyl rubber material shall be determined in accordance with ASTM D2240 [12]. Each lot of butyl rubber material shall have a hardness of 70 ±5 Shore A durometer (i.e., within the range of 65 to 75 Shore A durometer).

8.1.5.2.2 Tensile Strength and Elongation

The tensile strength of each lot of the butyl rubber material shall be determined in accordance with ASTM D412 [13]. Each lot of butyl rubber material shall have a minimum tensile strength of 10 MPa and a minimum elongation of 250%.

8.1.5.2.3 Heat Resistance

The heat resistance of each lot of the butyl rubber material shall be determined in accordance with ASTM D573 [14]. Each lot of butyl rubber material shall experience a maximum 10 Shore A durometer hardness increase, a maximum reduction in tensile strength of 25%, and a maximum reduction in ultimate elongation of 25%, when tested at 70 °C.

8.1.5.2.4 Compression Set

The compression set of each lot of the butyl rubber material shall be determined in accordance with Method B of ASTM D395 [15]. After 22 hours at 70 °C, each lot of butyl rubber material shall have a maximum compression set of 25%.

8.1.5.2.5 Cold Temperature Resistance

The cold temperature resistance of each lot of the butyl rubber material shall be determined in accordance with Method A, 9.3.2 of ASTM D2137 [16]. After 3 minutes at -40 °C, each lot of butyl rubber material shall be non–brittle.

8.1.5.2.6 Cold Temperature Resiliency

The cold temperature resiliency of each lot of the butyl rubber material shall be determined in accordance with the TR–10 test of ASTM D1329 [17]. Each lot of butyl rubber material shall be resilient at a test temperature of -50 °C or less.

8.1.6 Shielding Integrity Tests

8.1.6.1 In–Situ Lead Shielding

In–situ or poured lead shielding integrity shall be confirmed via gamma scanning. Two gamma scan techniques are utilized. The primary difference is in the method used to determine acceptance criteria. Both gamma scan techniques are exactly the same in all other respects and are conducted as discussed below.

A gamma probe is used to scan the outer cask surface while a Cobalt–60 or similar gamma source of sufficient strength is positioned within a collimator or guide tube along the centerline of the cask cavity. The cask outer surface is marked with a grid and a chart is made to reflect the gridded surface. The source is first placed on the bottom of the cask cavity while the surface is scanned around its circumference. The source is then moved up the predetermined distance to the next gridline and the circumference scanned again. This sequence is repeated until the entire cask outer surface is scanned. Dose rates are recorded from each grid square by scanning every point in the grid and recording the maximum dose rates in the corresponding grid on the chart. This data then serves as the raw gamma scan results.

The dose rates are evaluated by comparing them to predetermined dose rate values for nominal lead thickness and nominal–less–10% lead thickness. The two methods utilized to determine acceptance criteria for this data are as follows:

The first method, the *Laboratory Calibration Method*, utilizes test blocks of the cask wall made up of lead and steel plates. The test blocks simulate nominal and nominal–less–10% lead thicknesses. The source is placed behind the nominal test block assembly at a distance equal to the inside radius of the cask. The probe is then placed on the outside of the test block assembly and the dose rate recorded. This test sequence is repeated on the nominal–less–10% test block assembly. The resultant dose rate values are then utilized as acceptance criteria for the actual cask gamma scan. Additionally, the expected dose rate values for nominal and reduced (nominal–less–10%) thickness shielding are calculated utilizing attenuation values for steel and lead as correlation verification.

The second, the *Field Calibration Method*, utilizes a specially fabricated test lid that incorporates a holder for various lead and steel plate thicknesses. The fixture is installed onto the cask with the test lid set up to simulate the nominal lead thickness. The source is placed below the test lid, inside the cask, at a distance equal to the inside radius of the cask, along the centerline of the cask body. The dose rate is then measured and recorded. The test lid is adjusted to establish the nominal–less–10% lead thickness configuration. The source is again placed below the test lid at a distance equal to the inside radius of the cask, and the dose rate is again measured and recorded. The value for nominal–less–10% lead thickness is utilized as the maximum acceptable dose rate value for the BRR packaging.

8.1.6.2 Plate or Sheet Lead Shielding

Plate or sheet lead is utilized in the bottom end of the cask body and in the removable shield plug. Ultrasonic examination of each plate or sheet is performed prior to installation to ensure that no voids exist in excess of 10% of the lead plate or sheet thickness.

8.1.7 Thermal Tests

Tests to demonstrate the heat transfer capability of the packaging are not required because the thermal evaluations presented in Chapter 3, *Thermal Evaluation,* are based on well established heat transfer properties and methodologies and demonstrate relatively large thermal margins for all components. As such, the uncertainties in the predicted temperature levels are small. Further, since the thermal modeling incorporates several conservative assumptions, it is expected that the peak temperatures achieved will be less than predicted. See Chapter 3, *Thermal Evaluation,* for further discussions.

Table 8.1-1 – Compressive Strength (psi) Parallel-to-Foam Rise at 65°F to 85°F

Strain	Minimum		Nominal	Maximum	
	Nom. –15%	Nom. –10%		Nom. +10%	Nom. +15%
20%	234	248	275	303	316
40%	252	267	297	327	342
70%	644	682	758	834	872

Table 8.1-2 – Compressive Strength (psi) Perpendicular-to-Foam Rise at 65°F to 85°F

Strain	Minimum		Nominal	Maximum	
	Nom. –15%	Nom. –10%		Nom. +10%	Nom. +15%
20%	225	239	265	292	305
40%	250	265	294	323	338
70%	652	690	767	844	882

8.2 Maintenance Program

This section describes the maintenance program used to ensure continued performance of the BRR packaging.

8.2.1 Structural and Pressure Tests

No structural or pressure tests are necessary to ensure continued performance of the packaging.

8.2.2 Maintenance/Periodic Leakage Rate Tests

This section provides the generalized procedure for maintenance/periodic leakage rate testing of the containment boundary penetrations during routine maintenance, or at the time of seal replacement or sealing area repair. Maintenance leakage rate testing shall follow the guidelines of Section 7.4, *Maintenance Leakage Rate Test*, and Section 7.5, *Periodic Leakage Rate Test*, of ANSI N14.5.

Maintenance/periodic leakage rate testing shall be performed on the main O–ring seal, the vent port sealing washer, and the drain port sealing washer for the containment boundary in accordance with Section 8.2.2.2, *Helium Leakage Rate Testing the Main Containment O–ring Seal*, 8.2.2.3, *Helium Leakage Rate Testing the Drain Port Sealing Washer*, and 8.2.2.4, *Helium Leakage Rate Testing the Vent Port Sealing Washer*. Each leakage rate test shall meet the acceptance criteria delineated in Section 8.2.2.1, *Maintenance/Periodic Leakage Rate Test Acceptance Criteria.*

Prior to leakage rate testing, internal components that are not permanently affixed to the containment boundary, such as shield plug and spent fuel baskets, shall be removed. For ease of leakage rate testing, the interior surfaces of the containment boundary should be thoroughly cleaned.

8.2.2.1 Maintenance/Periodic Leakage Rate Test Acceptance Criteria

Maintenance/periodic leakage rate test acceptance criteria are identical to the criteria delineated in Section 8.1.4.1, *Fabrication Leakage Rate Test Acceptance Criteria.*

8.2.2.2 Helium Leakage Rate Testing the Main Containment O–ring Seal

1. The maintenance/periodic leakage rate test of the BRR package containment O–ring seal integrity shall be performed following the guidelines of Section A.5.4, *Evacuated Envelope – Gas Detector*, of ANSI N14.5.
2. The BRR package shall be assembled with the two O–ring seals installed in the closure lid, and the vent and seal test ports are installed with their associated sealing washers. If not previously tightened, tighten the closure lid bolts to 200 – 240 ft-lb torque. Assembly is as shown in Appendix 1.3.3, *Packaging General Arrangement Drawings*.
3. Utilizing a port tool, attach a vacuum pump and a source of helium gas, in parallel, to the vent port.
4. Close the valve to the source of helium gas and open the valve to the vacuum pump.
5. Utilizing a port tool, rotate the vent port plug to the open position.

6. Evacuate the system to a 90% vacuum or better (≤ 10% ambient atmospheric pressure). Isolate the vacuum pump from the system.
7. Provide a helium atmosphere inside the evacuated cavity by backfilling with helium gas (99% purity or better) to ambient atmospheric pressure (+1 psi, -0 psi).
8. Utilizing the port tool, rotate the vent port plug to the closed position, and remove the helium–contaminated port tool from the vent port.
9. Install a clean (helium–free) port tool into the seal test port.
10. Utilizing appropriate fittings, attach a helium MSLD to the port tool.
11. Utilizing the port tool, rotate the seal test port plug to the open position.
12. Evacuate the cavity between the containment O–ring seal and the test O–ring seal until the vacuum is sufficient to operate the leak detector per the manufacturer's recommendations.
13. Perform the helium leakage rate test to the requirements of Section 8.2.2.1, *Maintenance/Periodic Leakage Rate Test Acceptance Criteria.* If, after repeated attempts, the BRR package containment O–ring seal fails to pass the leakage rate test, isolate the leak path and, prior to repairing the leak path and repeating the leak test, record on a nonconformance report and disposition prior to final acceptance in accordance with the cognizant quality assurance program.

8.2.2.3 Helium Leakage Rate Testing the Drain Port Sealing Washer

1. The maintenance/periodic leakage rate test of the drain port plug containment sealing washer integrity shall be performed following the guidelines of Section A.5.4, *Evacuated Envelope – Gas Detector*, of ANSI N14.5.
2. The BRR package shall be assembled with the two O–ring seals installed on the closure lid. Ensure the vent and seal test port plugs are installed with their associated sealing washers. Assembly is as shown in Appendix 1.3.3, *Packaging General Arrangement Drawings.*
3. Verify the presence of a helium atmosphere below the vent port plug containment sealing washer, as specified above in Steps 3 – 8 of Section 8.2.2.2, *Helium Leakage Rate Testing the Main Containment O–ring Seal.*
4. Install a port tool into the drain port.
5. Utilizing appropriate fittings, attach a helium MSLD to the port tool.
6. Evacuate the cavity above the drain port plug containment sealing washer until the vacuum is sufficient to operate the leak detector per the manufacturer's recommendations.
7. Perform the helium leakage rate test to the requirements of Section 8.2.2.1, *Maintenance/Periodic Leakage Rate Test Acceptance Criteria.* If, after repeated attempts, the drain port plug containment sealing washer fails to pass the leakage rate test, isolate the leak path and, prior to repairing the leak path and repeating the leak test, record on a nonconformance report and disposition prior to final acceptance in accordance with the cognizant quality assurance program.

8.2.2.4 Helium Leakage Rate Testing the Vent Port Sealing Washer

1. The maintenance/periodic leakage rate test of the vent port plug containment sealing washer integrity shall be performed following the guidelines of Section A.5.4, *Evacuated Envelope – Gas Detector*, of ANSI N14.5.
2. The BRR package shall be assembled with the two O–ring seals installed on the closure lid. Ensure the vent and seal test port plugs are installed with their associated sealing washers. Assembly is as shown in Appendix 1.3.3, *Packaging General Arrangement Drawings*.
3. Verify the presence of a helium atmosphere below the vent port plug containment sealing washer, as specified above in Steps 3 – 8 of Section 8.2.2.2, *Helium Leakage Rate Testing the Main Containment O–ring Seal*.
4. Install a port tool into the vent port.
5. Utilizing appropriate fittings, attach a helium MSLD to the port tool.
6. Evacuate the cavity above the vent port plug containment sealing washer until the vacuum is sufficient to operate the leak detector per the manufacturer's recommendations.
7. Perform the helium leakage rate test to the requirements of Section 8.2.2.1, *Maintenance/Periodic Leakage Rate Test Acceptance Criteria*. If, after repeated attempts, the vent port plug containment sealing washer fails to pass the leakage rate test, isolate the leak path and, prior to repairing the leak path and repeating the leak test, record on a nonconformance report and disposition prior to final acceptance in accordance with the cognizant quality assurance program.

8.2.3 Component and Material Tests

8.2.3.1 Fasteners

All threaded components shall be visually inspected before installation for deformed or stripped threads. Damaged threaded components shall be repaired or replaced prior to further use. The threaded components to be visually inspected include the closure lid bolts, vent port plug, and drain port plug.

8.2.3.2 Sealing Area Routine Inspection and Repair

Before each use and at the time of seal replacement, containment sealing surfaces shall be visually inspected for damage that could impair the sealing capabilities of the packaging. Perform surface finish inspections for the closure lid O–ring grooves, the mating sealing area on the cask body, and the surfaces that mate with the sealing washer in the vent port and drain port. Damage shall be repaired prior to further use (e.g., using emery cloth or other surface finishing techniques) to restore the sealing surfaces to the value specified on the drawings in Appendix 1.3.3, *Packaging General Arrangement Drawings*.

Upon completion of any surface finish repairs, perform a leakage rate test per Section 8.2.2, *Maintenance/Periodic Leakage Rate Tests*.

8.2.3.3 Impact Limiters

Before each use, the impact limiters shall be inspected for tears or perforations in the stainless steel sheets, and for the presence of the fire–consumable plastic plugs. The ball–lock pins that retain the impact limiters shall be visually inspected for any damage that could reduce their effectiveness. Any damage shall be repaired prior to further use.

8.2.3.4 Seals

The containment boundary O–ring seal, the vent port sealing washer, and the drain port sealing washer shall be replaced within the 12–month period prior to shipment or when damaged (whichever is sooner), per the size and material requirements delineated on the drawings in Appendix 1.3.3, *Packaging General Arrangement Drawings*. Following seal replacement and prior to a loaded shipment, the new seals shall be leakage rate tested to the requirements of Section 8.2.2, *Maintenance/Periodic Leakage Rate Tests*.

8.2.4 Thermal Tests

No thermal tests are necessary to ensure continued performance of the BRR packaging.

8.3 Appendix

8.3.1 References

1. Title 10, Code of Federal Regulations, Part 71 (10 CFR 71), Packaging and Transportation of Radioactive Material, 01–01–08 Edition.
2. ANSI/AWS D1.6/D.6M:2007, *Structural Welding Code–Stainless Steel*, American Welding Society (AWS).
3. American Society of Mechanical Engineers (ASME) Boiler and Pressure Vessel Code, Section III, *Rules for Construction of Nuclear Facility Components*, Division 1 – Subsection NB, *Class 1 Components*, and Section V, *Nondestructive Examination*, Article 2, *Radiographic Examination*, 2007 Edition.
4. American Society of Mechanical Engineers (ASME) Boiler and Pressure Vessel Code, Section III, *Rules for Construction of Nuclear Facility Components*, Division 1 – Subsection NB, *Class 1 Components*, and Section V, *Nondestructive Examination*, Article 4, *Ultrasonic Examination Methods for Welds*, 2007 Edition.
5. American Society of Mechanical Engineers (ASME) Boiler and Pressure Vessel Code, Section III, *Rules for Construction of Nuclear Facility Components*, Division 1 – Subsection NB, *Class 1 Components*, and Section V, *Nondestructive Examination*, Article 6, *Liquid Penetrant Examination*, 2007 Edition.
6. American Society of Mechanical Engineers (ASME) Boiler and Pressure Vessel Code, Section III, *Rules for Construction of Nuclear Facility Components*, Division 1 – Subsection NB, *Class 1 Components*, Article NB–6220, 2007 Edition.
7. ANSI N14.5–1997, *American National Standard for Radioactive Materials – Leakage Tests on Packages for Shipment*, American National Standards Institute (ANSI), Inc.
8. EPA Method 300.0, Revision 2.2 (October 1999), *Determination of Inorganic Anions by Ion Chromatography*, U.S. Environmental Protection Agency.
9. ASTM C518–04, *Standard Test Method for Steady–State Thermal Transmission Properties by Means of the Heat Flow Meter Apparatus*, American Society for Testing and Materials (ASTM).
10. ASTM E1269, *Standard Test Method for Determining Specific Heat Capacity by Differential Scanning Calorimetry*, American Society for Testing and Materials (ASTM).
11. ASTM D2000–05, *Standard Classification System for Rubber Products in Automotive Applications*, American Society for Testing and Materials (ASTM).
12. ASTM D2240–05, *Standard Test Method for Rubber Property – Durometer Hardness,* American Society for Testing and Materials (ASTM).
13. ASTM D412–98a(2002)e1, *Standard Test Methods for Vulcanized Rubber and Thermoplastic Rubbers and Thermoplastic Elastomers – Tension,* American Society for Testing and Materials (ASTM).

14. ASTM D573–04, *Standard Test Method for Rubber – Deterioration in an Air Oven,* American Society for Testing and Materials (ASTM).

15. ASTM D395–03, *Standard Test Methods for Rubber Property – Compression Set,* American Society for Testing and Materials (ASTM).

16. ASTM D2137–94(2000), *Standard Test Methods for Rubber Property – Brittleness Point of Flexible Polymers and Coated Fabrics,* American Society for Testing and Materials (ASTM).

17. ASTM D1329–02, *Standard Test Method for Evaluating Rubber Property – Retraction at Lower Temperatures (TR Test),* American Society for Testing and Materials (ASTM).